Doctoral theses at NTNU, 2013:4

Leonardo Carlos Ruspini

Experimental and numerical investigation on two-phase flow instabilities

Doctoral Thesis

Leonardo Carlos Ruspini

ISBN 978-82-471-3404-7 (printed version)
ISBN 978-82-471-3405-4 (electronic version)
ISSN 1503-8181

NTNU – Trondheim
Norwegian University of
Science and Technology

NTNU
Norwegian University of Science and Technology
Thesis for the degree of Philosophiae Doctor
Faculty of Engineering Science & Technology
Department of Energy and Process Engineering

Doctoral theses at NTNU, 2013:4

NTNU

NTNU – Trondheim
Norwegian University of
Science and Technology

Leonardo Carlos Ruspini

Experimental and numerical investigation on two-phase flow instabilities

Thesis for the degree of Philosophiae Doctor

Trondheim, January 2013

Norwegian University of Science and Technology
Faculty of Engineering Science & Technology
Department of Energy and Process Engineering

NTNU – Trondheim
Norwegian University of
Science and Technology

NTNU
Norwegian University of Science and Technology

Thesis for the degree of Philosophiae Doctor

Faculty of Engineering Science & Technology
Department of Energy and Process Engineering

ISBN 978-82-471-3404-7 (printed version)
ISBN 978-82-471-3405-4 (electronic version)
ISSN 1503-8181

Doctoral theses at NTNU, 2013:4

Printed by Skipnes Kommunikasjon as

To my sister

Preface

This thesis has been submitted in fulfilment of the Ph.D. degree at the Norwegian University of Science and Technology under the supervision of Professor Carlos A. Dorao and co-supervision of Assoc. Prof. Maria Fernandino and Prof. Jostein Petersen.

The present work was performed at the Department of Energy and Process Engineering, Faculty of Engineering Science and Technology in the period November 2008- November 2012. The position was financed though a consortium between the Norwegian University of Science and Technology and Statoil A.S. through the project “Two-phase flow instabilities” (40104800).

Abstract

Two-phase flow instabilities are experimentally and numerically studied within this thesis. In particular, the phenomena called *Ledinegg* instability, *density wave* oscillations and *pressure drop* oscillations are investigated.

The most important investigations regarding the occurrence of two-phase flow instabilities are reviewed. An extensive description of the main contributions in the experimental and analytical research is presented. In addition, a critical discussion and recommendations for future investigations are presented.

A numerical framework using a hp-adaptive method is developed in order to solve the conservation equations modelling general thermo-hydraulic systems. A natural convection problem is analysed numerically in order to test the numerical solver. Moreover, the description of an adaptive strategy to solve thermo-hydraulic problems is presented.

In the second part of this dissertation, a homogeneous model is used to study *Ledinegg*, *density wave* and *pressure drop oscillations* phenomena numerically. The dynamic characteristics of the Ledinegg (flow excursion) phenomenon are analysed through the simulation of several transient examples. In addition, *density wave* instabilities in boiling and condensing systems are investigated. The effects of several parameters, such as the fluid inertia and compressibility volumes, on the stability limits of *Ledinegg* and *density wave* instabilities are studied, showing a strong influence of these parameters. Moreover, the phenomenon called *pressure drop oscillations* is numerically investigated. A discussion of the physical representation of several models is presented with reference to the obtained numerical results. Finally, the influence of different parameters on these phenomena is analysed.

In the last part, an experimental investigation of these phenomena is presented. The designing methodology used for the construction of the experimental facility is described. Several simulations and a non-dimensional similitude analysis are used to support the design, regarding the occurrence of two-phase flow instabilities. Some experimental results are presented in order to validate the current design. A full characterisation of the pressure drop losses in the facility is presented. Both, distributed and local pressure drop losses are investigated and the experimental results are compared with the main correlations used in the literature for the analysis of pressure drop in two-phase flow systems. Finally, *pressure drop* and *density wave* oscillations are studied experimentally, with main focus on the interaction of these two oscillation modes. In addition, the influence of compressibility volumes on the stability limits for the *density wave* phenomenon is analysed.

Acknowledgements

Professionally, I would like to thank to my supervisor Carlos Dorao and co-supervisor Maria Fernandino. The interaction with my co-supervisor Jostein Pettersen has also been important during the development of the experimental project. Furthermore, all the experimental works could not be done without the help and patience of three fantastic persons. Thanks Håvard Rekstad, Marius Døllner and Reidar Tellebon. It was a pleasure for me to work with all of you. In addition, I should also thanks to the whole personal of the EPT department, in particular to the secretary and the library staff, to make our working life much more easy.

Personally I must say that four years far from home have been a long time and it would not have been possible for me to do this without the support and company of several persons. There is no words that can describe my gratitude with Fabio, Octavio and Emilio for their friendship during these years. I also have to thank a lot to Ale "il bambino" for helping me with corrections and suggestions for this thesis. In these four years I had the fortune to know a lot of fantastic people that I would like to thank. Ranghild and Gøril, I'am completely grateful to you for sharing this last time with me. Giova, Gursu and Luca thanks for so many good memories "boludos" and I should also thanks to: Aldito, il Maestro, Claudita, Tanita, Gabri, Turkan, Martita, Luisito, Nico, Ale Ottavi, Alejandro, la hiena, Sonja, Eze, Nicla, Max and many others that I probably forgot now. The "tangueros" Morten, Anita, Terje, Heidi, Emilia, Guro, Frederik, Karl Johan, Toril, Bjørn and Igor. Of course to my bandoneon professor Kåre. I will always have really good memories of all of you. To the friends back in Argentina, thanks to make me feel that I never left. Thanks: Juancito, Pela, Bruno, Marito, Fer, Pabel, Maria, Yagui, Saltita, Dieguito, Edu, Pablito, Guille.

Of course it would not be possible to make this without the complete support of my family: "Gracias por aguantar todas mis locuras. Los quiero"; and of course to my new family Cristoforetti.

Finally, I really need to thank to one of the most important persons during these last years, who managed to teach me a lot of things that I never though I was able to learn. Thanks Batata.

Leonardo Carlos Ruspini

Trondheim, 2012

Contents

Nomenclature

Abbreviations and acronyms

BWR	Boiling Water Reactor
PWR	Pressure Water Reactor
LNG	Liquid Natural Gas
FDM	Finite Differences Method
FEM	Finite Elements Method
FVM	Finite Volumes Method
LSQFEM	Least Squares Finite Element Method
LSSM	Least Squares Spectral Method
WRF	Weighted Residual Formulation
CHF	Critical heat flux
OFI	Onset of Flow Instability
ONB	Onset of Nucleate Boiling
OSB	Onset of Significant Boiling
ChP	Characterisation of the pressure drop vs. flow rate curve
DWO	Density wave oscillations
FDI	Flow distribution instability
FSH	Flashing induced instability
GES	Geysering
LED	Ledinegg instability or flow excursion
NBO	Natural boiling oscillations
PDO	Pressure drop oscillations

TAO	Thermo-acoustic oscillations
ThO	Thermal oscillations

Non-dimensional numbers

N_{sub}	Subcooling number
N_{Zu}, N_{pch}	Zuber or phase change number
N_{Drift}	Drift number
N_{ρ}	Density number (gas-liquid density ratio)
N_{τ}	Nondimensional throttling number
Fr	Froud number
Re	Reynolds number

Variables and parameters

t	Time coordinate, [s]
z	Space coordinate, [m]
ΔP	Pressure drop, [Pa]
ΔT	Temperature difference, [^oC]
ρ	Density, [kg/m^3]
G	Mass flow rate, [kg/m^{2}s]
P	Absolute pressure, [Pa]
Q	Total power, [W]
T	Temperature, [^{o}C]
h	Specific enthalpy, [J/kg]
x	Quality, []
A_{xs}	Cross sectional area, [m^2]
Cp	Heat capacity, [J/K]
D_H	Hydraulic diameter, [m]
f	Darcy friction factor, []
K	Local pressure drop constant, []
L	Length, [m]

l	Orifice valve length, [m]
P_H	Hydraulic perimeter, [m]
q''	Heat per unit area, [W/m^2]
V	Compressible volume, [m^3]

Subscripts

g	Gas phase
l	Liquid phase
$G0$	Only Gas phase
HS	Heated section
$L0$	Only liquid phase
TP	Two-phase
in	Inlet
out	Outlet
si	Surge tank upstream
so	Surge tank downstream

CHAPTER I

Overview

► A description of the motivation and challenges behind this dissertation is presented in this introductory chapter. The objectives, scope and the structure of the work are discussed.

1.1 Introduction

The growth of the total worldwide energy consumption have motivated and challenged the use of new ways of heat transfer. For the last decades, the research on thermo-hydraulic designs using two-phase flow has been a subject of considerable interest. In particular, in situations where very high heat fluxes are expected, the use of subcooled boiling results quite attractive due the improved heat transfer characteristics. Evaporating and condensing two-phase flow systems are widely used in power generation, thermal management, chemical, space, cryogenics and other industries. In addition, the rapidly increase of power density in electronics is also encouraging the development of two-phase components for practical high-power electronics applications. Nevertheless, it is well known that under unstable operation conditions, the efficiency of a two-phase systems can rapidly decrease. In addition, the continue occurrence of two-phase instabilities can cause failures such as: premature burn-out, thermal fatigue, mechanical vibrations and control problems, and consequently decrease significantly the operation life span of the involved systems. It is clear that the study of these phenomena plays an important role in the design and safety analysis of two-phase flow systems.

The study of instabilities occurring in two-phase flow systems was initiated approximately sixty years ago. Great attention was given to these problems in the sixties and seventies with the advent of high power density boilers and boiling water reactors (BWR). Nowadays, the different scenarios where these phenomena can take place are fairly well understood in the nuclear industry. Not only because of the phenomenological understanding but also because of the large amount of effort put into the analysis of accidents and transient phenomena. Today, more than 90 % of thermo-hydraulic research for nuclear reactors belongs to the field of nuclear safety (F. Mayinger (1997)). Regarding other kind of industries where two-phase flow components are important, the understanding on two-phase flow instabilities is still very poor. Many industrial systems such as cryogenic heat exchangers, where

both boiling and condensing phenomena take place (two different streams), refrigeration systems, etc, are designed without the proper stability analysis of the transient phenomena involved in such a complex processes.

With this scenario on mind, it is easy to see that more basic research is still needed in order to extend the present knowledge on these phenomena to other related industries. Moreover, from the state-of-the-art analysis presented in Chapter 2 it can be also seen that there are still several open questions regarding these complex phenomena. Some of the most important points that must be clarified are enumerated:

- The interaction among different kinds of instabilities.
- The mechanisms that take place in the occurrence of instabilities in condensing systems.
- The occurrence of high-order density wave oscillations.
- The effects of external parameters (pump response, inertia, compressibility) in the stability of the systems.

1.2 Objectives

The main objective of this work is to study the phenomena involved in the so called thermo-hydraulic instabilities with reference to other kind of industries, since most of the present investigations describes only nuclear components conditions. Specifically this work considers the following topics:

- Review the state-of-the-art of two-phase flow instabilities. The main mechanisms triggering these phenomena are identified and its effects in different industries are studied.
- Develop a numerical framework capable of solving these complex phenomena and their interaction. Analyse the potential use of high-order adaptive techniques to solve with high accuracy the different time and space involved scales.
- Study the influence of different parameters that normally are not taken into account in the literature, such as inertia in the inlet and outlet fluid, compressibility volumes and pump response.
- Design an experimental facility to study this kind of phenomena. Including the characterisation of several parameter of paramount importance in the occurrence of two-phase instabilities.
- Study experimentally several aspects related with these phenomena. In particular, study the interaction between different modes occurring at the same time.

1.3 Scope

In Chapter 2 a review on the present understanding of thermo-hydraulic instability phenomena is presented. From this analysis it can be seen that there are several kinds of phenomena occurring in two-phase flow systems. The current investigation is mainly focused in *Ledinegg* instability, *density wave* oscillations (DWO), and *pressure drop oscillations* (PDO). The models and simulations presented in this work are restricted to following conditions,

- Pure fluids are considered as the working refrigerant. In most of the cases, the analysis is made using the refrigerant "R134a" (fluorine-hydrocarbon).
- Only macroscopic phenomena are described. No microscopic phenomena such as Helmholtz and Taylor instabilities, bubble collapse, etc, are taken into account in this work.
- One-dimensional representation of the main thermo-hydraulic variables. This formulation is proved to describe most of the physical phenomena occurring in boiling and condensing components.
- In most of the cases the effects of gravity are disregarded, since horizontal flows are considered as a study condition.

1.4 Outline of the thesis

This thesis is divided in five parts. This and the next chapter constitute the introductory part (Part 0), where the main research questions are formulated. Part I presents the development of the numerical tools used in the rest of the work to analyse the different phenomena. Part II deals with different aspects of the modelling of two-phase flow instabilities. Part III contains the description of the designed loop and the experimental investigation made as a part of this work. Finally in Part IV, conclusions, final remarks and future works are presented. In the following, an overview of the topics discussed in each of the chapters are presented.

- Chapter 2: The main phenomena considered as two-phase flow instabilities and the physical mechanisms related with their occurrence are introduced, in order to present a general description of the systems where these phenomena can be found. The state-of-the-art of *Ledinegg*, *density wave* oscillations and *pressure drop oscillations* is described. A review of experimental, analytical and numerical works is presented. Finally a discussion of the main results and problems in the research of these phenomena is addressed.

Part I: Numerical framework

- Chapter 3: The *least squares method spectral method* is analysed as an attractive tool for the resolution of general thermo-hydraulics systems. A *hp*-adaptive solver is developed and some examples are used in order to test it.

- Chapter 4: A natural circulation single-phase loop is simulated using the adaptive solver in order to study the strategies for adaptation in a thermo-hydraulic problem.

Part II: Modelling of two-phase flow instabilities

- Chapter 5: A homogeneous model is described in order to model a general two-phase flow single channel. The Ledinegg instability (or flow excursion) is analysed through several simulations in order to investigate the dynamic characteristics of this phenomenon.

- Chapter 6: Density wave instability and Ledinegg phenomena are studied in boiling and condensing systems.

- Chapter 7: The effects of external parameters, such as the inertia of the fluid in the pipes and the compressibility of gases in the systems, on the stability of *density wave* phenomena are investigated.

- Chapter 8: A dynamic model is compared with the normally used steady-state models in the description of *pressure drop oscillations*. The impact of several parameters in the stability of the systems are studied.

Part III: Experimental investigation

- Chapter 9: The design methodology for two-phase components and the particular design of a facility to study instabilities are described. Some details from the construction of the loop developed as a part of this work are shown and in the last part some experimental results are used to test the validity of the proposed methodology.

- Chapter 10: The distributed and local two-phase and single-phase pressure drop losses in the experimental facility are characterised. The experimental data is compared with the results of the main correlations available in the open literature.

- Chapter 11: An experimental investigation regarding the interaction between *density wave* and *pressure drop oscillations* is presented, with main focus on the mechanism that takes place in this interaction. Finally, the influence of a compressible volume in the stability of density wave phenomena is analysed.

Part IV: Final Remarks & Conclusions

- Chapter 12: In this last chapter the main conclusions, observations and remarks are presented.

1.5 Publications and contributions produced in this work

Papers in international journals

Ruspini, L.C., "Inertia and compressibility effects on density waves and Ledinegg phenomena in two-phase flow systems", Nuclear Engineering and Design, 250:60-67, 2012.

Ruspini, L.C., Dorao, C.A. and Fernandino, M., "Two-Phase Flow Instabilities in Boiling and Condensing Systems", Journal of Power and Energy Systems, JSME, 6(2):302-313, 2012.

Ruspini, L.C., Dorao, C.A. and Fernandino, M., "Dynamic simulations of Ledinegg instability". Journal of Natural Gas Science and Engineering, 2:211-216, 2010.

Ruspini, L.C., Dorao, C.A. and Fernandino, M., "Simulation of a natural circulation loop using a least squares hp-adaptive solver", Mathematics and Computers in Simulation, 81:2517-2528, 2011.

Ruspini, L.C., Dorao, C.A. and Fernandino, M., "Dynamic modeling of pressure drop oscillations in two-phase flow systems", Submitted to International Journal of Multiphase flow, 2012.

Ruspini, L.C., Dorao, C.A. and Fernandino, M., "Design methodology for two-phase flow components: experimental study of two-phase flow instabilities", Submitted to Experimental Thermal and Fluid Science, 2012.

Papers in conference proceedings (Peer-Reviewed)

Ruspini, L.C., Dorao, C.A. and Fernandino, M., "Experimental study of two-phase flow thermal-hydraulic instabilities, 20th International Conference On Nuclear Engineering (ICONE'20), California, USA, July 2012.

Ruspini, L.C., Dorao, C.A. and Fernandino, M., "Study of density wave phenomena in boiling and condensing two-phase flow systems", The 14th International Topical Meeting on Nuclear Reactor Thermal Hydraulics (NURETH-14 Toronto, Canada, September 2011.

Ruspini, L.C., "Study of inertia effects on dynamic two-phase oscillation phenomena", The 14th International Topical Meeting on Nuclear Reactor Thermal Hydraulics (NURETH-14 Toronto, Canada, September 2011.

Stromsvag, D., **Ruspini, L.C.**, Dorao, C.A. and Fernandino, M., "Influence of subcooling on density wave oscillations in a heated pipe", 8th International Conference on CFD in Oil & Gas, metallurgical and Process Industries, SINTEF/NTNU, Trondheim, Norway, June 2011.

Ruspini, L.C., Dorao, C.A. and Fernandino, M., "Modeling of dynamic instabilities in boiling systems", 19th International Conference On Nuclear Engineering (ICONE'19) Osaka, Japan, May 2011.

Ruspini, L.C., Dorao, C.A. and Fernandino, M., "Study of fast transient phenomena in the transportation of super-critical fluids", Computational mechanics conference (Mekit'11), Trondheim, Norway, May 2011.

Ruspini, L.C., Dorao, C.A. and Fernandino, M., "Design of a two-phase forced convection loop for stability analysis", Experimental Fluid Mechanics (EFM'10), Liberec, Czech Republic, 2010.

Ruspini, L.C., Dorao, C.A. and Fernandino, M., "Simulation of a natural circulation loop using an adaptive strategy ", Computational mechanics conference (Mekit'09), Trondheim, Norway, May 2009.

Oral presentations

Ruspini, L.C., Dorao, C.A. and Fernandino, M., "Study of density wave phenomena in boiling and condensing two-phase flow systems", The 14th International Topical Meeting on Nuclear Reactor Thermal Hydraulics (NURETH-14 Toronto, Canada, September 2011.

Ruspini, L.C., "Study of inertia effects on dynamic two-phase oscillation phenomena", The 14th International Topical Meeting on Nuclear Reactor Thermal Hydraulics (NURETH-14 Toronto, Canada, September 2011.

Ruspini, L.C., Dorao, C.A. and Fernandino, M., "Modeling of dynamic instabilities in boiling systems", 19th International Conference On Nuclear Engineering (ICONE'19) Osaka, Japan, May 2011.

Ruspini, L.C., Dorao, C.A. and Fernandino, M., "Study of fast transient phenomena in the transportation of super-critical fluids", Computational mechanics conference (Mekit'11), Trondheim, Norway, May 2011.

Ruspini, L.C., Dorao, C.A. and Fernandino, M., "Dynamical analysis of steady-state criteria for Ledinegg instability", Gas Technology Conference (SINTEF/NTNU). Trondheim, Norway. September 2009.

Ruspini, L.C., Dorao, C.A. and Fernandino, M., "Design of a two-phase forced convection loop for stability analysis", Experimental Fluid Mechanics (EFM'10), Liberec, Czech Republic, 2010.

Ruspini, L.C., Dorao, C.A. and Fernandino, M., "Simulation of a natural circulation loop using an adaptive strategy ", Computational mechanics conference (Mekit'09), Trondheim, Norway, May 2009.

Poster presentations

Ruspini, L.C., Dorao, C.A. and Fernandino, M., "Modeling of dynamic instabilities in boiling systems", 19th International Conference On Nuclear Engineering (ICONE'19) Osaka, Japan, May 2011.

Ruspini, L.C., Dorao, C.A. and Fernandino, M., "Design of a two-phase forced convection loop for stability analysis", Experimental Fluid Mechanics (EFM'10), Liberec, Czech Republic, 2010.

Ruspini, L.C., Dorao, C.A. and Fernandino, M., "Dynamical simulation of two-phase Ledinegg instability ", Gas Technology Conference (SINTEF/NTNU). Trondheim, Norway. September 2009.

Supervision

- **Co-advisor**: Bachelor Thesis. Bieito Gomez, "Study of two-phase pressure drop in orifice valves", Energy and Process department, NTNU, Norway, 2012.
- **Co-advisor**: MSc Thesis. Dag Stromsvag, "Influence of sub-cooling on density wave oscillations in a heated pipe", Energy and Process department, NTNU, Norway, 2010.
- **Co-advisor**: Bachelor Thesis. Dag Stromsvag. "Analysis of pressure drop in a boiling channel", Energy and Process department, NTNU, Norway, 2009.

1.5.1 About this thesis

The main idea behind the structure of this thesis is to assure that the chapters can be read independently. For this reason, a brief abstract and an introduction are included at the beginning of each chapter and a summary, with the main results and conclusions, is included at the end.

CHAPTER II

Two-phase flow instabilities: A review

► A review of two-phase flow instabilities is presented. The main physical mechanisms involved in the occurrence of these phenomena are introduced. A review of experimental and analytical investigations regarding *Ledinegg* instability, *density wave* and *pressure drop* oscillations is presented. Moreover, the current research state and the needs for future works are critically discussed.

2.1 Introduction

Historically, the study of two-phase flow instabilities started with the pioneering article of M. Ledinegg [115] (1938). Several years later, around 1960, the development of industrial high density boilers and boiling water reactors (BWR) turned the attention of many researchers into this kind of phenomena occurring in two-phase flow systems. During those years, several experimental studies described different kinds of phenomena occurring in boiling channels. As described by Yadigaroglu [43, chap. 17] (1981), "a period of relative confusion followed, with many authors attempting to explain various widely different observations". Thus, it is not until late 60's that the main instability mechanisms were understood, especially due to the development of analytical tools and computational tools [26, 239, 87, 88]. During the 70's and early 80's, several analytical works made a significant contribution on the understanding basis of thermo-hydraulic instabilities [61]. In parallel, lot of effort was made to study the stability of different kind of nuclear reactor components. With the development of computational tools, the study of transient phenomena related with accident analysis in nuclear reactors started to grow rapidly. Nowadays, the different scenarios where these phenomena can take place are fairly well understood in the nuclear industry. This is mainly due to the big effort put into the accident analysis and transient simulations. Today more than 90 % of thermo-hydraulic research in nuclear reactors belongs to the field of nuclear safety [137]. Regarding other industries where two-phase flow components are important, the understanding of the two-phase flow instability phenomena is still poor. In the last 50 years, several works reported the occurrence of this kind of phenomena in components such as

heat-exchangers, re-boilers, economisers, steam-generators, condensers, petroleum well components, thermo-syphons, etc. Several excellent reviews of experimental and analytical research have been published, such as J.A. Bouré et al. [25] (1973), M.Ishii [141] (1976), A.E. Bergles [22] (1977), G. Yadigaroglu [222] (1981), R.T. Lahey and D.A. Drew [112] (1980), S. Nakanishi [143] (1981) and R.T. Lahey and M.Z. Podowski [114] (1989). More recently, some reviews describe some particular aspects of two-phase flow instabilities L.A. Belblidia and C. Bratianu [17], G.V.D. Prasad et al. [165] (2007), L. Tadrist [196] (2007), A.K. Nayak and P.K. Vijayan [148] (2008) and S. Kakac and B. Bon [97] (2007).

The objective of this chapter is to review the main kinds of instabilities occurring in two-phase flows. In the first section, a description of the main mechanisms involved in the occurrence of two-phase flow instabilities is made. In the Sections 2.4 and 2.5, some of the most important experimental and analytical investigations are described. Moreover, a critical discussion of some relevant aspects of the current research state and future needs are presented in Section 2.6.

2.2 Two-phase flow instability mechanisms

In order to get a clearer picture of the phenomena taking place in two-phase flow systems it is necessary to introduce some common terms used in this field. The first distinction should be made between *microscopic* and *macroscopic* instabilities. The term *microscopic* instabilities is used for the phenomena occurring locally at the liquid-gas interface; for example, the Helmholtz and Taylor instabilities, bubble collapse, etc. The treatment of this kind of instabilities is out of the scope of this work. On the other hand, the macroscopic instabilities involve the entire two-phase flow system. In this brief review, the main focus is kept on the macroscopic phenomena.

The most used classification, introduced in J.A. Bouré et al. (1973), divided two-phase flow instabilities in *static* and *dynamic*. In the first case, the threshold of the unstable behaviour can be predicted from the steady-state conservation laws. On the other hand, to describe the behaviour of *dynamic* instabilities it is necessary to take into account different dynamic effects, such as the propagation time, the inertia, compressibility, etc. In addition, the term compound instability is normally used when several of the basic mechanisms, described later, interact with each other. In this way, it is said that a phenomenon is compound when is the consequence of a primary phenomenon. In more recent reviews, the distinction between natural and forced convection instabilities is made [148, 165], even when the nature of involved phenomena in the different cases is the same. In the following sections, this distinction is not considered and all the common phenomena are described. In this work a classification similar to the one presented in G. Yadigaroglu (1981) is used. Moreover, this classification is extended by the one presented in K. Fukuda and T. Kobori [61] (1979) and other more recent investigations.

In the next sections, the main mechanisms related with the occurrence of two-phase flow instabilities are described.

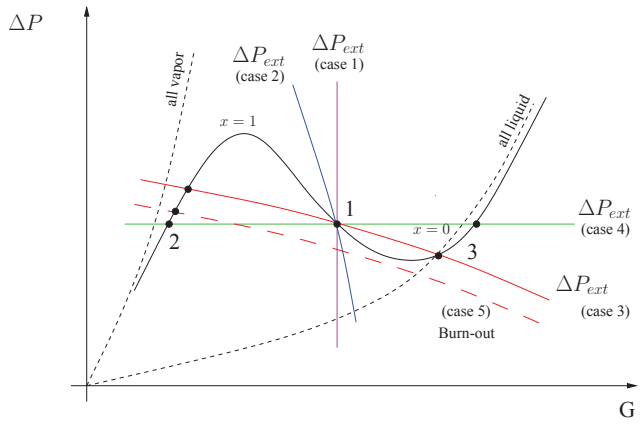

Figure 2.1: *Internal pressure drop vs. flow rate characteristic curve for a boiling system. In addition, five different external characteristics curves (cases) are presented.*

2.2.1 Characteristic pressure drop vs. flow rate instabilities

The static methodology comes from considering two different steady-state systems, external and internal. Thus, the intersecting points gives the steady-state operation points. It is well-know that under certain conditions the pressure drop vs. flow rate characteristic curve of a boiling system (internal curve) may exhibit a N-shape (or S-shape). Consequently depending on the pressure drop vs. flow rate characteristic curve of the external system, the operation points can be stable or unstable. An operation point is called stable when the slope of the internal characteristic is smaller than the slope of the external characteristic curve [115]. That is

$$\left.\frac{\partial \Delta P}{\partial G}_{int}\right|_w > \left.\frac{\partial \Delta P}{\partial G}_{ext}\right|_w \qquad stability\ condition \tag{2.1}$$

In Figure 2.1 the typical N-shape curve for a boiling system and several external curves are plotted. In addition, the total pressure drop for the theoretical cases of *all vapor* and *all liquid* (dotted line) are also shown. These two curves correspond to the limit cases for the two-phase pressure drop. As can be seen, the external curves of the *case 1* and *case 2* intersect the internal curve in only one point (1). As the internal curve slope is larger than the external curve slope, then this point is stable. An opposite behaviour is observed when the external curves of *case 3* and *case 4* intersect the same point. In these two cases the point (1) becomes unstable. Furthermore, two new stable operation points are fulfilling the steady-state operation condition, points (2) and (3).

Before continuing, it is interesting to analyse the different sources of the pressure drop vs. flow rate characteristic curve.

2.2.1.1 The characteristic pressure drop vs. flow curve

In a general steady-state case, this curve has three main components; momentum, frictional and potential pressure drops. According to the stability criteria,

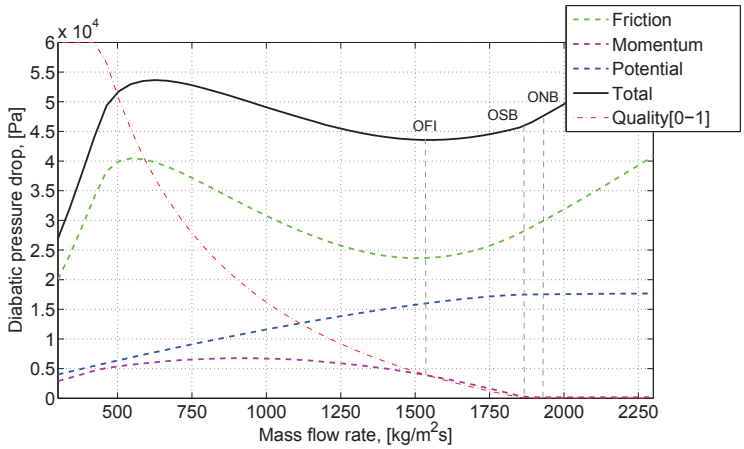

Figure 2.2: *Decomposition of the different pressure drop components in the characteristic pressure drop vs. flow rate curve of an upward flow boiling system.*

Eq. (2.1), the influence of the different terms stabilises or destabilises the system in the measure of how much they increase or decrease the characteristic curve slope. Figure 2.2 shows the different components for an upward boiling channel. In this case, the potential term is stabilising the system, while the momentum and frictional terms are destabilising the system in some flow regions. Notice that in the case of downward flow, then the potential term will also destabilise the system. K. Fukuda and T. Kobori (1979) propose to classify the instabilities depending on which of the terms is dominant. Even if according to the steady-state analysis this distinction is not strictly necessary, it is still not clear if a difference exists in how the different source terms influence the evolution of the system as will be discussed in the next sections.

In addition regarding to the literature common terminology for subcooled flow boiling in conventional-sized channels, three different physical points are distinguished. They are named; Onset of Nucleate Boiling (ONB), the Onset of Significant Boiling (OSB) or Net Vapor Generation (NVG) and the Onset of Flow Instability (OFI). The location of ONB and OSV points can be obtained through the void fraction distribution along the heated channel. G. Yadigaroglu [221] defines the OSB or NVG point as the point where the subcooled boiling void fraction starts growing appreciably. For most practical purposes the region between ONB and OSB is not analysed individually. Furthermore, the OFI denotes the minimum point of the total pressure drop characteristic curve. Normally, this last point is used to indicate the beginning of the unstable region, even when it is not a sufficient condition to assure an unstable behaviour.

On the other hand it should also be mentioned that the N-shape curve is not only particular of boiling systems, but it is also reported in general gas-liquid mixtures [155, 95, 86]. There are several instabilities triggered by this mechanism. In the following sections some of them are explained.

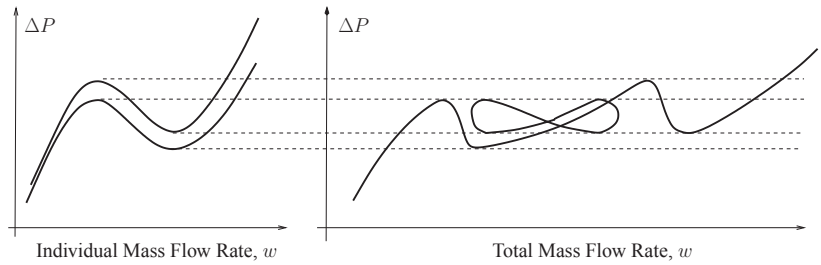

Figure 2.3: *Characteristic pressure drop vs. flow rate for two parallel channels with different individual characteristics.*

2.2.1.2 Ledinegg instability

Ledinegg instability or flow excursion is one of the most analysed instabilities in the literature. It is classified as a static instability by J.A. Bouré et al. (1973). It was first introduced by M. Ledinegg [115] and later named as *Ledinegg* instability. It is necessary to remark that the term *Ledinegg* instability is used in the literature in a general way to denote the unstable region.

This is the basic phenomena associated with the characteristic pressure drop vs. flow curve. It is said that the system experiments a flow excursion when it turns from an unstable to a stable operation point. In most of the practical cases this situation will never happen. Conversely, the modification of the external characteristic (or internal) can change the stability of an operation point. This effect is shown as (case 5) in Figure 2.1. If the external characteristic of a system, having initially three operation points (case 3), is for some reason modified to case 5, then the system will experiment a flow excursion from point 3 to point 2. When the flow is decreasing from the single-phase liquid region (point 3), the system suddenly turns in a two-phase state with a high generation of vapour. On the contrary, the same phenomenon can occur from an operation point in the two-phase region to a point in the all liquid zone. In [174] it is shown that from an unstable point the system can evolve in both direction, increasing or decreasing the flow with the same probability. Several examples describing the occurrence of this and other related phenomena, and their interaction, are included in the next sections.

2.2.1.3 Flow distribution instability

In this section, the flow distribution instability in parallel channels due to negative characteristic slope is analysed. Before continuing, it is necessary to distinguish between single and parallel channel for the formulation of the boundary conditions. In the case of a parallel array of tubes, connected by an inlet and exit plenum, whenever the conditions at the channel limits are sufficiently specified at all times, the problem reduces to a single-channel instability. Furthermore, the term "parallel channel" has been frequently used to recall a *constant pressure drop* boundary condition, while it might have been used more properly to denote flow distribution phenomena.

In the case of multiple channels, flow distribution in the different channels may result when some of the channels operate in the negative slope region. In Figure 2.3 the case of two parallel channels with different characteristic curves is shown. As can be seen, there are several regions of multiple solutions. Thus according to the external characteristic curve intersecting this curve, the system may have several possible operation points. In the case of a horizontal external characteristic (constant pressure difference) then the system can intersect until 9 operation points. It is easy to see that when the amount of channels grows, the complexity of the multiple solution region increases.

This phenomenon was first systematically analysed by K. Akagawa and T. Sakaguchi [3]. In this last work, several two-phase phenomena are analysed in an array of long parallel tubes. It is found that under the negative slope condition, the flow rate in the different tubes is not only mal-distributed but also flow excursions between the channels are observed.

2.2.1.4 Flow pattern transition

This kind of instability has been described in the literature since the 70's. Nevertheless, this phenomenon is not reported in industrial systems as an important issue. The main mechanism can be explained through the static characteristic curve in the same way as for the *Ledinegg* flow excursion. In the proximity of a flow pattern transition (normally considered as bubbly to annular, or slug), the pressure drop vs. flow rate will exhibit a transition point due to the different local pressure drop of the different regimes. When the characteristic curve has a negative slope, then any perturbation to the initial state can provoke an excursion to a new operation point. This would be the main mechanism of the flow pattern transition. In some particular cases, the modification of the operation point can produce a change in the main variables (void fraction) and the boundary conditions. Hence, the system will evolve again to the initial state, through another flow excursion. Under very specific conditions, this process can be repeated producing a periodic oscillations.

In the last years, some works have attempted to explain this phenomenon analytically. A.K. Nayak et al. [149] analyse the internal characteristic curve of a natural circulation pipe, using different pressure drop models for the different flow patterns, based on the maps of [198]. The characteristic curves show a multiple solution region for the flow pattern transition between annular and slug flow. Although this phenomenon can produce a flow excursion, the amplitude of flow excursion is always smaller than the amplitude of the *Ledinegg* flow excursion in the same system. Very brief experimental examples of this phenomenon can be found in [91, 208, 29].

2.2.1.5 Pressure Drop Oscillations (PDO)

Considering a boiling system with an N-shape characteristic curve, such as the one presented in Figure 2.4(b), a flow oscillation will be induced if a sufficient large amount of compressible volume is placed upstream from the heated section. This kind of phenomena is mainly due to the interaction between the flow excursion

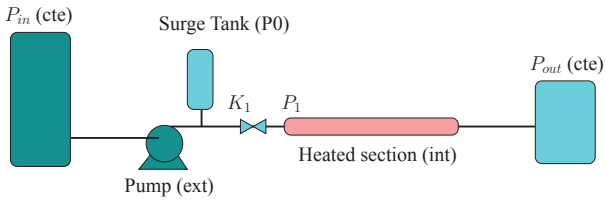

(a) Total system

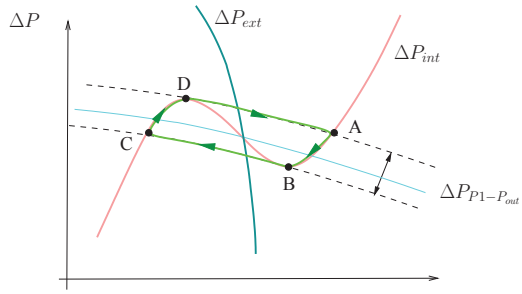

(b) External and internal characteristics curves

Figure 2.4: *Mechanism of Pressure Drop Oscillation. (a) System capable of sustaining oscillations. (b) Characteristic curves of the different parts of the system.*

phenomena and the surge tank compressibility. It was introduced and sistematically analysed in the pioneer studies of A.H. Stenning (1964) [189, 191, 133, 134].

Consider the system shown in Figure 2.4(a), where a surge tank (compressible volume) is situated upstream from a boiling channel. In accordance to Figure 2.4, the internal characteristic exhibits the N-shape curve. Consequently, the boundary conditions of the heated section would correspond at each time to the curve given by the valve K_1 and the constant pressures P_0 and P_{out} (cyan line in Figure 2.4(b)). When the intersection of this boundary condition curve and the boiling channel do not satisfy the stability condition of Eq. (2.1), thus the system may experience a transient phenomenon called *pressure drop oscillations*. Considering a full developed oscillation, this mechanism is composed by: a compression in the surge tank, CD; a flow excursions from a two-phase state to a liquid state, DA; a decompression in the surge tank, AB; and a flow excursion from a low quality to a high quality two-phase state, BC. In [133], it is proved that for high power density systems, the amount of compressible volume needed to sustain the oscillation is very low. In case of no interference with other phenomena, the frequency of the oscillations is mainly controlled by the compressible volume dynamics and the fluid inertia. Nevertheless, the occurrence of this phenomenon is normally associated with other kind of instabilities as will be discussed in the next sections.

2.2.2 Density Wave Oscillations, (DWO)

This is by far the most studied kind of two-phase flow instability. A thermo-hydraulic system and its associate boundary conditions constitute a complex dynamic system. The main two mechanisms related with the generation and propagation of this phenomenon are the delay in the propagation of disturbances and the feedback processes conditioning the inlet parameters. While delay effects are the product of transport phenomenon within the channel, feedback effects are related with the characteristics of the boundary conditions. In the classical description, the time period of these phenomena is considered to be between 1.5 and 2 times the time required for the fluid to travel through the system.

In general the name density wave instability was used in the literature to denominate one particular phenomenon occurring at high outlet qualities (DWO$_{II}$). K. Fukuda and T. Kobori (1979) presented a classification of different types of density wave instabilities. The authors of this last work classify the different kinds of phenomena according to the main mechanisms involved in their occurrence. In their model a heated channel and riser section are described. Moreover, they present five different kinds of DWO: due to gravity in the heated section, $D_{I,H}$; due to gravity in the riser section, $D_{I,R}$; due to friction in the heated section, $D_{II,H}$; due to friction in the riser sections, $D_{II,R}$; and due to inertia-momentum in the heated section, $D_{III,H}$.

The present classification, based in Fukuda's results, and taking into account experimental and analytical evidence, is divided in three types of *density wave* instabilities, based on the three main mechanisms that provoke them: due to gravity DWO_I; due to friction DWO_{II}; and due to momentum DWO_{III}. This last classification is in agreement with the analysis carried out by J.A. Bouré and A. Mihaila [26] (1967).

2.2.2.1 Type I: Due to gravity, DWO$_I$

This kind of instability is experimentally reported in upward vertical systems with a long unheated riser section downstream from the heated section. It was experimentally reported and systematically analysed in [61]. At low quality conditions, any disturbance can generate a significant change in the void fraction and in consequence a change in the flow conditions. At low pressures the hydrostatic head (heated section and riser) is very sensitive to flow rate variations. In consequence, the feedback between flow, void fraction, and head can lead into a cyclic evolution. In particular, this phenomenon is very important in natural convection loops, but it was also reported in forced convection systems [37]. It plays an important role in BWR safety analysis, as described in the experimental and analytical studies presented in the following sections.

2.2.2.2 Type II: Due to friction, DWO$_{II}$

This type of density wave phenomena is the most common *density wave* instability described in the literature. The theoretical basis and non-dimensional analysis, used to analyse this phenomenon, were introduced in [193, 26, 239, 88]. The main

cause of this phenomenon is the different propagation speed of the flow perturbations in the single phase and in the two phase region. Any change in flow or void fraction in the two phase region results in a pressure drop variation. Since the perturbation propagates rather slowly along the two phase region, a significant delay marks the onset of perturbations in the two phase region, hence the two phase pressure drop and the single phase pressure drop oscillate out-of-phase. A discussion of the complex interaction between the mechanisms taking place in the occurrence of this phenomenon will be presented in Section 2.5.4.

2.2.2.3 Type III: Due to momentum, DWO$_{III}$

This type of *density wave* instability have received very few attention. It was first presented as high-order *density waves* in the experimental study of G. Yadigaroglu and A. Bergles [224]. Moreover, in J.L. Achard et al. [2] the term "stability islands" was used to describe the parameter region where this phenomenon makes the system unstable. As described in [61], the basic cause of this phenomenon is the interaction between the inertia and momentum pressure drop terms and the thermo-hydraulic propagation delays.

2.2.3 Compound density wave phenomena

In this section, several phenomena related with the basic forms of the *density wave* instabilities are presented.

2.2.3.1 Density wave oscillations in parallel channels

Several investigations regarding the occurrence of *density wave* oscillations in parallel boiling channels have been published. Different aspects of this complex phenomenon have been introduced in [68, 59]. The basic *density wave* mechanisms, explained before, also occurs in parallel channel systems. As concluded by K. Fukuda and S. Hasegawa [59] (1979), the system stability depends on the local stability for each channel. Moreover, different modes of oscillations are possible according to the different characteristics of the channels. In general terms, out-of-phase and in-phase oscillations are reported and they are the result of the interaction between different channels. Several experimental and analytical investigations are analysed in the following sections.

2.2.3.2 Coupled neutronic thermo-hydraulic instabilities

During the 80's, several nuclear power plant events (BWR) [69, 150] have triggered the attention of thermo-hydraulic researchers and nuclear reactors vendors. As described before, the *density wave* instabilities are the consequence of feedback between the propagation phenomena and the different pressure drop terms in the single- and two-phase regions. In BWRs, since water is used as a refrigerator and as a moderator, the neutron flux (in consequence the power) depends strongly on the void fraction. Thus, there is a feedback effect between the void fraction and the neutronic flux called *reactivity feedback*. In conclusion, this new feedback effect

is coupled with the basic mechanism triggering the *density wave* instabilities and can produce the phenomenon named as neutronic-coupled *density wave* instability. An excellent review of the state-of-art regarding neutronic-coupled instabilities was presented by J. March-Leuba and J.M. Rey [128] (1993). In general, two different modes are described in the literature. They are: *Core wide*, when the whole core behaves as one (in the sense of the neutron flux); *Out-of-phase*, when the neutron flux oscillates azimuthally in the core of the reactor. In the last decades, lot of effort was made in order to understand and predict the occurrence of this phenomenon in nuclear reactors.

2.2.4 Flashing instability, (FSH)

This phenomenon is generally described in natural convection systems, in which an unheated section (riser) is placed downstream from the boiler. As described by M. Furuya [63] (2006), the flashing-induced mechanism can be resumed in the following steps:

(a) The fluid heated in the core flows into the chimney.

(b) Boiling is initiated at a location where the liquid temperature exceeds the local saturation temperature.

(c) A decrease in the static head promotes further evaporation (flashing).

(d) The natural circulation flow rate increases due to an enlarged vapor volume, resulting in an outflow of vapour bubbles. The temperature at the chimney inlet decreases due to the higher flow.

(e) After the chimney is filled with subcooled liquid, the flow rate decreases and the process repeat itself from the point (a).

It is found that the oscillation period agrees with the time required for the single-phase liquid to pass through the unheated section region (chimney). For that reason it is considered in some works as a *density wave* phenomenon. A basic thermo-hydraulic model to analyse this phenomenon is presented in [223, 125, 126].

2.2.5 Thermal oscillations (ThO)

The name *thermal oscillation* phenomenon is associated with the large fluctuations of the heated channel wall temperature. It was first presented by A.H. Stenning and T.N. Veziroglu [190]. This phenomenon is considered as a compound dynamic instability in the classification presented in J.A. Bouré et al. [25], since it is observed as a result of other thermo-hydraulic instabilities. In the original study [190], this phenomenon is triggered by *density wave* oscillations (DWO_{II}).

This phenomenon is associated with the movement of the dryout and nucleate boiling boundaries (H.T. Liu et al. [122]). When this phenomenon is triggered by low frequency oscillations (PDO), as described in [102, 97], the temperature fluctuantions are simply the result of the boiling boundary movement. In these cases

the oscillation frequency is equivalent to that of the primary phenomenon, as any other thermo-hydraulic variable in the system. On the other hand, when this phenomenon is triggered by high frequency oscillations (DWO), then the temperature fluctuations have two distinct modes: a high frequency and small amplitude mode (corresponding to the DWO); and a low frequency and large amplitude mode. The high frequency mode is simply due to the boiling boundary movement, similar to the case of PDO. The low frequency mode is a system mode and depends on the heater wall capacity, axial conduction, and transition boiling characteristics, as described by H.T. Liu et al. (1994). Strictly speaking, this last mode is the only phenomenon that can be considered apart from the primary phenomenon and received the name of *thermal oscillations*. According to the experimental evidence [190, 102, 122, 49], this last mode occurs only as a result of the *density wave* oscillations.

2.2.6 Geysering (GES)

Geysering phenomenon has been observed in upward vertical boilers with long unheated section downstream from the heated section. This phenomenon occurs for low power and low flow rates. It has been reported in natural and forced convection systems and in single and parallel channels. It was first reported by P. Griffith [73] (1962) for a vertical heated section with no circulation.

The mechanism triggering this instability mode was presented in M. Ozawa et al. [156]. The whole process is explained as occurring in three different parts: boiling delay, condensation (or expulsion of vapor) and liquid returning. Figure 2.5 shows a representation of the geysering phenomenon. The main mechanism, as explained by M. Aritomi et al. [11], could be summarised as: a large slug of bubbles is generated as a result of the heating and the decrease of the hydrostatic head as it moves up; when the vapor mixes with the subcooled liquid in the upper plenum, then the large slug of bubbles is suddenly condensed; due to the bubbles collapse the subcooled liquid reenters the channels and restores the non-boiling condition; the heating of the liquid increase again the void in the heater and the whole process repeats. This phenomenon is most of the times reported in interaction with DWO_I and flashing phenomena.

Several experimental investigations have shown that the period of flow oscillation is proportional to the boiling delay time t_{bd}, since it is considered that the boiling delay time is much longer than the condensation and liquid return times. The boiling delay time is defined as the time required for the subcooled liquid to be heated to saturation temperature. As shown in [156], it can be expressed by the following equation,

$$t_{bd} = \frac{\rho_l C p_l \Delta T_{sub} A_{xs} L_{HS}}{q''} \tag{2.2}$$

where ρ_l is the density of the subcooled liquid; Cp_l the heat capacity; ΔT_{sub} the subcooling temperature difference of the liquid; A_{xs} the cross section; L_{HS} the length of the heated section; and q'' the heat per unit area.

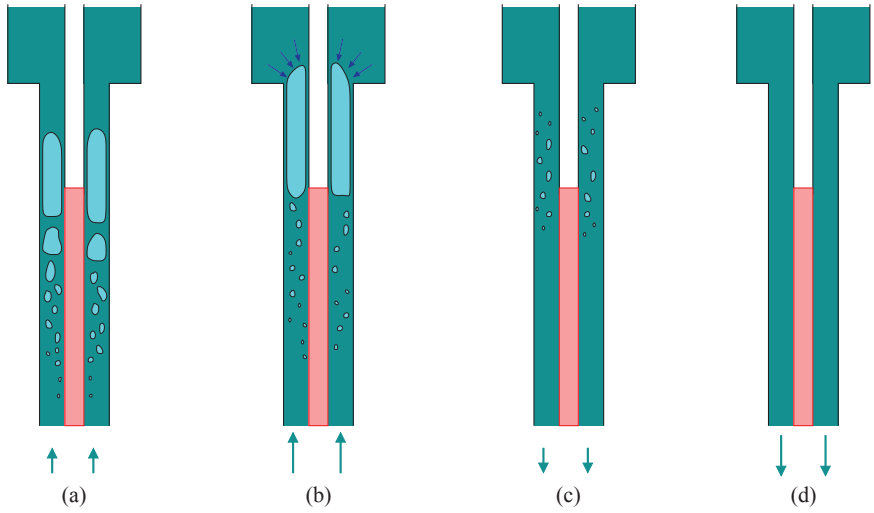

Figure 2.5: *Mechanism of geysering [12]. (a) Boiling starts in the heated section and a large slug of bubbles is formed. As the hydrostatic head decrease the flow gets accelerated. (b) when the large slug of bubbles reach the subcooled liquid in the outlet plenum, it gets condensed. (c) as an effect of the condensation the void decrease and the flow decelerates. As the hydrostatic head the flow change the direction from the outlet plenum to the heated section. (d) the system turns into a subcooled liquid state. The liquid is heated in the bottom part, so it turns again the direction and the process repeats from (a).*

2.2.7 Natural boiling oscillation, (NBO)

J.H. Chiang et al. (1993) described a new kind of flow instabilities in natural convection systems called *natural circulation instability*. This phenomenon is caused by the accumulation of vapor downstream from the heated section. The main mechanism occurring during this transient phenomenon is described as:

(a) Under conditions of low vaporisation rate, the vapor accumulates in a non-heated section downstream from the heated section (in [33] the vapor accumulates in the pipes connecting the outlet plenum with the separation tank). As a consequence, the hydrostatic head decreases and the circulation rate increases.

(b) As a consequence of the flow rate increase, the accumulated vapor flows out and water fills the non-heated section. Thus, the hydrostatic head increases again and the circulating rate decreases. It repeats from (a).

This phenomenon is characterised by about 180 degrees shift between the flow rate and the pressure drop oscillation in the region where the vapor accumulates (between the outlet plenum and the separator). The period of *natural circulation oscillation* is much longer than the corresponding to the transit time of a fluid particle (*density wave*).

2.2.8 Thermo-acoustic oscillations (TAO)

This phenomenon has received very little attention in the last 50 years. According to [20], one of the first survey regarding the occurrence of acoustic phenomena in boiling systems was presented by H. Firstenberg et al. (1960) under the title “Boiling songs and mechanical vibrations”. This last term was used in reference to the high frequency sounds (1000-10000 Hz) occurring in boiling systems under boiling conditions. These sounds are mostly produced by bubbles collapse and depend on the subcooling temperature and heat flux. On the other hand, the terms *acoustic oscillation* or *thermo-acoustic oscillations* (TAO) are used in reference to a lower frequency phenomenon (5-100 Hz). According to H.F. Smirnov et al. (1997), the main mechanism triggering this kind of instability is the acoustic resonance of the vapor-liquid media at the existence of a forced oscillation source. The resonance occurs when the frequency of the vaporisation centres coincides with the natural acoustic frequencies of the vapour-liquid flows, which depends on the pressure, flow patterns, channel geometry and the boundary conditions (open-end, closed-end, U-shape tube or valves).

As this phenomenon is not further treated in this work but it can affect the stability of other instabilities, a brief description of the main works that have investigated it are described in this section. A.J. Cornelius [39] (1965) presented one of the first systematic studies describing the occurrence of *thermo-acoustic oscillations* in forced and natural convection systems. In this investigation, a closed loop using freon-114 is used to study flow instabilities in supercritical conditions. *Thermo-acoustic oscillations* and what seems to be DWO_I and geysering phenomena are reported. It is necessary to remark that in some cases the *thermo-acoustic oscillations* are observed at the same time with the other two phenomena (*geysering*, DWO_I). Nevertheless, the interaction between this high frequency phenomena and the other oscillatory phenomena is not investigated. Acoustic oscillations of around 10 Hz are observed during boiling heat transfer studies in [72]. This phenomenon seems to be caused by small bubbles that appear to "blink" (i.e., rapidly collapse and then expand) in the high-speed photographs system. A. Bergles et al. (1967) described some experimental results in a boiler under subcritical conditions. Water is used as a refrigerant and the reported oscillation frequencies are higher than 35 Hz. The setup boundary conditions are not closed-end or open-end but valves are used and it seems to influence the period of the oscillation with respect to the theoretical one.

The oscillatory behaviour encountered during heat transfer to a fluid appears to be similar, regardless of whether the fluid is at a subcritical or supercritical pressure. Several investigations report the occurrence of thermo-acoustic oscillations in supercritical systems using helium, hydrogen, nitrogen and other fluids, [230, 50, 109, 58]. In the studies [205, 55], this phenomenon is reported in a cryogenic boiler using dense hydrogen as a fluid. A non-dimensional analysis is presented in order to understand the similarity of the phenomena occurring in other systems. According to this investigations the *thermo-acoustic* phenomenon is excited by film oscillations.

E. Steward et al. [195] studied this phenomenon in a supercritical pressured wa-

ter system. High frequency audio oscillations (500-2000 Hz) and *thermo-acoustic oscillations* are reported. The modes of oscillation are identified as Helmholtz and open-open pipe resonance. During almost 30 years, very few investigations analysed this phenomenon. H.F. Smirnov et al. (1997) presented one of the most complete studies in the field. Several test sections with different shapes and sizes are used. The main mechanism explained in the previous parragraphs was proposed in this last study. Nevertheless, it is still not clear if this phenomenon is the result of the bubbles collapse or the interaction with microscopic instabilities in the boiling film, as described for supercritical fluids.

2.2.9 Instabilities in Condensing flows

At least 12 different phenomena have been explained in the previous sections for boiling systems. However, very few research has been done regarding the study of two-phase flow instabilities in condensing flows. As suggested in [43], the microscopic and macroscopic particular characteristics of condensing systems are completely different than those triggering the physical mechanisms described for boiling systems.

One of the pioneer studies on instabilities in condensing flow was carried out by W.H. Westendorf and W.F. Brown [217] (1966). In this work, three different stability regions are reported, as shown in Figure 2.6. In addition, two different oscillatory phenomena are described. One corresponding with high frequencies (50-200 Hz) and the other with frequencies between 1 and 10 Hz. The main explanation for the first phenomenon is the occurrence of acoustic resonance, similar to the *thermo-acoustic* instability described in Section 2.2.8. As shown in this last work, the mechanism triggering the low frequency phenomenon do not fulfil the required characteristics of *density wave* or *pressure drop* oscillations. In [186, 185] a transparent channels array is used in order to investigate flow patterns, stability and gravity effects. Several different microscopic phenomena associated with the liquid film behaviour produce pressure and flow oscillations.

2.2.9.1 Self-sustained oscillations

A low frequency phenomenon ($\approx$ 1-20 Hz), similar to the one described in [217], was investigated by B.L. Bhatt and G.L. Wedekind [23] (1980). In this last study the mechanism triggering the oscillation is explained as the dynamic energy exchange between the vapor compressibility upstream from the cooled channel and the inertia of the subcooled liquid. Under this kind of phenomenon, the system evolves in a limit cycle oscillation. The time period of the oscillations is lower than the corresponding to the DWO_{II}. B.D. Boyer et al. (1995) described the occurrence of a similar phenomenon in a vertical annular channel. The main parameters affecting the oscillations are heat transfer, vapor-liquid density ratio, vapor compressibility, downstream liquid inertia, upstream vapor, upstream and downstream throttling. Even when this phenomenon is associated with a compressible volume upstream from the test section, it is still not clear if it is related with the mechanism triggering *pressure drop oscillations* in boiling systems. In [24] a brief experimental analysis suggests, without being totally conclusive, that this phenomenon is particular

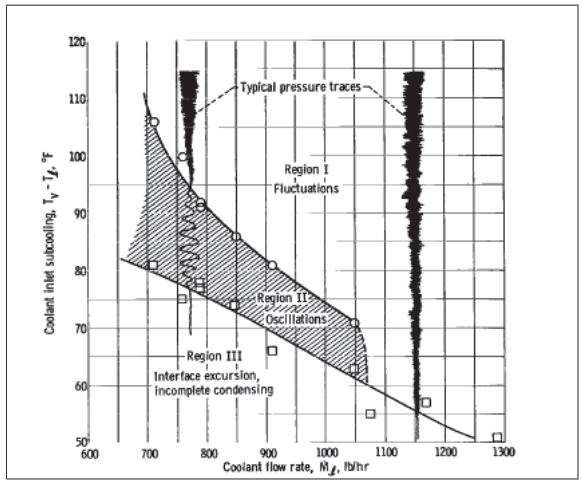

Figure 2.6: *Stability map for a condensing system, presented in [217].*

of condensing systems. As described in Section 2.2.1.5, a necessary condition for the occurrence of PDO is the negative slope of the characteristic pressure drop vs. flow rate curve. The characteristic curve for condensing systems is described in the following section.

2.2.9.2 Characteristic pressure drop vs. flow rate curve for condensing systems

In Figure 2.7 the static characteristic pressure drop vs. flow rate curve for a downward condensing case is shown. In contrast with the boiling case, in the condensing systems the friction pressure drop curve has not a negative slope region. This effect can be easily understood by analysing the limit cases of *all vapor* and *all liquid* as presented in Figure 2.1. Thus in accordance with Figure 2.7, the only term that can destabilise the system (negative slope) is the momentum term. It is necessary to remark that the effect of the momentum term will be important only for low non-dimensional friction numbers, Λ[1] [87]. In addition, when condensing takes place in an upward system then the slope of the potential pressure drop term will be negative, especially for low flow rates. In conclusion, condensing systems are, in theory, also able to experiment instabilities related to the negative region of the pressure drop vs. flow rate characteristic curve (e.g. Ledinegg, flow re-distribution instability, PDO). J. M. Delhaye et al. (1981) refers to this problem stating that the acceleration pressure drop may be destabilising for condensing flow in tubes.

[1] $\left(\Lambda = f_{tp}\frac{L}{D_H}\right)$

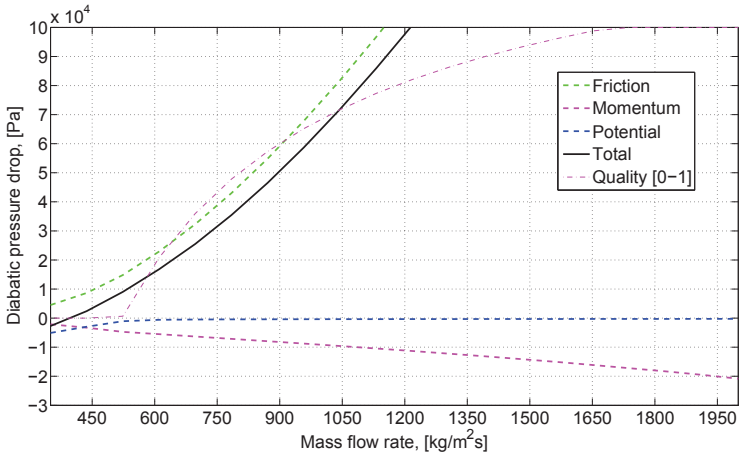

Figure 2.7: *Decomposition of the different pressure drop components of the pressure drop vs. flow rate characteristic curve of a downward flow condensing system.*

2.2.9.3 Oscillations in parallel condensing channels

Very few studies analyse the occurrence of macroscopic instabilities in condensing systems. Following the investigations describing *self-sustained oscillations* in single channels, C.J. Kobus and B.L. Bhatt (2001) investigated this phenomenon in a parallel channels system. The same kind of low frequency oscillations associated with the inertia of the subcooled liquid and the compressibility upstream the cooled section are reported. Similarly to the phenomenon described for single channels, the primary physical parameters responsible for this particular type of unstable behaviour include the condenser heat flux, downstream inertia of the subcooled liquid, compressibility in the upstream vapor volume, flow resistance and liquid-vapor density ratio, being this last one the primary physical parameter responsible for the amplitude of the oscillations. An analytical model representing these parameters is also described in this last investigation and the results agree well with the experimental data.

2.3 Other types of two-phase transient phenomena

In this section a brief description of other phenomena affecting two-phase flow systems is presented.

2.3.1 Water-hammer phenomena

Modern hydraulic systems operate over a broad range of working regimes. Any sudden change can induce a pressure wave, that in some cases can exceed several times the normal pressure level, and cause breakages in pipelines, valves or other

components. W. Yow et al. (1988) noted three basic types of severe water hammer occurring at industrial plants that can result in significant damages. They are:

- Rapid valve operation events: when a sudden change occurs in any hydraulic system, a pressure wave is generated and it can produce damages in valves, pipes or other components. M.S. Guidaoui et al. [75] present a review on the experimental and modelling research on water hammer phenomenon. Most of the phenomena reported in this last work correspond to single-phase components.

- Water-slug induced events: when slugs of liquids (accelerated by a high flow of gas) collapse or crash with the pipe walls, then a pressure wave is generated within the gas. A. Bergant et al. [19] review the water-hammer studies reported in several two-phase flow systems.

- Condensation-induced events: The fast collapse of gas can produce, under some conditions, pressure waves of high amplitudes. Moon-Hyun Chun and Seon-Oh Yu [34] analyse the condensation-induced water hammer phenomenon. They found that condensation-induced water hammer events were responsible of about 34 % of the 283 events compiled by [211]. Four different kinds of phenomena are classified in [232]: (1) steam and water counter-flow in a horizontal pipe; (2) subcooled water with condensing steam in a vertical pipe (water cannon); (3) pressurised water entering a vertical, steam-filled pipe; and (4) hot water entering a lower pressure line.

2.3.2 Flow-induced instabilities

These phenomena are one of the major problems in several industrial components. Flow-induced vibration is an important concern for the designers of heat exchangers subjected to high flows of gases or liquids. Two-phase cross-flow occurs in industrial heat exchangers, such as nuclear steam generators, condensers, boilers, etc. Under certain flow regimes and fluid velocities, the fluid forces result in tube vibration and damage due to fretting and fatigue. It is known that four mechanisms are responsible for the excitation of tube arrays in cross-flow [161]. These mechanisms are: (1) turbulence buffeting; (2) vortex shedding; (3) acoustic resonance; and (4) fluid-elastic instability. The latter is proved to be the most damaging in two-phase components [56]. M.J. Pettigrew et al. [161] (1991) presented a review of all these phenomena occurring in industrial systems. Moreover, a complete review regarding the occurrence of fluid-elastic instabilities can be found in S. Khushnood et al. [106] (2004).

2.4 Experimental investigations

In this section a description of some of the most important experimental studies describing several two-phase flow instabilities is presented. However, only the phenomena considered in the scope of this work (LED, PDO and DWO) are described with detail.

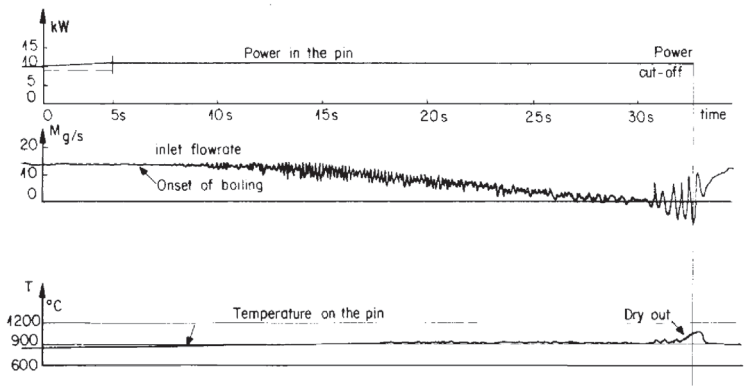

Figure 2.8: *Flow excursion in a sodium boiling system, [181] (taken from [40]).*

2.4.1 Ledinegg or flow excursion

Although there are several articles describing experimentally the characteristic pressure drop vs. flow rate curve or the Onset of Flow Instability (OFI) [183, 188, 238], there are only a few articles analysing experimentally the occurrence of flow excursion phenomenon in two-phase systems. In Figure 2.8 an experimental case of flow excursion is shown [40, 181]. This transient evolution occurred in a Liquid Metal Fast Breeder Reactor (LMFBR) using sodium as refrigerant fluid after the coast-down of the main pump. The total time of the transition is in the order of 30 [sec]. In the last part of this flow excursion dryout is induced and consequently the wall temperature increases. Moreover, what seems to be *density wave* oscillations can be observed. S.Y. Jiang et al. [94] (2000) describe the occurrence of flow excursion transients in a natural circulation loop (HRTL-5). The reported evolution is a slow and long-term process in which both the mass flow rate and the inlet temperature of the heated section decrease while the exit temperature increases. In addition, *density wave* oscillations are reported in the process of the static flow excursion. X.T. Yang et al. [229] (2005) studied the flow excursion phenomena in the same system described above. In contrast with the forced convection systems, in natural convection it is proved that under some conditions it could be a multivalued operation region. It means that for a given mass flow rate, it is possible to find several total pressure drop that satisfy the steady-state operation point condition.

More recently, Z. Tao et al. [203] studied experimentally the flow excursion phenomena in a narrow rectangular channel using a natural convection loop. Before and during the flow excursion oscillations, DWO_{II} are reported. During this transient, the flow pattern regime change has an important effect on the evolution of the system. It is proved that the effect of narrow channels plays a significant role promoting flow excursion.

2.4.1.1 Flow distribution instability

There are several studies reporting flow distribution problems in two-phase flow systems. As described in the case of Figure 2.8, most of the times the occurrence of this phenomenon in industrial systems triggers the dryout and it may provoke burnout. In [129], flow excursion and flow mal-distribution are reported in a preheater used to recover heat from ammonia plants. K. Akagawa and T. Sakaguchi [3] (1971) presented one of the most complete investigation in the field. In a loop using freon-113, long parallel channels (approximately 40 [m] long) are used to study several two-phase flow instabilities. The circular heater tubes, of 4 [mm] internal diameter, are electrically heated. Flow mal-distribution, due to negative slope of the characteristic curve is observed. Furthermore, flow excursion between the different channels is also reported. PDO and DWO modes are briefly described. They established a graphical stability criterion for the flow-distribution instability in parallel channels using ΔP vs. G curves. In [153] an air/water experimental system is used to study flow distribution and pressure drop oscillations in twin parallel channels. The reported flow distribution and the PDO are proved to be of similar characteristics than those observed in boiling channels.

In recent years due to the use of direct steam generation (DSG) for solar heating, some investigations have been carried out in order to understand the flow distribution instability in those kind of systems. In [206] the splitting of a two-phase air/water mixture in a system of two parallel channels with a common feed and a common exit is investigated experimentally. Several parameter maps showing the symmetric and asymmetric flow splitting in the heated channels are described. The results show that at low flow rates and in inclined channels the flow is not symmetric. Similarly, Y. Taitel et al. [200] (2003) use four parallel channels in an inclined array with a mixture of air/water to study distribution phenomena. It is found that for low liquid and gas flow rates the two-phase mixture prefers to flow in a single channel, while stagnant liquid fills part of the other three channels. As the flow rates of liquid and gas increase, flow in two, three and eventually in four channels takes place. U. Minzer et al. [140] (2004) presented the experimental results of a boiling system where the flow splits in two parallel channels using water at atmospheric pressure. They prove that, in the zone of multiple stable solutions, all possible solutions are practically obtained and the actual solution depends on the direction leading to the steady state (hysteresis phenomenon). In [16] similar results are obtained for a four parallel channel boiling system. More recently in [220], a parallel array of two upward vertical channels using supercritical water is studied. Flow distribution between the channels is reported in connection with other oscillatory phenomena, (DWO_{II}).

2.4.2 Pressure drop oscillations

R.S. Daleas and A.E. Bergles [41] (1965) report that the Ledinegg-type instability interacted with the upstream compressibility volume to cause oscillations triggering the premature CHF (Critical Heat Flux) in a boiling section. The term *pressure drop oscillation* was given by A.H. Stenning [189] (1964). In this last work DWO_{II} and PDO are reported in a subcooled boiling horizontal channel using freon-11 as

refrigerant [190, 193]. Several steady-state pressure drop vs. flow characteristic curves are shown. Moreover the dynamic evolution of the PDO mode is plotted together with the steady-state characteristic curves. Similar plots to the curves shown in Figure 2.4 are presented. The influence of different compressible volumes, upstream of the heated section, on the amplitude of the oscillation is studied. In some of the experimental cases, DWO_{II} are observed in interaction with the PDO mode. Another fundamental investigation about PDO corresponds to J.S. Maulbetsch and P. Griffith [133, 134, 135]. In these studies PDO and DWO_{II} modes are experimentally investigated. A very controversial conclusion is presented, stating that: "In cases of very long test sections (L/D > 150), there can be sufficient compressibility inherent in the test section itself due to vapour generation to initiate this type of instability.". There is sufficient experimental evidence to prove that this conclusion is not well supported, since no other work in the field reported this effect. Furthermore, there are several experimental cases in which the ratio L/D is higher than 150 and do not report self-sustained oscillatory phenomena without a compressible volume. A clear example is the investigation presented in [3], where L/D = 10000 and the occurrence of PDO modes are not observed. In addition, it should be noted that the characteristics of the DWO phenomena were not known at that time, and these two phenomena could be confused. In [100, 101] a vertical four parallel channels test section is used to investigate PDO and DWO during boiling conditions. Cross-connection between the channels is investigated, proving to stabilise the PDO mode. Moreover, the use of cross-connection reduce significantly the period of the oscillations.

M. Ozawa et al. [155] (1979) reported some experimental results regarding the occurrence of PDO mode in a freon-113 vertical channel. High amplitude DWO_{II} are reported in some parts of the PDO cycle. Another interesting investigation was presented by M. Ozawa et al. [154] (1979), reporting PDO in an air/water system. Oscillations with time periods between 200 and 300 [sec] are observed. During the oscillations, due to the capillarity of the tubes, flow pattern changes between slug and bubbly flow are reported. In addition, high frequency oscillations are also reported when the flow is decreasing (bubbly flow). In the same manner as for boiling systems, the oscillations occur when the hypothetical equilibrium point is in the negative slope region of the static characteristic curve of the pressure drop and flow. Years later, M. Ozawa et al. [153] (1989) studied PDO in a parallel array using a mixture of air/water. Three different modes were observed: In-phase mode, all the channels oscillate with the same frequency; U-tube mode, the gas flow and the liquid flow oscillate 180^o out of phase in the two channels; Multi-mode, the gas flow in each channel oscillates independently (i.e. the oscillation period in each channel differs from the others).

A. Mentes et al. [138] (1983) investigate the effect of different heater surface configurations on two-phase flow instabilities. A single channel, forced convection, open loop, up-flow system using freon-11 and six different heater tubes with several inside surface configurations are tested. Heat transfer coefficients change during the oscillations and among the tubes up to 90 %. In addition, changes in the oscillation periods are also observed. For the DWO mode every tube has similar periods, but for the PDO mode there is a great difference among the tubes, although the amount of

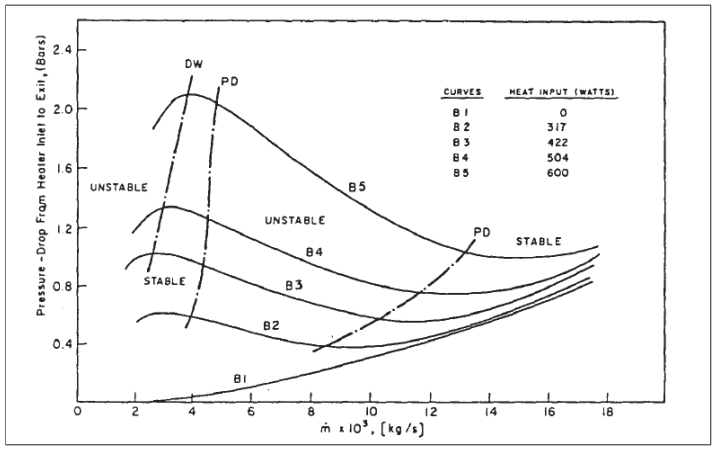

Figure 2.9: *Characteristic pressure drop vs. flow curves and the stability boundaries of DWO_{II} and PDO modes [235].*

air in the surge tank remained constant. In the same year, T. Dogan et al. [51] (1983) used an upflow forced convection loop with freon-11 to study PDO. Experimental steady-state characteristic pressure drop vs. flow curves ($\Delta P\ vs.\ G$) are obtained. PDO and DWO_{II} are reported as pure phenomena and also the interaction between these two modes is reported. In addition the stable and unstable regions are shown in the characteristic pressure drop vs. flow curves. Similar to the experimental setup described before, in [234, 235] a horizontal boiling channel is used. In all the experimental cases DWO are superimposed to the PDO mode. Several stability maps are reported using the characteristic pressure drop curves as shown in Figure 2.9. In [102, 157] PDO are reported in a vertical channel of similar characteristics to the one described before. The main focus of these studies is the variations of temperature at the outlet of the heated section. Superimposed DWO on the PDO mode are also observed. The same experimental setup is used by H.T. Liu and S. Kakac [121] (1991) in a very interesting investigation. This is the first study analysing the superimposed DWO on the PDO mode. The density wave mode take place in the lower mass flow rate region of the characteristic pressure drop vs. flow curve (higher qualities). The superimposed DWO are observed for different inlet temperatures and power conditions. Nevertheless, no systematic conclusion of how the DWO mode influence the frequency and amplitude of the PDO mode is reported.

Y. Ding et al. [49] (1995) presents a complete parameter analysis. The effects of mass flux rate and inlet temperature on the time period and amplitude of the oscillations, both PDO and DWO modes, are investigated. Under the DWO mode *thermal oscillations* are observed. It is also proved that the DWO mode can take place in the negative slope region of the characteristic curve, in contrast with the vertical cases where this mode is reported in the positive slope region, as indicated in Figure 2.9. In addition, the chaotic position of the two-phase/over-heated vapour boundary is investigated in relation with the occurrence of the *thermal oscillation* phenomena. As reported in [216], under some conditions the motion of this point

can be highly chaotic.

M. Xiao et al. [219] (1993) reported the occurrence of DWO_I, DWO_{II} and PDO using two vertical parallel channels and water as refrigerant. In this study the DWO_I mode is called 2^{nd} DWO. In some cases, the PDO are reported to occur without surge tank due to the parallel array condition. In addition, flow reversal is observed in each of the channels and superimposed DWO occurs during the PDO mode. Even though this is one of the most interesting experiments, due to its conditions, no further information about the PDO mode is reported. In [166] an interesting investigation reported pressure drop oscillations in a downward vertical tube, in order to analyse the occurrence of these phenomena related to the monolithic reactors. The main focus of this study is the modelization of the system as be described in the next sections.

Another interesting study was presented in L. Guo et al. [78], where PDO are studied in a forced convection loop with water and a helical heated section at a medium pressure (@ 30 [bar]). In this investigation the compressible gas volume positions, non-uniform heat flux distributions and various helix-axis inclinations are studied. For a given set of parameters, the existence of a critical compressible volume is experimentally proved. Moreover, it is also proved that moving the surge tank upstream (farther from the test section) increases notably the stability of the system. When the surge tank is placed right before the test section, the non-uniform heat flux distribution has not significant effect on the stability of the system. On the other hand, when the the surge tank is farther form the test section the non-uniform heat flux distribution influences the stability limits. Finally, the helix-axis inclination has not significant influence in the occurrence of PDO. L. Guo et al. [79] use the same experimental system to study the heat transfer properties of the system under pressure drop oscillations. As a result of the PDO, the transient local heat transfer coefficient oscillates with a reverse phase characteristics (respect to the flow rate) and it shows an asymmetrical and non-uniform feature.

In [152] the influence of mass flow rate and inlet temperature on the stability of PDO and DWO phenomena are analysed. Using the same system, S. Karsli et al. [104] studied the effect of heat transfer enhancement in the stability of different instabilities modes: PDO, DWO and ThO (Thermal Oscillations). The heat transfer is modified by using five tubes with different characteristics and different pitch. The unstable region for PDO is larger for tubes with enhanced surfaces than for the bare tube. Periods and amplitudes of pressure-drop type oscillations and density-wave type oscillations change depending on the heater tube configurations. The same system and same experimental results are presented in [231].

S. Kakac and Liping Cao [98] (2009) studied *pressure drop* and thermal oscillations in vertical and horizontal channels. Even though this investigation is related to the modelling of those instability modes, several experimental data are presented. Density wave oscillations are observed in interaction with PDO and ThO modes.

2.4.3 Density wave instabilities

Density wave instabilities have been the most studied phenomena in the literature. As presented in Section 2.2.2 there are three main types of *density wave*

instabilities according to the mechanism that induce the instability. Historically, only the phenomenon classified as DWO_{II}, induced by friction terms, has been normally considered as *density wave* oscillations. Even when the distinction between these phenomena was introduced by K. Fukuda and T. Kobori (1979), it took several years until this classification was adopted by the researchers. In this section, the experimental investigations for the *density wave* modes are described.

As mentioned in [97] several articles reported oscillations in subcooled single and parallel systems during the 50's [182, 213]. Nevertheless, it is not until the middle 60's that this kind of phenomena started to be systematically investigated. F.A. Jeglic and K.T Yang [91] (1965) study the incipience of flow oscillations in a boiling single vertical channel. A transparent test section is used in order to study visually the flow patterns during the unstable phenomena. Flow excursions with associated burning of the system and superimposed DWO_{II} are reported. Two different kinds of test section are used: an electrically heated test sections (Iconel); and a porous wall transparent test section. In this last case, the injection of air or steam is used to simulate the oscillatory phenomenon of diabatic systems in an adiabatic condition. When steam is injected, the system behaves in the same manner as in the diabatic case (metallic test section). On the contrary when air is injected, no oscillatory phenomena are reported. A.H. Stenning and T.N. Veziroglu [192] (1967) used an air/water system to study in a controlled manner the occurrence of DWO_{II} phenomenon. It is proved that the oscillation also takes place in adiabatic systems (air/water). Stability maps of the density ratio vs. normalised pressure drop are presented.

A.H. Stenning et al. [193] (1967) used a forced convection single boiling channel with freon-11 and water as working fluids. Three different kind of instabilities are described, they are called type I, II, III, corresponding respectively with PDO, DWO and ThO instabilities. DWO_{II} oscillations are associated with the dryout condition at the outlet of the test section. In addition, the interaction of PDO and DWO_{II} modes are reported in most of the cases. In a similar way it is proved that the ThO mode is triggered by the occurrence of the higher frequency phenomena (DWO_{II}), as explained in Section 2.2.5. Static characteristic curves are obtained and the PDO evolution, with superimposed DWO, are shown on these curves. It is proved that the increase in the inlet throttling stabilise the system. On the other hand, the high stabilising effect of the liquid-vapor ratio is observed. Low pressure (higher liquid-vapour ratio) destabilises the system. Furthermore, a high decrease of the boiling heat transfer during the oscillations is reported. Even though some stability maps of mass flow rate vs. subcooled temperature are shown, no significant conclusion about the stability limits prediction is presented. Most of the results of this investigation are the extension of the studies presented in [190, 191].

F.J.M. Dijkman et al. [48] (1967) investigate these phenomena in a loop using water under natural and forced convection. In accordance to the described oscillations and the characteristics of the system, it is possible to conclude that the phenomenon reported is DWO_{II}. It is proved that the forced convection mode is more stable than the natural convection mode. The study is focused on the experimental description of the transfer functions in order to characterise the dynamic of the

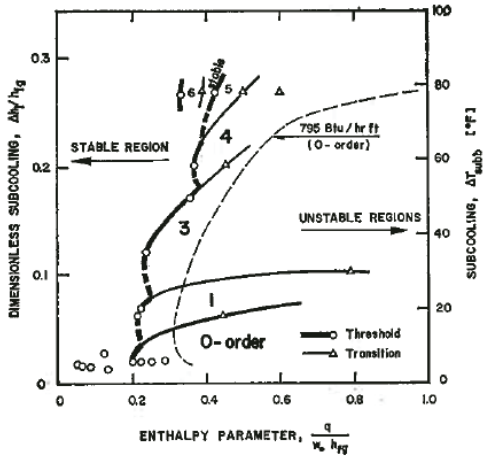

Figure 2.10: *Stability map for different density wave oscillations modes, printed from [225].*

system (power → inlet mass flow rate; power → void fraction). In a similar manner, R.G. Dorsh [52] use a forced convection loop with freon-113 to evaluate the frequency response functions (impedance maps) to forced oscillations in order to evaluate the dynamic of the boiler system. Moreover, R.P. Mathisen [130] presents a study in a natural parallel channel system using water as working fluid. A very complete steady-state characterisation of the power vs. flow rate curve is presented. Burnout of some of the channels is reported in association with the starting of flow oscillations. The effects of pressure, subcooling and exit throttling are analysed for a single channel. In reference to the two-parallel channels analysis, it is observed a 180^o shift (out-phase) between the channels flow when DWO_{II} occurs. The parallel system configuration results more unstable than the single channel configuration.

One of the most discussed studies regarding *density wave* phenomena is presented by G. Yadigaroglu and A. Bergles [224] (1969). They use a boiling, single channel, upward system with freon-13 to study stability regions. High-order modes (DWO_{III}) are reported in interaction with the normal mode (DWO_{II}). The stability limits are plotted as a function of the enthalpy parameter vs. a dimensionless subcooling, as show in Figure 2.10. In this figure the limits for the higher frequencies modes corresponding to the DWO_{III} are shown.

D.B. Collins and M. Gacesa [37] (1969) performed an experimental programme to investigate parallel-channel instabilities in a full-scale simulated nuclear reactor channel operating in vertical, high-pressure, upward conditions and using water as refrigerant. In this investigation two 19-rod electrically heated bundles are connected in parallel with an unheated by-pass between a common inlet and an outlet headers. Two different kinds of phenomena are reported. A high frequency random oscillation, associated probably with the mechanism explained for TAO (thermoacoustic oscillations) (28 Hz) and *density wave oscillations* with high quality conditions (DWO_{II}). During this last oscillations mode, a low frequency modulation,

or what the authors identify as beating, is reported. The frequency of this beating is not constant, indicating that it is produced for two oscillations of similar frequencies more than as an independent phenomenon. Moreover when the power is increased the amplitude of the oscillations grows and the beating phenomenon becomes less significant. Regarding the occurrence of oscillations in parallel channels, T.N. Veziroglu and S.S. Lee [212] (1971) study two cross connected parallel channels. It is shown that the cross-connection makes the system more stable. In addition, without the cross-connection the oscillation has a shift of 180^{o} in the inlet flow, while instead, when the cross-connection is used the oscillations between the two channels are in-phase.

In [131, 132] a vertical upward closed loop is used under forced and natural convection. One of the particularities of this study is the use of n-pentane as a refrigerant. These are one of the first investigations reporting DWO_{I} (low quality). Moreover, even though this kind of phenomena is normally associated with natural convection systems, the oscillatory phenomenon is observed for both forced and natural convection. When forced convection is used, a reduction of the unstable region is observed. Moreover, a photographic study of the flow pattern during the oscillations is shown and flow pattern changes during the oscillation are reported. In [109] the stability of a heated channel using nitrogen is investigated. Thermoacoustic oscillations (TAO) are found and the DWO mode is proved to be stable. Moreover, J.C. Friedly [58] (1976) investigated DWO in a similar experimental system, reporting DWO in interaction with TAO. In this last case the nitrogen was subcooled at a fixed temperature and pressure drop was dominated by the pressure drops in the inlet an outlet restrictions.

P. Saha [175] (1974) presents an experimental investigation of DWO_{II} phenomenon in a forced convection loop using freon-113. One of the advantages of using the freon-xx refrigerant family is that under the unstable conditions it is more difficult to trigger the channels burnout. In this last work, a fixed pressure drop boundary condition is imposed to the heated section by using a parallel by-pass branch with a known single phase pressure drop valve. Some of the plots show back-flow due to this parallel configuration. Oscillations of pressure and flow are reported, however no information on the temperature evolution is presented. One of the features of this investigation is to report the stability limits using the N_{Zu} vs. N_{sub} stability maps [240]. Moreover, the effects of inlet-outlet restrictions and system pressure are analysed. As explained before, it is found that an increase in the inlet restriction stabilises the system while an increase in the outlet restriction destabilises it. In addition, the system is proved to be completely stable to the high-order mode (DWO_{III}). The results presented in this experimental investigation are the extension of the studies published in [176, 177]. K. Fukuda and T. Kobori [61] (1979) use an upward double channel ([60]) to study DWO_{I} and DWO_{II} phenomena. Both phenomena are reported in forced and natural circulation. A model of the mechanisms involved in the occurrence of these two phenomena is proposed. A cross-sectional valve is used to mix the flows at the exit the channels before the risers (one for each channel). When the valve is open, the system behaves in a more stable manner, showing that cross-connections at the outlet stabilise the system.

H.C. Ünal et al. [210] (1977) studied DWO_{II} in an industrial upward steam-

generator heated by sodium flowing downward inside an array of 139 tubes. The temperature at any point in a cross-section in the superheated steam region of such a steam-generator tube oscillates irregularly owing to thermodynamic non-equilibrium between the phases. A correlation for the oscillation periods is presented and these periods are proved to be between one and two times the transit period as described in other investigations. Moreover in [208, 207, 209], the same authors analysed this phenomenon in a controlled experimental setup. DWO_{II} phenomenon is investigated in forced and natural convection using water as a refrigerant. Single, parallel and a helicoidal test sections are used. The different test sections are heated through a counter-current stream of sodium in order to fulfil the conditions in steam-generators. In all the cases are used long heaters, with L/D between 1272 and 2468. It is found that the steam quality at the outlet of the tube at the inception of the DWO is practically only a function of pressure for a given inlet throttling, whereas the effect of all the other operating conditions on this steam quality are of secondary importance. In addition, for once-through steam-generator tubes of L/D > 4100, the effect of inlet throttling on the outlet steam quality at the inception conditions of the DWO disappears. This last fact seems to be related with the hypothesis discussed above, for the PDO phenomenon [133], that for high L/D ratios the oscillations are independent of the inlet throttling.

A very interesting investigation was carried out by D.E. Daney et al. [42] (1979). In this work, DWO_{II} are studied in a long test section (L = 185 m) using supercritical helium as a working fluid in order to simulate the conditions of superconducting power transmission lines. In this system the L/D ratio corresponds to 46000. The growing of the enthalpy waves under unstable conditions is reported and analysed. DWO_{II} with a time period of several minutes are described. Moreover, the vapour-liquid density ratio is proved to be important in the system stability. The time period is found to coincide with two times the transit time. Another interesting problem to take into account was described by R.P. Roy et al. [172] (1988), where a closed forced loop with freon-113 at low-pressure and an annular test section are used to study these phenomena. Multiple instability frequencies (DWO_{III}) are detected in the experiments although a dominant frequency is always found (DWO_{II}). The cumulative amount of energy associated with the non-dominant frequencies is not trivial, amounting typically to about one-third of the total flow oscillation energy. Should also be remarked that due to the big hydraulic diameter (annular test section) the momentum terms could influence inducing DWO_{III}, as described in Section 2.2.2.3. R.C. Yang et al. [228] (1988) reported a phenomenon identified as a DWO in a vertical U-tube evaporator using Freon-12 as working medium. The experiments show that flow oscillations in the vertical U-tube evaporator may lead to serious heat transfer deterioration and it results in large temperature excursions at the tube wall.

M. Aritomi et al. [11] (1992) presented an investigation of the thermo-hydraulics phenomena during start-up in a natural circulation boiling water reactors (BWR). Geysering, natural boiling oscillation and density wave instability (DWO_{II}) are reported. The driving mechanisms of the geysering and the natural circulation instability are discussed using the experimental results. DWO_{II} are observed at high heat flux, but the main focus is taken for the GES and NBO phenomena. In [44] oscil-

lations in a natural convection loop using water as refrigerant are presented. In this last work, the chaotic nature of the experimental phase trajectories of the DWO_{II} are analysed. Several phase diagrams showing the evolution of the oscillations are shown. H.T. Liu et al. [122] (1994) analysed the characteristics of transition boiling and thermal oscillations (ThO) in a single-channel, forced convection, upflow system using freon-22. As commented above, the ThO mode is triggered by the *density wave* oscillations. Under the unstable hydrodynamic state the storage and exchange of energy from the tube wall to the fluid provokes the oscillations of the nucleate and transition boiling boundaries. As a consequence, oscillations in the wall temperature are induced. In this last work the wall capacity and the axial conduction are proved to have a high influence on the thermal oscillations. In a similar manner, Q. Wang et al. [215] (1994) studied DWO_{II} in a single-channel, high-pressure forced convection, boiling system. The effects of the system pressure, inlet subcooling, mass flow rate and exit throttling are investigated. All the conclusions agree with the results discussed in previous studies. In [104] the effects of heat transfer enhanced tubes on PDO and DWO are analysed. Even though this work is more focus on PDO, it is proved that the use of different heat transfer enhancement tubes has an influence on the amplitude and period of the DWO_{II} phenomenon. In all the cases the enhanced tubes give higher amplitudes and smaller period oscillations than the bare tube.

In the last years, the study of natural convection systems received a lot of attention. J.M. Kim and S.Y Lee [107] (2000) analyse the different interacting modes induced in a natural circulation loop with an expansion tank. Geysering, DWO_{I}, Natural boiling oscillation, DWO_{II} and PDO are reported. Moreover, since several phenomena occur at the same time it is not clear how the different phenomena interact with each other. Several experimental stability maps (heat flux vs. inlet subcooling) are shown and the stability regions for different phenomena are identified. The effect of the outlet resistance is analysed. The region of pressure drop oscillations shrinks down with the increase of friction resistance at the expansion tank line. W.J.M. Kruijf et al. [110] (2004) presented the experimental case of a natural convection system with a complex geometry. Experimental data in the whole operational range is gathered and a N_{Zu} vs. N_{sub} stability map is constructed. In opposition of what is expected, for low subcooling values, the stability of the facility increases as the power is increased to higher values, when keeping the subcooling number constant. Similarly, M. Furuya et al. [64] (2005) studied instabilities in a natural convection experiment simulating the start-up conditions in a BWR. Two types of instabilities are reported: an intermittent oscillation at higher channel inlet subcoolings and sinusoidal oscillation at lower subcoolings. The intermittent and sinusoidal oscillations are suggested to be flashing-induced DWO_{II} (high qualities) and the sinusoidal oscillation simply DWO_{II}. The stability maps (N_{Zu} vs. N_{sub}) for the *flashing phenomena* are plotted. The shape of the stability limits are similar to the ones presented in [110], suggesting that this shape is typical for the flashing-induced DWO phenomenon. These results are described with more detail in [63]. A. Baars and A. Delgado [14] (2006) reported *geysering*, DWO_{I} and DWO_{III} (high-order oscillations) in a natural convection, vertical, boiling loop using water as working fluid. The *density wave* phenomena is reported for low vapour

quality, which are characteristics of type DWO_I. The reported oscillations show a strong correlation between the time period and the travelling time of enthalpy perturbations in the liquid phase of the heated tube. Even when a frequency decomposition of these modes is presented, it is not clear in which parameter region each of the modes will be dominant. No stability maps are reported in this last investigation. In [125, 126] a very complete study on the natural convection instabilities in single and parallel channels is presented. This investigation makes special focus on the study of *geysering* and *flashing* phenomena. In the single channel case, intermittent and sinusoidal oscillations are reported. Both phenomena are identified as *flashing*-induced instability. A wavelet decomposition of the experimental signals are presented, showing for some cases interacting oscillation modes. Several stability maps are presented, the same stability limit shape as described before for *flashing* instabilities are observed. In the case of two parallel channels, similar phenomena as the ones observed for a single channel are identified. In-phase oscillations are reported in the intermittent oscillations region. In addition, out-phase oscillations are reported for higher heat fluxes. Several details of this experimental investigation can be found in C.P. Marcel [127] (2007).

Recently, G. Yun et al. [233] (2010) study these phenomena in twin parallel channels. The influence of system pressure, non-uniform heating and asymmetric entrance throttling is studied. Out-phase and in-phase oscillations corresponding to the DWO_{II} mode in parallel channels are reported. The parallel system is in general more unstable than the single channel case. Non-uniform heating is proved to destabilise the system. This last fact has a large impact on the design of industrial components since normally non-uniform heating conditions are employed. In order to study these phenomena for the refrigeration industry conditions, in [119, 120] a straight horizontal tube using freon-22 is analysed. PDO, ThO and DWO_{II} instabilities are reported. Moreover, several static characteristic curves for different conditions are shown. In the reported results the DWO_{II} mode has the shortest period and the lowest amplitude. Nevertheless, the time acquisition seems to be in the same order of the oscillation period, thus the phenomenon can not be described accurately. The ThO occurs with the longest periods and the highest amplitude among the three modes.

2.4.4 Instabilties in micro- and nano- channels

In the last years several works analysed two-phase flow instabilities in micro- and nano- channels [105, 28, 84, 21, 103]. L. Tadrist [196] (2007) made a literature review with two-phase flow instabilities in narrow channel systems. As these kinds of systems are out of the scope of this work, they will not be discussed further.

2.4.5 Summary of experimental studies

In Table 2.1 a summary of several experimental investigations reporting two-phase flow instabilities is shown.

Table 2.1: *Experimental studies analysing two-phase flow instabilities in boiling systems*

Author	Phenomena	Type	Fluid	Conf.	Ch.	Comments
G.B. Wallis and J. H. Heasley [213] (1961)	DWO_I, DWO_{II}	nat	pentane	upw	2	Three parallel channel oscillation modes are identified
R.S. Daleas and A.E. Bergles [41] (1965)	PDO	forc	water	hor	1	CHF induced by oscillations
A.H. Stenning and T.N. Veziroglu [190] (1965)	ChP, DWO_{II}, PDO, ThO	forc	freon-11	hor	1	Propose a model for PDO. This exp. is used in [189, 191, 193]
F.A. Jeglic and K.T Yang [91] (1965)	LED, DWO_{II}	forc	air/water	upw	1	Transparent sections, porous wall (air injection)
A.J. Cornelius [39] (1965)	TAO, DWO_I, GES	nat/forc	freon-114	hor	1	Supercritical conditions
J.S. Maulbetsch and P. Griffith [133] (1965)	PDO, DWO_{II}	forc	water	hor	1	Influence of the compressible volume
A.H. Stenning and T.N. Veziroglu [192] (1967)	DWO_{II}	forc	air/water	down	1	DWO in an adiabatic system
F.J.M. Dijkman et al. [48] (1967)	DWO_{II}	nat/forc	water	upw	1	Evaluation of transfer functions
R.P. Mathisen [130] (1967)	DWO_{II}	nat	water	upw	2	Very complete parameter analysis
R.G. Dorsh [52] (1967)	DWO_{II}	forc	freon-113	upw	1	Frequency response of the system
G. Yadigaroglu and A. Bergles [224] (1969)	DWO_{II}, DWO_{III}	forc	freon-13	upw	1	High-order modes
D.B. Collins and M. Gacesa [37] (1969)	DWO_{II}, DWO_I	forc	water	upw	2	Bundles with 19 rod heaters
K. Akagawa and T. Sakaguchi [3] (1971)	ChP, FDI, DWO_{II}	forc	freon-113	hor	3	flow distribution mechanisms. L = 40 m (L/D = 10000)
G. Matsui [131] (1971)	DWO_I	forc/nat	n-pentane	upw	1	Forced convection increase stability
P. Saha and N. Zuber [178] (1974)	DWO_{II}	forc	freon-11	upw	1	Stability maps. Parameter analysis (K_{in}, K_{out}, P_{in})
V.S. Krishnan and J.C. Friedly [109] (1974)	TAO, DWO_{II}	forc	nitrogen	hor	1	Stable in the DWO sense

S. Kakac et al. [101] (1977)	DWO_{II}, PDO	forc	freon-113	upw	4	Cross connection between channels
K. Fukuda and T. Kobori [60] (1978)	DWO_I, DWO_{II}	forc/nat	water	vertical	2	DWO_I mechanism model
M. Ozawa et al. [154] (1979)	ChP, PDO	forc	air/water	hor	1	Capillary tubes, flow pattern changes
M. Ozawa et al. [155] (1979)	ChP, DWO_{II}, PDO	forc	freon-113	upw	1	Interacting DWO_{II} and PDO
D.E. Daney et al. [42] (1979)	DWO_{II}	forc	helium	helical	1	L = 185 m helical test section (L/D = 46000)
H.C. Ünal [208] (1981)	DWO_{II}	forc/nat	water	upw	-	Several test sections (helical, parallel, single). Heated with sodium
T. Dogan et al. [51] (1983)	ChP, DWO_{II}, PDO	forc	freon-11	upw	1	Interacting DWO_{II} and PDO
A. Mentes et al. [138] (1983)	DWO_{II}, PDO	forc	freon-11	upw	1	Effect of heat transfer augmentation
K. Mishima et al. [142] (1985)	CHF, PDO, DWO_{II}, CHF	forc	water	upw	1	Relation between burnout and instabilities
R.C. Yang et al. [228] (1988)	DWO_I or GES	forc	freon-22	upw	1	U-tube test section
R.P. Roy et al. [172] (1988)	DWO_{II}, DWO_{III}	forc	freon-113	upw	1	Annular test section and high-order frequencies
M. Ozawa et al. [153] (1989)	ChP, FDI, PDO	forc	air/water	hor	2	Three modes: In-phase, U-tube mode; multichannel mode
H. Yuncu [234] (1990)	ChP, PDO, DWO_{II}	forc	freon-11	hor	1	Use of characteristic curves as stability maps
M.M. Padki et al. [157] (1991)	PDO, ThO	forc	freon-11	upw	1	Influence of thermal effects
M. Aritomi et al. [11] (1992)	GES, DWO_I, DWO_{II}, NBO	nat	water	upw	2	Study of start-up conditions, focused on BWR
M. Xiao et al. [219] (1993)	DWO_I, DWO_{II}, PDO	forc	water	upw	2	High pressure (30-210 [bar])
M. Aritomi et al. [12] (1993)	GES	nat	water	upw	2	Discussion of Geysering phenomena
V. Jovic et al. [95] (1994)	FDI, PDO	forc	air/water	upw	3	PDO in an adiabatic system
H.T. Liu et al. [122] (1994)	ThO, DWO_{II}	forc	freon-12	upw	1	Wall capacity, axial conduction
D. Delmastro and A. Clausse [44] (1994)	DWO_I	nat	water	upw	1	Phase trajectories and chaos analysis

Q. Wang et al. [215] (1994)	DWO_{II}	forc	water	upw	1	Parameters analysis (T_{in}, P_{in}, G_{in})
I.S. Kyung and S.Y. Lee [111] (1994)	DWO_I, DWO_{II}	nat	freon-13	upw	1	Stability maps
Y. Ding et al. [49] (1995)	PDO	forc	freon-11	hor	1	Parameter analysis (T_{in}, G_{in})
S.Y. Jiang et al. [93] (1995)	GES, FSH, DWO_I	nat	water	upw	2	Start up analysis
M. Tshuva et al. [206] (1999)	FDI	forc	air/water	inclined	2	Flow distribution is studied
J.M. Kim and S.Y Lee [107] (2000)	DWO_I, DWO_{III}, GES, PDO	nat	water	upw	1	Several instability interacting modes
L. Guo et al. [78] (2001)	PDO	forc	water	helical	1	Parameter analysis, critical volume
O.Komakli et al. [152] (2002)	DWO_{II}, PDO, ThO	forc	freon-11	hor	1	Parameter analysis (T_{in}, G_{in})
Y. Taitel et al. [200] (2003)	FDI	forc	air/water	inclined	4	Flow distribution is studied
U. Minzer et al. [140] (2004)	ChP, FDI	forc	water	inclined	2	Flow splitting and the static characteristics are studied
W.J.M. Kruijf et al. [110] (2004)	DWO_{II}	nat	freon-12	upw	1	Atypical stability limit (N_{Zu},N_{sub})
A. Baars and A. Delgado [14] (2006)	DWO_I, DWO_{III}	nat	water	upw	1	Interaction of the DWO_I and DWO_{III}
S. Kakac and B. Bon [97] (2007)	ChP, PDO, DWO_{II}, THO	forc	freon-11	upw/hor	1	DWO interact with PDO and ThO modes
C.P. Marcel [127] (2007)	GES, FLS, DWO_I	nat	water	upw	4	Two chimneys and bypass channels are included, [125, 126]
G. Yun et al. [233] (2010)	DWO_{II}	forc	water	upw	2	Stability maps (N_{Zu},N_{sub})
Vikas Jain et al. [90] (2010)	DWO_I, DWO_{II}	nat	water	upw	4	Several riser sections
Zhian Deng et al. [47] (2011)	DWO_{II}, PDO	forc	water	upw	2	Rifled channels
Nan Liang et al. [120] (2011)	ChP, DWO_{II}, PDO	forc	freon-22	upw	1	Not significant conclusion
T. Xiong et al. [220] (2012)	FDI, DWO_{II}	forc	water	upw	2	Super critical conditions
Z. Tao et al. [203] (2013)	LED, DWO	nat	water	upw	1	Narrow rectangular channel

ChP - *characteristic pressure drop vs. flow rate curve*; LED - *Ledinegg or flow excursion*; FDI - *flow distribution instability*; PDO - *pressure drop oscillations*; DWO - *density wave oscillations*; ThO - *thermal oscillations*; TAO - *thermo-acoustic oscillations*; GES - *geysering*; FSH - *flashing induced instability*; NBO - *natural boiling oscillations*.

2.5 Analytical investigations

Several works in the literature describe the modelling of two-phase flow systems. One of the first summarising different analytical and empirical models was Graham B. Wallis [214] (1969). Several years later, Mamoru Ishii and Takashi Hibiki [89] presented a rigorous mathematical formulation for the models describing multi-phase flow systems. Nevertheless, the field of two-phase flow is empirically based. It is rarely possible to make calculations solely based on first principles, but instead it is common the use of correlations synthesised from experimental data. The prediction of pressure drop and heat transfer coefficients is a particularly good example of the empirical basis of these calculations. Good reviews of boiling and condensing models and correlations are presented in [194, 218, 83].

2.5.1 Models, formulations and numerical schemes

As described above, the description of two-phase flow phenomena is based on conservation principles. Several forms of the conservation equations have been obtained [240, 227, 43]. On the other hand, in most of the investigations regarding the occurrence of two-phase flow instabilities, one-dimensional models are used. In the literature it is possible to find mainly four models:

- **TFM, Two-Fluid Model**: This is the most general formulation for two-phase flow modelling. Six equations, three for each phase need to be solved and several consecutive laws (friction, heat transfer and interfacial) at the boundary and at the interface are required [97]. However, it is necessary the use of accurate models of the constitutive relations for interfacial and wall transfer, which are very dependent on the particular characteristics of each situation. In addition, most of the correlations used in two-phase flow modelling are obtained under steady-state conditions. For this last reason, separated models are not normally used in the description of transient two-phase flow phenomena. Examples of this model implementation can be found in [53, 54].

- **DFM, Drift-Flux Model**: The *drift-flux model* introduced by N. Zuber and J. A . Findlay [240] (1965) is an approximation of the two-fluid model [214]. It allows to represent the velocity difference between the different phases (slip) and the radial void distribution. There are several versions of DFM, mainly depending on the assumption for the void distribution parameter [240, 169].

- **SFM, Slip-Flow Model**: In this kind of model the two phases are considered to be segregated in two different streams, liquid-vapor. It is useful to represent flow regimes such as annular where the two streams assumption is close to the real case [113].

- **HM, Homogeneous Model**: This is the simplest and most used model to represent transient phenomena in two-phase flow systems. In this model the two-phase flow is treated as a single-phase compressible fluid. The velocity of the phases is considered equal and in most of the cases a thermo-dynamic

equilibrium condition between the phases is assumed. In this case the model is called Homogeneous Equilibrium Model (HEM).

The conservation equations for the different models can be found elsewhere in the literature mentioned above. Several techniques are used in order to obtain a solution to these system of equations.

- **Frequency-domain formulation**: Normally, the Laplace transform of the equations is taken in order to transform from the time-domain to the frequency-domain. The spacial dependencies are normally eliminated by taking a lumped model (integral method) but it can also be solved by discretizing in space or applying the method of characteristics [151]. Some examples of the frequency-domain formulation can be found in [87, 177, 1, 13, 202, 114].

- **Time-domain formulation**: The equations are discretized in time using different numerical techniques such as finite difference methods, finite volumes methods, etc. The spatial dependence is normally treated using two different techniques:

  - **Lumped formulation**: A lumped formulations of the conservation equations is normally obtained by the *integral method*. The integral method is used for the purpose of reducing the dimension of the problem. It consists on integrating the governing equations over the domain of interest to substitute the continuous dependence of parameters by an average dependence [7, 168]
  - **Distributed formulation**: It consists in discretizing the spatial dependence and formulate an algebraic problem based in the values of the variables at the discretized nodes. Two techniques are used to select the discretization nodes.
    - **FNS, Fixed Nodes Scheme**: The discretization nodes are distributed in a fixed spacial position and the different terms of the model are evaluated according to the nodal variables values. Several numerical techniques such FDM, FVM, FEM can be used. [7, 160, 173]
    - **MNS, Moving Nodes Scheme**: In this case the discretization is defined according to a fixed distribution in some variable (enthalpy) and the model is reformulated according to this new discretization. [35, 66, 204, 160]

In the following sections, a brief review of different analytical investigations regarding two-phase flow instabilities is presented. Several studies have summarised some particular aspects of the two-phase flow instabilities modelling [97, 148, 71]. In the next section only the analytical investigations of the phenomena considered in the scope of this work (LED, PDO and DWO) are described.

2.5.2 Ledinegg or flow excursion

Based on the condition of negative slope of the characteristic pressure drop vs. mass flow rate, there are several studies proposing simple models and correlations

to calculate the Onset of Fluid Instability (OFI) based on steady-state calculations [124, 188, 92, 15, 118, 96, 238]. Nevertheless, in this section a summary of the studies describing the transient process of flow excursion is described.

J.L. Achard et al. [1] (1981) presented a comprehensive linear stability study based in a frequency-domain lumped parameter model. In this investigation, the analytical results predicts excursive instability (i.e. Ledinegg) for the zero-frequency limit. A similar analysis is developed in [77], where an analytical expression for the stability limit of the Ledinegg phenomena is obtained based in a lumped parameter linear model. This stability limit is function of the N_{Zu} and N_{sub} numbers and the concentrated inlet/outlet friction factors. M.M. Padki et al. [158] (1992) presented a linearised stability analysis of *Ledinegg* and *pressure drop* oscillations. A stability criterion based on a bifurcation analysis is derived in terms of the steady-state external and internal pressure drop vs. mass flow rate characteristic curves. It is proved that the Ledinegg instability is caused by a saddle-node bifurcation while the PDO are cause by a super-critical Hoft bifurcation.

More recently, several investigations reported numerical examples of the dynamic evolution during the flow excursion. For example in [7] a lumped parameter model is used to simulate a boiling channel and the Ledinegg stability limit is predicted in a N_{pch} vs. N_{sub} non-dimensional map. Using a similar analysis, the existence of a negative slope region in supercritical conditions is studied numerically in [6, 70]. W. Schlichting et al. [180] (2010) present a few transient simulations showing flow excursion and DWO phenomena. Nevertheless, this phenomenon is not analysed in deep in these last mentioned investigations.

2.5.2.1 Flow distribution instability

K. Akagawa and T. Sakaguchi [3] (1971) presented one of the first investigations analysing systematically the flow distribution instability, both experimentally and analytically. A geometrical criterion based on the shape of the steady-state characteristic curves is presented. More recently, S. Natan et al. [146] analyse a two parallel boiling channels in connection with the use of Direct Steam Generation (DSG) for solar heating. A flow pattern based model is used to analysed the flow distribution and steady-state characteristic curves. It is found that the flow splitting between the two parallel channels is not equal even for symmetric heating. For asymmetric heating conditions, most of the liquid tends to flow in the pipe which absorbs less heat. U. Minzer et al. [139] (2006) present a simple transient model to simulate the behaviour of a parallel boiling system. Similarly to the flow excursion in a single channel, the simulations show the trajectories of the system evolving from the unstable to the stable operation points. In addition, whenever several stable solutions are possible, the obtained solution depends on the inlet flow rate history (hysteresis phenomenon). In [199] a control system using the total flow and the inlet valves is proposed in order to control the flow distribution instability. M. Baikin et al. [16] (2011) presented the experimental and numerical analysis of four parallel boiling channels. In the case where only some of the channels are heated, it is found that most of the flow tends to take place in the unheated channels.

Y. Taitel and D. Barnea [197] (2011) present a flow pattern based model to study the transient evolution of the flow-distribution phenomenon. The transient responses to finite disturbances in flow and heating power are analysed. The simulations show that depending on the amplitude of the perturbations, in some cases the transient trajectories can even provoke the excursion to other final states. Finally in [236], a homogeneous model is used to study the stability and controllability of parallel boiling channels. As a main conclusion it is proved that the most stable systems are those where the characteristics of each channel are distinct. In addition when the channels are identical, there is not change in the total flow as a results of the flow-distribution variations in the individual channels. Thus, in general for parallel arrays, it is recommended the use of uneven channel conditions.

2.5.3 Pressure drop oscillations

Several analytical and experimental studies were presented during the 60's regarding the occurrence of oscillations in boiling systems [81, 82]. A.H. Stenning and T.N. Veziroglu [190] (1965) propose a model to study the PDO phenomenon. As in most of the experimental results the oscillation periods are much longer than the residence time of a fluid particle, a quasi-steady state for the heated section is assumed. The mathematical model used in this study includes the pressure drops in the valves and inertia in the pipelines. Moreover, the pressure drop of the heater is calculated using a steady-state model. In addition, a compressible ideal gas model is used for the calculation of the compressible volume evolution. This first model is extended in [193, 192] to take into account the thermal capacity of the pipe and the heat exchange with the fluid. In these last works, a perturbation linear analysis is applied in order to obtain the system stability boundaries. In addition, a non-linear analysis of the limit cycles is performed by solving numerically the ODE system. The necessary parameters are measured or estimated from experimental data. Therefore using the linearised model, the oscillation periods are 300 % longer than the experimental ones, even when the predicted analytical stability limits are in accordance with the experimental data. In the case of the non-linear model, the predicted periods are between 40-100 % longer than those obtained experimentally. J.S. Maulbetsch and P. Griffith [134] (1965) present a linear stability analysis of the PDO phenomena. The assumptions of this model are similar to the one described previously, but the effects of heat transfer and thermal capacity are neglected. An analytical formulae for the frequency of the oscillations is obtained. The stability limits agree with the experimental ones but the periods are not compared. M. Ozawa et al. [155] (1979) studied the PDO phenomenon experimentally and analytically. A lumped parameter model and a linearization technique, similar to the ones described before, are presented. The effects of the wall thermal capacity and the inlet valves are neglected. Moreover, the channel pressure drop is approximated by a cubic polynomial. The results show that even though the stability limits are predicted accordingly to the experimental values, the differences of the theoretical and experimental periods is close to 100 %. In addition, most of the previous investigations, DWO are superimposed to the PDO in the experimental data used to compare with the theoretical cases.

In [5, 4] a finite difference scheme is used to solve the non-linear system representing a single vertical channel. A homogeneous equilibrium model, similar to the one described above, is implemented and the wall thermal storage is neglected. This theoretical analysis is conservative in predicting the stability boundaries for pressure-drop type oscillations. Moreover, the amplitude of the oscillations is well predicted but the periods are underestimated. In this last investigation no DWO phenomena are observed in the compared experimental data. This fact should be remarked, since in most of the works the results obtained using a quasi-steady model for the heater section (no DWO) are compared with experimental data where DWO are superimposed to the PDO phenomenon. H. Gürgenci et al. [80] (1983) present a simplified non-linear analysis. The effects of wall heat storage, the fluid properties variations and the inertia terms are neglected. The non-linear system is solved by a FDM. It should be remarked that in this case a vertical channel system is described so the gravitational terms are included in the model. The amplitude of the predicted limit cycles is in agreement with the experimental data. Nevertheless, the oscillations periods are 100 % longer than the experimental values. In [51] a model (HEM) similar to the one described above is implemented. It is proved that the variations of the heat transfer to the fluid plays an important role in generating and sustaining the PDO. Moreover, a relatively good agreement between the experiments and calculations is reported. In [235] a frequency-domain analysis is used to obtain the stability limits of the PDO phenomenon. A steady-state homogeneous equilibrium model is used to describe the heater section. The system is transformed by the Laplace transform and Nyquist graphics are used in order to determine the stability boundaries. The stability predictions agrees within the 50 % with the experimental values.

In [102, 157] a steady-state drift-flux model is used to represent a vertical, boiling test section. The effects of wall thermal capacity are taken into account. In addition, a FDM is used in order to solve the non-linear system. As a result, a relatively good agreement between the experimental and theoretical results is obtained. It is found that, the period and amplitudes of the oscillations increase with decreasing mass flow rate. M.M. Padki et al. [158] (1992) was the first using the bifurcation theory to analyse these phenomena, based on a lumped parameter integral model. In this study it is proved that PDO is caused by a Hopf bifurcation as the heat input is increased. The necessary conditions for the occurrence of PDO and Ledinegg phenomena based on the slope of the characteristic curve are obtained, see Section 2.2.1.5. In [123] a comparison of dynamic simulations and the experimental data obtained in [121], using the model developed in [102] is described. In addition a bifurcation analysis is presented, based in a planar system developed by using a lumped parameter model. Several limit cycles are analysed concluding that, for increasing mass flow rates, the PDO limit-cycles are generated after a supercritical Hopf bifurcation and they converge again to an asymptotically stable equilibrium point after a reverse supercritical Hopf bifurcation takes place.

N. Reinecke and D. Mewes [166] (1999) present an analytical and experimental investigation of PDO in a vertical tube system using an air/water mixture. A simple mathematical model is presented, using the experimental characteristic curve and a ideal gas model for the compressible volume. The agreement of the numerical results and the experimental data is good, both in frequency and amplitude. L. Cao

et al. [30] (2000) presented an experimental and an analytical investigation. As in the experimental results it is found that the larger pressure drop takes place at the exit restriction, therefore, a model for the exit valve is developed in order to fit the experimental results. A drift-flux model is proposed to describe the steady-state heated section and the heater wall effects are neglected. The theoretical oscillation amplitudes are overestimated and periods are reasonably good predicted. In [31] the same model is improved by using a subcooling boiling model. The pressure drop vs. mass flow rate characteristic curves are predicted more accurately than for the previous case and, as a consequence, the stability limit is also predicted more accurately. In [187] a homogeneous equilibrium model is used to study the stability limits and dynamic behaviour of PDO. A singularity theory is implemented and several bifurcation diagrams used to determine the stability regions for Ledinegg and PDO phenomena. The stability boundaries are described in a K_{in} vs. N_{sub} non-dimensional stability map. Moreover, some examples of dynamic simulations using the scheme developed in [145] are shown. Oscillations with really sharp transitions, much more faster than the fluid particle transit time are reported. However, no discussion about the validity of the steady-state assumption for the heated channel under those conditions is presented.

More recently, P.R. Mawasha and R.J. Gross [136] (2001) analysed PDO in an horizontal boiling channel. An empirical third order polynomial correlation is used in order to represent the characteristic pressure drop vs. mass flow rate curve from a given boiling system [234]. The effect of the wall heater is considered by the model. The periods of the numerical simulations agree with the experimental ones. Nevertheless, the amplitude is over-predicted by the theoretical model. The heater thermal capacity do not produce any significant effect in the simulated oscillations. Similar to the reported results in previous studies, it is possible to see that some of the variables (flow) are changing very fast (much more faster than the transit time of a fluid particle) and, as mentioned above, none of these studies mentioned the limitations of the quasi-steady assumptions. S. Kakac and Liping Cao [98] (2009) study this phenomenon in vertical and horizontal systems. A steady-state drift-flux model for the heater is implemented, with similar characteristics to the investigations described above. The theoretical and experimental data are compared, finding a relatively good agreement. A very similar analysis is presented in [99]. T. Zhang et al. [237] (2011) present the numerical analysis of PDO in parallel channels, with focusing in the design of a control system to avoid this kind of phenomena in electronics cooling systems. Two control strategies are proposed, control through the inlet valve and control using the supply pump. In addition, the effect of the wall capacity is proved to have an influence on the oscillations. In [74], PDO in parallel and single channels are analysed. The thermal and hydrodynamic interaction between the heated channels are considered using a very simple model. Synchronous and asynchronous oscillations in the neighbouring channels are observed. The general evolution of the system is proved to be strongly dependent on the shape of the characteristic curve and in the thermal interaction of the channels. Moreover, the existence of chaotic regions due to the nature of these interactions is demonstrated.

Without any doubt, the most interesting study, since the pioneer article of A.H.

Stenning and T.N. Veziroglu [190] (1965), is the one presented by W. Schlichting [179] (2008). In this study a *dynamic* homogeneous model is used to model the heated section. An ideal gas compressible volume is simulated upstream of the heated channel. The features of this model allow to simulate PDO, DWO and Ledinegg phenomena using the same model. The interaction between DWO and PDO is briefly analysed. Nevertheless, the simulated conditions differ from the normal experimental conditions of the literature investigations. A summary of the results presented in this investigation is presented in [180].

2.5.4 Density wave instabilities

G.B. Wallis and J. H. Heasley [213] (1961) was one of first articles analysing oscillations in two-phase flow systems. Moreover, it took some years until the different phenomena were identified and studied in a systematic manner. A.H. Stenning et al. [193] (1967) implement a lumped parameter model of a heated section with inlet and outlet throttling. The predicted oscillations are in the order of 1.5 to 2.0 times the residence time of a fluid particle in the heated section. The stability boundaries of the system are obtained using a frequency-domain analysis. J.A. Bouré and A. Mihaila [26] (1967) propose the density effect mechanism, involving time delays, to explain the oscillatory behaviour of boiling channels. Several experimental results are used to prove that this effect is, in most of the cases, triggering this phenomenon (DWO_{II}). N. Zuber [239] (1967) presents a distributed formulation expressed in terms of the mixture center of mass. In addition, the slip velocity between the phases is considered in this formulation. M. Ishii and N.Zuber [87] (1970) extend this formulation and propose a set of non-dimensional numbers in order to establish a similitude criterion between different two-phase flow systems. The subcooling (N_{sub}), phase change (N_{Zu}), drift (N_D) , density (N_ρ), Froud (Fr) and Reynolds (Re) non-dimensional numbers are proposed to analyse the phenomena taking place in boiling systems, as explained in Section 9.2. Following this theoretical investigation, Mamoru Ishii [88] (1971) uses a frequency-domain analysis to obtain the system characteristic equation, assuming no slip between the phases. The stability limits for several cases are plotted in N_{Zu} vs. N_{sub} maps. It is proved that the stability of the boiling system is proportional to: subcooled temperature, system pressure, slip velocity, inlet restriction; and inversely proportional to: heat flux, outlet restriction (very strongly). These last investigations introduced the theoretical basis for the understanding of the *density wave* phenomenon (DWO_{II}). A simple correlation to predict the DWO_{II} stability limit is proposed. In [177] this formulation is extended with a thermal non-equilibrium model. For low subcooling this model fits better the experimental data. However, in the high subcooling region the equilibrium model is proved to fit better to the experimental data.

An interesting study was presented in [224, 225], where the authors attempt to explain analytically the high-order *density wave* modes (DWO_{III}) by using transfer functions of the system main variables. K. Takitani [201] (1978) presented a simplified lumped parameter model with moving boundaries. The stability limits obtained using this model agree the experimental data but the oscillation periods have differences up to 150 %. R.T. Lahey and F.J. Moody [113] (1977) made a complete anal-

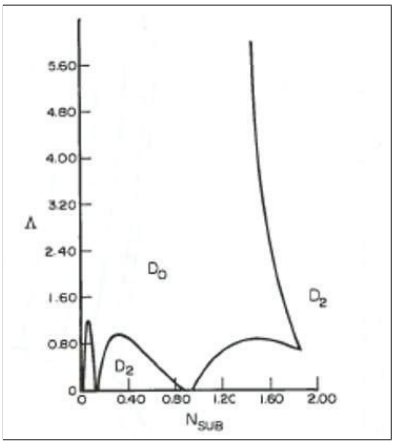

Figure 2.11: *Friction vs. Subcooling non-dimensional numbers stability map. presented by [1]. Stability islands are reported corresponding with the high-order modes (DWO$_{III}$).*

ysis of the two-phase flow modelling in Boiling Water Reactors, including the study of Ledinegg and *density wave* phenomenon using frequency-domain methods. This instability analysis is an extension of the analytical results presented in previous investigations [226]. Based in a frequency-domain analysis and using a homogeneous equilibrium model, K. Fukuda and T. Kobori [61] (1979) introduced the concept of the *density wave* oscillations induced by the gravity terms in a riser section (DWO$_I$). Five different kinds of *density wave* instabilities modes are described: due to gravity in the heated section and in the riser DWO$_I$; due to friction in the heated section and in the riser DWO$_{II}$; and due to acceleration in the heated section DWO$_{III}$. L.A. Belblidia and E. Weaver [18] (1980) performs a linear stability analysis. The stability influence of several parameters is studied, obtaining similar conclusions as the ones presented in previous investigations. J.L. Achard et al. [1] (1981) implemented a lumped parameter model in order to perform a linear stability analysis of a boiling channel. The effects of the gravity and friction are analysed through the Fr and friction $(\Lambda)^2$ non-dimensional numbers respectively. "Stability islands" are detected for low friction numbers and for different Fr numbers. This stability islands are found to be related with the occurrence of high-order oscillations (DWO$_{III}$) as reported experimentally. In [2] a similar investigation is made by using a non-linear analysis through the use of Hopf-bifurcation analysis techniques, valid near the marginal-stability boundaries. It is shown that the non-linear terms can change significantly the stability limits for both normal and high order modes. The analysis also describe cases where a finite-amplitude forced perturbation can cause a divergent instability on the stable region of the linear-stability boundary.

Another interesting study was presented by M.J. Atkinson and J.C. Friedly [13] (1983), where the influence of the thermal wall capacity of the heater is analysed. It is shown that this effect do not change significantly the stability limits but

[2] $\Lambda = f_{tp}\frac{L}{D}$ (friction number)

it is of paramount importance in the non-linear evolution of high amplitudes oscillations. It is proved that this effect is sufficient to guaranty bounded oscillations, as the ones seen in the experiments.

In [144] a D-partition method is used to make a linear analysis based in a homogeneous flow model. A stability map based on the inlet and outlet resistances is used to analyse the stability of the system. The stability limits are proved to be in accordance with experimental data. It is also proved that in the case of superheated exit conditions the gravity has no effect on the stability threshold. R.C. Dykhuizen et al. [53, 54] describe the application of a *two-fluid* model to make a linear stability analysis of the DWO_{II} phenomenon. The predicted limits are in agreement with the experimental data for high subcooling numbers, however, for low subcooling this boundary is predicted conservatively. A parameter analysis shows that the effect of the interfacial drag, the mass exchange between the phases and the void distribution have no significant influence in the stability thresholds. M. Furutera [62] (1986) study the validity of the homogeneous model in the description of the stability limits. Several pressure, subcooling and heat capacity models are compared with experimental data. It is proved that in general terms, the best approximation is made with no subcooling model and heat capacity of the wall when that mechanism is physically important (massive tubes).

R.T. Lahey and M.Z. Podowski [114] (1989) make a very complete description of the use of frequency-domain tools (such as the Nyquist graphics) in the study of these phenomena in BWR. An extensive summary with the results of previous studies and the analysis of single and parallel channel systems are presented. U. Rizwan and J.J. Dorning [169] (1986) present linear and non-linear techniques to study the stability limits of a boiling channel. A drift-flux model including the void distribution parameter C_0, see [240, 214], is implemented. This factor seems to be important for thermal equilibrium analysis since it leads to limits that agrees considerably better with the experimental data. In subsequent studies [170, 171] the effect of a periodic perturbation imposed to the pressure drop boundary condition is studied. It is shown that the system can exhibit a sub-harmonic, quasi-periodic or chaotic evolution depending on the amplitude and the frequency of the periodic forcing. Following this kind of analysis, A. Clausse and R.T. Lahey [35] (1991) use a homogeneous equilibrium model to study the chaotic nature of the DWO limit cycles. It is shown that periodic limit cycles and aperiodic chaotic response are induced in this kind of systems. In this last work, it is introduced the use of a Moving Node Scheme (MNS) for the numerical discretization. D.F Delmastro et al. [46] (1991) analysed the effect of gravity in the N_{Zu} vs. N_{sub} stability limits. A destabilising effect of the gravitational term for higher subcoolings and a stabilising effect at lower subcoolings is reported. A simple natural convection loop is used to compare experimental and analytical results finding a good agreement.

U. Rizwan [168] (1994) presented a critical view of the classical mechanisms used to explain the DWO_{II} phenomenon. Using numerical simulations and experimental data, it is concluded that the density waves travelling in the pipe do not play a significant role in the generation of the oscillations. The two fundamental processes for these non-linear oscillations are the delayed change of the pressure drop according to the inlet velocity and the feedback process (i.e. outlet throttling) by which

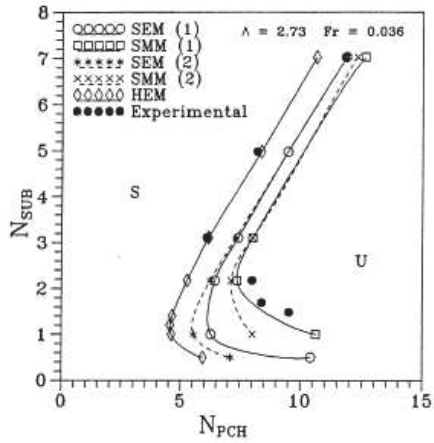

Figure 2.12: *The effects of different models on the marginal stability boundary for DWO_{II} presented in [162]. SEM thermodynamic equilibrium model with slip; SMM mechanistic model of subcooling boiling with slip ; HEM Homogeneous equilibrium model, no slip; (1) distributed parameters; (2) average steady-state parameters.*

the inlet velocity is modified according to the pressure drop changes. Unfortunately the mechanisms triggering DWO_I and DWO_{III} phenomena are not considered in this investigation. In [167] the same investigation is extended to a distributed heat source. The numerical results show that the channel becomes less stable by the introduction of a different axial heat flux profile if it increases the two-phase region length. Several heat sources examples are described. Respect to the uniform distribution, when a single humped distribution is used then the channel becomes less stable for low inlet subcooling and more stable for high inlet subcoolings. C.J. Chang and R.T. Lahey [32] (1997) analyse the occurrence of instabilities with view on the safety of BWRs. It is found that chaos may occur in a boiling channel coupled with an adiabatic riser. Moreover, in some cases the heated wall dynamics is proved to have a significant destabilising effect.

M.Z. Podowski and M.P. Rosa [162] (1997) study the effects of various modelling concepts and numerical approaches on the transient response and stability of boiling channels. It is analysed the impact of the numerical discretization on the convergence and accuracy of computations. Four different models are investigated: (a) Homogeneous equilibrium model (HEM), (b) Thermodynamic equilibrium model with plastic slip (SEM), (c) profile-fit model of subcooled boiling with slip (SPFM), (d) mechanistic model of subcooled boiling with slip (SMM). In addition, the effect of distributed and average parameters is investigated. Figure 2.12 shows the differences of the Marginal Stability Boundary (MSB) for different models. As can be seen, the homogeneous model predicts conservatively the stability boundaries respect to the models considering slip and subcooling boiling. In [145] the effects of heat distribution and the response to forced perturbations are studied. The interaction of the natural frequency of the DWO and a fixed forcing frequency of

the imposed pressure drop gives rise to various phenomena: relaxation oscillations, sub-harmonic oscillations, quasi-periodic and chaotic solutions. In [65, 66] the application of a general MNS to the calculation of DWO stability boundaries is made. Several numerical aspect of the implementation of these schemes are discussed.

W. Ambrosini et al. [7] (2000) use the homogeneous equilibrium balance equations and present a comparison between lumped and distributed parameter models. The prediction of the marginal stability boundaries is quite similar using both of them. The main mechanism triggering DWO_{II} are discussed with relation to the criticisms introduced by U. Rizwan [168]. The results indicate that for high inlet subcoolings the mechanism proposed by Rizwan is more adequate than the classical mechanism. Under these conditions: the period of oscillations is considerably longer than twice the fluid transit time; the outlet density does not oscillate in phase with outlet pressure drop and the density-wave phenomenon looks mostly governed by flow perturbations rather than by actual density wave propagation. On the other hand, for low inlet subcooling conditions it is found that the classical description of the main mechanisms is more accurate. Under these conditions: the period of oscillations is closer to twice the fluid transit time; the outlet density oscillations are correlated with outlet pressure drop oscillations; density wave propagation can be observed along the channel. D. Delmastro and A. Clausse [45] (2001) describe a simple mathematical model based on delay equations, derived from a homogeneous model. Using a linear perturbation method it is proved a good agreement with a distributed parameter model.

S.Y. Lee and Y.L. Kim [117] (1999) describe numerically a natural convection loop. The stability boundaries of Ledinegg instability, DWO_{I} and DWO_{II} are analysed numerically. The influence of a expansion tank upstream from the heated section is investigated. In all the cases the compressible volume destabilise the system. A.K. Nayak et al. [147] (2002) describe the application of a homogeneous model for the simulation of a BWR natural convection reactor. Both DWO_{I} and DWO_{II} modes are predicted. The frequency of DWO_{II} instability is larger than that corresponding to DWO_{I}. The effect of neutronic feedback is investigated. These effects are also investigated by G.V.D. Prasad and M. Pandey [163] (2008). In this last investigation, the boiling system undergo into chaotic oscillations (DWO_{II}) when a strong reactivity feedback is applied (neutron flux-void fraction). For the DWO_{I}, subcritical Hopf bifurcation leading to unstable limit cycle, as well as supercritical Hopf bifurcation leading to stable limit cycle have been found. A review of several modelling investigations in single- and two-phase flow natural convection is presented in [71]. In order to simulate the geysering phenomenon in a steam-water natural circulation loop, S. Paruya and P. Bhattacharya [159] derived a moving nodal model (lumped parameter model).

Very recently, S. Paruya et al. [160] (2012) investigated the difference between the fixed node scheme (FNS) and the moving node scheme (MNS) in the prediction of DWO phenomenon. The analysis suggests that MNS is more efficient and has a better convergence compared to FNS, using a finite difference method. Numerical simulations of long and short channels show that in the case of short channels with high Froude number the "islands of instability" appear in the N_{Zu}-N_{sub} plane. Moreover, the strong effect of the subcooling in the period of the oscillations, as

described in [168, 7], is reported. Should also be mentioned that the occurrence of these phenomena in systems under supercritical conditions is described in [6, 8, 70].

2.5.4.1 DWO in parallel channels

V.A. Gerliga and R.A. Dulevskiy [68] (1970) presented one of the first analytical investigations regarding the occurrence of thermo-hydraulic oscillations in parallel channels. In this work the characteristic equation for a parallel system is derived. K. Fukuda and S. Hasegawa [59] (1979) derived the governing equations for a general array of parallel boiling channels with different characteristics. M. Aritomi et al. [9] (1983) study the *density wave* phenomena in a forced convection upflow boiling system with parallel channels. A drift-flux model is implemented and a linear stability analysis is performed using a transfer function method. The experimental and analytical results for a twin-parallel channel system are compared, obtaining a good agreement between them. This last investigation is extended in [10], where the DWO phenomenon is studied in more than two channels. In the case of more than three channels, it is shown a behaviour quite similar to a twin channel system regardless of whether there are an odd or even number of channels. For more than three channels, the flow instability first occurs in the most unstable pair of channels.

A very extensive investigation is presented by R.P. Taleyarkhan et al. [202], using a model that accounts for subcooled boiling, arbitrary heat flux distribution, distributed and local hydraulic losses, heated wall dynamics and slip flow in ventilated parallel channels. This study is focused in the description of thermo-hydraulic phenomena in BWRs. This analysis suggests that radial variations of power, subcooling and ventilation between parallel channels can have a substantial impact on the predicted stability margins. Comparison with experimental data confirms the basic predicted trends and good agreement with the stability limits is observed.

G. Guido et al. [76] [77] presented an analytical stability analysis of parallel boiling channels. Explicit expressions for the stability limits of Ledinegg and DWO_{II} are obtained. In addition, the oscillation periods for twin parallel channels are calculated. The reported modes correspond with in-phase and out-of-phase oscillations. In the case of a non-identical channels system, the normal modes are not longer in-phase or out-of-phase, but the phase shift depends on the individual conditions. In addition for intermediate and large inlet subcooling lengths, when different power distribution between the channels is used the system becomes more unstable. A. Clausse et al. [36] (1989) extended this analysis using a perturbation method to analyse the feedback between the boiling channels and the external system. For different channels, the in-phase and out-of-phase modes interact with each other and complicated modes, involving coupling between the channels and the loop, can be induced. The results of this study explain the differences of the modes reported in experimental investigations. Moreover, it is proved that the phase shift is very dependent on small differences between channels.

J.D. Lee and C. Pan [116] (1999) studied the behaviour of a system with 1-5 channels using a MNS. It is proved that the multiple channel system becomes more unstable with an increase of the channel number. In all simulations the most heated channel exhibits the largest oscillation, and is out-of-phase with the other channels.

When a forced perturbation is imposed periodic, quasi-periodic and chaotic oscillations may appear. In [85], a lumped-parameter model is used to study a two parallel channel with natural convection. In-phase (loop instability) and out-of-phase (channel-to-channel) oscillations are found. The effects of various parameters in the stability limits are analysed. For example the resistance coefficients in the single-phase flow region K_{in} (total flow) and K_i (each channel) are stabilising factors. In contrast, the resistance coefficients in the two-phase flow region K_{out} (total flow) and K_e (each flow) are destabilising factors, as described in other investigations. G.V.D. Prasad et al. [164] (2008) simulate a twin-parallel in a natural circulation system using a lumped parameter and a commercial code (RELAP5/MOD3.4). The lumped parameter model predicts similar trends to the observed in the RELAP5 simulations. The DWO_I and DWO_{II} modes in a twin-parallel channel system are investigated. The effects of gravitational and frictional pressure drops and geometrical parameters on the oscillation modes are investigated. The two channels oscillate out-of-phase in the DWO_I region due to dominant gravitational pressure drop at low powers. On the other hand in the DWO_{II} region, the channels oscillate in-phase and out-of-phase depending on the dominance of two-phase frictional pressure drop and the downcomer inertia. The downcomer inertia can be varied by varying the dimensions of the boiling system. Thus, geometrical parameters influence the DWO_{II} mode but not the DWO_I.

X. Genglei et al. [67] (2012) study oscillations in 1-2-4-9 parallel channels using the commercial code RELAP5. A comparison with experimental data is made in order to validate the results. It is found that in some cases the non-equilibrium model overestimates the stable region. In contrast, the homogeneous equilibrium model predicts conservative limits in all the cases. The DWO, Ledinegg instability and flow distribution instability are investigated. The stability limits for the DWO_I and DWO_{II} modes are analysed. Moreover, the system pressure increases are proved to increase the system stability of both modes. Similarly, M. Colombo et al. [38] (2012) use the RELAP5 code to investigate a parallel twin-channel system. In this investigation it is also found that the non-equilibrium model (RELAP5) is non-conservative for the prediction of the stability boundaries. A parameter influence analysis shows that an increase in the inlet resistances and an increase in the system pressure stabilise the system. On the contrary, nonuniform heating makes the system more unstable with the increase of nonuniform degree.

2.6 Discussion

In the previous sections a comprehensive assessment of the main mechanisms triggering two-phase flow instabilities has been presented. In particular, a detailed presentation of the main experimental and analytical results concerning the Ledinegg instability, flow distribution instability, density wave oscillations and pressure drop oscillations has been made. In this section a discussion of those results is presented. It is apparent, however, that further research is needed. The recommendations for further work are tabulated bellow:

Experimental research needed

- As described in section Section 2.2.9, the knowledge on two-phase flow instabilities in condensing systems is still very limited. In total not more than ten articles can be found in the open literature analysing these phenomena. For these reason two-phase flow instabilities in condensing system should be investigated.
- The interaction between *pressure drop oscillations* and *density wave* phenomena, should be studied. This statement is based in the fact that several investigations reported the DWO superimposed to the PDO. In particular, as seen in [179], horizontal boiling channels are more vulnerable to the interaction between these two modes. This interaction could be the cause of the discrepancies seen in the amplitudes and frequencies observed for the PDO, in the experimental cases [235, 152, 49].
- None of the previous works analyse the effects of compressible volumes downstream the heated section on two-phase flow instability phenomena, especially for PDO and DWO modes. The effect on PDO and DWO of different amounts of gas upstream and downstream the heated channel should be studied. In particular, the PDO phenomenon in systems with small compressible volumes near the test section and the influence of compressibility volumes in the stability limits of the DWO modes should also be investigated.
- Experimental analysis of DWO in short test sections (small friction numbers Λ) would help to understand more about the influence of the momentum terms on DWO phenomena. Moreover, the use of this kind of test section would be interesting to analyse if PDO are generated only due to the compressibility of the two-phase mixture.
- In addition the interaction mechanism between DWO and thermo-acoustic oscillations and microscopic instability should be studied.

Analytical research needed

- More analytical investigations should be conducted in order to understand the different mechanisms related with condensing instabilities.
- As described in Section 2.5.3, most of the theoretical studies analysing PDO assume a *quasi-steady* state model for the heater channel (proposed by [190]). Nevertheless, none of these investigations study the limitations of this assumption in the representation of physical systems. In the other hand, none of these studies are able to describe the interaction between PDO and DWO modes, present in most of the experimental results. In conclusion, the use of proper models representing the physics described in the experiments should be investigated.
- The analytical study of the influence of other parameters than: the inlet/outlet throttling, system pressure, channels number, inlet subcooling, heat flux and mass flow rate on the stability of DWO modes should be addressed.

- More analytical investigations are needed in order to clarify the mechanism and parameter influence on high-order density wave oscillations (DWO_{III}).

2.7 Summary

A brief review of the main mechanisms triggering two-phase flow instabilities were introduced. The main phenomena were described in order to give the reader the necessary tools to distinguish among them. The main experimental and analytical investigations regarding the occurrence of the phenomena studied in this work were analysed. Several aspects of the current state-of-the-art in the two-phase flow instabilities field were critically discussed.

Bibliography

[1] ACHARD J., DREW D., AND LAHEY R. The effect of gravity and friction on the stability of boiling flow in a channel. *Chemical Eng. Comm.*, 11, 1981. (Cited on page 41, 42, 47, 255)

[2] ACHARD J., DREW D., AND LAHEY R. The analysis of nonlinear density-wave oscillations in boiling channels. *J. Fluid Mechanics*, 155:213–232, 1985. (Cited on page 17, 47)

[3] AKAGAWA K. AND SAKAGUCHI T. Study on distribution of flow rates and flow stabilities in parallel long evaporatos. *Bulletin of JSME*, 14:837–848, 1971. (Cited on page 14, 27, 28, 37, 42)

[4] AKYUZLU K., VEZIROGLU T. N., KAKAC S., AND DOGAN T. Finite difference analysis of two-phase flow pressure-drop and density-wave oscillations. *Wärme- und Stoffübertragung*, 14:253–267, 1980. (Cited on page 44)

[5] AKYUZLU K. *Mathematical Modelling Of Two-Phase Flow Oscillations*. PhD thesis, University of Miami, 1980. (Cited on page 44)

[6] AMBROSINI W. On the analogies in the dynamic behaviour of heated channels with boiling and supercritical fluids linear and nonlinear analysis of density wave instability phenomena. *Nuclear Engineering and Design*, 237: 1164–1174, 2007. (Cited on page 42, 51)

[7] AMBROSINI W., DI MARCO P., AND FERRERI J. Linear and nonlinear analysis of density wave instability phenomena. *International Journal of Heat and Technology*, 18:27–36, 2000. (Cited on page 41, 42, 50, 51)

[8] AMBROSINI W. AND SHARABI M. Assestment of stability maps for heated channels with supercritical fluids versus the predictions of a system code. *Nuclear Engineering and Technology*, 39(5), 2007. (Cited on page 51)

[9] ARITOMI M., AOKI S., AND INOUE A. Instabilities in parallel channel of forced-convection boiling upflow system, (v) consideration of density wave instability. *Journal of Nuclear and Technology*, 20(4):286–301, 1983. (Cited on page 51)

[10] ARITOMI M., AOKI S., AND INOUE A. Thermo-hydraulic instabilities in parallel boiling channel systems: Part 1. a non-linear and a linear analytical model. *Nuclear Engineering and Design*, 95:105–116, 1986. (Cited on page 51)

[11] ARITOMI M., CHIANG J., AND MORI M. Fundamental studies on safety-related thermohydraulics of nat. circ. boiling parallel channel flow systems under start-up conditions (mechanism of geysering in parallel channels). *Nuclear Safety*, 33:170–182, 1992. (Cited on page 19, 34, 38)

[12] ARITOMI M., CHIANG J., AND MORI M. Geysering in parallel boiling channels. *Nuclear Engineering and Design*, 141:111–121, 1993. (Cited on page 20, 38, 255)

[13] ATKINSON M. AND FRIEDLY J. Limitations of simple models in describing two-phase flow oscillations. *National heat transfer conference*, 21:147–157, 1983. (Cited on page 41, 47)

[14] BAARS A. AND DELGADO A. Multiple modes of a natural circulation evaporator. *Int. Journal Heat Mass Transfer*, 49:2304–2314, 2006. (Cited on page 35, 39)

[15] BABELLI I. AND ISHII I. Flow excursion instability in downward flow systems part ii: two-phase instability. *Nuclear Engineering and Design*, 206: 97–104, 2001. (Cited on page 42)

[16] BAIKIN M., TAITEL Y., AND BARNEA D. Flow rate distribution in parallel heated pipes. *International Journal of Heat and Mass Transfer*, 54:4448–4457, 2011. (Cited on page 27, 42)

[17] BELBLIDIA L. AND BRATIANU C. Density-wave oscillations. *Annals of Nuclear Energy*, 6:425–444, 1979. (Cited on page 10)

[18] BELBLIDIA L. AND WEAVER E. Linear stability analysis of density-wave oscillations. *Annals of Nuclear Energy*, 7:13–23, 1980. (Cited on page 47)

[19] BERGANT A., A.R. S., AND TIJSSELING A. Water hammer with column separation: A historical review. *Journal of Fluids and Structures*, 22:135–171, 2006. (Cited on page 25)

[20] BERGLES A., GOLDBERG P., AND MAULBETSCH J. Acoustic oscillations in high-pressure single channels boiling system. *EUROATOM, Symposium of two-phase flow dynamics, Eindhoven*, pages 525–550, 1967. (Cited on page 21)

[21] BERGLES A., LIENHARD J., KENDALL G., AND GRIFFITH P. Boiling and evaporating in small diameter channels. *Heat tranfer engineering*, 24:18–40, 2003. (Cited on page 36)

[22] BERGLES A. *A review of instabilities in two-phase systems*, volume 1. Hemisphere, Washington, 1977. (Cited on page 10)

[23] BHATT B. AND WEDEKIND G. A self sustained oscillatory flow phenomenon in two-phase condensing flow system. *ASME Journal of Heat Transfer*, 102:695–700, 1980. (Cited on page 22)

[24] BHATT B., WEDEKIND G., AND JUNG K. Effects of two-phase pressure drop on the self-sustained oscillatory instability in condensing flows. *ASME Journal of Heat Transfer*, 111:538–545, 1989. (Cited on page 22)

[25] BOURÉ J., BERGLES A., AND TONG L. Review of two-phase flow instabilities. *Nuclear Engineering and Design*, 25:165–192, 1973. (Cited on page 10, 13, 18)

[26] BOURÉ J. AND MIHAILA A. The oscillatory behaviour of heated channels. *EUROATOM, Symposium of two-phase flow dynamics, Eindhoven*, pages 695–720, 1967. (Cited on page 9, 16, 46)

[27] BOYER B., ROBINSON G., AND HUGHES T. Experimental investigation of flow regimes and oscillatory phenomena of condensing steam in a single vertical annular passage. *Int. Journal of multiphase flow*, 21:61–74, 1995. (Cited on page 22)

[28] BRUTIN D., TOPIN F., AND TADRIST L. Experimental study of unsteady convective boiling in heated minichannels. *Int. J. Heat and Mass transfer*, 46:2957–2965, 2003. (Cited on page 36)

[29] BUYEVICH Y. AND NATALUKHA I. Self-oscillating regimes of nucleate, transition and film boiling. *Int. J. Heat Mass Transfer*, 38(2):2363–2373, 1996. (Cited on page 14)

[30] CAO L., KAKAC S., LIU H., AND SARMA P. The effects of thermal non-equilibrium and inlet temperature on two-phase flow pressure drop type instabilities in an upflow boiling system. *Int. J. Therm. Sci.*, 39:886–895, 2000. (Cited on page 45)

[31] CAO L., KAKAC S., LIU H., AND SARMA P. Theoretical analysis of pressure-drop type instabilities in an upflow boiling system with an exit restriction. *Heat and Mass Transfer*, 37, 2001. (Cited on page 45)

[32] CHANG C. AND LAHEY R. Analysis of chaotic instabilities in boiling systems. *Nuclear Engineering and Design*, 167:307–334, 1997. (Cited on page 49)

[33] CHIANG J., ARITOMI M., AND MORI M. Fundamental study on thermo-hydraulics during start-up in natural circulation boiling water reactors, (ii) natural circulation oscillation induced by hydrostatic head fluctuation. *Journal of Nuclear Science and Technology*, 30(3), 1993. (Cited on page 20)

[34] CHUN M.-H. AND YU S.-O. A parametric study and a guide chart to avoid condensation-induced water hammer in a horizontal pipe. *Nuclear Engineering and Design*, 201:239–257, 2000. (Cited on page 25)

[35] CLAUSSE A. AND LAHEY R. The analysis of periodic and strange attractors during density-wave oscillations in boiling flow. *Chaos, Solitons and Fractals*, 1(2), 1991. (Cited on page 41, 48)

[36] CLAUSSE A., LAHEY R., AND PODOWSKI M. An analysis of stability and oscillation modes in boiling multichannel loops using parameter perturbation methods. *Int. Journal Heat Mass Transfer*, 32(11):2055–2064, 1989. (Cited on page 51)

[37] COLLINS D. AND GACESA M. Hydrodynamic instability in a full-scale simulated reactor channel. *Proceedings of the Institution of Mechanical Engineers*, 184:115–126, 1969. (Cited on page 16, 32, 37)

[38] COLOMBO M., CAMMI A., PAPINI D., AND RICOTTI M. Relap5/mod3.3 study on density wave instabilities in single channel and two parallel channels. *Progress in Nuclear Energy*, 52:15–23, 2012. (Cited on page 52)

[39] CORNELIUS A. *An investigation of instabilities encountered during heat transfer to a supercritical fluid*. PhD thesis, Faculty of the Graduate School of the Oklahoma State University, 1965. (Cited on page 21, 37)

[40] COSTA J. Two-phase flow problems in liquid-metal fast-breeder reactors. *ch.2 in Thermohydraulics of two-phase systems for industrial design and nuclear engineering*, pages 11–35, 1981. (Cited on page 26, 255)

[41] DALEAS R. AND BERGLES A. Effects of upstream compressibility on subcooled critical heat flux. *ASME Paper 65-HT-77*, 1965. (Cited on page 27, 37)

[42] DANEY D., LUDTKE P., AND JONES M. An experimental study of thermally-induced flow oscillations in supercritical helium. *Journal of Heat Transfer*, 101:9–14, 1979. (Cited on page 34, 38)

[43] DELHAYE J. M., GIOT M., AND RIETHMULLER M. L. *Thermohydraulics of Two-phase systems for industrial design and nuclear engineering*. Von Karman, Hemisphere Publising Corporation and McGraw-Hill Book Company, 1981. (Cited on page 9, 22, 23, 40)

[44] DELMASTRO D. AND CLAUSSE A. Experimental phase trajectories in boiling flow oscillations. *Experimental Thermal and Fluid Science*, 9:47–52, 1994. (Cited on page 34, 38)

[45] DELMASTRO D. AND CLAUSSE A. A delay theory for boiling ¯ow stability analysis. *International Journal of Multiphase Flow*, 27:657–671, 2001. (Cited on page 50)

[46] DELMASTRO D., CLAUSSE A., AND CONVERTI J. The influence of gravity on stability of boiling flows. *Nuclear Enginneering and Design*, 127:129–139, 1991. (Cited on page 48)

[47] DENG Z., LUO Y., WANG H., AND CHEN T. Experimental study of two-phase flow instability of vertical parallel rifled tube with different sizes at low-mass flow rate. *Asia-Pacific Journal of Chemical Engineering*, 2011. (Cited on page 39)

[48] DIJKMAN F., TUMMERS J., AND SPIGT C. The stability characteristics of a boiling system with natural and forced convection circulation. *EUROATOM, Symposium of two-phase flow dynamics, Eindhoven*, pages 307–323, 1967. (Cited on page 31, 37)

[49] DING Y., KAKAC S., AND X.J.CHEN . Dynamic instabilities of boiling two-phase flow in a single horizontal channel. *Experimental Thermal and Fluid Science*, 11:327–342, 1995. (Cited on page 19, 29, 39, 53)

[50] DMITREVSKIY Y. AND MEL'NIK Y. Observation of thermal-acoustic oscillations in hydrogen, nitrogen, oxygen and argon. *Cryogenics*, January 1976. (Cited on page 21)

[51] DOGAN T., KAKAC S., AND VEZIROGLU T. Analysis of forced-convection boiling flow instabilities in single-channel upflow system. *Int. J. heat and fluid flow*, pages 145–156, 1983. (Cited on page 29, 38, 44)

[52] DORSH R. Frequency response of a forced-flow single-tube boiler. *EUROATOM, Symposium of two-phase flow dynamics, Eindhoven*, 1:291–306, 1967. (Cited on page 32, 37)

[53] DYKHUIZEN R., ROY R., AND KALRA S. A linear two-fluid model analysis of dynamic instability in boiling flow systems. *J. Heat Transfer*, 108:100–108, 1986. (Cited on page 40, 48)

[54] DYKHUIZEN R., ROY R., AND S.P. K. Two-fluid model simulation of density-wave oscillations in a boiling flow system. *Nucl. Sci. Engng.*, 94: 167–179, 1986. (Cited on page 40, 48)

[55] EDESKUTY F. AND THURSTON R. Similarity of flow oscillations induced by heat transfer in cryogenic systems. *EUROATOM, Symposium of two-phase flow dynamics, Eindhoven*, pages 552–567, 1967. (Cited on page 21)

[56] FEENSTRA P. *Modelling two-phase flow-excited fluidelastic instability in heat exchanger tube arrays*. PhD thesis, McMaster University, Ontario, 2000. (Cited on page 25)

[57] FIRSTENBERG H., GOLDMANN K., AND HUDSON J. Boiling songs and mechanical vibrations. *NDA 2132-12*, 1960. (Cited on page 21)

[58] FRIEDLY J. An experimental study of oscillations in a liquid nitrogen evaporator. *UKAEA Report, AERE-R8487*, 1976. (Cited on page 21, 33)

[59] FUKUDA K. AND HASEGAWA S. Analysis on two-phase flow instability in parallel multichannels. *Journal of Nuclear Science and Technology*, 16(3): 190–199, 1979. (Cited on page 17, 51)

[60] FUKUDA K. AND KOBORI T. Two-phase flow instability in parallel channels. *Proc. 6th Int. Heat Transfer Conf. FB-17*, pages 369–374, 1978. (Cited on page 33, 38)

[61] FUKUDA K. AND KOBORI T. Classification of two-phase flow instability by density wave oscillation model. *Journal of Nuclear and Technology*, 16: 95–108, 1979. (Cited on page 9, 10, 12, 16, 17, 31, 33, 47)

[62] FURUTERA M. Validity of homogeneous flow model for instability analysis. *Nuclear Engineering and Design*, 95:65–77, 1986. (Cited on page 48)

[63] FURUYA M. *Experimental and Analytical Modeling of Natural Circulation and Forced Circulation BWRs*. PhD thesis, Nuclear Technology Research Laboratory, Central Research Institute of Electric Power Industry (CRIEPI), Tokyo, 2006. (Cited on page 18, 35)

[64] FURUYA M., INADA F., AND HAGEN V. D.T. Flashing-induced density wave oscillations in a natural circulation bwr-mechanism of instability and stability map. *Nuclear Engineering and Design*, 235:1557–1569, 2005. (Cited on page 35)

[65] GAREA V. *Nodal analysis of two-phase flow instabilities*. PhD thesis, Rensselaer Polytechnic Institute, 1998. (Cited on page 50)

[66] GAREA V., DREW D., AND LAHEY R. A moving-boundary nodal model for the analysis of the stability of boiling channels. *Int. Journal Heat Mass Tranfer*, 42:3575–3584, 1999. (Cited on page 41, 50)

[67] GENGLEI X., MINJUN P., AND GUO Y. Research of two-phase flow instability in parallel narrow multi-channel system. *Annuals of Nuclear Energy*, 48:1–16, 2012. (Cited on page 52)

[68] GERLIGA V. AND DULEVSKIY R. The thermohydraulic stability of multichannel steam generating systems. *Heat transfer Sov. Res.*, 2:63–72, 1970. (Cited on page 17, 51)

[69] GIALDI E. Core stability in operating bwr: Operational experience. *Proceedings of SMORN-IV, Dijon, France*, 1984. (Cited on page 17)

[70] GOMEZ T. O., CLASS A., LAHEY R., AND SCHULENBERG T. Stability analysis of a uniformly heated channel with supercritical water. *Nuclear Engineering and Design*, 238:1930–1939, 2008. (Cited on page 42, 51)

[71] GOSWAMI N. AND PARUYA S. Advances on the research on nonlinear phenomena in boiling natural circulation loop (review). *Progress in Nuclear Energy*, 53:673–697, 2011. (Cited on page 41, 50)

[72] GOUSE S. AND ANDRYSIAK C. Flow oscillations in a closed loop with transparent parallel vertical heated channels. Technical Report Report 8973-2, MIT Engineering Projects Laboratory, 1963. (Cited on page 21)

[73] GRIFFITH P. Geysering in liquid-filled lines. *ASME Paper 62-HT-39*, 1962. (Cited on page 19)

[74] GRZYBOWSKI H. AND MOSDORF R. Modelling of pressure-drop instability in single and multichannels. *Acta Mechanica et Automatica*, 6(3):45–51, 2012. (Cited on page 45)

[75] GUIDAOUI M., ZHAO M., MCINNIS D., AND AXWORTHY D. H. A review of water hammer theory and practice. *Applied Mechanics Reviews*, 58:49–75, 2005. (Cited on page 25)

[76] GUIDO G., CONVERTI J., AND CLAUSSE A. Stability of twoparallel boiling channels. *Proc. XVI Argentine Nuclear Technology Association, Annual Conf, Bariloche, Argentina*, 1987. (Cited on page 51)

[77] GUIDO G., CONVERTI J., AND CLAUSSE A. Density wave oscillations in parallel channels – an analytical approach. *Nuclear engineering and Design*, 125:121–136, 1991. (Cited on page 42, 51)

[78] GUO L., Z.P.FENG , AND X.J.CHEN . Pressure drop oscillation of steam-water two-phase flow in a helically coiled tube. *Int. J. of Heat and Mass Transfer*, 44:1555–1564, 2001. (Cited on page 30, 39)

[79] GUO L., Z.P.FENG , AND X.J.CHEN . Transient convective heat transfer of steam/water two-phase flow in a helical tube under pressure drop type oscillations. *Int. J. of Heat and Mass Transfer*, 45:533–542, 2002. (Cited on page 30)

[80] GÜRGENCI H., VEZIROGLU T., AND KAKAC S. Simplified nonlinear descriptions of two-phase flow instabilities in vertical boiling channel. *Int. J. Heat Mass Transfer*, pages 671–679, 1983. (Cited on page 44)

[81] HAYAMA S. A study on the hydrodynamic instability in boiling channels (1st report, the stability in single boiling channel). *JSME*, 6(23), 1963. (Cited on page 43)

[82] HAYAMA S. A study on the hydrodynamic instability in boiling channels (2th report, the instability of two parallel boiling channels). *JSME*, 6(23), 1963. (Cited on page 43)

[83] HETSRONI G. *Handbook of multiphase systems*. Hemisphere, 1982. (Cited on page 40)

[84] HETSRONI G., MOSYAK A., SEGAL Z., AND POGREBNYAK E. Two-phase flow patterns in parallel micro-channels. *International Journal of Multiphase Flow*, 29:341–360, 2003. (Cited on page 36)

[85] HIRAYA M., UMEKAWA H., AND OZAWA M. Parallel channel instability in natural circulation systems. *Multiphase Science and Technology*, 18(4): 305–333, 2006. (Cited on page 52)

[86] HU B. *Characteristing gas-lift instabilities*. PhD thesis, Departament of petroleum engineering and applied geophysics, Norwegian University of Science and Technology, 2004. (Cited on page 12)

[87] ISHII M. AND N.ZUBER . Thermally induced flow instabilities in two-phase. *Proceedings of the forth international heat transfer metting*, 1970. (Cited on page 9, 23, 41, 46)

[88] ISHII M. *Thermally induced flow instabilities in two-phase mixtures in thermal equilibrium*. PhD thesis, Georgia Institute of Technology, Michigan, 1971. (Cited on page 9, 16, 46)

[89] ISHII M. AND HIBIKI T. *Thermo-fluid dynamics of two-phase flow*. Springer, 2005. (Cited on page 40)

[90] JAIN V., NAYAK A., VIJAYAN P., SAHA D., AND SINHA R. Experimental investigation on the flow instability behavior of a multi-channel boiling natural circulation loop at low-pressures. *Experimental Thermal and Fluid Science*, 34:776–787, 2010. (Cited on page 39)

[91] JEGLIC F. AND YANG K. The incipience of flow oscillations in force-flow subcooled boiling. Technical Report N66-15248, Heat transfer and Fluid Mechanics Institute University of California, 1965. (Cited on page 14, 31, 37)

[92] JENG H. AND PAN C. Analysis of two-phase flow characteristics in a natural circulation loop using the drift-flux model taking flow pattern change and subcooled boiling into consideration. *Annuals of Nuclear Energy*, 26:1227–1251, 1999. (Cited on page 42)

[93] JIANG S., YAO M., BO J., AND WU S. Experimental simulation study on start-up of the 5 mw nuclear heating reactor. *Nuclear Engineering and Design*, 158:111–123, 1995. (Cited on page 39)

[94] JIANG S., ZHANG Y., WU X., BO J., AND JIA H. Flow excursion phenomenon and its mechanism in natural circulation. *Nuclear Engineering and Design*, 202:17–26, 2000. (Cited on page 26)

[95] JOVIC V., AFGAN N., JOVIC L., AND SPASOJEVIC D. An experimental study of the pressure drop oscillations in three parallel channel two phase flow. *Proceedings of the International Heat Transfer Conference, Brighton (Ed: Hewitt, G.F), UK*, pages 193–198, 1994. (Cited on page 12, 38)

[96] K. F. A model for predicting static instability in two-phase flow systems. *Progress in Nuclear Energy*, 51:805–812, 2009. (Cited on page 42)

[97] KAKAC S. AND BON B. A review of two-phase flow dynamic instabilities in tube boiling systems. *Int. Journal Heat Mass Tranfer*, 51:399–433, 2007. (Cited on page 10, 18, 31, 39, 40, 41)

[98] KAKAC S. AND CAO L. Analysis of convective two-phase flow instabilities in vertical and horizontal in-tube boiling systems. *Int. Journal Heat Mass Transfer*, 52:3984–3993, 2009. (Cited on page 30, 45)

[99] KAKAC S., VENKATARAMAN M., PRAMUANJAROENKIJ A., AND KOTCIOGLU I. Modeling of two-phase flow instabilities in convective in-tube boiling horizontal systems. *J. of Thermal Science and Technology*, 29(1): 107–116, 2009. (Cited on page 45)

[100] KAKAC S., VEZIROGLU T., AKYUZLU K., AND BERKOL O. Sustained and transient boiling flow instabilities in a cross-connected four-parallel-channel upflow system. *Proc. of the 5th int. conf. Heat Tranfer, Tokyo*, pages 235–239, 1974. (Cited on page 28)

[101] KAKAC S., VEZIROGLU T., OZHOYA N., AND LEE S. Transient boiling flow instabilities in a multi-channel upflow system. *Wårme- und Steffubertragung*, 10:175–188, 1977. (Cited on page 28, 38)

[102] KAKAC S., VEZIROGLU T., PADKI M., FU L., AND CHEN X. J. Investigation of thermal instabilities in a forced convection upward boiling system. *Experimental Thermal and Fluid Science*, 3:191–201, 1990. (Cited on page 18, 19, 29, 44)

[103] KANDLIKAR S., KUAN W., WILLISTEIN D., AND BORRELLI J. Stabilization of flow boiling in drop elements and fabricated nucleation sites. *Journal of heat transfer, Trans. ASME*, 128:389–396, 2006. (Cited on page 36)

[104] KARSLI S., YILMAZ M., AND COMAKLI O. The effect of internal surface modification on flow instabilities in forced convection boiling in a horizontal tube. *International Journal of Heat and Fluid Flow*, 23, 2002. (Cited on page 30, 35)

[105] KENNEDY J., ROACH JR. D., ABDEL-KHALIK M., GHIAASSIAAN S., JETER S., AND QUERSHI S. The onset of flow instability in uniformly heated horizontal micro-channels. *J. Heat Transfer*, 122:118–125, 2000. (Cited on page 36)

[106] KHUSHNOOD S., KHAN Z., MALIK M., KORESHI Z., AND KHAN M. A review of heat exchanger tube bundle vibrations in two-phase cross-flow. *Nuclear Engineering and Design*, 230:233–251, 2004. (Cited on page 25)

[107] KIM J. AND LEE S. Experimental observation of flow instability in a semi-closed two-phase natural circulation loop. *Nuclear enginnering and design*, 196:359–367, 2000. (Cited on page 35, 39)

[108] KOBUS C. AND BHATT B. Predicting the onset of a low-frequency, limit-cycle type of oscillatory flow instability in multitube condensing flow systems. *Journal of Heat Transfer*, 123:319–330, 2001. (Cited on page 24)

[109] KRISHNAN V. AND FRIEDLY J. Pressure oscillations in forced convection heating of gases. *Int. Heat Transfer Conf. 5th Porc., Tokyo*, pages 358–362, 1974. (Cited on page 21, 33, 37)

[110] KRUIJF W., SENGSTAG T., DE HASS D., AND VAN DER HAGEN T. Experimental thermohydraulic stability map of a freon-12 boiling water reactor facility with high exit friction. *Nuclear Engineering and Design*, 229:75–80, 2004. (Cited on page 35, 39)

[111] KYUNG I. AND LEE S. Experimental observations on flow characteristics in an open twp-phase natural circulation loop. *Nuclear engineering and design*, 159:163–176, 1994. (Cited on page 39)

[112] LAHEY R. AND DREW D. An assesstment of the literature related to LWR instability modes. Technical Report NUREG/CR-1414, Rensselaer Polytechnic Institute, U.S. Nuclear Regulatory Commission, 1980. (Cited on page 10)

[113] LAHEY R. AND MOODY F. *The thermal hydraulics of a boiling water nuclear reactor*. Amer Nuclear Society, 1977. (Cited on page 40, 46)

[114] LAHEY R. AND PODOWSKI M. On the analysis of varius instabilities in two-phase flows. *Multiphase Science and Technology*, pages 183–370, 1989. (Cited on page 10, 41, 48)

[115] LEDINEGG M. Instability of flow during natural and forced circulation. *Die Wärme*, 61(8):891–898, 1938. (Cited on page 9, 11, 13)

[116] LEE J. AND PAN C. Dynamics of multiple parallel boiling channel systems with forced flows. *Nuclear Engineering and Design*, 192:31–44, 1999. (Cited on page 51)

[117] LEE S. AND KIM Y. An analytical investigation of role of expansion tank in semi-closed two-phase natural circulation loop. *Nuclear Engineering and Design*, 190:353–360, 1999. (Cited on page 50)

[118] LI Y., YEOH G., AND TU J. Numerical investigation of static flow instability in a low-pressure subcooled boiling channel. *Heat and Mass Transfer*, 40: 355–364, 2004. (Cited on page 42)

[119] LIANG N., SHAO S., XU H., AND TIAN C. Instability of refrigeration system – a review. *Energy Conversion and Management*, 51, 2010. (Cited on page 36)

[120] LIANG N., SHUANGQUAN S., TIAN C., AND YAN Y. Two-phase flow instabilities in horizontal straight tube evaporator. *Applied Thermal Engineering*, 31:181–187, 2011. (Cited on page 36, 39)

[121] LIU H. AND KAKAC S. An experimental investigation of thermally induced flow instabilities in a convective boiling upflow system. *Wärme- und Stoffübertragung*, 26:365–376, 1991. (Cited on page 29, 44)

[122] LIU H., KAKAC S., AND MAYINGER F. Characteristics of transition boiling and thermal oscillation in an upflow convective boiling system. *Experimental Thermal and Fluid Science*, 6:195–205, 1994. (Cited on page 18, 19, 35, 38)

[123] LIU H., KOCAK H., AND KAKAC S. Dynamical analysis of pressure-drop type oscillations with planar model. *Int.J. Multiphase Flow*, 20:1129–1142, 1995. (Cited on page 44)

[124] LORENZINI E. A simplified method proposal for practical determination of aperiodic to-phase flow instability. *International Journal of Multiphase flow*, 7(6):635–645, 1981. (Cited on page 42)

[125] MARCEL C., ROHDE M., AND VAN DER HAGEN T. Experimental and numerical investigations on flashing-induced instabilities in a single channel. *Experimental Thermal and Fluid Science*, 33:1197–1208, 2009. (Cited on page 18, 36, 39)

[126] MARCEL C., ROHDE M., AND VAN DER HAGEN T. Experimental investigations on flashing-induced instabilities in one and two-parallel channels: A comparative study. *Experimental Thermal and Fluid Science*, 34:879–892, 2010. (Cited on page 18, 36, 39)

[127] MARCEL C. *Experimental and numerical stability investigations on natural circulation boiling water reactors*. PhD thesis, Technische Universiteit Delft, october 2007. (Cited on page 36, 39)

[128] MARCH-LEUBA J. AND REY J. Coupled thermohydraulic-neutronic instabilities in boiling water nuclear reactors: a review of the state of the art. *Nuclear Engineering and Design*, 145:97–111, 1993. (Cited on page 18)

[129] MARGETTS R. Excursive instability in feedwater coils. *AIChE Paper prepared for presentation at 13th National Heat Transfer Conference, Denver, Colorado*, 1972. (Cited on page 27)

[130] MATHISEN R. Out of pile channel instability in the loop skalvan. *EUROATOM, Symposium of two-phase flow dynamics, Eindhoven*, pages 19–63, 1967. (Cited on page 32, 37)

[131] MATSUI G. Flow instability in boiling channels systems. *International Chemical Engineering*, 11(3):554–560, 1971. (Cited on page 33, 37)

[132] MATSUI G. An experimental study of flow instability in boiling channel systems. *Heat Tranfer, Japanese Research*, 1:46–52, 1972. (Cited on page 33)

[133] MAULBETSCH J. AND GRIFFITH P. A study of system-induced instabilities in forced-convection flows with subcooled boiling. *MIT engineering projects Lab Report 5382-35*, 1965. (Cited on page 15, 28, 34, 37)

[134] MAULBETSCH J. AND GRIFFITH P. System induced instabilities in forced convection with subcooled inlet. *Procedings of the fifth International Heat Tranfer*, 4:247–257, 1965. (Cited on page 15, 28, 43)

[135] MAULBETSCH J. AND GRIFFITH P. Prediction of the onset of system-induced instabilities in subcooled boiling. *EUROATOM, Symposium of two-phase flow dynamics, Eindhoven*, 1:799–825, 1967. (Cited on page 28)

[136] MAWASHA P. AND GROSS R. Periodic oscillations in a horizontal single boiling channel with thermal wall capacity. *Int. J. of Heat and Fluid Flow*, 22:643–649, 2001. (Cited on page 45)

[137] MAYINGER F. Status of thermohydraulic research in nuclear safety and new challenges. *eight International Topical Meeting on Nuclear Reactor Thermal-hydraulics*, 1997. (Cited on page 9)

[138] MENTES A., YILDIRIM O., GURGENCI H., KAKAC S., AND VEZIROGLU T. Effect of heat transfer augmentation on two-phase flow instabilities in a vertical boiling channel. *Heat and Mass Transfer*, 17:161–169, 1983. (Cited on page 28, 38)

[139] MINZER U., BARNEA D., AND TAITEL Y. Flow rate distribution in evaporating parallel pipes - modeling and experimental. *Chemical Engineering Science*, 61:7249–7259, 2006. (Cited on page 42)

[140] MINZER U., BARNEA D., AND TAITEL Y. Evaporation in parallel pipes - splitting characteristics. *Int. J. Multiphase Flow*, 30:763–777, 2004. (Cited on page 27, 39)

[141] M.ISHII . Study of flow instabilities in two-phase mixtures. *ANL-76-23*, 1976. (Cited on page 10)

[142] MISHIMA K., NISHIHARA H., AND MICHIYOSHI I. Boiling burnout and flow instabilities for water flowing in a round tube under atmospheric pressure. *Int. J. Heat Mass Transfer*, 28:1115–1129, 1985. (Cited on page 38)

[143] NAKANISHI S. Recent japanese research on two-phase flow instabilities. *Two-phase flow dynamics, Hemisphere*, 1981. (Cited on page 10)

[144] NAKANISHI S. AND KAJI M. Aa approximation method for construction of a stability map for density wave oscillations. *Nuclear Engineering and Design*, 95:55–64, 1986. (Cited on page 48)

[145] NARAYANAN S., SRINIVAS B., PUSHPAVANAM S., AND BHALLAMUDI S. M. Non-linear dynamics of a two-phase flow system in an evaporator: The effects of (i) a time varying pressure drop, (ii) an axially varying heat flux. *Nuclear Engineering and Design*, 178:279–294, 1997. (Cited on page 45, 49)

[146] NATAN S., BARNEA D., AND TAITEL Y. Direct steam generation in parallel pipes. *Int. Journal of multiphase flow*, 29:1669–1683, 2003. (Cited on page 42)

[147] NAYAK A., VIJAYAN P. K., SAHA D., VENKAT RAJ V., AND ARITOMI M. Study on the stability behaviour of a natural circulation pressure tube type boiling water reactor. *Nuclear Engineering and Design*, 215:127–137, 2002. (Cited on page 50)

[148] NAYAK A. AND VIJAYAN P. Flow instabilities in boiling two-phase natural circulation systems: A review. *Science and Technology of nuclear installations*, 2008. (Cited on page 10, 41)

[149] NAYAK A., VIJAYAN P., JAIN V., SAHA D., AND SINHA R. Study on the flow-pattern-transition instability in a natural circulation heavy water moderated boiling light water cooled reactor. *Nuclear Engineering and Design*, 225:159–172, 2003. (Cited on page 14)

[150] NRC . Power oscillations in boiling water reactors. Technical Report NRC Bulletin 88-07 Supplement 1, LaSalle, US, 1988. (Cited on page 17)

[151] OKAZAKI M. Analysis of density wave instability in a boiling flow using a characteristic method. *Nonlinear Analysis, Theory, Mehods and Application*, 30(5):2787–2795, 1995. (Cited on page 41)

[152] O.KOMAKLI , KARSLI S., AND YILMAZ M. Experimental investigation of two-phase flow instabilities in a horizontal in tube boiling system. *Energy Conversion and Management*, 43:249–268, 2002. (Cited on page 30, 39, 53)

[153] OZAWA M., AKAGAWA K., AND SAKAGUCHI T. Flow instabilities in parallel-channel flow systems of gas-liquid two-phase mixtures. *Int. Journal of multiphase flow*, 15:639–657, 1989. (Cited on page 27, 28, 38)

[154] OZAWA M., AKAGAWA K., SAKAGUCHI T., TSUKAHARA T., AND FUJII T. Oscillatory flow instabilities in air water two-phase flow systems. *Bulletin of JSME*, 22(174):1763–1773, 1979. (Cited on page 28, 38)

[155] OZAWA M., NAKANISHI S., ISHIGAI S., MIZUTA Y., AND TARUI H. Flow instabilities in boiling channels: Part 1, pressure drop oscillations. *Bulletin JSME*, 22(170), 1979. (Cited on page 12, 28, 38, 43)

[156] OZAWA M., NAKANISHI S., ISHIGAI S., MIZUTA Y., AND TARUI H. Flow instabilities in boiling channels: Part 2, geysering. *Bulletin JSME*, 22(170), 1979. (Cited on page 19)

[157] PADKI M., LIU H., AND KAKAC S. Two-phase flow pressure drop type and thermal oscillations. *Int. Journal of heat and fluid flow*, 12:240–248, 1991. (Cited on page 29, 38, 44)

[158] PADKI M., PALMER K., KAKAC S., AND VEZIROGLU T. Bifurcation analysis of pressure-drop oscillations and the ledinegg instability. *Int. Journal Heat Mass Transfer*, 35:525–532, 1992. (Cited on page 42, 44)

[159] PARUYA S. AND BHATTACHARYA P. Moving-boundary analysis of net vapor generation point in a steam generator. *Int. J. Numer. Methods Fluids*, 61: 569–590, 2009. (Cited on page 50)

[160] PARUYA S., MAITI S., KARMAKAR A., GUPTA P., AND SARKAR J. Lumped parameterization of boiling channel - bifurcations during density wave oscillations. *Chemical Engineering Science*, 74:310–326, 2012. (Cited on page 41, 50)

[161] PETTIGREW M., CARLUCCI L., TAYLOR C., AND FISHER N. Flow induced vibration and related technologies in nuclear components. *Nuclear Engineering and Design*, 131:81–100, 1991. (Cited on page 25)

[162] PODOWSKI M. AND ROSA M. Modeling and numerical simulation of oscillatory two-phase flows, with application to boiling water nuclear reactors. *Nuclear Engineering and Design*, 177:179–188, 1997. (Cited on page 49, 256)

[163] PRASAD G. AND PANDEY M. Stability analysis and nonlinear dynamics of natural circulation boiling water reactors. *Nuclear Engineering and Design*, 238:229–240, 2008. (Cited on page 50)

[164] PRASAD G., PANDEY M., PRADHAN S., AND GUPTA P. Study of flow instabilities in double-channel natural circulation boiling systems. *Nuclear Engineering and Design*, 238:1750–1761, 2008. (Cited on page 52)

[165] PRASAD G., PANDLEY M., AND KALRA M. Review of research on flow instabilities in natural circulation boiling systems. *Progress in Nuclear Energy*, 49:429–451, 2007. (Cited on page 10)

[166] REINECKE N. AND MEWES D. Oscillatory transient two-phase ¯ows in single channels with reference to monolithic catalyst supports. *International Journal of Multiphase Flow*, 25:1373–1393, 1999. (Cited on page 30, 44)

[167] RIZWAN U. Effects of double-humped axial heat flux variation on the stability of two phase flow in heated channels. *Int. J. Multiphase flow*, 20:721–737, 1994. (Cited on page 49)

[168] Rizwan U. On density wave oscillations in two-phase flows. *Int. J. Multiphase flow*, 20:721–737, 1994. (Cited on page 41, 48, 50, 51)

[169] Rizwan U. and Dorning J. Some nonlinear dynamics of a heated channel. *Nuclear Engineering and Design*, 93:1–14, 1986. (Cited on page 40, 48)

[170] Rizwan U. and Dorning J. A chaotic attractor in a periodically forced two phase flow system. *Nucl. Sci. Engng.*, 100, 1988. (Cited on page 48)

[171] Rizwan U. and Dorning J. Chaotic dynamics of a triply forced two phase flow system. *Nucl. Sci. Engng.*, 105, 1990. (Cited on page 48)

[172] Roy R., Jain P., and S.P. K. Dynamic instability experiments in boiling flow system. *Int. J. Heat Mass Transfer*, 31:1947–1952, 1988. (Cited on page 34, 38)

[173] Ruspini L. Inertia and compressibility effects on density waves and ledinegg phenomena in two-phase flow systems. *Nuclear Engineering and Design*, 250:60–67, 2012. (Cited on page 41)

[174] Ruspini L., Dorao C., and Fernandino M. Dynamic simulation of ledinegg instability. *Journal of Natural Gas Science and Engineering*, 2: 211–216, 2010. (Cited on page 13)

[175] Saha P. *Thermally induced two-phase flow instabilities, including the effect of thermal non-equilibrium between the phases*. PhD thesis, Georgia Instituta of Technology, 1974. (Cited on page 33)

[176] Saha P., Ishii M., and N.Zuber . An experimental investigation of the thermally induced flow oscillations in two-phase systems. *Transactions of the ASME*, 1:616–622, 1976. (Cited on page 33)

[177] Saha P. and N.Zuber . An analytic study of the thermally induced two-phase flow instabilities including the effect of thermal non-equilibrium. *Int. J. Heat Mass Transfer*, 21:415–426, 1978. (Cited on page 33, 41, 46)

[178] Saha P. and Zuber N. Point of net vapor generation and vapor void fraction in subcooled boiling. *Procedings of the fifth International Heat Tranfer*, B4.7:175–179, 1974. (Cited on page 37)

[179] Schlichting W. *An analysis of the effect of gravity on interacting DWO/PDO instability modes*. PhD thesis, Faculty of Rensselaer Polytechnic Institute, 2008. (Cited on page 46, 53)

[180] Schlichting W., Lahey R., and Podowski M. An analysis of interacting instability modes, in phase change system. *Nuclear Engineering and Design*, 240:3178–3201, 2010. (Cited on page 42, 46)

[181] Schmitt F. *Contribution experimentale et theretique a l'etude d'un type particulier d'ecoulement transitoire de sodium en ebullition*. PhD thesis, Universite scientifique et medicale et Institute National Polytechnique, Grenoble, 1974. (Cited on page 26, 255)

[182] SEMENOVKEL I. On the onset of pulsation in the boiling tubes of high-pressure boilers. *Hydrodynamics and boiling heat transfer in high-pressure boilers, USSR*, 1955. (Cited on page 31)

[183] SIMAN-TOV M., FELDE D., MCDUFFE J., AND YODER G. Experimental study of static flow instability in subcooled flow boiling in parallel channels. *4th ASME/JSME Thermal Engineers Joint Conference, Hawaii*, 1995. (Cited on page 26)

[184] SMIRNOV H., ZRODNIKOV V., AND BOSHKOVA I. Thermoacoustic phenomena at boiling subcooled liquid in channels. *Int. Journal Heat Mass Tranfer*, 40(3):1977–1983, 1997. (Cited on page 21, 22)

[185] SOLIMAN M. AND BERENSON P. Flow instability and gravitational effects in condenser tubes. *Paper no. Cs. 1.8, Proceedings of the fourth international conference on heat transfer*, 1970. (Cited on page 22)

[186] SOLIMAN M. AND BERENSON P. Flow stability and gravitational effects in multitube condensers. *NASA technical note, N76-71971*, 1970. (Cited on page 22)

[187] SRINIVAS B. AND PUSHPAVANAM S. Determining parameters where pressure drop oscillations occur in a boiling channel using singularity theory and the d-partition method. *Chemical Engineering Science*, 55:3771–3783, 2000. (Cited on page 45)

[188] STELLING R., MCASSEY E., AND DOUGHERTY Y. The onset of flow instability in uniformly for downward flow in vertical channels. *J. Heat Transfer*, 3:709–714, 1996. (Cited on page 26, 42)

[189] STENNING A. Instabilities in the flow of a boiling liquid. *Journal of basic Engineering*, pages 213–217, 1964. (Cited on page 15, 27, 37)

[190] STENNING A. AND VEZIROGLU T. Flow oscillation modes in forced convection boiling. *Heat Transfer and Fluid Mech. Stanford Univ. Press*, pages 301–316, 1965. (Cited on page 18, 19, 28, 31, 37, 43, 46, 53)

[191] STENNING A. AND VEZIROGLU T. Density-wave oscillations in boiling freon-11. *ASME Paper 66-WA/HT-49*, 1966. (Cited on page 15, 31, 37)

[192] STENNING A. AND VEZIROGLU T. Oscillations in two-phase component two-phase flow. Technical Report CR-72121, NASA Lewis Research Center Cleveland, Ohio, 1967. (Cited on page 31, 37, 43)

[193] STENNING A., VEZIROGLU T., AND CALLAHAN G. M. Pressure-drop oscillations in forced convection flow with boiling. *EUROATOM, Symposium of two-phase flow dynamics, Eindhoven*, pages 405–427, 1967. (Cited on page 16, 28, 31, 37, 43, 46)

[194] STEPHAN K. *Heat transfer in condensation and boiling*. Springer-Verlag, 1992. (Cited on page 40)

[195] STEWARD E., STEWARD P., AND WATSON A. Thermo-acoustic oscillations in forced convection heat transfer to supercritical pressure water. *Int. Journal Heat Mass Tranfer*, 16:257–270, 1973. (Cited on page 21)

[196] TADRIST L. Review on two-phase flow instabilities in narrow spaces. *International Journal of Heat and Fluid Flow*, 28:54–62, 2007. (Cited on page 10, 36)

[197] TAITEL Y. AND BARNEA D. Transient solution for flow of evaporating fluid in parallel pipes using analysis based on flow patterns. *International Journal of Multiphase Flow*, 37:469–474, 2011. (Cited on page 43)

[198] TAITEL Y. AND DUKLER A. A model for predicting flow regime transitions in horizontal and near horizontal gas-liquid flow. *AIChE Journal*, 22:47–55, 1976. (Cited on page 14)

[199] TAITEL Y., MINZER U., AND BARNEA D. A control procedure for the elimination of mal flow rate distribution in evaporating flow in parallel pipes. *Solar Energy*, 82:329–335, 2008. (Cited on page 42)

[200] TAITEL Y., PUSTYLNIK L., TSHUVA M., AND BARNEA D. Flow distribution of gas and liquid in parallel pipes. *International Journal of Multiphase Flow*, 29:1193–1202, 2003. (Cited on page 27, 39)

[201] TAKITANI K. Density wave instability in once-through boiling flow system, (ii). *Journal of Nuclear Science and Technology*, 15(6):389–399, 1978. (Cited on page 46)

[202] TALEYARKHAN R., PODOWSKI M., AND LAHEY R. A stability analysis of ventilated boiling channels. *Nuclear Engineering and Design*, 93:39–50, 1986. (Cited on page 41, 51)

[203] TAO Z., DEXUN H., KE R., AND ZIWEI S. Research on mechanism of flow excursion in narrow rectangle channel under natural circulation. *Nuclear Engineering and Design*, 254:1–4, 2013. (Cited on page 26, 39)

[204] THELER G., CLAUSSE A., AND BONETTO F. The mouving boiling-boundary model of a vertical two-phase flow channel. revisited. *Mecánica Computacional*, 29:3949–3976, 2010. (Cited on page 41)

[205] THURSTON R. AND ROGERS J. Pressure oscillation induced by forced convection heating of dense hydrogen. *Cryogenic Engineering Conference, CONF-660605-4, Bolder*, 1966. (Cited on page 21)

[206] TSHUVA M., BARNEA D., AND TAITEL Y. Two-phase ¯ow in inclined parallel pipes. *Int. Journal of multiphase flow*, 25:1491–1503, 1999. (Cited on page 27, 39)

[207] ÜNAL H. Density wave oscillations in sodium heated once-througt steam generator tubes. *J. Heat Transfer*, 103:485–491, 1981. (Cited on page 34)

[208] ÜNAL H. *Some aspects of two-phase flow, heat transfer and dynamic instabilities in medium and high pressure steam generators*. PhD thesis, Technological University of Delft, The Netherlands, 1981. (Cited on page 14, 34, 38)

[209] ÜNAL H. The period of density wave oscillations in forced convection steam generator tubes. *Int. J. Heat Mass Transfer*, 25(3):419–422, 1982. (Cited on page 34)

[210] ÜNAL H., VAN GASSELT M., AND LUDWIG P. Dynamic instabilities in tubes of large capacity, straight-tube, once-throut sodium heated steam generator. *Int. J. Heat Mass Transfer*, 20:1389–1399, 1977. (Cited on page 33)

[211] VAN DUYNE D., YOW W., AND SABIN J. Water hammer prevention, mitigation, and accommodation. Technical Report EPRI NP-6766, Electric Power Research Institute, Palo Alto, USA, 1992. (Cited on page 25)

[212] VEZIROGLU T. AND LEE S. Boiling flow instabilities in a cross-connected parallel channel upflow system. *ASME Paper 71-HT-12*, 1971. (Cited on page 33)

[213] WALLIS G. AND HEASLEY J. H. Oscillations in two-phase flow systems. *J. Heat Transfer*, 83(3):363, 1961. (Cited on page 31, 37, 46)

[214] WALLIS G. B. *One-dimensional two-phase flow*. McGraw-Hill, 1969. (Cited on page 40, 48)

[215] WANG Q., CHEN X. J., KAKAC S., AND Y.DING . An experimental investigation of density-wave-type oscillations in a convective boiling upflow system. *Int. J. Heat and Fluid Flow*, 15, 1994. (Cited on page 35, 39)

[216] WEDEKIND G. An experimental investigation into the oscillatory motion of the mixture-vapor transition point in horizontal evaporating flow. *J. Heat Transfer*, 93, 1971. (Cited on page 29)

[217] WESTENDORF W. AND BROWN W. Stability of intermixing of high-velocity vapor with its subcooled liquid in cocurrent streams. *NASA technical note, TN D-3553*, 1966. (Cited on page 22, 23, 255)

[218] WHALLEY P. *Boiling, Condensation and Gas-Liquid Flow*. Oxford University Press, New York, 1987. (Cited on page 40)

[219] XIAO M., CHEN X. J., ZHANG M. Y., VEZIROGLU T. N., AND KAKAC S. A multivariable linear investigation of two-phase flow instabilities in parallel boiling channels under high pressure. *Int. J. Multiphase Flow*, 19:65–77, 1993. (Cited on page 30, 38)

[220] XIONG T., YAN X., XIAO Z., LI Y., HUANG Y., AND YU J. Experimental study on flow instability in parallel channels with supercritical water. *Annuals of Nuclear Energy*, 48:60–67, 2012. (Cited on page 27, 39)

[221] YADIGAROGLU G. Regime transitions in boiling heat transfer. *Thermohydraulics of two-phase systems for industrial design and nuclear engineering, McGraw-Hill book Company*, 1981. (Cited on page 12)

[222] YADIGAROGLU G. Two-phase flow instabilities and propagation phenomena. *ch.17 in Thermohydraulics of two-phase systems for industrial design and nuclear engineering*, 1981. (Cited on page 10)

[223] YADIGAROGLU G. AND ASKARI B. Boiling water reactor stability revisited: The effects of flashing. *Nuclear Engineering and Design*, 235:1093–1105, 2005. (Cited on page 18)

[224] YADIGAROGLU G. AND BERGLES A. An experimental and theoretical study of density-wave phenomena oscillations in two-phase flow. Technical report, Department of Mechanical Engineering Mas sachus etts Institute of Te chnology imbridge, Massachusetts, 1969. (Cited on page 17, 32, 37, 46)

[225] YADIGAROGLU G. AND BERGLES A. Fundamental and higher mode density-wave oscillations in two-phase flows. *Journal of heat transfer, Trans. ASME*, 94:189–195, 1972. (Cited on page 32, 46, 255)

[226] YADIGAROGLU G. AND LAHEY R. A lagrangian analysis of two-phase hydrodynamic and nuclear-coupled density wave oscillations. *Proceeding of the fifth international Heat Transfer Conference, Tokyo*, 4, 1975. (Cited on page 47)

[227] YADIGAROGLU G. AND LAHEY R. On the various forms of the conservation equations in two-phase flow. *Int. J. Multiphase Flow*, 2:477–494, 1976. (Cited on page 40)

[228] YANG R., FENG J., AND LU Z. The analysis of two-phase flow instability in a vertical u-tube evaporator. *Wårme- und Steffubertragung*, 23:127–136, 1988. (Cited on page 34, 38)

[229] YANG X., JIANG S., AND ZHANG Y. Mechanism analysis on flow excursion of a natural circulation with low steam quality. *Nuclear Engineering and Design*, 235:2391–2406, 2005. (Cited on page 26)

[230] YAZAKI T., TOMINAGA A., AND NARAHARA Y. Stability limit for thermally driven acoustic oscillation. *Cryogenics*, pages 393–396, July 1979. (Cited on page 21)

[231] YILMAZ M., COMAKLI O., AND KARSLI S. The e!ect of inlet subcooling on two-phase #ow instabilities in a horizontal pipe system with augmented surfaces. *International Journal of Energy Research*, 26:110–131, 2002. (Cited on page 30)

[232] YOW W., VAN DUYNE D., AND CHIU C. Analysis of root causes of water hammer. *In: The Third International Topical Meeting on Nuclear Power Plant Thermal Hydraulics and Operations (NUPTHO-3)*, pages 103–109, 1988. (Cited on page 25)

[233] YUN G., JUN H., GENGLEI X., AND HEYI Z. Experiment investigation on two-phase flow instability in a parallel twin-channel system. *Annals of Nuclear Energy*, 37:1281–1289, 2010. (Cited on page 36, 39)

[234] YUNCU H. An experimental and theorethical study of density wave and pressure drop oscillations. *Heat transfer engineering*, 11:45–56, 1990. (Cited on page 29, 38, 45)

[235] YUNCU H., YILDIRIM O., AND KAKAC S. Two-phase flow instabilities in a horizontal single boiling channel. *Applied Scientific Research*, 481:83–104, 1991. (Cited on page 29, 44, 53, 255)

[236] ZHANG T., WEN J., JULIUS A., PELES Y., AND JENSEN M. K. Stability analysis and maldistribution control of two-phase flow in parallel evaporating channels. *Int. Journal Heat Mass Transfer*, 54:5298–5305, 2011. (Cited on page 43)

[237] ZHANG T., WEN J., PELES Y., CATANO J., ZHOU R., AND JENSEN M. Two-phase refrigerant flow instability analysis and active control in transient electronics cooling systems. *International Journal of Multiphase Flow*, 37: 84–97, 2011. (Cited on page 45)

[238] ZHANG T., TONG T., CHANG J.-Y., PELES Y., PRASHER R., K. M., JENSEN , WEN J. T., AND PHELAN P. Ledinegg instability in microchannels. *International Journal of Heat and Mass transfer*, 52:5661–5674, 2009. (Cited on page 26, 42)

[239] ZUBER N. Flow excursions and oscillations in boiling, two-phase flow systems with heat addition. *EUROATOM, Symposium of two-phase flow dynamics, Eindhoven*, pages 1071–1089, 1967. (Cited on page 9, 16, 46)

[240] ZUBER N. AND . FINDLAY J. A. Average volumetric concentration in two-phase flow systems. *J. Heat Transfer*, 1965. (Cited on page 33, 40, 48)

PART I

Numerical investigation

CHAPTER III

Least Squares Spectral Method for thermo-hydraulic problems

► The main objective of this chapter is to evaluate the application of the Least Squares method for solving thermo-hydraulic problems. A brief analysis of the typically used numerical methods is presented. In a general context, the *weighted residual* method is described in order to introduce the *least squares formulation*. The application of this method for a general system of equations is described in order to show the practical details of its implementation. In addition, the development of a general *hp-adaptive* solver for the resolution of thermo-hydraulic space-time problems is depicted. Finally, a numerical example is used to analyse the characteristics of the final scheme.

3.1 Introduction

As previously mentioned in Chapter 2, the numerical investigation of thermo-hydraulic systems was mainly developed for the study of *nuclear industry* safety. Nowadays, transient phenomena in thermo-hydraulic systems are simulated using several commercial codes, such as

- ATHLET(Germany, 1D, FVM 1^{st} order)
- CATHARE(France, 1D – 3D, FVM-FDM 1^{st} order)
- CATHENA(Canada, 1D, FDM 1^{st} order)
- RELAP5 (USA, 1D – 3D, FDM 1^{st} order)
- TRAC (USA, 1D – 3D, FDM 1^{st} order)

Moreover, in the oil and gas industries there are several commercial codes for simulating diabatic and adiabatic multi-phase and multi-component systems, such as

- OLGA(Norway, 1D/3D, 1^{st} order)

- PLAC (England, 1D 1^{st} order)
- TACITE (France, 1D 1^{st} order)
- PIPEPHASE, SimSci (England, 1D 1^{st} order)
- Aspen HYSIS (USA, 1D 1^{st} order)
- TRAFLOW (1D 1^{st} order)

In general, all of these commercial codes are developed based on three main numerical schemes:

- Finite Difference Methods (FDM), see G.A Sod [23]
- Finite Volumes Methods (FVM), see R. Leveque [15], S.V. Patankar [19]
- Galerkin-Finite Elements Methods (FEM), see P.G. Ciarlet [7], S. Brenner and R.L. Scott [5]

A large number of different numerical techniques to solve partial differential equations is available nowadays, although they have not been widely used in industrial applications. Some of them are: Orthogonal Collocation Method [24], Mesh Free Collocation Method [17], several versions of the FEM (Generalized Finite Element Method (GFEM), Extended Finite Element Method (XFEM), Spectral Finite Element Method (SFEM)). In particular, during the last years the *Least Squares Spectral Method* (LSSM) has gained a lot of attention, [4, 13]. Several advantages can be mentioned:

- Independent of the underlying equation, for any problem a well- or bad- posed problem results in a symmetric positive–definite systems of linear algebraic equations, which can be efficiently solved.
- For incompressible flows, least–squares can be applied without the limitation of the Ladyzhenskaya-Babuŝka-Brezzi (LBB) condition for the approximation order of the velocity and pressure fields, [2, 6].
- The Courant-Friedrichs-Lewy (CFL) number poses often as a stability criterion for explicit time integration methods. Since the time stepping method used in this work is unconditionally stable (fully implicit) there is no need to use a CFL number for stability reasons.
- For first order problems (e.g. an advective transport equation) the least squares method does not require special numerical treatment like the up–wind discretization in the Finite Difference Method. Thus, no numerical diffusion is introduced.
- The LSM meets the need for a-posteriori error analysis by supplying an error indicator in the form of the residuals that are minimized by the procedure. In particular, this is a very reliable indicator which can be used for adaptation.

The main disadvantages of using LSSM are: (1) the higher condition of the matrix system, compared with other methods such as Galerkin; (2) the regularity requirements for the global solution, also higher than Galerkin formulations.

The main objective of this chapter is to evaluate the implementation of LSSM, in the resolution of transient phenomena in thermo-hydraulic systems. In the next section, the method of *weighted residual* is introduced to derive the *least square formulation*. Then, the application of the LSSM in a general set of linear equations is used to describe the implementation of the methods. Finally, a general high-order adaptive framework for thermo-hydraulic systems and some applications are presented.

3.2 Method of weighted residuals

Given a general problem

$$\left\{ \begin{array}{rcll} \mathcal{L}\mathbf{u} & = & \mathbf{g} & in \quad \Omega \\ \mathcal{B}\mathbf{u} & = & \mathbf{u}_0 & on \quad \Gamma \subset \partial\Omega \end{array} \right. \tag{3.1}$$

where: $\mathbf{u}$ is the main unknown variable defined in a domain Ω; $\mathcal{L}$ is any linear partial differential operator; $\mathcal{B}$ is the boundary condition operator; $\mathbf{g}$ is a source term independent of $\mathbf{u}$; and $\mathbf{u}_0$ is the value of $\mathbf{u}$ at the boundary of the domain Γ. Then, the residual can be defined as

$$\mathcal{R}(\mathbf{u}) = \mathcal{L}\mathbf{u} - \mathbf{g} \tag{3.2}$$

The *Weighted Residual Formulation* (WRF) consists on seeking for the minimum of the residual function, weighted by a general function ϕ, over the entire domain. That is

$$\mathcal{J}(\mathbf{u}) \; = \; \int_{\Omega} \mathcal{R} \; \phi \; d\Omega \; \rightarrow \; \textbf{minimum} \tag{3.3}$$

In this context, according to the *weighting function* ϕ, different methods are obtained. In the Box 3.1, a summary of different methods and their particular *weighting functions* is presented. As it is possible to see, the *finite difference method* and the *finite volume method* depend on particular points $\mathbf{r}_j$. This family of methods is called "point discretization methods". Conversely, the methods depending on a set of basis functions are called "spectral approximation methods" (i.e. Galerkin, Least Squares, Orthogonal Collocation, etc).

Box 3.1: Weighted Residual Formulation

Method	Weighting Function
Finite differences	$\phi(\mathbf{r}) = \delta(\mathbf{r} - \mathbf{r}_j)$
Finite volumes	$\phi(\mathbf{r}) = 1 \;\; if \; \mathbf{r} \in \Omega_j$
	$= 0 \;\; if \; \mathbf{r} \notin \Omega_j$
Galerkin	$\phi(\mathbf{r}) = \psi_j$
Least-Squares	$\phi(\mathbf{r}) = \mathcal{R}$

where the functions ψ_j are the components of a complete set of basis functions in Ω.

3.3 The Least Squares formulation

As described before, the *least squares method* is a particular case of the *weighted residual formulation*. Given the system defined in Eq. (3.1) and assuming that it is well-posed, $\mathcal{L}$ is a linear differential operator and there are two Hilbert scales $X(\Omega)$ and $Y(\Gamma)$ x $Y(\Omega)$ such that $(\mathcal{L}, \mathcal{B})$ has a complete set of homeomorphisms, [21]. Then, the norm-equivalent functional becomes

$$\mathcal{J}(\mathbf{u}) \;=\; \frac{1}{2}\left(||\mathcal{L}-\mathbf{g}||^2_{Y(\Omega)} \;+\; ||\mathcal{B}-\mathbf{u}_0||^2_{Y(\Gamma)}\right) \tag{3.4}$$

In consequence, minimising the functional $\mathcal{J}$ for $\mathbf{u}$ means:

Find $\mathbf{u} \in X(\Omega)$ such that

$$\lim_{\epsilon \to 0} \frac{d}{d\epsilon} \mathcal{J}(\mathbf{u} + \epsilon \, \mathbf{v}) = 0 \quad \forall \, \mathbf{u} \in X(\Omega) \tag{3.5}$$

Hence, the necessary condition for the minimisation of $\mathcal{J}$ is equivalent to:

Find $\mathbf{u} \in X(\Omega)$ such that

$$\mathcal{A}(\mathbf{u}, \mathbf{v}) = \mathcal{F}(\mathbf{v}) \quad \forall \mathbf{v} \in X(\Omega) \tag{3.6}$$

with

$$\mathcal{A}(\mathbf{u}, \mathbf{v}) \;=\; \int_\Omega \mathcal{L}\mathbf{u} \; \mathcal{L}\mathbf{v} \; d\Omega \;+\; \int_\Gamma \mathcal{B}\mathbf{u} \; \mathcal{B}\mathbf{v} \; d\Gamma \tag{3.7}$$

$$\mathcal{F}(\mathbf{v}) \;=\; \int_\Omega \mathbf{g} \; \mathcal{L}\mathbf{v} \; d\Omega \;+\; \int_\Gamma \mathbf{u}_0 \; \mathcal{B}\mathbf{v} \; d\Gamma \tag{3.8}$$

where $\mathcal{A} : X \times X \to \mathbb{R}$ is a symmetric, continuous bi-linear form, and $\mathcal{F} : X \to \mathbb{R}$ a continuous linear form. The introduction of the boundary residual allows the use of spaces $X(\Omega)$ that are not constrained to satisfy the boundary conditions.

3.3.1 Element splitting

The domain Ω is divided into N_e non-overlapping sub-domains Ω^e, called spectral elements, such that

$$\Omega = \bigcup_{e=1}^{N_e} \Omega^e, \qquad \Omega^e \cap \Omega^l = \emptyset, \quad e \neq l \tag{3.9}$$

In consequence, the global function $\mathbf{u}$ can be expressed as the union of the local functions in each element

$$\mathbf{u} = \bigcup_{e=1}^{N_e} \mathbf{u}^e \tag{3.10}$$

3.3.2 The discretized formulation

After partitioning the domain, a *series expansion* of the solution in each element is defined in order to approximate the functions $\mathbf{u}^e$, such as

$$\mathbf{u^e} \simeq \mathbf{u_h^e} = \sum_{j=0}^{N_a} u_j^e \psi_j \qquad \psi_j \in X_h^e(\Omega^e) \subset X^e(\Omega^e) \tag{3.11}$$

notice that the approximated space $X_h^e(\Omega^e)$ has a finite-dimension while the space $X^e(\Omega^e)$ has an infinite-dimension.

Therefore, the approximated solutions in each elements will be restricted to a linear combination of the functions $\{\psi_j\}$ defined in $X_h^e(\Omega^e)$. In consequence, replacing Eq. (3.11) in Eqs. (3.7, 3.8) the solution, in each element, is given by

$$\sum_{j=0}^{N_a} \mathcal{A}^e(\psi_j, \psi_i)\, u_j^e = \mathcal{F}^e(\psi_i) \qquad \forall \psi_i \in X_h^e(\Omega^e) \tag{3.12}$$

where

$$\mathcal{A}^e(\psi_j, \psi_i) = \int_\Omega \mathcal{L}\psi_j \, \mathcal{L}\psi_i \, d\Omega + \int_\Gamma \mathcal{B}\psi_j \, \mathcal{B}\psi_i \, d\Gamma \tag{3.13}$$

$$\mathcal{F}^e(\psi_i) = \int_\Omega \mathbf{g} \, \mathcal{L}\psi_i \, d\Omega + \int_\Gamma \mathbf{u}_0 \, \mathcal{B}\psi_i \, d\Gamma \tag{3.14}$$

3.3.3 Numerical integration and quadratures

As shown in Eqs. (3.13) and (3.14), within each element it is still necessary to evaluate the integral function. The *Gaussian quadrature method* consists on taking an approximation of order O_q over the integral, such as

$$\int_\Omega f(r)\, d\Omega \simeq \sum_{q=0}^{O_q} w_q \, f(r_q) \tag{3.15}$$

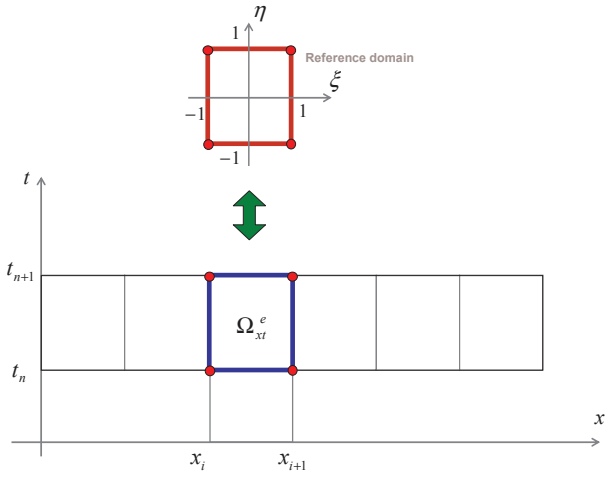

Figure 3.1: *Time–space formulation to solve a one-dimensional transient problem. The space is divided in different elements and in every time step the solution, in each element, is converged.*

with $(O_q + 1)$ number of quadrature points (r_q) and quadrature weights (w_q). Therefore, the choice of the points and weights will define the accuracy of the quadrature integration.

Finally, the integrals of Eqs. (3.13 and 3.14) are approximated by quadratures $(\mathbf{r}_q, w_q)$ in Ω and $(\mathbf{r}_m, w_m)$ in Γ. Thus, the general discretized formulation of the problem is reduced to an algebraic system, that is expressed as

$$\begin{aligned}
\mathcal{A}^e(\psi_j, \psi_i) \simeq A^e_{ij} &= \sum_{q=0}^{N_q} w_q \, \mathcal{L}\psi_j(\mathbf{r}_q) \, \mathcal{L}\psi_i(\mathbf{r}_q) + \sum_{m=0}^{N_m} w_m \, \mathcal{B}\psi_j(\mathbf{r}_m) \, \mathcal{B}\psi_i(\mathbf{r}_m) \\
\mathcal{F}^e(\psi_i) \simeq F^e_i &= \sum_{q=0}^{N_q} w_q \, \mathbf{g}(\mathbf{r}_q) \, \mathcal{L}\psi_i(\mathbf{r}_q) + \sum_{m=0}^{N_m} w_m \, \mathbf{u}_0(\mathbf{r}_m) \, \mathcal{B}\psi_i(\mathbf{r}_m) \quad (3.16)
\end{aligned}$$

3.4 One-dimensional transient problems

Until now, the general formulation for a *least squares spectral method* was presented. In this section, the problem is restricted to a two-dimensional space-time domain. This formulation is based on a time-space formulation using a time marching approach, such as the ones presented in [20, 8]. In each time strip, the solution will be converged before moving to the next time–space strip. Thus, the domain becomes $\Omega^e = \Omega^e_x \times \Omega^e_t = (x_e, x_{e+1}) \times (t_n, t_{n+1})$, with $\Delta t = t_{n+1} - t_n$, as indicated in Figure 3.1.

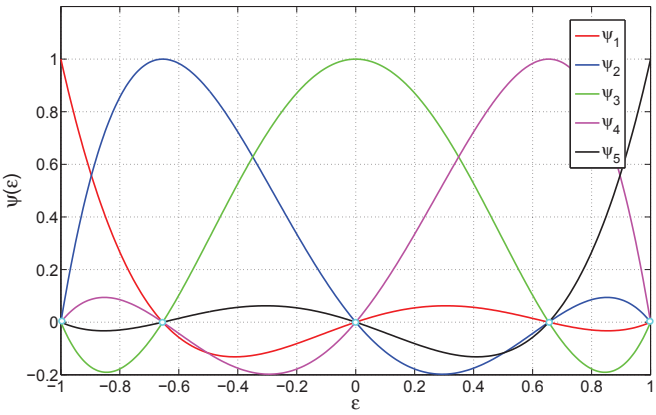

Figure 3.2: *Legendre polynomials defined over a set of GLL collocation points, in a one-dimensional generic domain [-1,1].*

In this work, the discretization points for each element of the space-time domain are based on the Gauss Lobatto Legendre (GLL) set of collocation points. In addition, the nodal series expansion is also based on the same discretization, by taking the Legendre polynomials defined over the Gauss-Lobatto collocation points. In the Figure 3.2, the polynomials corresponding to a GLL discretization of order 4 (4+1 points) in a general one-dimensional domain are shown. The local approximated solution $\mathbf{u}_h^e$ can be finally expressed as

$$\mathbf{u}_h^e(z,t) = \sum_{i=0}^{N_z} \sum_{j=0}^{N_t} u_{ij}^e \, \varphi_i(z) \, \varphi_j(t), \quad \text{with} \quad u_{ij}^e = u(z_i, t_j) \tag{3.17}$$

where $\varphi_i(z)$ and $\varphi_j(t)$ are the one-dimensional set of Legendre polynomials mentioned before.

Box 3.2: Legendre polynomials through GLL collocation points

For example the polynomial $\varphi_j(z)$ defined in the reference domain $\hat{\Omega} = [-1, 1]$ is given by

$$\varphi_j(z) = \frac{(z^2-1)\dfrac{dL_{N_z}(z)}{dz}}{N_z(N_z+1)L_{N_z}(z)(z-z_j)} \tag{3.18}$$

where the $(N_z + 1)$ GLL–points, z_j, are the roots of the first derivative of the Legendre polynomial of degree N_z, extended with the boundary nodes as described in [9].

In summary, for a general problem given by the operators $(\mathcal{L}, \mathcal{B})$, Eq. (3.1), the final algebraic system can be expressed as:

Find the coefficients u^e_{ij}, such that

$$\sum_{i=0}^{N_z}\sum_{j=0}^{N_t} A^e_{ijkm} u^e_{ij} \;=\; F^e_{km} \qquad \forall\, k = 0, ..., N_z \quad m = 0, ..., N_t \tag{3.19}$$

where

$$A^e_{ijkm} \;=\; \sum_{iz=0}^{N_z}\sum_{it=0}^{N_t} w_{iz}\, w_{it}\, \mathcal{L}(\varphi_i(z_{iz})\varphi_j(t_{it}))\, \mathcal{L}(\varphi_k(z_{iz})\varphi_m(t_{it})) \tag{3.20}$$

$$F^e_{km} \;=\; \sum_{iz=0}^{N_z}\sum_{it=0}^{N_t} w_{iz}\, w_{it}\, \mathcal{L}(\varphi_k(z_{iz})\varphi_m(t_{it}))\, g_{km}\varphi_k(z_{iz})\varphi_m(t_{it}) \tag{3.21}$$

in this case the boundary conditions would be imposed in a weakly form in the borders $z = z_{min}$ and $z = z_{max}$ according to the problem. Respectively the initial condition, $\mathbf{u_0}$, would be imposed in $t = t_n$. Notice also that the source terms given by $\mathbf{g}$ were approximated by taking the GLL expansion series as shown in Eq. (3.21).

Finally, the problem can be rearranged in a global matrix-vector system,

$$\bar{\bar{A}}\, \bar{\mathbf{u}}_h = \bar{F} \tag{3.22}$$

where the dimension of the vector $\bar{\mathbf{u}}_h$ will be $N_D = N_e \mathrm{x} N_z \mathrm{x} N_t$ and $\bar{\bar{A}}$ will be a positive-definite square matrix of dimension $N_D \mathrm{x} N_D$. As commented before, several numerical methods allow to solve this kind of square symmetric systems in a very efficient manner (e.g. conjugate gradient method).

3.4.1 Numerical error estimator and adaptivity

The residual defined by the functional $\mathcal{J}(\mathbf{u})$ can be expressed as

$$\mathcal{J}(\mathbf{u}) = \int_\Omega \left(\mathcal{L}\mathbf{u}_h - \mathbf{g}\right)^2 d\Omega \tag{3.23}$$

where $\mathbf{u}_h$ is the numerical approximated solution. This residual can be used as an error estimator, since it indicates how big the error of the numerical solution is. Following the steps presented in the Section 3.4, the error estimator in each element becomes

$$\mathcal{R}^e \;=\; \sum_{iz=0}^{N_z}\sum_{it=0}^{N_t} w_{iz}\, w_{it} \sum_{i=0}^{N_z}\sum_{j=0}^{N_t} \left(u^e_{ij}\mathcal{L}(\varphi_i(z_{iz})\varphi_j(t_{it})) - g_{ij}\varphi_i(z_{iz})\varphi_j(t_{it})\right)^2 \tag{3.24}$$

In conclusion, the $\mathcal{R}^e$ error estimator can be used locally, in each element, for local adaptation or the sum over all the elements can be used to adapt the main parameters of the global marching scheme [20, 8]. Hence, according to the numerical formulation proposed in the previous sections, there are four main parameters that would define the accuracy of the numerical scheme. They are

- O_z: $(N_z - 1)$ Approximation Order of the space variable
- O_t: $(N_t - 1)$ Approximation Order of the time variable
- N_e: Elements number in the space domain
- Δt: Time step

As can be seen, several possible adaptation strategies can be implemented, depending on the choice of the discretization parameters to be modified. The strategy in normally decided based on the experience of the user and the particular problem. In [8] more details of the residual and the convergence of the problem can be founded. In general, when the order of approximation is modified it is said that the scheme is *p-adaptive* (O_z, O_t). Moreover, when the size of the elements is modified the scheme is called *h-adaptive* $(\Delta t, N_e)$. Different adaptation strategies will be presented and analysed in the next chapter. In the next section, the general description of a hp-adaptive framework for thermo-hydraulic systems is described.

3.5 General hp-adaptive framework for the resolution of thermo-hydraulic systems

In the previous sections, the basic concepts of the LSSM implementation for a general linear problem were presented. The main idea in this section is to describe the particular application of the LSSM to the resolution of thermo-hydraulic problems, based on conservation equations. In the Figure 3.3 a flow chart of the numerical solver is presented. The solver framework is divided in four main parts: *Definitions and initialisation*, *Time steps loop*, *Non-linear loop* and the *Elements loop*. In the next sections, a brief description of these parts is presented.

3.5.1 Definitions and initialisation

In this first part, the general conditions of the problems are set up. First, the two-dimensional space-time mesh is generated. Then, all the variables of the problem are created and initialised. If necessary, a stable point calculation is performed and set as initial state, depending on the problem.

3.5.2 Time steps loop

This is the main loop of the solver. Following the Figure 3.3 the different stages are described in the following.

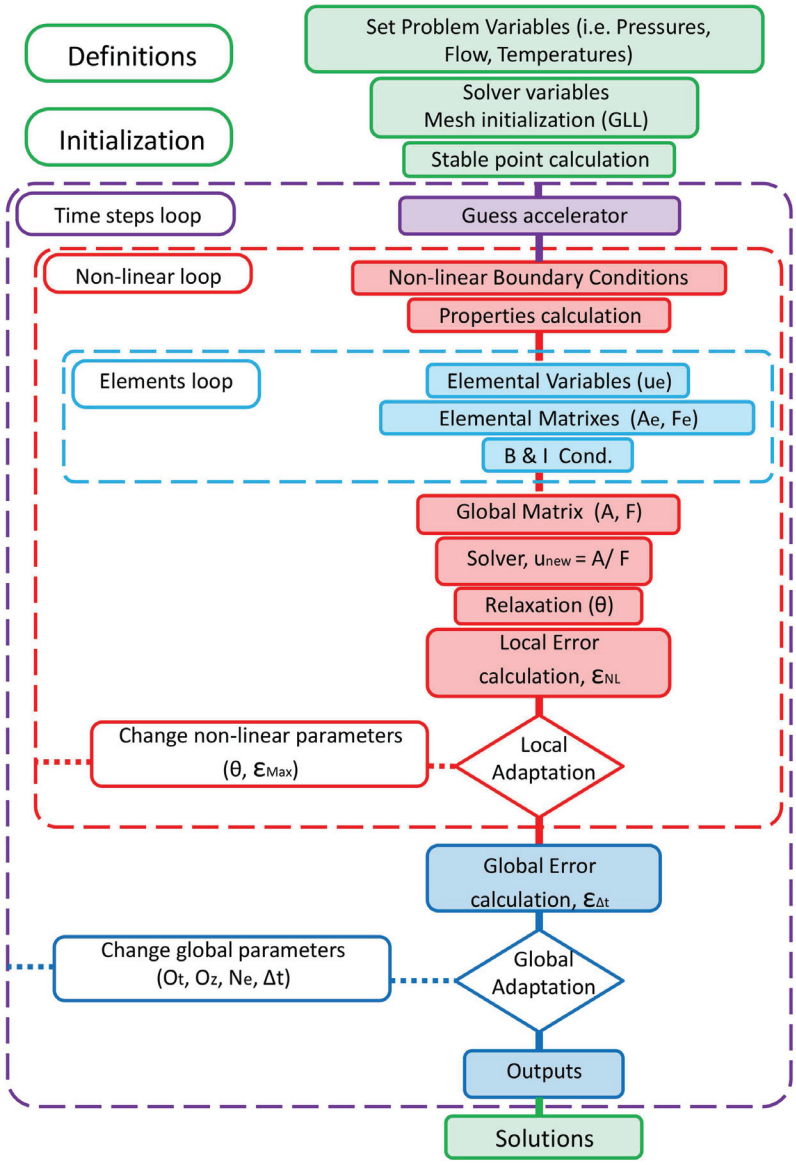

Figure 3.3: *Flow chart of the non-linear solver based on a least squares spectral method.*

- **Guess accelerator:** A guess solution for the main variable, $\mathbf{u}_h$, is set up. This guess step is simply to save computational time (non-linear iterations), since the solution of the previous step $\mathbf{u}_{h\_prev}$, is normally differing from the non-linear solution in the current step. Thus, according to the time evolution of the different variables and the boundary conditions a guess solution is taken.

- **Non-linear loop:** As presented before, the LSSM is derived assuming a linear operator $\mathcal{L}$. Therefore, the set of equations describing the problem must be linearised and, consequently, a non-linear loop have to be implemented in order to deal with the non-linear components, typical from any thermo-hydraulic system. In this work, a *Picard* method is chosen for the iteration process. The following list describe the main steps performed inside this non-linear loop.

  - **Non-linear Boundary Conditions:** Normally, for thermo-hydraulic systems, the boundary conditions depend on the main variables values (e.g. the pressure drop in a valve). In this step, the boundary conditions are updated according to the current non-linear step solution, $\mathbf{u}_h$.
  - **Properties Calculation:** The main properties (density, void fraction, temperature, etc.) may depend on the variables (enthalpy, pressure, etc.). According to the chosen models and closing laws, the properties are updated to the value of the current non-linear solution of the main variables normally contained in $\mathbf{u}_h$.

  - **Elements loop:** The elements loop consists in the following steps:
    - *Elements Variables:* The local element variables, u_h^e and main properties are calculated from the global variables u_h.
    - *Elemental Matrices:* Using the results of the Eq. (3.20), the elemental matrix and source terms are assembled.
    - *Boundary and Initial Conditions:* The boundary and initial conditions are imposed weakly to the specific nodes, as explained before.

  - **Global matrix assembling and solver:** The global matrix and source vector $(\bar{\bar{A}}, \bar{F})$ are assembled by gathering the elemental matrices and sources vectors, (A^e, F^e). The system is solved by using a conjugate gradient method and a new solution, $\mathbf{u}_{h\_sol}$ is obtained.
  - **Relaxation:** A relaxation technique is used in order to improve the convergence of the system in the case of highly non-linear problems. In the following equation the relaxation technique is applied to the solution $\mathbf{u}_{h\_sol}$,

$$\mathbf{u}_{h\_new} \;=\; (\theta)\mathbf{u}_{h\_sol} \;+\; (1-\theta)\,\mathbf{u}_{h\_prev} \tag{3.25}$$

    where $\mathbf{u}_{h\_prev}$ corresponds with the solution of the previous nonlinear step and θ is the relaxation parameter bounded in the interval $(0, 1)$. The

new solution will be a linear combination of the previous step and the new non-linear solutions.

- **Local Error:** the local error is calculated as

$$\varepsilon_{NL} = \mathbf{u}_{h\_new} - \mathbf{u}_{h\_prev} \tag{3.26}$$

according to this error, the non-linear loop will stop when ε_{NL} becomes smaller than the maximum non-linear error ε_{Max}.

- **Local Adaptation:** According to the strategy of adaptation the parameters (θ, ε_{Max}) can be modified. Generally this parameters are not modified, but for the cases of expensive problems, this kind of local adaptivity can improve significantly total computational time.

- **Global error calculation, $\varepsilon_{\Delta t}$:** Using the Eq. (3.24) for the element error estimator, the global error for each time step is calculated as the sum of all the elements error estimators. That is

$$\varepsilon_{\Delta t} = \sum_{e=1}^{N_e} \mathcal{R}^e \tag{3.27}$$

- **Global adaptation:** According to the value of $\varepsilon_{\Delta t}$ and the adaptive strategy chosen for each problem there exist two options:

  Adaptation The time step solution is dismiss. Some of the parameters, (O_z, O_t, N_e, Δ_t), are changed and the mesh and variables are initialised for this new domain with the conditions of the previous time step.

  No-adaptation The time step solution is accepted.

- **Outputs:** The time step solutions are saved as the output variables

In this section the main description of the solver developed and utilised in this work was presented. In the next and finally part, a numerical example is presented.

3.6 Numerical example: Fast transient phenomena in supercritical fluids

A pressure wave propagation problem in a supercritical fluids will be presented in this section. This kind of problems are of particularly interesting to evaluate numerical methods performance for the numerical complexity and also for the involved physical phenomena.

A super-critical fluid presents physio-chemical properties that are between those of liquids and gases, according to the thermodynamic state. These particular properties have motivated the application of super-critical fluid in several technological

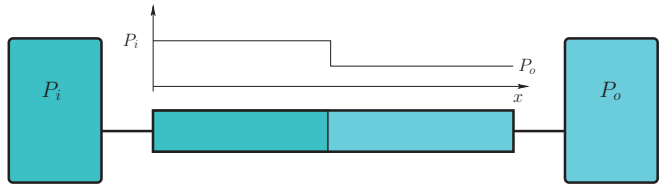

Figure 3.4: *Scheme of the shock tube problem.*

areas, such as pulse cleaning [18], solute formation of powders [16], etc. In addition, these phenomena are investigated in the transport of CO_2 in supercritical conditions as described by [3] and the development of super-critical nuclear reactors, see [10].

The numerical modelling and simulation of transient phenomena in super-critical fluids is quite challenging due to the complexity of the physical process and the temporal and spatial scales involved. In [14] the simulations of shock tube problems for gas and super-critical CO_2, using the *finite volume method*, are described. Moreover, several articles describe the use of first order methods in the simulation of these kind of phenomena in supercritical CO_2, [11, 12, 25, 1]. The introduction of numerical diffusion using traditional finite difference method is described in [23]. As described in this last work, the influence of numerical diffusion is an undesirable effect that can notably influence the numerical solution.

3.6.1 The Model

The shock tube problem consists of a diaphragm that divides a tube in two regions at different pressures and same temperature, as sketched in Figure 3.4. At time $t > 0$ the diaphragm bursts and three different kinds of waves move into the domain, Figure 3.5. A rarefaction wave (R) moves to the left at the speed of the sound (interaction between pressure and flow). This rarefaction wave is not discontinuous even when the initial conditions are discontinuous, since the slope of the wave decreases when it moves. A second wave called contact discontinuity (C) moves to the right with the velocity of a particle in the fluid (slow enthalpy wave). In this case no discontinuity is observed in the pressure profile but discontinuities are shown in the rest of the variables. The last wave is called shock wave (S) and it is moving to the right with discontinuities in the main variables profiles, due to the negative gradient of the velocity.

The mathematical model used to describe the evolution of the system is based on conservation laws. Mass, momentum and energy equations can be expressed as

$$\frac{\partial \rho}{\partial t} + \frac{\partial G}{\partial z} = 0 \tag{3.28}$$

$$\frac{\partial G}{\partial t} + \frac{\partial}{\partial z}\left(\frac{G^2}{\rho}\right) + \frac{\partial P}{\partial z} + \frac{f}{D_H}\frac{|G|G}{2\rho} = 0 \tag{3.29}$$

$$\frac{\partial \rho h}{\partial t} + \frac{\partial G h}{\partial z} = \frac{DP}{Dt} \tag{3.30}$$

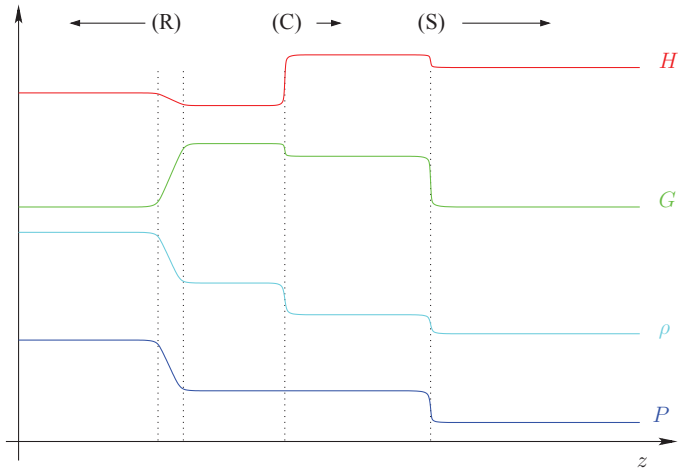

Figure 3.5: *Scheme of the shock waves in enthalpy, flow, density and pressure, after for the shock tube problem.*

where G is the mass flux; P is the static pressure; h is the specific enthalpy; ρ is the density; f is the Darcy-Weisbach friction factor; D_H is the diameter of the pipe; z is the space coordinate and t the time coordinate. The friction factor f, is calculated using the "Colebrook and Blasius" pressure drop correlation. Friction losses and temperature diffusion are neglected in the energy equation, due to the low influence ($\approx 10^{-4}$) respect to the $\frac{DP}{Dt}$ term. In this example, the system is closed calculating in each point the density with the specific enthalpy and absolute pressure using REFPROP V 8.0 [22].

The initial condition for the pressure profile is a step function corresponding with the values of P_{in} and P_{out} as shown in Figure 3.4. The initial flow is set to zero and the initial enthalpy profile is calculated with the values of the pressure and the initial constant temperature, T_{in}.

3.6.2 Linearization

The linear set of equations of the system described in Eqs. (3.28) and (3.30) results in

$$\begin{aligned} \frac{\partial \rho^*}{\partial t} + \frac{\partial G}{\partial z} &= 0 \\ \frac{\partial G}{\partial t} + \frac{\partial}{\partial z}\left(\frac{G^{*2}}{\rho^*}\right) + \frac{\partial P}{\partial z} + \frac{f}{D_H}\frac{G^{*2}}{2\rho^*} &= 0 \\ \frac{\partial \rho^* h}{\partial t} + \frac{\partial G^* h}{\partial z} - \frac{DP}{Dt} &= 0 \end{aligned}$$

where G^* and ρ^* correspond to the values of the previous non-linear step, as explained before. Hence, using the operator description of Eq. (3.1)), it is possible to

rewrite the linearised system as

$$\mathcal{L} = \begin{Bmatrix} \frac{\partial \bullet}{\partial z} & 0 & 0 \\ \frac{\partial \bullet}{\partial t} & \frac{\partial \bullet}{\partial z} & 0 \\ 0 & -\frac{D \bullet}{Dt} & \rho^* \frac{\partial \bullet}{\partial t} + G^* \frac{\partial \bullet}{\partial z} \end{Bmatrix} \tag{3.31}$$

$$\mathbf{g} = \begin{Bmatrix} -\frac{\partial \rho^*}{\partial t} \\ -\frac{\partial}{\partial z}\left(\frac{G^{*2}}{\rho^*}\right) - \frac{f}{D_H}\frac{G^{*2}}{2\rho^*} \\ 0 \end{Bmatrix} \tag{3.32}$$

$$\mathbf{u} = \begin{Bmatrix} G \\ P \\ h \end{Bmatrix} \tag{3.33}$$

3.6.3 Numerical Results

The numerical simulation of the shock wave in super-critical CO2 was performed using a 4 order approximation for both time and space, with a time slag of $\Delta t = 2\ 10^{-6} sec$ and $Ne = 100$ (number of elements). The non-linear maximum error was set as $\varepsilon_{Max} = 10^{-6}$. The main parameters of the simulations are:

- Fluid: CO2
- L = 1m, D_H = 25mm
- P_{in} = 90 10^5 Pa, P_{out} = 80 10^5 Pa, T_{in} = 32 ^oC

In the Figures 3.6(a) to 3.7 the evolution of the main variables and the dynamic of the three waves are shown. (S) and (R) waves move with a velocity $\approx$ 300 $\frac{m}{s}$ (sound velocity), whereas the (C) wave moves with a velocity of $u = \frac{G}{\rho} \approx 2.3 \frac{m}{s}$ (particle velocity).

Figure 3.6(a) shows the evolution of the pressure in the moment after the diaphragm breaking. As described by [23], the discontinuity in the pressure split in two shock waves, (R) and (S). Nevertheless the pressure profile does not change with the (C) contact wave. In Figure 3.6(b) the evolution of the flow is presented. In contrast with the pressure profile the (C) wave is also present in the flow profile. These variations in the flow profile are due to the changes in density. This effect is not described in [14], probably due to diffusion of the method used to simulate this transient behaviours.

The other thermodynamic variables, enthalpy, density and temperature, are plotted in the Figure 3.7. An enthalpy dependence with the pressure changes is observed due to the last term in Eq. (3.30). These changes in the enthalpy profile also affect

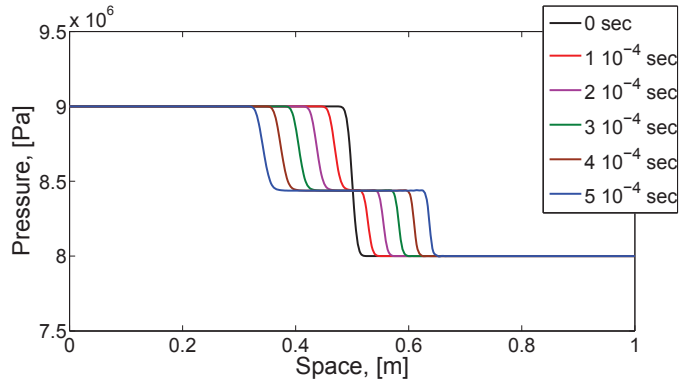

(a) Pressure profile

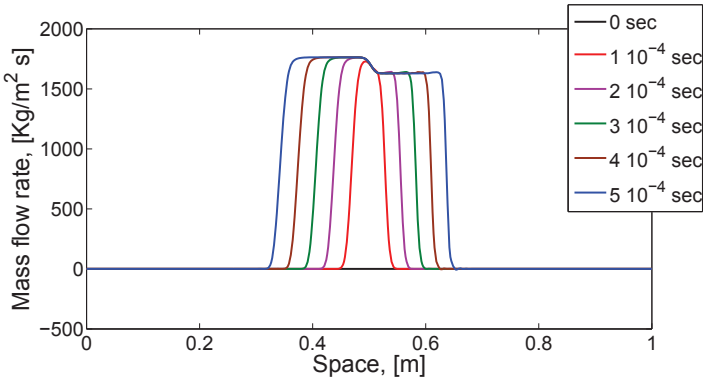

(b) Flow profile

Figure 3.6: *Evolution of pressure and flow profiles during the shock tube simulation.*

the values of the density and temperature profiles, according with the working conditions. The three waves described are observed in the density profile. However, for the density profile the (C) wave is the most influencing ($\approx 60\%$ of the total change). Finally a non-negligible discontinuity, of more than one centigrade degree in the temperature profiles is observed. These phenomena are due to the variations in the pressure and the enthalpy as a result of the shock waves.

3.6.4 Discussion

A transient shock tube problem with super-critical CO2 was described in the previous sections. The *least squares method* have proved to correctly describe the evolution of this system. Moreover, as a result of the low diffusion of the numerical method, it is possible to see the contact shock wave phenomenon in the flow profile. The high accuracy of the method allows to make a detailed description of the wave propagation for the shock tube.

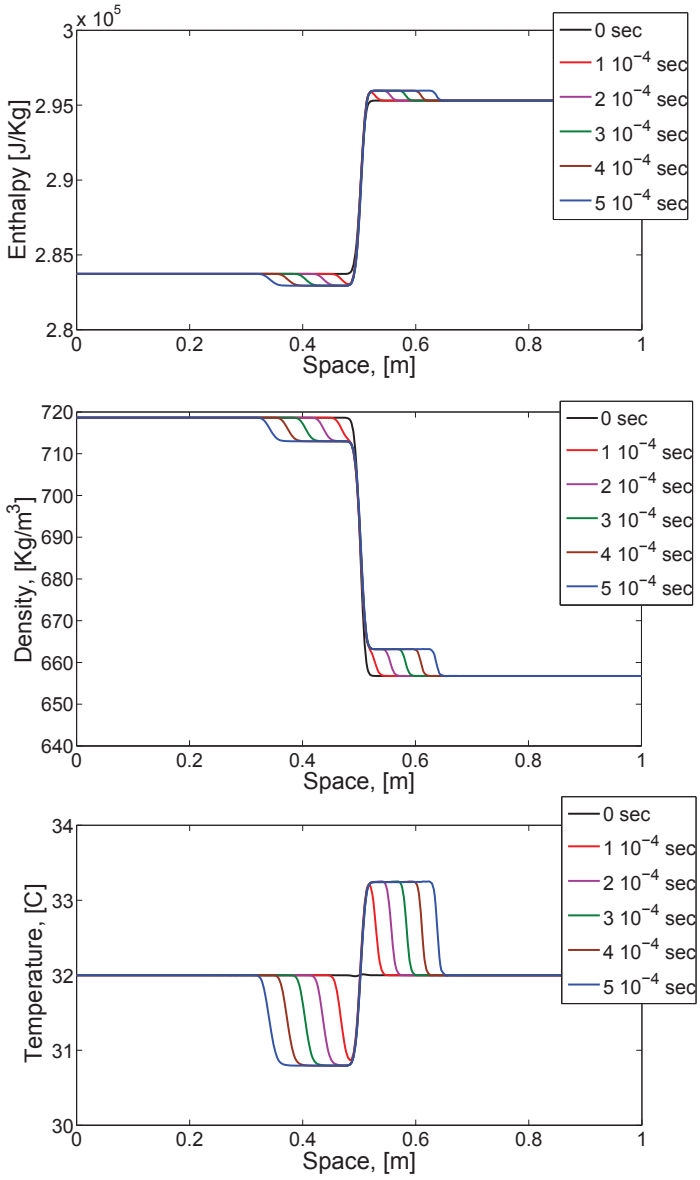

Figure 3.7: *Evolution of the enthalpy, density and temperature profiles during the shock tube simulation.*

3.7 Summary

The Least Squares Method for the simulation of transient problems was presented. The most relevant aspects of a numerical framework used to solve one-dimensional transient problems were described. The framework was based on a coupled space-time formulation. Furthermore, the use of hp-adaptivity in the resolution of thermo-hydraulic non-linear problems was presented. Finally, numerical examples were used in order to test the developed framework.

Bibliography

[1] AMBROSINI W. On the analogies in the dynamic behaviour of heated channels with boiling and supercritical fluids linear and nonlinear analysis of density wave instability phenomena. *Nuclear Engineering and Design*, 237:1164–1174, 2007. (Cited on page 89)

[2] BABUSKA I. s on the schwarz algorithm in the theory of differential equations of mathematical physics. *Tchacosl. Math. J. (Russian)*, 8:328–342, 1958. (Cited on page 78)

[3] BARRIE J., BROWN K., HATCHER P., AND SCHELLHASE H. Carbon dioxide pipelines: A preliminary review of design and risk. *In Greenhouse Gas Control Technologies 7. Vancouver, Canada.*, 2004. (Cited on page 89)

[4] BONAN J. The least-square finite element method: Theory and applications in computational fluid dynamics and electromagnetics. *Springer*, 1998. (Cited on page 78)

[5] BRENNER S. AND SCOTT R. *The Mathematical Theory of Finite Element Methods*. Springer, 2nd edition, 2005. (Cited on page 78)

[6] BREZZI F. On the existence, uniqueness, and approximation of saddle-point problems arising from lagrange multipliers. *R.A.I.R.O.*, 8:479–506, 1974. (Cited on page 78)

[7] CIARLET P. *The Finite Element Method for Elliptic Problems*. North-Holland, 1978. (Cited on page 78)

[8] DE MAERSCHALCK B. AND GERRISTMA M. I. Least-squares spectral element method for non-linear hyperbolic differential equations. *Journal of Computational and Applied Mathematics*, 215(2):357–367, 2008. (Cited on page 82, 85)

[9] DEVILLE M., FISHER P., AND MUND E. High-order methods for incompressible fluid flow. *Cambridge University Press.*, 2002. (Cited on page 83)

[10] DOSTAL V., DRISCOLL M., AND HEJZLAR P. A supercritical carbon dioxide cycle for next generation nuclear reactors. *MIT-ANP-Series, MIT-ANP-TR-100*, 2004. (Cited on page 89)

[11] GARCIA-VALLADARES O. Numerical simulation of trans-critical carbon dioxide flow through short tube orifices. *Applied Thermal Engineering*, 26: 144–151, 2006. (Cited on page 89)

[12] HAGHSHENAS FARD M., HOOMAN K., AND CHUA H. Numerical simulation of a supercritical co2. *International Communications in Heat and Mass Transfer*, 2010. (Cited on page 89)

[13] KARNIADAKIS G. E. AND SHERWIN S. *Spectral/hp Element Methods for Computational Fluid Dynamics*. Oxford Science Publications, 2005. (Cited on page 78)

[14] KSIBI H. AND MOUSSA A. Numerical simulation of a one-dimensional shock tube problem at critical fluid conditions. *Internal Journal of physical Sciences*, 3:314–320, 2008. (Cited on page 89, 91)

[15] LEVEQUE R. *Finite Volume Methods for Hiperbolic Problems*. Cambridge University Press, 2002. (Cited on page 78)

[16] MATSON D., FULTON J., PETERSEN R., AND SMITH R. Rapid expansion of supercritical fluid solutions: solute formation of powders, thin films, and fibers. *Industrial & Engineering Chemistry Research*, 26:2298–2306, 1987. (Cited on page 89)

[17] NETUZHYLOV H. AND ZILIAN A. Space-time meshfree collocation method: methodology and application to initial-boundary value problems. *International Journal for Numerical Methods in Engineering*, 80(3):355–380, 2009. (Cited on page 78)

[18] OTA K. AND TSUTSUMI A. Supercritical CO_2 pulse cleaning in deep microholes. *Journal of advanced mechanical design, systems, and manufacturing*, 2:619–628, 2008. (Cited on page 89)

[19] PATANKAR S. *Numerical Heat Transfer and Fluid Flow*. McGraw-Hill, 1980. (Cited on page 78)

[20] PONTAZA J. AND REDDY J. Space–time coupled spectral/hp least squares finite element formulation for the incompressible navier–stokes equation. *Journal of Computational Physics*, 190(2):418–459, 2004. (Cited on page 82, 85)

[21] PROOT M. AND GERRITSMA M. Application of the least-squares spectral element method using chebyshev polynomials to solve the incompressible navier-stokes equations. *Numerical Algorithms*, 38:155–172, 2005. (Cited on page 80)

[22] REFPROP V 8.0 , 2007. Reference fluid thermodynamics and transport properties, NIST Standard Reference Database 23, Gaithersbug, MD 20899, USA. (Cited on page 90)

[23] SOD G. A survey of several finite difference methods for systems of nonlinear hyperbolic conservation laws. *Journal of Computational physics*, 21:1–31, 1978. (Cited on page 78, 89, 91)

[24] VILLADSEN J. AND STEWART W. Solution of boundary-value problems by orthogonal collocation. *Chemical Engineering Science*, 22(11):1483–1501, 1967. (Cited on page 78)

[25] ZHONGXUAN D., WENSHENG L., AND ANZHONG G. Numerical investigation of cooling heat transfer to supercritical co2 in a horizontal circular tube. *J. of Supercritical Fluids*, 2010. (Cited on page 89)

CHAPTER IV

Simulation of a single-phase natural circulation loop using a least squares hp-adaptive solver

► In this chapter the performance of the adaptive high-order method, developed in the previous chapter, is analysed. A single-phase natural circulation loop is simulated in order to evaluate the accuracy and the computational time in the resolution of non-linear systems. Finally, several numerical simulations are discussed in relation to the development of the adaptive strategies for this kind of transient thermo-hydraulic problems.

4.1 Introduction

The study of thermo-hydraulic instabilities represents a challenging topic of research in thermal fluid dynamics both in the industry and in academics. As discussed in Chapter 2, the investigation of thermo-hydraulic instabilities is of interest in the design and operation of many industrial systems and equipment, such as steam generators [6] , boiling water nuclear reactors [12, 9], heat exchangers [5], refrigeration plants and in the oil industry [8]. Flow instabilities are undesirable since they can induce mechanical vibrations, problems of system control and disturbance of heat transfer in certain areas of the equipment. A particular case of thermo-hydraulic instability occurs in single-phase natural circulation system. This case presents several applications in nuclear reactors, solar energy units, thermosyphons, etc. The problem of single phase natural circulation presents a complex non-linear behaviour that has motivated a systematic investigation both experimentally and analytically ([1], [10], [13]).

The simulation of nonlinear systems can be accomplished by several methods. A relevant aspect in the selection of the numerical method is the introduction of artificial dissipative and dispersive effects which may mislead the underlying behaviour of the system. For that reason, a suitable method for solving the problem should minimise the numerical errors. As explained in the previous chapter, for time dependent problems the space-time formulation allows high order accuracy both in

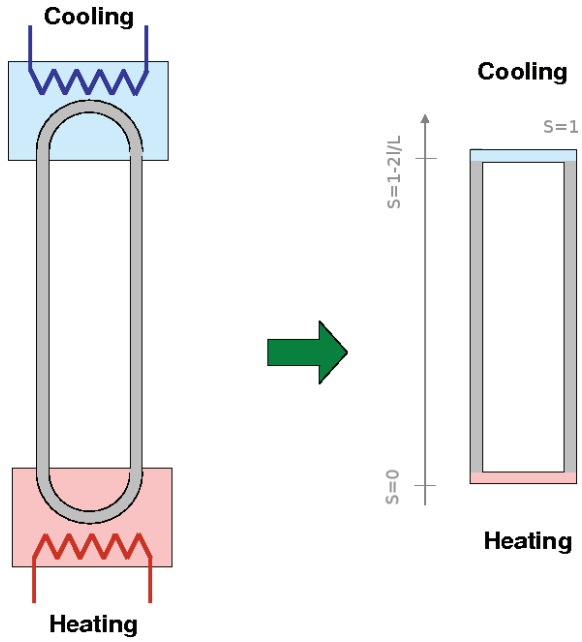

Figure 4.1: *Welander problem, the chaotic natural circulation loop.*

space and time, [3, 11].

The main goal of this chapter is to discuss the application of the time-space adaptive least squares formulation, developed in Chapter 3, to describe the evolution of a single phase natural circulation loop.

4.2 The Welander problem

The Welander problem, proposed by Pierre Welander (1967), is one of the simplest thermo-hydraulic examples where very complex behaviours could be found. It consists of a closed single phase thermo-syphon with two adiabatic legs and two point constant temperature sources as can be seen in Figure 4.1.

The mathematical model, presented by Welander, consists in the conservation of mass, momentum and energy. The main assumptions are: Boussinesq approximation (changes in the density just in the momentum balance); laminar and Newtonian flow; constant wall temperature and heat transfer coefficient; adiabatic legs. In this study a turbulent regime is assumed, following the model described in [2, 1]. When the initial conditions are anti-symmetrical the loop preserves this antisymmetry, as shown experimentally by [7]. This characteristic could be used to simplify the mathematical formulation of the problem, modelling just one of the two legs and assuming an anti-symmetrical behaviour in the other leg. Thus, following the model described in [1] and taking into account the length of the heater as [2, 4], the

s	$=$	$\dfrac{2x}{L}$	dimensionless space coordinate	x	space coordinate
τ	$=$	$\dfrac{2\kappa l t}{L}$	dimensionless time	Q	mass flow
q	$=$	$\dfrac{Q}{A\kappa l}$	dimensionless flow	l	heater length
θ	$=$	$\dfrac{T - T_0}{\Delta T}$	dimensionless temperature	h	heat transfer coefficient
ΔT	$=$	$\dfrac{T_{heater} - T_{cooler}}{2}$		A	cross section area
T_0	$=$	$\dfrac{T_{heater} + T_{cooler}}{2}$		ρ	density
κ	$=$	$\dfrac{P_w\, h}{A\, \rho C_p}$		β	expansion coefficient
ξ	$=$	1.75		C_p	specific heat
α	$=$	$\dfrac{g\beta\Delta T L}{2(\kappa l)^2}$		D	diameter
ϵ	$=$	$\dfrac{\alpha}{16}\left(\dfrac{\rho D\kappa l}{\mu}\right)^{0.75}\dfrac{RL}{2\kappa l}$		L	loop length
R	$=$	$32\dfrac{\mu}{\rho D^2}$		P_w	wetted perimeter

Table 4.1: *Nomenclature of the variables defined for the Welander problem*

dimensionless conservation system can be written as

$$\begin{cases} \dfrac{dq}{d\tau} &= \alpha \int_0^1 \theta ds - \epsilon q|q|^{\xi-1} \quad for\ \tau > 0 \\ \dfrac{\partial\theta}{\partial\tau} + q\dfrac{\partial\theta}{\partial s} &= \begin{cases} 0 & 0 < s < (1 - 2l/L) \\ -\dfrac{L}{2l}(1+\theta) & 2l/L < s < 1 \end{cases} \quad and\ \tau > 0 \end{cases} \tag{4.1}$$

The dimensionless variables used in this chapter are given in the Table 4.1. Boundary conditions result from the imposition of the antisymmetric behaviour in both legs, then the non-dimensional temperatures in $s = 0$ and $s = 1$ are given by

$$\theta(0, \tau) = -\theta(1, \tau) \tag{4.2}$$

Initial conditions for the dimensionless temperature and flow are imposed as external functions according to the problem as

$$\begin{cases} q(0) &= q_0 \\ \theta(s, 0) &= \theta_0(s) \quad \text{for } 0 < s < 1. \end{cases} \tag{4.3}$$

Eqs. (4.1) to (4.3)) define the dimensionless Welander problem for turbulent flow depending just on the three parameters ξ, α and ϵ. As previous works show, these parameters control the stability of the system.

4.3 Problem linearization

The Welander's problem, equation (4.1), is linearised in order to use the method described above as

$$\begin{cases} \dfrac{dq}{d\tau} &= \alpha \int_0^1 \theta ds - \epsilon q|q^*|^{\xi-1} & \text{for } \tau > 0 \\ \dfrac{\partial\theta}{\partial\tau} + q^* \dfrac{\partial\theta}{\partial s} &= 0 & \text{for } 0 < s < 1 \ \ and \ \ \tau > 0 \end{cases} \tag{4.4}$$

The operator $\mathcal{L}$ can be written as

$$\mathcal{L} = \begin{bmatrix} \dfrac{\partial \bullet}{\partial\tau} + \epsilon|q^*|\bullet & 0 \\ 0 & \dfrac{\partial \bullet}{\partial\tau} + \dfrac{\partial \bullet}{\partial s} \end{bmatrix} \tag{4.5}$$

where $\mathbf{u} = [q\ \theta]$, $\mathbf{g} = [0\ \ \alpha \int_0^1 \theta ds]$, $\mathbf{u}_0 = [q_0\ \theta_0]$ and q^* is the linearised dimensionless flow. The solver presented in the previous chapter is used to solve this non-linear iterative problem.

4.3.1 Error estimators

As described, the residual defined by the functional $\mathcal{J}(\mathbf{u})$ is given as

$$\mathcal{J}(\mathbf{u}) = \int_\Omega \left(\mathcal{L}\mathbf{u}_h - \mathbf{g}\right)^2 d\Omega \tag{4.6}$$

with $\mathbf{u}_h$ the numerical approximation. As shown before, this residual can be used as an error estimator, since it indicates how big is the error of the numerical solution. The main problem of using this operator is the complex matrix operations required to calculate it, Eq. (3.24). Hence, in order to take a more suitable error estimator, it is possible to use the fact that the initial conditions are imposed in a weak way. Thus, the numerical error is also reflected at the boundary. In this way, it could be possible to use the error in the boundary as an estimator of the numerical error of the solution. The error given by imposing the boundary conditions in a weak manner can be written as

$$\mathcal{E}_{IC}(t) = \int_\Gamma \left(\mathbf{u}_\Gamma(t) - \mathbf{u}_h(t)\right)^2 d\Gamma \tag{4.7}$$

where Γ is the boundary of the domain where boundary and initial conditions, $\mathbf{u}_\Gamma(t)$, are imposed. As we can see from equation (4.7), this measure does not represent the residual on the boundary. It represents the difference between the imposed solution and the numerical solution. Hence the values of these two estimators should not necessarily be of the same magnitude. One possible disadvantage regarding the use of this estimator is how penalties in the boundary conditions could affect its behaviour. It implies that when the imposed conditions in the boundary are penalised the error estimator is reduced. Numerical examples in the next section are performed in order to analyse all these questions.

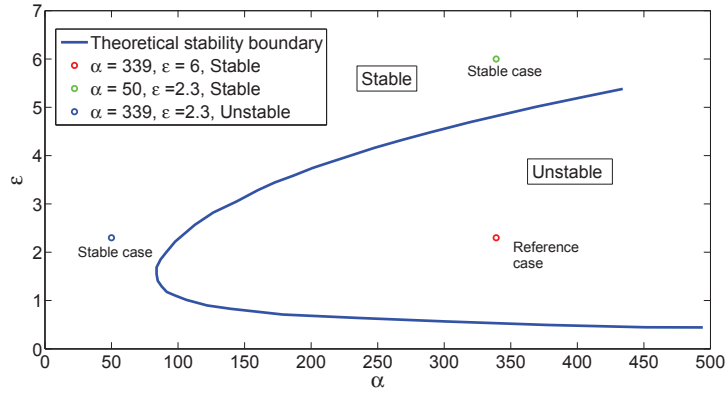

Figure 4.2: *Theoretical stability map, [1] for a positive flow steady-state conditions,* $\xi = 1.75$*,* $l = 0.05$*.*

4.4 Numerical Examples

A stability parameter map of the system is shown in Figure 4.2. The stability limit, from [1], is plotted on this figure. A length of source of 5% of the total length (point source) of the loop is used, in order to approach to this referred case.

The plots in Figure 4.3 show the three different behaviours of the system. These operating points are also plotted in the stability map of Figure 4.2. As it is possible to see, stable states are damped achieving the steady state solution after a certain time. Stable and unstable states agree with solutions presented by [1], both in characteristic times as in the magnitude of the dimensionless temperature and flow. These simulations are solved on successive space-time strips $\Omega_\tau = [0, 1] \times \Delta\tau$, using $\Delta\tau = 0.01$, $Ne = 10$, $O_x = 4$, $O_t = 3$ and $\varepsilon_{Max} = 10^{-6}$.

The trajectory of the dimensionless flow rate versus the integral of the dimensionless fluid temperature is shown in Figure 4.4. The two attractors corresponding to the clock-wise and anti clock-wise motion are clearly observed. The location of the attractors as well as the shape and magnitude of this diagram are in agreement with the case presented by [1] in their Figure 3.

4.4.1 Low order and high order methods

Previous works pointed out the importance of the diffusion effect of low order methods in similar problems [1]. Figure 4.5 shows a comparison between the solution obtained with a low order discretization, ($O_x = 1$, $O_t = 1$), and with a high order discretization, ($O_x = 5$, $O_t = 5$), using $Ne = 10$ elements in both cases. The low order discretization case introduces a significant amount of numerical diffusion which damps the oscillatory behaviour of this unstable case.

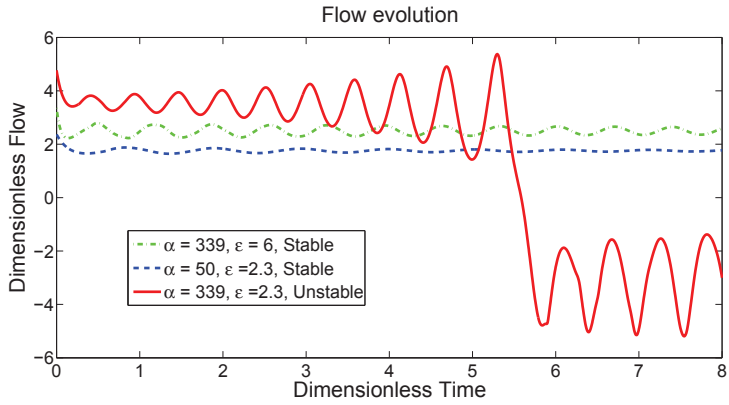

Figure 4.3: *Comparison between different regimes*

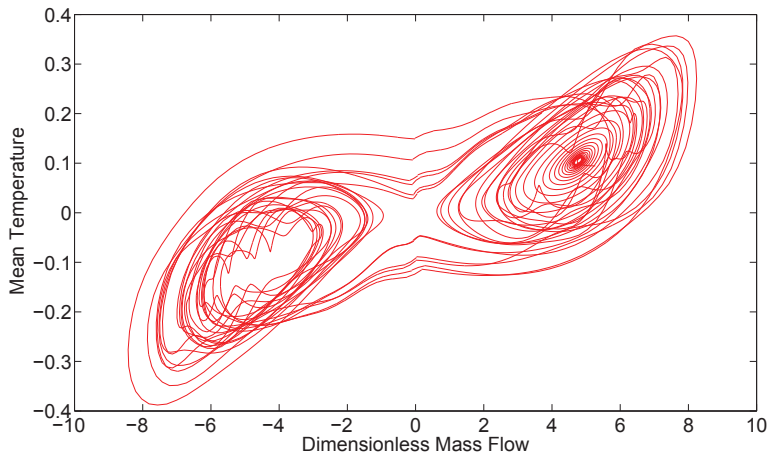

Figure 4.4: *Projection of the attractor in the phase space* ($\alpha = 339$, $\xi = 1.75$, $\epsilon = 2.3$, $l = 0.05$).

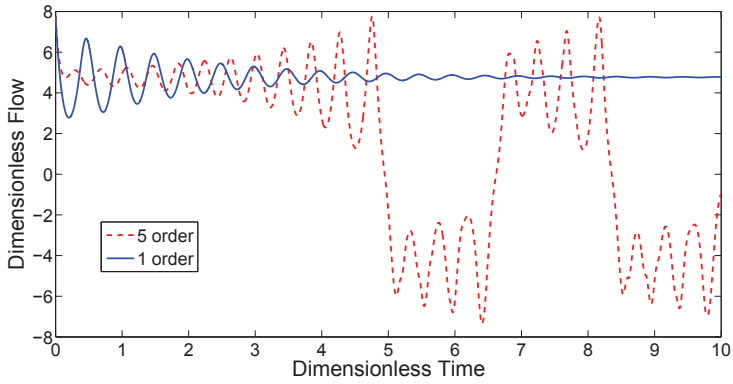

Figure 4.5: *Comparison between a first order diffusive method and high order methods. Using an initial condition different from the steady state point. ($\alpha = 339$, $\xi = 1.75$, $\epsilon = 2.3$, $l = 0.05$).*

4.4.2 Estimator validation and convergence

During the evolution of the system, the flow rate changes the sign when the flow is reversed. In the flow reversal phenomena, the temperature of the system increases significantly which results in strong gradients increasing the value of the residual, Figure 4.6. It is also interesting to note that the numerical error, measured by the residual $\mathcal{R}^e$ and by the initial condition error $\mathcal{E}_{IC}$, follows a similar trend, even when penalties for boundary conditions are applied. For the case shown in Figure 4.6, a penalty of 1000 was applied to the boundary conditions and accordingly that value corresponds to the difference between the magnitude of $\mathcal{E}_{IC}$ with and without penalties. This example shows that even when the magnitude of the estimators are different, the trend in all the cases results the same. Moreover this example shows that the implementation of this estimator in an adaptive solver is possible even when penalties on boundary conditions are used.

One important advantage of using a high order method is the flexibility for changing the approximation order of the solution. Figure 4.7 shows the convergence of the solution when increasing the order of approximation for both space and time, keeping the same discretization, $Ne = 10$ and $\Delta\tau = 0.1$. Hence, increasing the approximation order can reduce the error in the approximation significantly, but this can result in a significant increase of the computational time.

4.4.3 High order *hp*-adaptive scheme

Based on the observed behaviour of the residual, a possible manner of improving the simulation of this problem while reducing the computational cost is to selectively modify the numerical parameters (Ne, $\Delta\tau$, O_x, O_t) during the simulation. For this purpose, the boundary conditions error estimator $\mathcal{E}_{IC}$ determines the discretization and the order used in each time step. The adaptive strategy consists in

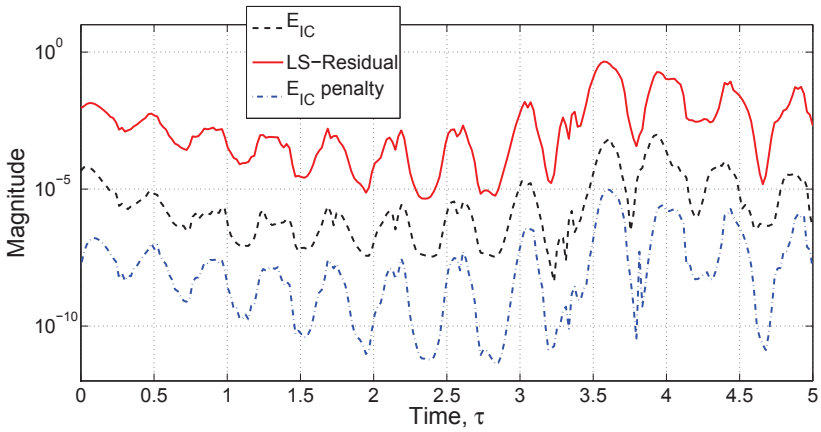

Figure 4.6: *Comparison between the boundary error estimator $\mathcal{E}_{IC}$, for no penalty and for a penalty of 1000 in the boundary conditions, and the R residual estimator. ($\alpha = 339$, $\xi = 1.75$, $\epsilon = 2.3$, $l = 0.01$).*

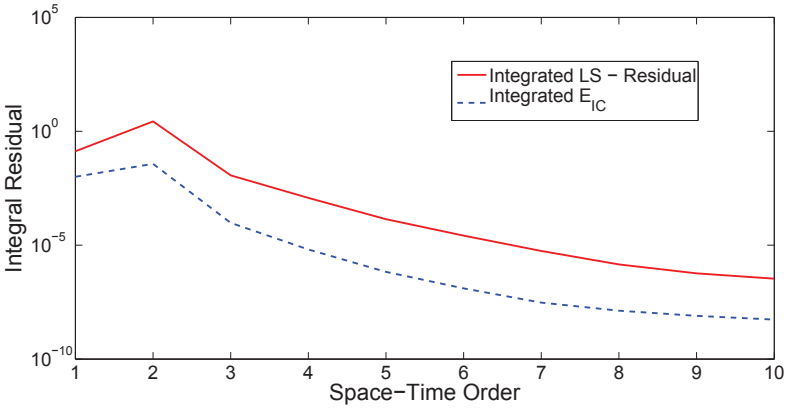

Figure 4.7: *Convergence of the integral error for the boundary error estimator, $\mathcal{E}_{IC}$ and the residual estimator, R, changing the order of approximation for the space and time description. ($\alpha = 339$, $\xi = 1.75$, $\epsilon = 2.3$, $l = 0.05$).*

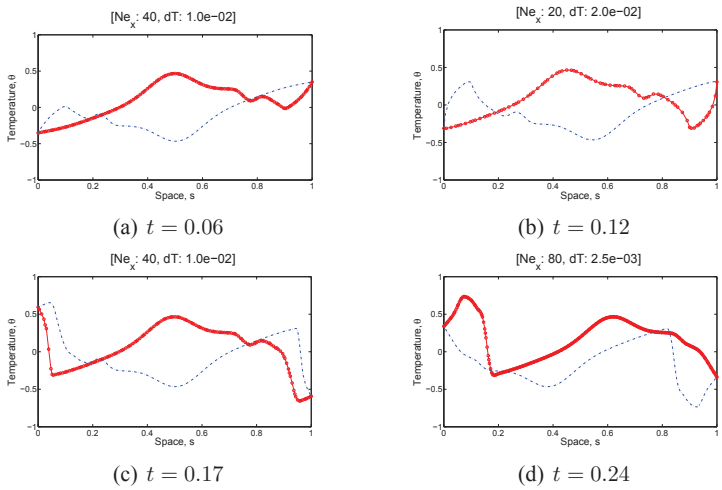

(a) $t = 0.06$ (b) $t = 0.12$

(c) $t = 0.17$ (d) $t = 0.24$

Figure 4.8: *Evolution of the temperature profile using an h-adaptive strategy for both time and space, in the case of an unstable condition. Solid line represents the simulated leg while the dotted line represents the antisymmetric leg. [$\alpha = 339$, $\xi = 1.75$, $\epsilon = 2.3$, $l = 0.05$].*

defining a maximum and a minimum error and when the error estimator gets over these limits the discretization and the order are changed.

As it was commented before, flow reversals introduce an important error. Then in this example, different strategies to simulate a flow reversal are tested. Figure 4.8 shows the evolution of the temperature profile using an *h*-adaptive strategy. The discretization of space and time was doubled when the numerical error was bigger than the upper limit and divided by two when the estimator was smaller than the lower limit. The order of approximation for space and time were respectively $O_x = 4$ and $O_t = 3$. In the figure, the solid line with dots represents the temperature profile in one of the legs while the discontinuous line corresponds to the antisymmetric leg (not simulated). The figure shows the different discretization used at different times during the evolution of the solution. The corresponding evolution of the flow vs. time can be seen in Figure 4.9.

In order to study the different strategies of adaptation, a simulation using a *p*-adaptive strategy was also performed. For this case the order of the space and time was increased or decreased an order according to the magnitude of the error estimator. In all the cases $O_x = O_t + 1$, $Ne = 25$ and $\Delta\tau = 2\ 10^{-2}$.

The evolution of the error estimator for both previous cases is presented in Figures 4.11 and 4.12. The error can not exceed the maximum value imposed. Thus the problem can be solved in a cost-effective manner, since the solver uses the lower order or bigger discretization without exceeding error limits.

In order to compare the performance of adaptive strategies with respect to conventional methods, two different fixed schemes were simulated for the same case. The values of the numerical parameters were fixed in order to have a numerical error lower than the same upper limit as in the cases above during all the simulation.

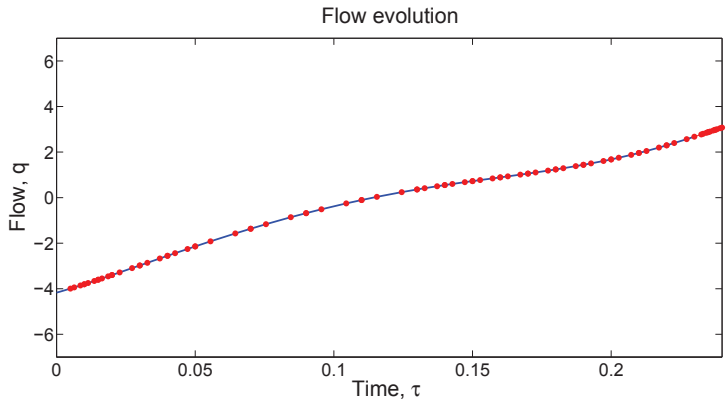

Figure 4.9: *Evolution of the flow using the h-adaptive strategy, figure(4.8), for the case of an unstable condition. [$\alpha = 339$, $\xi = 1.75$, $\epsilon = 2.3$, $l = 0.05$].*

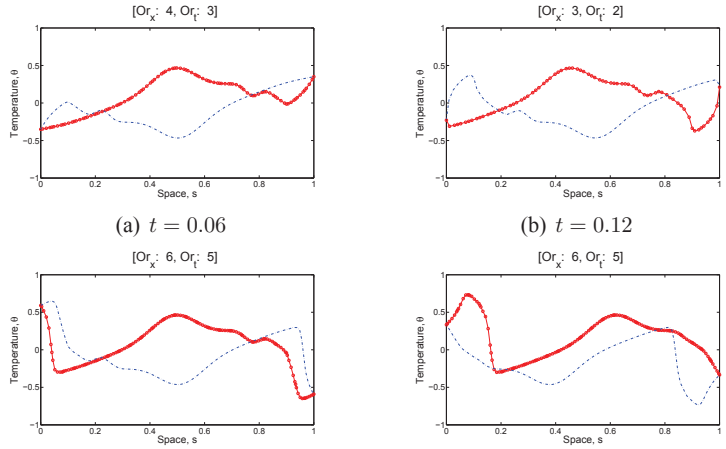

(a) $t = 0.06$ (b) $t = 0.12$

(c) $t = 0.18$ (d) $t = 0.24$

Figure 4.10: *Evolution of the temperature profile using an p-adaptive strategy for time and space, in the case of an unstable condition. Solid line represents the simulated leg while the dotted line represents the antisymmetric leg. [$\alpha = 339$, $\xi = 1.75$, $\epsilon = 2.3$, $l = 0.05$].*

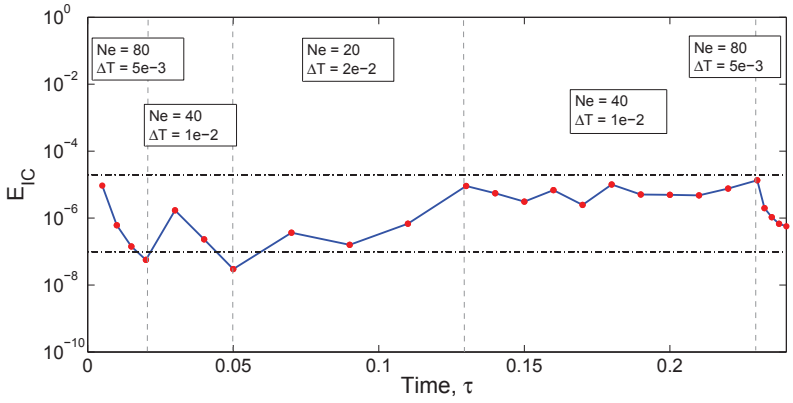

Figure 4.11: *Error evolution using an h-adaptive strategy for the case [*$\alpha = 339$, $\xi = 1.75$, $\epsilon = 2.3$, $l = 0.05$*].*

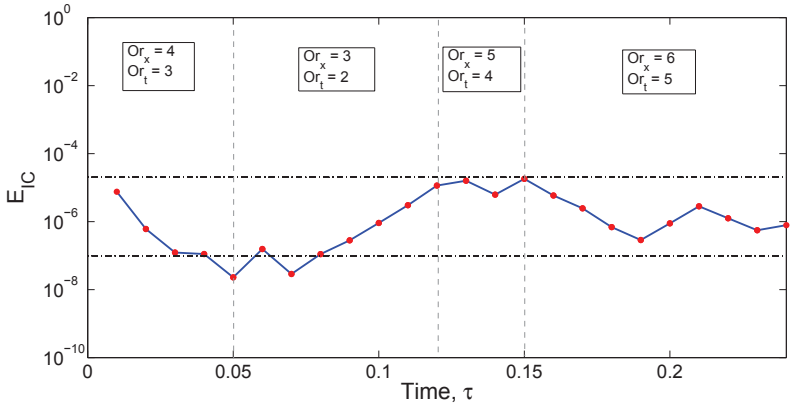

Figure 4.12: *Error evolution using an p-adaptive strategy for the case [*$\alpha = 339$, $\xi = 1.75$, $\epsilon = 2.3$, $l = 0.05$*].*

Computational times are presented in table 4.2, where it is possible to see that for both adaptive schemes the computational time was improved with respect to fixed schemes. Indeed a big difference in computational time, less than 25 % in the worse case, was achieved using the *p*-adaptive and *hp*-strategy. It shows that increasing the approximation order for the space is more effective in terms of the computational time than decreasing the discretization size. On the other hand a small difference between *hp*-adaptive and *p*-adaptive computational times, table 4.2, indicates that, regarding the computational time, it is more effective to decrease discretization size of the time than the order of approximation.

Table 4.2: *Computational times for different strategies*

Solver	Ne	$\Delta\tau$	O_x	O_t	Comp. time [sec]	Estimator limits
Fixed	80	5e-3	4	3	838	$< 10^{-5}$
Fixed	25	2e-2	6	5	179	$< 10^{-5}$
h-adaptive	x2	/2	4	3	137	$10^{-5} - 10^{-7}$
p-adaptive	25	2e-2	+1	+1	30	$10^{-5} - 10^{-7}$
hp-adaptive	25	/2	+1	3	27	$10^{-5} - 10^{-7}$

4.5 Summary

The *hp*-adaptive time-space least squares spectral method was discussed for solving a natural circulation loop given by the so called Welander's problem. The method has shown to be quite robust for solving this kind of problems using different order of approximation and discretization. It was shown that low order discretization approaches can affect the nature of the problem by damping the dynamics of an unstable case. The implementation of the weak imposed boundary conditions error as an estimator was analysed. It was also proved that the use of an adaptive strategy reduces significantly the computational costs. Different *hp*-adaptive strategies were developed based on maintaining the value of the numerical error limited by an upper and lower value. Finally p-adaptation in the space was in terms of computational time, the best strategy.

Bibliography

[1] AMBROSINI W. AND FERRERI J. The effect of truncation error in the numerical prediction of linear stability boundaries in a natural circulation single phase loop. *Nuclear Engineering and Design*, 183(1-2):53–76, 1998. (Cited on page 97, 98, 101, 256)

[2] CHEN K. On the oscillatory instability of closed-loop thermosyphons. *J. Heat Transactions of the ASME*, 107:826–832, 1985. (Cited on page 98)

[3] De Maerschalck B. and Gerristma M. I. Least-squares spectral element method for non-linear hyperbolic differential equations. *Journal of Computational and Applied Mathematics*, 215(2):357–367, 2008. (Cited on page 98)

[4] Ferreri J. and Ambrosini W. Verification of relap5/mod3 with theoretical and numerical stability results on single-phase, natural circulation in a simple loop. *NUREG IA/151*, 1999. (Cited on page 98)

[5] Fowler A. Linear and non-linear stability of heat exchangers. *J. Inst. Maths Applics*, 22:361–382, 1978. (Cited on page 97)

[6] Ge-Ping W., Sui-Zheng Q., Guang-Hui S., and Dou-Nan J. Analysis of flow instabilities next term in forced-convection steam generator. *Nuclear Science and Techniques*, 17:185–192, 2006. (Cited on page 97)

[7] Greif R., Zvirin Y., and Mertol A. The transient and stability behaviour of a natural convection loop. *ASME Journal of heat transfer*, 101:684–688, 1981. (Cited on page 98)

[8] Hu B. *Characteristing gas-lift instabilities*. PhD thesis, Departament of petroleum engineering and applied geophysics, Norwegian University of Science and Technology, 2004. (Cited on page 97)

[9] Lahey R. and Moody F. *The thermal hydraulics of a boiling water nuclear reactor*. Amer Nuclear Society, 1977. (Cited on page 97)

[10] Pilkhwa D., Ambrosini W., Forgione N., Vijayan P. K., Saha D., and Ferreri J. C. Analysis of the unstable behaviour of a single-phase natural circulation loop with one-dimensional and computational fluid-dynamic models. *Annals of Nuclear Energy*, 34(5):339–335, 2007. (Cited on page 97)

[11] Pontaza J. and Reddy J. Space–time coupled spectral/hp least squares finite element formulation for the incompressible navier–stokes equation. *Journal of Computational Physics*, 190(2):418–459, 2004. (Cited on page 98)

[12] Van der Hagen T., Stekelenberg A., and Van bragt D. Reactor experiments on type-i and type-ii bwr stability. *Nucl. Eng. Des.*, 2000. (Cited on page 97)

[13] Welander P. On the oscillatory instability of a differentially heated fluid loop. *Journal Fluid Mechanics*, 29:17–30, 1967. (Cited on page 97, 98)

PART II

Modeling of two-phase flow instabilities

CHAPTER V

Dynamic simulation of Ledinegg instability

► The flow excursion instability (*Ledinegg*) could produce severe damages in thermo-hydraulic components due to fast changes in the main variables. In this chapter, this phenomenon is studied by simulating the transient behaviour of the system during the process. The effects of dynamic changes in the pressure drop vs. flow characteristic curve are analysed. Finally, some numerical aspects related to the application of an adaptive high-order method to the resolution of these complex thermo-hydraulic problems are discussed.

5.1 Introduction

The investigation of two-phase flow instabilities results quite relevant for the design and operation of many industrial systems and equipment, such as steam generators, boiling water nuclear reactors, heat exchangers, thermo-syphons, re-boilers, refrigeration plants and some chemical processing systems, as seen in Chapter 2. M. Ledinegg (1938) described a phenomenon later named *Ledinegg* instability or flow excursion. This is the most common type of static oscillations, according to the classification introduced in [1] and it is associated with a sudden change in the flow rate. The main mechanisms involved in the occurrence of this phenomenon are explained in detail in the Section 2.2.1.2.

In Figure 5.1 a typical pressure drop curve as a function of the mass flow for the case of a heated section is shown. There are two limiting cases which correspond to the case of all vapor and all liquid (dotted lines). For a given set of parameters (Q, T_{in}, K_i, P), the characteristic pressure drop of two-phase flow systems may show the N-shape curve. Thus, according to the characteristic pressure drop of the external system, the operation points would result stable or unstable, as it was commented in Chapter 2. In some cases the occurrence of *Ledinegg* instability in industrial systems may trigger the burn-out of the system due to the sudden change in the operation state ([4]). This effect is shown in dashed line in Figure 5.1. When the flow is decreased from a single-phase liquid region, the system turns suddenly to a two-phase state, with a high generation of vapor.

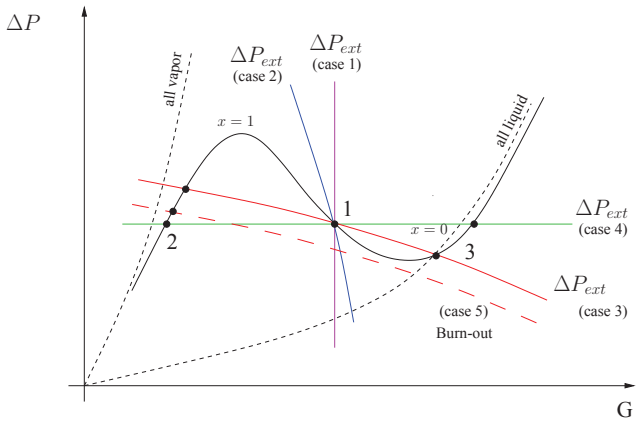

Figure 5.1: *Characteristic pressure drop vs. flow rate. In the plot, four different external characteristics (cases) are presented.*

M.M. Padki et al. (1992) performed a theoretical bifurcation analysis of *Ledinegg* phenomena. He concluded that the necessary conditions for its occurrence corresponds to the case of: internal characteristic curve (pressure drop - flow rate) with negative slope; internal characteristic curve steeper than external curve; and multiple intersections of the internal and external characteristic curves. Different scenarios are plotted in the Figure 5.1. For cases 3 and 4, point 1 fulfils the mentioned stability condition. The standard way to avoid this kind of instabilities is to make the slope of the external characteristic curve steeper than the internal curve. The analysis of the evolution of the flow during the occurrence of the *Ledinegg* instability is quite relevant. However, little information has been found in the open literature about this process.

The main goal of this chapter is to study the dynamic of a heated pipe with focus on the *Ledinegg* instability. In particular, a detailed description of the dynamic effects on the main variables is presented. In Section 5.2, the mathematical model is discussed. The numerical solver presented in previous chapters is used to solve the mathematical equations modelling the phenomena. The possibility of using an adaptive solver is also discussed. Finally, in Section 5.4, several simulations are presented and the numerical and physical aspects related to the occurrence of *Ledinegg* instability are discussed.

5.2 The model

The simplest model used to study these kinds of thermo-hydraulic instabilities consists of two pressurised tanks, two valves and a heated section, Figure 5.2. In this model, the pressure difference between both tanks acts as driving force (external) and according to the valves opening the external characteristic results in a quadratic decreasing curve, Figure 5.1. When the valve K_{in} is almost closed the slope is close

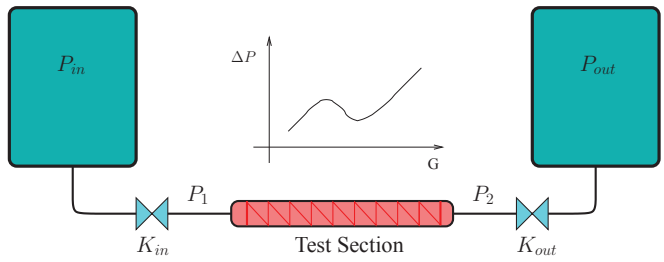

Figure 5.2: *Diagram of the model used to simulate the Ledinegg phenomenon.*

to infinity (case 1) and when this valve is fully open the slope of the curve is zero (case 4). The high slope case is equivalent a large serial array (thermo-hydraulic circuit), so even when the pressure drop changes, the flow remains constant. On the other hand, the case of a zero slope is equivalent to a parallel array of components (tubes in a heat exchanger).

The mathematical model used to describe the evolution of the system is based on the following assumptions:

- One-dimensional.
- Thermodynamic equilibrium between phases.
- Two-phase homogeneous model, [7].
- Two-phase Müller-Steinhagen and Heck pressure drop correlation [5], see Appendix A.

The mass, momentum and energy equations can be expressed as

$$\frac{\partial \rho}{\partial t} + \frac{\partial G}{\partial z} = 0 \tag{5.1}$$

$$\frac{\partial G}{\partial t} + \frac{\partial}{\partial z}\left(\frac{G^2}{\rho}\right) + \frac{\partial P}{\partial z} + \left[\frac{f}{D_H} + \sum_{i=1}^{N} K_i \delta(z - z_i)\right] \frac{|G|G}{2\rho} = 0 \tag{5.2}$$

$$\frac{\partial \rho h}{\partial t} + \frac{\partial G h}{\partial z} = Q\frac{P_H}{A_x} \tag{5.3}$$

where G is the mass flux; P is the static pressure; h is the specific enthalpy; ρ is the density; Q is the heat source; f is the Darcy friction factor; K_i is the constant value of concentrated local pressure drop for valves; D_H is the diameter of the pipe; P_H is the perimeter; A_x is the cross section area; z is the space coordinate and t the time coordinate. The pressure drop in the valves is calculated using a pressure drop concentrated value, K_i, for each valve. Friction losses are neglected in the energy equation.

5.3 Linearization

From Eqs. (5.1) to (5.3) it is possible to see that the system is highly non-linear. As shown in Chapter 3, it is necessary to find a linear form for this set of equations in order to use LSSM (Least Square Spectral Method). The linearization of the equations system described results in

$$\frac{\partial \rho^*}{\partial t} + \frac{\partial G}{\partial z} = 0 \tag{5.4}$$

$$\frac{\partial G}{\partial t} + \frac{\partial}{\partial z}\left(\frac{G^{*2}}{\rho^*}\right) + \frac{\partial P}{\partial z} + \left[\frac{f}{D_H} + \sum_{i=1}^{N} K_i\right]\frac{|G|G}{2\rho^*} = 0 \tag{5.5}$$

$$\frac{\partial \rho^* h}{\partial t} + \frac{\partial G^* h}{\partial z} = Q\frac{P_H}{A_x} \tag{5.6}$$

where G^* and ρ^* correspond to the old values of flow and density respectively. Hence, using the operator description of Eq. 3.1, it is possible to rewrite the linearised system as

$$\mathcal{L} = \begin{Bmatrix} \frac{\partial \bullet}{\partial z} & 0 & 0 \\ \frac{\partial \bullet}{\partial t} & \frac{\partial \bullet}{\partial z} & 0 \\ 0 & 0 & \rho^*\frac{\partial \bullet}{\partial t} + G^*\frac{\partial \bullet}{\partial z} \end{Bmatrix} \tag{5.7}$$

$$\mathbf{g} = \begin{Bmatrix} -\frac{\partial \rho^*}{\partial t} \\ -\frac{\partial}{\partial z}\left(\frac{G^{*2}}{\rho^*}\right) - \left[\frac{f}{D_H} + \sum_{i=1}^{N} K_i\delta(z - z_i)\right]\frac{|G|G}{2\rho^*} \\ Q\frac{P_H}{A_x} \end{Bmatrix} \tag{5.8}$$

$$\mathbf{u} = \begin{Bmatrix} G \\ P \\ h \end{Bmatrix} \tag{5.9}$$

the corresponding initial nodes are set to the initial values for flow, pressure and enthalpy. The boundary conditions for enthalpy, flow and pressure are set in $z = 0$. This case is equivalent to taking an infinity slope for the external characteristic, case 1 in Figure 5.1.

5.4 Numerical Results

All the simulations in this section have been done in a system with the following parameters:

- Fluid: Water

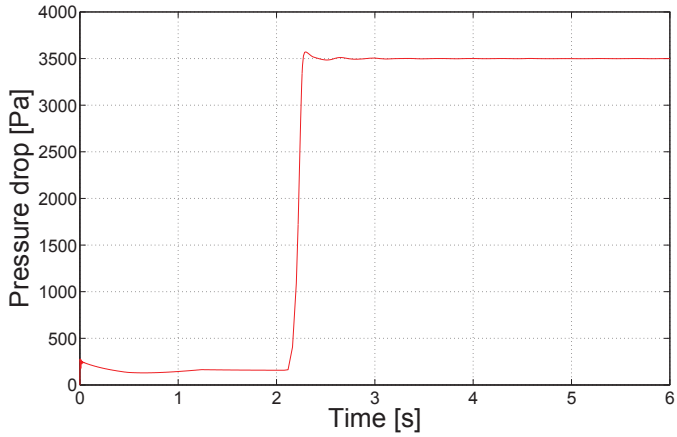

Figure 5.3: *Evolution of the pressure drop during a cold start of the system from an unheated initial condition.*

- L = 1m, D_H = 5mm
- Q = 6kW
- $P_{in} = 10^5$ Pa, T_{in} = 20 C
- $K_{in} = K_{out} = 0$ (horizontal external characteristic)

The adaptive strategy used in these examples corresponds to varying just the time step and a constant high order for both time and space, in this case $O_z = 5$ and $O_t = 4$. The number of elements in which the space is discretized is $N_e = 20$ and the maximum non-linear error, as described in Eq. (3.26), is $\varepsilon_{NL} = 10{-}6$.

5.4.1 Stable point simulation

In this section, the evolution of the system corresponding to the cold starting of the system from an initial condition of constant flow (200 kg/m^{2}s) and constant subcooling temperature (20 C) is presented. The flow and pressure at the inlet are imposed as boundary conditions. This case is equivalent of having an infinite slope for the external characteristic, case 1 in Figure 5.1. Therefore even if the slope of the internal characteristic is negative, this point does not fulfil the criteria necessary for *Ledinegg* instability and result in a stable behaviour of the system.

In this first example the start-up of the system is simulated. The heat source is started at $t = 0$ and fix to a constant value during the simulation. In Figure 5.3, the pipe pressure drop evolution (head),during the starting of the system, is plotted. The first region ($t < 0.7$ sec) is characterised by a small decrease in the pressure due to changes in the viscosity; in the second region (0.7 sec $< t <$ 2.0 sec) the small increase in the pressure is due to changes in the density. In the subcooled liquid

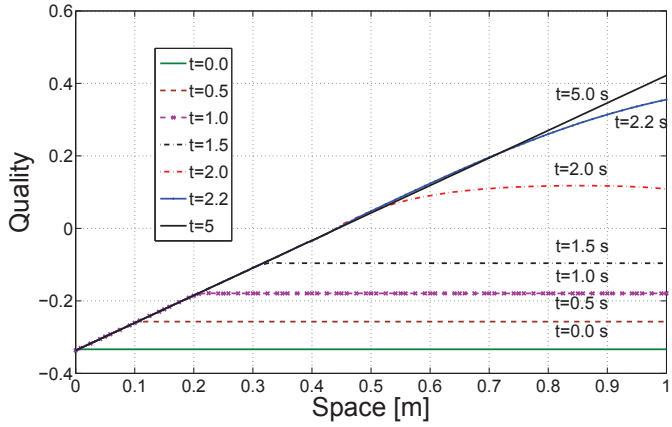

Figure 5.4: *Evolution of the quality profile during a cold start of the system from an unheated initial condition.*

region these two effects (density, viscosity) are always present, but their influence varies depending on the thermodynamic state. At approximately 2.2 sec vapor is spontaneously generated in half of the domain. Hence a high jump in the pressure drop in the system is produced. Finally the system achieves a steady state. The evolution of the thermodynamic quality is presented in Figure 5.4, where a sudden generation of vapor in a big region of the domain, between $t = 1.5$ and $t = 2$, is observed. This phenomenon is due to the constant increment of the temperature in the domain because of the constant heat source. It means that in the starting up of these two-phase flow systems it is always necessary to limit the slope of the heat source in order to avoid a spontaneous generation of vapor that can produce some damage in the system.

Figure 5.5 shows the changes in the time discretization according to the error estimator. The adaptive strategy implemented consists in doubling the time step when the estimator is smaller than a *minimum error limit* value and dividing the time step by two when this estimator is larger than a *maximum error limit*. The evolution of the time step is written in the top of this figure for a better understanding of the adaptive solver behaviour.

This example where the flow is imposed, is directly related with the simulation of large systems. In such big systems the flow could be considered constant with respect to the pressure drop of the component simulated and therefore the pressure drop becomes the target of the calculations.

5.4.2 Ledinegg instability simulation

The characteristic curve corresponding to the steady-state N-shape of the problem described above is shown in Figure 5.6. The N-shape curve was obtained using

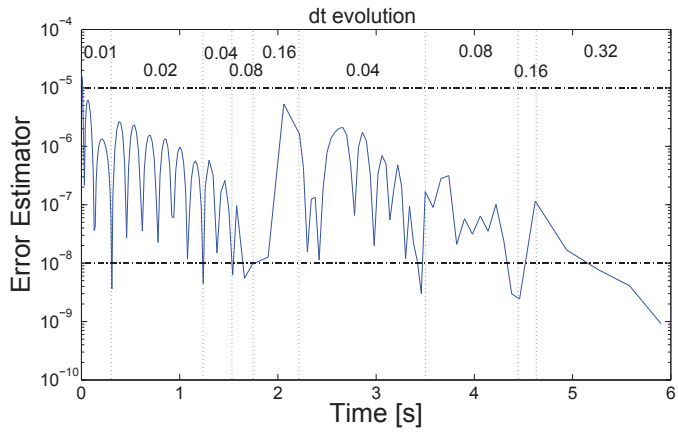

Figure 5.5: *Evolution of the error estimator (residual) during the simulation. This estimator is used to adapt the solver parameters in order to improve computational time and accuracy of the solution.*

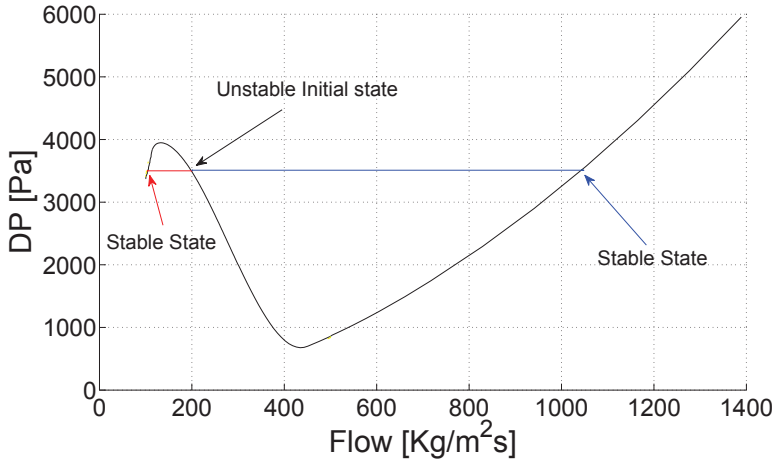

Figure 5.6: *Evolution of the system during two different flow excursions (flow* 200 *kg/m*^{2}*s). The perturbation of the boundary conditions were* P_{out} = 996510 *Pa,* P_{out} = 996490 *Pa, respectively for each simulation. The static characteristic of the system is shown as the black line.*

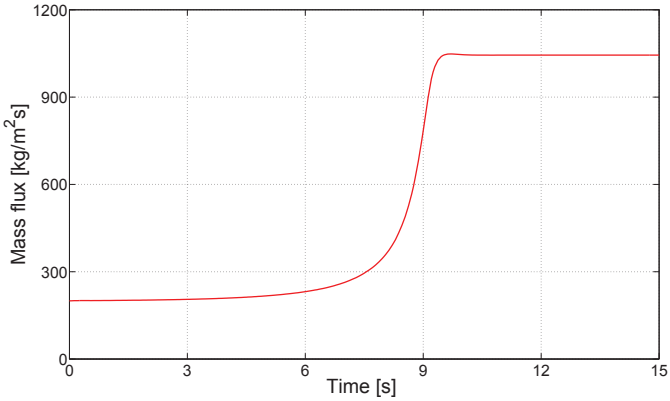

Figure 5.7: *Evolution of the inlet flow during a transient flow excursion corresponding to the simulation in Figure 5.6 with increasing flow.*

the same model for steady state calculations. The initial condition of the system simulated here is the final state of the previous example. As one can see in Figure 5.6, this initial condition corresponds to a negative slope of the internal characteristic. It means that by changing the slope of the external characteristic to a smaller slope than the internal, this point becomes unstable.

In this example the outlet pressure is set as a boundary condition thus getting a horizontal slope (case 4 in Figure 5.1). The value of the pressure is the same as the one obtained in the previous final state, $P_{out} = 996490$ Pa. The evolution of the system under these conditions corresponds to the positive flow displacement evolution from the unstable point, Figure 5.6. In this figure, the simulation corresponding to a perturbed higher value of the pressure outlet $P_{out} = 996510$ Pa is presented. This case corresponds to the system going to smaller flow rates. These two simulations are showing equal probability to evolve in both directions (greater or lower flow rates) and not just to lower flow rates as described in most of the previous works [1, 2]. For the first flow excursion simulation (i.e. towards greater flow rates) the evolution of the inlet flow, density profile and pressure profile are plotted in Figures 5.7-5.8. The characteristic evolution time (time to go from 10 - 100 % of the initial and final value of the mass flux respectively) for this case is approximately 3 sec.

An important fact is that the nature of the dynamic effects results from delays in the propagation of the thermodynamic information (enthalpy) instead of the fluid dynamic information (pressure).

5.4.3 Influence of dynamic effects on the N-shape characteristic curve

In order to study the dynamic changes in the pressure drop response of the system due to dynamic effects, the ΔP vs. G curve during a linear variation of the flow in time is obtained. Some dynamic N-shapes curves for different flow variations are

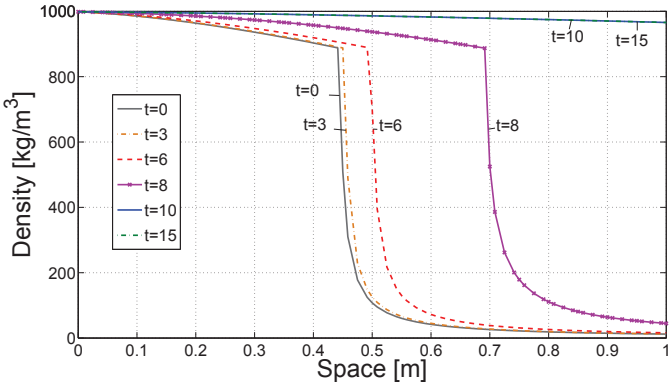

(a) Density profiles

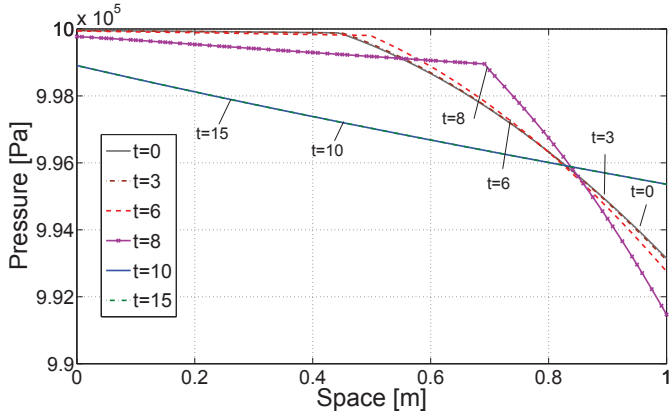

(b) Pressure profiles

Figure 5.8: *Evolution of density and pressure from an unstable initial state, Ledinegg excursive instability.*

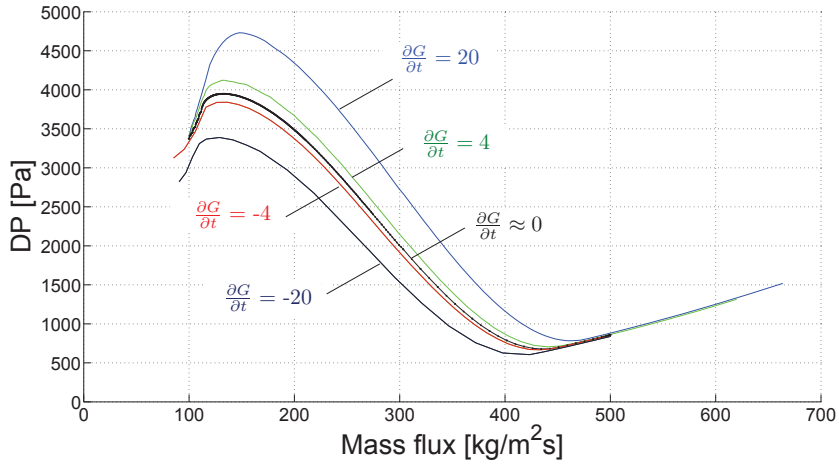

Figure 5.9: *Modification of the characteristic N-shape due to dynamic effects during constant flow variations.*

shown in Figure 5.9.

During the increasing of the mass flow rate, the delays in the propagation produce a positive curvature of the enthalpy profile and, in consequence, the pressure drop is higher if compared to the steady-state case. On the other hand, when the flow is decreasing the negative curvature of the enthalpy profile will produce lower values of the pressure drop, as shown in Figure 5.9. These changes in the characteristic curve are of particular importance when analysing *pressure drop oscillation* phenomena (PDO). As explained, PDO implies the successive occurrence of increasing and decreasing flow excursions. However, as will be exposed in Chapter 8, most of the models used in the calculation of PDO assume a steady-state characteristic curve, even when the described phenomenon is dynamic as shown in these examples.

5.5 Summary

In this chapter the *Ledinegg* transient evolution was simulated for several conditions. In these simulations is possible to see that for an unstable point the system can evolve to both lower and higher flow rates. The dynamic changes of the characteristic pressure drop vs. flow rate curve due to delays in the propagation of the enthalpy information were studied. A high-order hp-adaptive method was implemented in order to improve both the computational time as well as the accuracy of the numerical solution.

Bibliography

[1] BOURÉ J., BERGLES A., AND TONG L. Review of two-phase flow instabilities. *Nuclear Engineering and Design*, 25:165–192, 1973. (Cited on page 113, 120)

[2] KAKAC S. AND BON B. A review of two-phase flow dynamic instabilities in tube boiling systems. *Int. Journal Heat Mass Tranfer*, 51:399–433, 2007. (Cited on page 120)

[3] LEDINEGG M. Instability of flow during natural and forced circulation. *Die Wärme*, 61(8):891–898, 1938. (Cited on page 113)

[4] MARGETTS R. Excursive instability in feedwater coils. *AIChE Paper prepared for presentation at 13th National Heat Transfer Conference, Denver, Colorado*, 1972. (Cited on page 113)

[5] MULLER-STEINHAGEN H. AND HECK K. A simple friction pressure drop correlation for two-phase flow pipes. *Chem. Eng. Prog.*, 20:297–308, 1986. (Cited on page 115)

[6] PADKI M., PALMER K., KAKAC S., AND VEZIROGLU T. Bifurcation analysis of pressure-drop oscillations and the ledinegg instability. *Int. Journal Heat Mass Transfer*, 35:525–532, 1992. (Cited on page 113, 114)

[7] WALLIS G. B. *One-dimensional two-phase flow*. McGraw-Hill, 1969. (Cited on page 115)

CHAPTER VI

Two-phase flow instabilities in boiling and condensing systems

► In this chapter *density wave* and *Ledinegg* instabilities are analysed in a single channel systems. Both phenomena are analysed for boiling and condensing conditions. The analysis is based on the direct numerical simulation of the conservation equations using a homogeneous approach. Stability limits are constructed and compared with available correlations. In the case of boiling conditions, the analysis is extended to subcooled, saturated and over-heated inlet conditions. Finally a discussion regarding the occurrence of these phenomena in condensing systems is presented.

6.1 Introduction

In Chapter 2 the phenomena known as *Density Wave Oscillations* (DWO) and *Ledinegg* instability were introduced. The main mechanisms involved in the occurrence of these transient phenomena were explained and a review of the main experimental and analytical investigations was presented. As explained, the stability in thermo-hydraulic variables such as flow, pressure and temperature should be studied in detail to better understand and characterise the conditions for the occurrence of these phenomena. In particular *Ledinegg* and DWO_{II} are the two most studied instabilities due to their occurrence and relevance.

Regarding the modelling and theoretical background of *density wave* oscillations, the investigations carried out in [7, 8] constitute the theoretical basis in the understanding of *density wave* phenomenon. In these works a thermal equilibrium model was used to describe the system in a one-dimensional model. The Ishii-Zuber stability map is the most used map for two-phase flow stability analysis. In [16] the use of a non-equilibrium theory was proposed. For low subcooling this model seems to fit better to the experimental data. Nevertheless, in the high subcooling cases the equilibrium model fits better the experimental data. In [5] the validity of the homogeneous model was discussed. In this last work several pressure, subcooling and heat capacity models were compared with experimental data. It was proved that in general terms the best approximation is made with no subcooling model and

heat capacity of the wall when that mechanism could be important (massive tubes). More recently [15, 14], a homogeneous equilibrium model (no subcooling) was used to study DWO. Several aspects of the classical theoretical description of DWO were critically discussed. The introduction of non-uniform heating was discussed in [13, 14]. These studies consider that the mechanism responsible of the oscillatory behaviour are the change in the exit density (related with the spatial slope of the density profile) and the change of the exit flow. For different subcooling conditions those effects have a stronger or weaker influence over the system.

Nevertheless, it is still not clear how the *density wave* mechanisms affect the systems for condensing and saturated boiling flows. In [10] an experimental and numerical study showed the occurrence of oscillations in the condensing secondary side of a heat exchanger, stating that condensation processes are similar to the boiling processes in the sense of occurrence of density wave oscillations. However, no theoretical analysis was presented to support the previous statement. In addition, several studies described the occurrence of oscillations in condensing systems [1, 2, 11, 3]. These experimental investigations indicate that the nature of the oscillations seems to be very different from *density wave* phenomena, regarding the time periods.

The purpose of this chapter is to study how the involved mechanisms in DWO_{II} and *Ledinegg* phenomena affect condensation and boiling systems with subcooled, saturated and over-heated inlet conditions. A homogeneous model is used to describe the nature of the involved phenomena for different operation regions. Non-dimensional stability maps, $N_{pch}\ vs\ N_{sub}$, are constructed and several simulations show the behaviour of a simple thermo-hydraulic system. In addition the application of a high-order method to solve the conservation equations is described and implemented.

6.2 The Model

The thermo-hydraulic model used to study these kinds of instabilities is the same as the model presented in Section 5.2. It consists of two constant pressure tanks, two valves and a horizontal heated section, as shown in Figure 6.1. The mathematical model used to describe the system is the same as the model presented in the previous chapter. It is based on the assumptions,

- One-dimensional.
- Thermodynamic equilibrium between phases.
- Two-phase homogeneous model [17].
- Two-phase Müller-Steinhagen and Heck pressure drop correlation [12], see Appendix A.

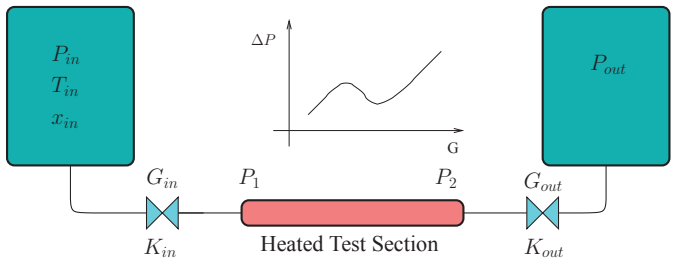

Figure 6.1: *Scheme of the implemented model to analyze DWO and Ledinegg phenomena.*

6.2.1 Stability Criteria

The stability of these phenomena is normally analysed by the construction of non-dimensional stability maps. In this chapter the Sub-cooling and Zuber (phase-change) numbers are used following [7]. They correspond to

$$N_{sub} = \frac{h_f - h_{in}}{h_{fg}} \frac{\rho_{fg}}{\rho_g} \qquad N_{Zu} = N_{pch} = \frac{Q}{GA_{xs}h_{fg}} \frac{\rho_{fg}}{\rho_g} \tag{6.1}$$

The numerical stability limits obtained in this chapter are compared to existing stability limit correlations. One the most used limits to analyze the DWO stability is the Ishi's simplified stability criterion [7]. It is obtained by the development of a thermal equilibrium homogeneous model and it is only applicable for high subcooling numbers ($N_{sub} > \pi$). It is expressed as

$$N_{sub} = N_{Zu} - \text{-}2(K_{in} + K_{out} + f_{TP})1 + \frac{1}{2}(2K_{out} + f_{TP}) \tag{6.2}$$

where K_{in} and K_{out} represent the constant inlet and outlet pressure losses and f_{TP} is the two-phase mixture friction factor.

Another more recent stability limit for DWO is Guido's criterion [6]. This stability limit is obtained using a simple lumped model assuming all the pressure losses represented by an inlet and outlet valves. The representative values of these valves are assumed constant, represented with * in Eq (6.4). The expression of this limit is given by

$$N_{pch} = \frac{\tau}{2}\left(1 + \frac{2}{N_{sub}}\right) - \frac{5}{2} + \left(\left(\frac{\tau}{2}\left(1 + \frac{2}{N_{sub}}\right) - \frac{5}{2}\right)^2 + \tau\right)^{\frac{1}{2}} + N_{sub} \tag{6.3}$$

where the value of τ is given by

$$\tau = 2\frac{K_{in} * + K_{out} *}{K_{out} * + 1} \tag{6.4}$$

The latter limit for DWO is valid for all the range of subcooling numbers. As this criterion does not represent distributed friction losses it is only valid in the

cases where the local pressure losses in the valves are significant respect to the total pressure drop in the system. In the analysis presented by Guido it is also obtained the classical stability limit for *Ledinegg* phenomenon as

$$N_{sub} = \frac{N_{Zu} + \tau}{2} \tag{6.5}$$

6.3 Numerical description

The linearization of the systems is presented in Section 5.3. The main difference with respect to the problems presented in the previous chapters is that the boundary conditions for enthalpy and pressure are set up at $z = 0$ and the third boundary condition corresponds to the outlet pressure at $z = L$.

6.3.1 Numerical solution stability

To evaluate the stability of the numerical solution the evolution of the inlet flow is fitted with the function,

$$f(t) = Ae^{-\alpha t} sin(\beta t + \gamma) + B \tag{6.6}$$

then a stability criterion could be defined as

$$\alpha > 0 \quad Stable \qquad \alpha < 0 \quad Unstable \tag{6.7}$$

Figure 6.2 shows two different simulations and its corresponding fitted curve, Eq. (6.6). These simulations correspond respectively with a stable and an unstable cases. For these two cases the (N_{pch},N_{sub}) pairs are (5.2, 1.1) and (10, 0.6) respectively.

6.4 Numerical results

The approximation order for the space and time are $O_z = O_t = 4$. The number of elements in which the space is discretized is $N_e = 50$ and the time step is $\Delta t = 10^{-2}$ sec for all the cases. The non-linear relative error tolerance for the Picard loop is $\varepsilon_{NL} = 10^{-8}$. In this chapter is not used any adaptive strategy, since only the system stability is analysed. In this case the simulated times are in the order of a few oscillations cycles.

All the simulations in this section are done in a system with the following characteristics:

- Fluid: R134a
- L = 1m, D_H = 5mm
- P_{out} = 8 10^5 Pa, $P_{in} = P_{stationary}(G_{in} = 500$ [kg/m^{2}s])
- K_{in} = 2, K_{out} = 1

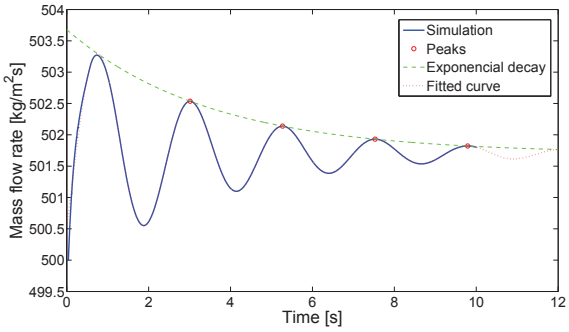

(a) Stable case

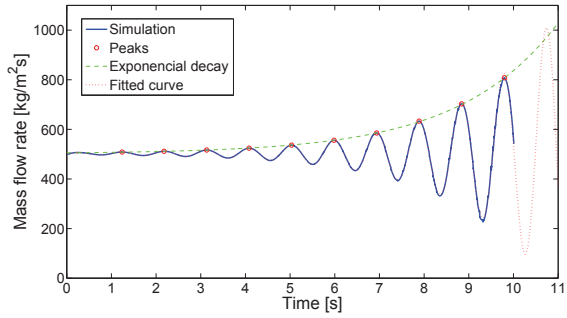

(b) Unstable case

Figure 6.2: *Density wave oscillations and fitted functions. The (N_{pch},N_{sub}) for each case is: (a) (5.2, 1.1) and (b) (10, 0.6).*

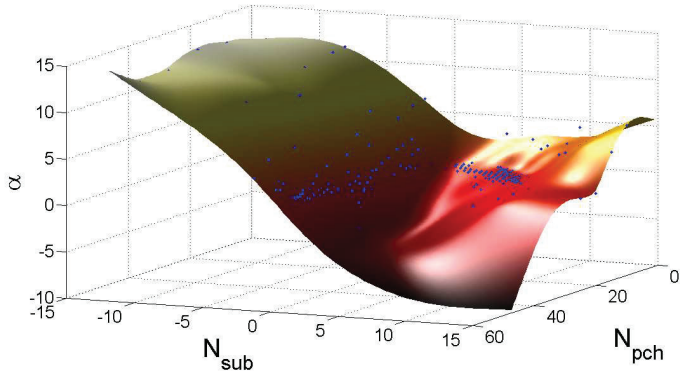

Figure 6.3: *Stability map of α as a function of (N_{pch},N_{sub}) for a boiling system. The blue points correspond with the simulations.*

6.4.1 Boiling

Figure 6.3 shows a three-dimensional map of the stability function α as a function of (N_{pch},N_{sub}). This plot is generated by a total number of 355 simulations where according to the evolution of the system the alpha coefficient is computed. The boiling region is defined for positives N_{pch} numbers.

It is observed that for low negative subcooling numbers ($N_{sub} < -5$) the system response becomes stable and with a fast time response (i.e. $\alpha >> 1$). This situation corresponds with a high-saturated ($x_{in} > 0.5$) and over-heated inlet conditions. The stability of this region is due to the low density change from the saturated to the over-heated states. On the other hand, for $N_{sub} > -5$ the stability of the system decreases and in some regions alpha becomes negative. The stability of the low saturated and subcooled region is analysed in the following sections.

6.4.1.1 Sub-cooled inlet region

The stability map for the subcooled region is presented in Figure 6.4. In this plot the unstable regions due to *Ledinegg* and *density wave* instabilities are observed. For the cases of *Ledinegg* excursion α is imposed to be $\alpha = -0.1$ and no fitting is made. An example of *Ledinegg* excursion is plotted in Figure 6.5, where the system evolution to a new operation point is shown. The classical limit introduced by Guido [6] for *Ledinegg* instability is plotted in red line in the Figure 6.4. It does not fit the boundary found in this analysis for any subcooled region. This differences are probably due to the simplifications used in Guido's lumped model, such as not friction in the pipe and the homogeneous pressure drop model for the valves.

The simplified stability limits, described before, are presented in Figure 6.4. The simplified correlation presented by Ishii [7] predicts conservatively the limit of stability for DWO. Nevertheless, the differences between Ishii's correlation and the

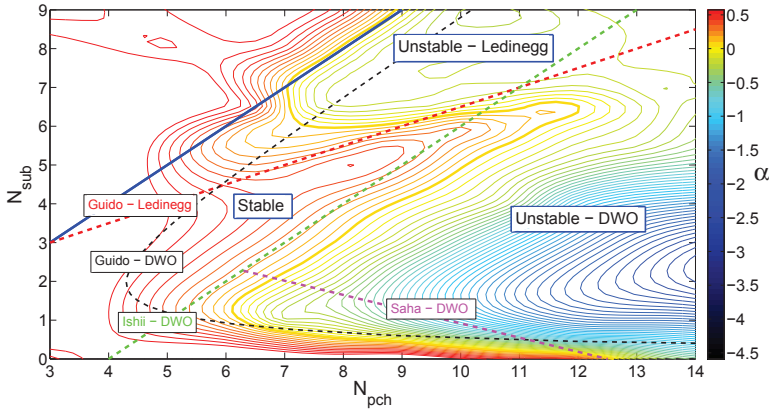

Figure 6.4: *Stable and unstable regions for a boiling system with a subcooled inlet conditions. Ochre line shows the stability limit for $\alpha = 0$. Ishii's [7] and Guido's [6] stability limits are shown in the map.*

limit obtained in this chapter could be due to the pressure drop correlation and used in the present model. Another important difference with Ishii's model is that in the present study the density profile, for the single- and two-phase regions, is updated according to the local enthalpy and pressure. In addition, Saha's limit [16], for low subcooling numbers, is also plotted. It is necessary to remark that this last limit is in the region where subcooled boiling is important. Moreover, this limit is not an independent criteria since it is necessary to give the critical N_{pch} for which $N_{sub} = 0$. In conclusion, the usage of Saha's limit does not seem appropriate for predicting the occurrence of DWO. The simplified Guido's limit for DWO is also presented in the figure. It does not predict accurately the unstable limit for DWO. The main reason of this notable discrepancy is that in this last model the friction losses in the pipe are neglected and a homogeneous model is taken in the valves. Consequently, the results of these criteria (*Ledinegg* and DWO) are only valid in those cases where the local pressure losses (inlet and outlet valves) are much more higher than the pressure loss in the pipe.

6.4.1.2 Saturated inlet region

In Figure 6.6 the stability map of the saturated inlet region is presented. This region is characterised by a low stability. The DWO stability limit follows the same trend as in the low part of the subcooling region ($N_{sub} > 0$). An inflection point in the stability limit is observed when the outlet reaches the single phase gas conditions, red line in Figure 6.6. This change in the behaviour corresponds to the difference in the local pressure drop at the exit restriction between the single gas and the two-phase flow cases. An extrapolation of Saha's limit for DWO is plotted in the figure. For $N_{sub} < 0$, it does not exist any subcooling boiling in the system

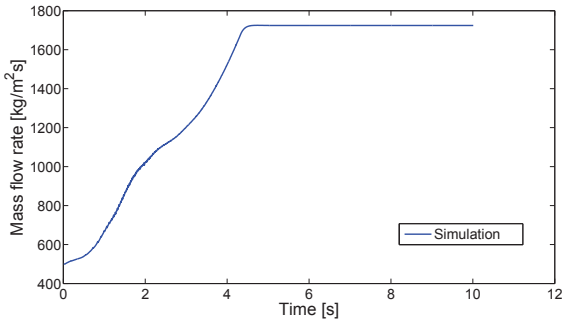

Figure 6.5: *Transient response of the system in a Ledinegg flow excursion. In this case (N_{sub},N_{pch}) are (7,8).*

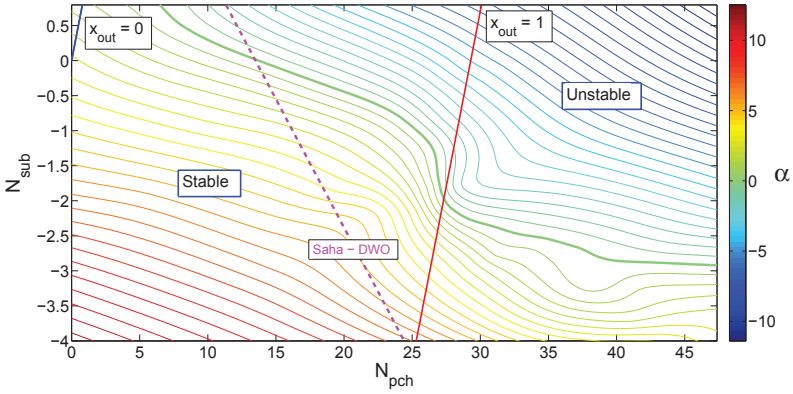

Figure 6.6: *Stable and unstable regions for the saturated case. Green line shows the stability limit for $\alpha = 0$.*

(saturated inlet) and the simplified limit predicted by Saha does not fit the limit obtained in this chapter. In conclusion, it is possible to say that this limit does not give an accurate representation of the main phenomena occurring in the low subcooling region.

Even when no other work analyses oscillations in the saturated inlet region, it is necessary to remark its importance since there is a great number of industrial systems that work in saturated conditions with a low amount of vapor. In addition, the observed oscillations are much faster than those for high subcooling, making it harder to control. However none of the existing correlation is able to predict the position of this limit accurately.

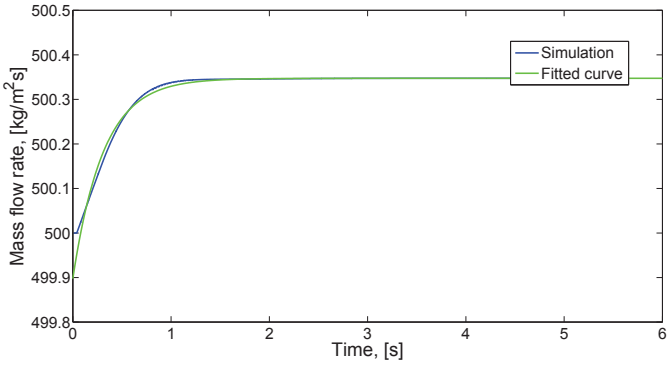

Figure 6.7: *Transient response of the condensing system. This case corresponds to (N_{pch}, N_{sub}) = (-30,-2).*

6.4.2 Condensing

An example of the response of condensing systems is presented in Figure 6.7. In this case, in contrast with the behaviour of a boiling system, the system evolves in an over-damped manner. An exponential curve is fitted to analyze the stability of the system. The stability map for the condensation region is presented in Figure 6.8. In all the cases the system behaves in a stable fashion ($\alpha > 0$). Moreover the minimum value for the parameter α is 3.5, Figure 6.8. A total of 250 cases have been simulated in order to obtain the stability map for a condensing system. In this stability map the region of N_{sub} between 2 and -50 is analysed. The region with positive subcooling number is not analysed since it corresponds with the just liquid region. No *Ledinegg* or *density wave* instability are observed. A discussion of the nature of two-phase flow instabilities in condensing systems is presented in the next section.

6.5 Discussion

6.5.1 Density wave oscillations

As described in [15] for the subcooled inlet conditions, DWO_{II} are mainly the consequence of the regenerative feedback between friction pressure drop and delay effects. In general terms, it is well known that friction losses at the inlet valve stabilise the system while the outlet friction losses destabilise it. In addition, it is also known that the variations in the flow and density at the exit restriction control the oscillation occurrence, since a constant pressure is imposed to the system. While changes in the density produce a positive feedback (destabilising), the changes on the exit flow tend to stabilise the system, as described in [15]. Furthermore it can be easily seen that density profile slopes of opposite sign will affect the system in opposite manner, since the same perturbation will produce an opposite reaction in the two-phase friction losses (pipe and valve). For example, in the case of positive

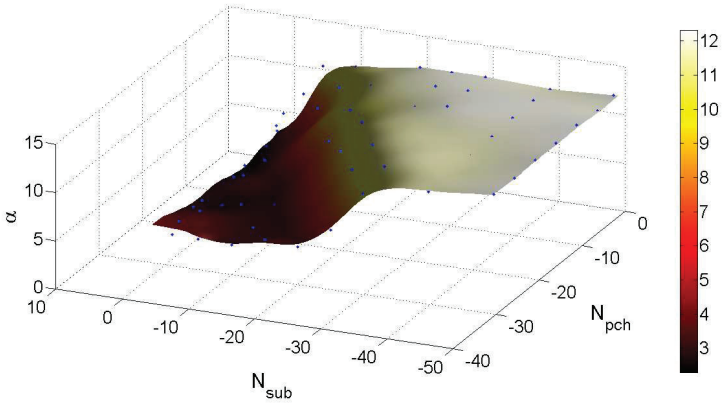

Figure 6.8: *Stability map of α as a function of (N_{pch},N_{sub}). In all the cases α is positive and then the system is stable. The blue points correspond with the simulations.*

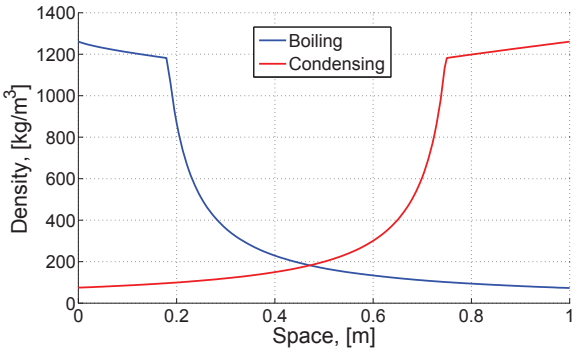

Figure 6.9: *Density profiles for boiling and condensing cases. Boiling case (N_{pch} = 19, N_{sub} = 5); Condensing (N_{pch} = -19, N_{sub} = -15).*

slope (cooling) any increase in the flow produces a decrease in the density at the outlet, while in the case of negative slope (heating) any increase of the flow produces an increase in the exit density. In Figure 6.9 the density profiles for the boiling (heating) and condensing (cooling) cases are presented. For these cases the gradient of the density profile monotonously fulfils

$$\frac{\partial \rho}{\partial z} < 0 \qquad \text{(Heating case)} \tag{6.8}$$

$$\frac{\partial \rho}{\partial z} > 0 \qquad \text{(Cooling case)} \tag{6.9}$$

and these statements are valid for any distribution of heat and any inlet condition (subcooled, saturated or over-heated). Consequently due to the characteristic positive slope of the density profile for condensing flows, the outlet two-phase friction

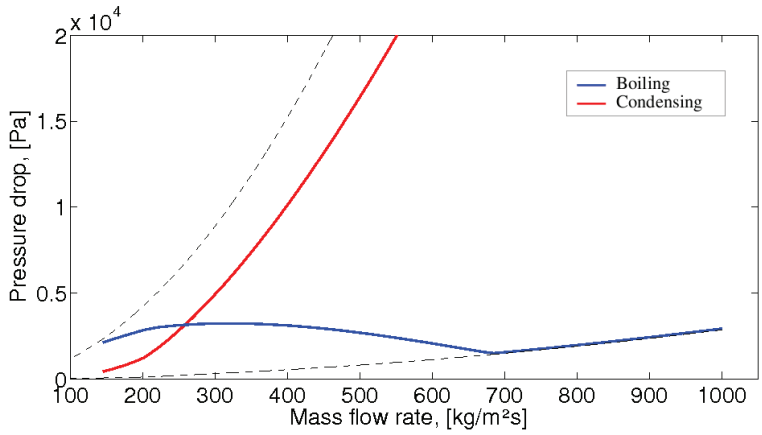

Figure 6.10: *Comparison between the internal characteristic curves of a boiling and a condensing systems. Dashed lines represent the "all vapor" and "all liquid" cases.*

terms will have a stabilising effect. Thus, the system will be stable in the DWO_{II} sense, as shown by the simulations of condensing systems in Figure 6.7. This last conclusion is also in accordance with the experimental data reported in [1, 2], where it is shown that the oscillations in condensing systems are not according with *density wave* and they seem to be related with the amount of compressible volume in the system such as pressure drop oscillations for boiling systems [9, 4]. The main difference with the oscillations occurring in those systems are the characteristic periods of the oscillations. Nevertheless, it is still not clear how the DWO type I and type III could affect condensing systems and its relation with the experimental oscillations described by [1, 2].

6.5.2 Ledinegg instability

The occurrence of *Ledinegg* instability is related with the shape of the pressure drop vs. flow characteristic curve of the system. Steady simulations for both, boiling and condensing systems are presented in Figure 6.10. The system is equivalent to the one described in the previous sections and the inlet temperatures are -23^oC and 107^oC for the boiling and condensing cases, respectively. When the flow tends to zero, in the boiling case, the total pressure drop tends to the all vapor curve. In contrast, when the flow tends to infinite then the pipe would be full of subcooled liquid and the total pressure drop would tend to the all liquid case. As the vapor have a higher pressure drop than the liquid (higher velocity), the two-phase flow characteristic curve will be higher then the one corresponding to the liquid case and for some cases the N-shape would be observed. On the other hand in a condensing system, the mechanism result exactly the opposite. When the flow tends to zero, the total pressure drop will approach to the all liquid case and when the flow tends to infinite the curve will tend to the all vapor case. As it is possible to see in Figure 6.10,

the pressure drop for the all vapor case is always greater (2 orders of magnitude) than the all liquid case.

In consequence, for systems in which the friction pressure drop is dominating (see Section 2.2.1.1 and Section 2.2.1.1), the characteristic curve for the condensing systems will show a steeper slope than the boiling case following the pressure drop curve of the all vapor case. As shown in the figure, the characteristic curve for condensing systems do not show the typical N-shape of boiling systems. Due to these reasons condensing systems do not have the problem of *Ledinegg* instability when the friction terms dominate the total pressure drop (most of the real systems). It is important to notice, that for upward condensing systems the potential component could still create a negative slope of the characteristic pressure drop vs. flow curve, as explained in Section 2.2.1.2.

6.6 Summary

Density wave and *Ledinegg* phenomena were analysed for boiling and condensing in a single channel. A high-order spectral method was used to solve the constitutive conservation equations of the system in order to avoid the typical numerical diffusion of low order methods. A comparison with previous *density wave* stability criteria was presented. In general terms, only Ishii's simplified criterion for *density wave* oscillations predicts accurately the stability limits. A saturated inlet case is analysed. None of the stability correlations describe the stability limit in this case. The *Ledinegg* limits are also characterised and a significant difference between the limit obtained in this chapter and the classical criterion is observed. In addition a condensing system was also analysed. No unstable oscillatory behaviour is observed. A discussion of the occurrence of *density wave* oscillations and *Ledinegg* phenomena in condensing systems is presented. It is found that due to the characteristic positive slope of the density profile it is not possible to find *density wave* (type II) phenomenon in such systems. It is also proved that *Ledinegg* instabilities are not occurring in horizontal condensing systems.

Bibliography

[1] BHATT B. AND WEDEKIND G. A self sustained oscillatory flow phenomenon in two-phase condensing flow system. *ASME Journal of Heat Transfer*, 102: 695–700, 1980. (Cited on page 126, 135)

[2] BHATT B., WEDEKIND G., AND JUNG K. Effects of two-phase pressure drop on the self-sustained oscillatory instability in condensing flows. *ASME Journal of Heat Transfer*, 111:538–545, 1989. (Cited on page 126, 135)

[3] BOYER B., ROBINSON G., AND HUGHES T. Experimental investigation of flow regimes and oscillatory phenomena of condensing steam in a single vertical annular passage. *Int. Journal of multiphase flow*, 21:61–74, 1995. (Cited on page 126)

[4] DING Y., KAKAC S., AND X.J.CHEN . Dynamic instabilities of boiling two-phase flow in a single horizontal channel. *Experimental Thermal and Fluid Science*, 11:327–342, 1995. (Cited on page 135)

[5] FURUTERA M. Validity of homogeneous flow model for instability analysis. *Nuclear Engineering and Design*, 95:65–77, 1986. (Cited on page 125)

[6] GUIDO G., CONVERTI J., AND CLAUSSE A. Density wave oscillations in parallel channels – an analytical approach. *Nuclear engineering and Design*, 125:121–136, 1991. (Cited on page 127, 130, 131, 257)

[7] ISHII M. AND N.ZUBER . Thermally induced flow instabilities in two-phase. *Proceedings of the forth international heat transfer metting*, 1970. (Cited on page 125, 127, 130, 131, 257)

[8] ISHII M. *Thermally induced flow instabilities in two-phase mixtures in thermal equilibrium*. PhD thesis, Georgia Institute of Technology, Michigan, 1971. (Cited on page 125)

[9] KAKAC S. AND BON B. A review of two-phase flow dynamic instabilities in tube boiling systems. *Int. Journal Heat Mass Tranfer*, 51:399–433, 2007. (Cited on page 135)

[10] KOLEV N. I. *"Multiphase Flow Dynamics 4: Nuclear Thermal Hydraulics"*. Springer, 2004. (Cited on page 126)

[11] LIAO N. S. AND WANG C. C. Transient responce characteristics of a two-phase condensing flows. *Int. J. Multiphase Flow*, 16:139–151, 1990. (Cited on page 126)

[12] MULLER-STEINHAGEN H. AND HECK K. A simple friction pressure drop correlation for two-phase flow pipes. *Chem. Eng. Prog.*, 20:297–308, 1986. (Cited on page 126)

[13] NARAYANAN S., SRINIVAS B., PUSHPAVANAM S., AND BHALLAMUDI S. M. Non-linear dynamics of a two-phase flow system in an evaporator: The effects of (i) a time varying pressure drop, (ii) an axially varying heat flux. *Nuclear Engineering and Design*, 178:279–294, 1997. (Cited on page 126)

[14] RIZWAN U. Effects of double-humped axial heat flux variation on the stability of two phase flow in heated channels. *Int. J. Multiphase flow*, 20:721–737, 1994. (Cited on page 126)

[15] RIZWAN U. On density wave oscillations in two-phase flows. *Int. J. Multiphase flow*, 20:721–737, 1994. (Cited on page 126, 133)

[16] SAHA P., ISHII M., AND N.ZUBER . An experimental investigation of the thermally induced flow oscillations in two-phase systems. *Transactions of the ASME*, 1:616–622, 1976. (Cited on page 125, 131)

[17] WALLIS G. B. *One-dimensional two-phase flow*. McGraw-Hill, 1969. (Cited on page 126)

CHAPTER VII

Inertia and compressibility effects on Ledinegg and density wave phenomena

► In this chapter *Ledinegg* and *density wave* oscillations are studied. The main focus of this study is the analysis of the effects of different parameters related to real systems. The effect on the stability of the fluid inertia and the presence of compressible gases in the system is analysed. DWO_{III} (high-order) modes are found to be related with the fluid inertia of external piping. The occurrence of these high-order modes, reported in the literature, is analysed based on the numerical simulation results. In particular it is found that both inertia and compressibility have a high impact on the stability limits of the systems. Finally, the use of wavelet decomposition analysis is proved to be an efficient tool in stability analysis of several frequencies oscillations.

7.1 Introduction

As explained in Chapter 2, the occurrence of oscillations and instabilities may cause severe damages in many industrial systems. Consequently the stability in thermo-hydraulic variables such as mass flux, pressure and temperature should be studied in detail to better understand and characterise the conditions for the occurrence of these phenomena.

In the Sections 2.2.1.2 and 2.2.2 the main mechanisms involved in the occurrence of *Ledinegg* and *density wave* instabilities are presented. In the last two chapters, a homogeneous model is used to describe the evolution and stability of a single channel system. In this chapter, the main focus will be taken in the description of the external system (pump, piping, valves, surge tanks) to study the influence of different parameters in the stability of a boiling single channel. As explained, there exist several experimental and theoretical works describing the occurrence of *density wave* phenomenon [5, 13, 9, 14, 11, 2]. One of the contradictions between those works was the description of DWO_{III} (high-order) modes. While in Yadigaroglu's work [13] higher-order modes were experimentally observed, in Saha's investiga-

tion [9] no higher modes were reported, even if special focus is made on searching for these modes. In addition, regarding the experimental study performed in the latter work, it is necessary to remark that in Saha's experiment the heated section was fixed in a by-pass configuration to assure a constant pressure drop condition (parallel channel condition). Moreover, all the pipes were 50 mm inside diameter and the heater was 10 mm inside diameter. From the given information, the section before the heater (where the pre-heater, turbine flow-meter and flex-joint were situated) was at least 2 meters long. It means that the inlet external inertia was higher than the inertia terms in the heated section. As it is shown later, the fluid inertia is playing an important role in the occurrence of high-order modes. Most of the experimental research do not focus on high-order modes. Actually by the data reported in [14, 11, 2] where the main focus is given to *pressure drop oscillations* (slow oscillations), it is possible to see that the acquisition system was not able to sample fast enough to describe high-order phenomena. In particular previous studies have not analysed the influence of the external parameters of the thermo-hydraulic loop such as compressibility (gases) and external fluid inertia (piping). In some studies (e.g. [3]), a non-heated vertical riser was modelled but the main focus is given to the gravity and pressure drop influence, as explained in Chapter 2.

The purpose of this chapter is to analyse the influence of the fluid inertia and compressibility volumes in different parts of the thermo-hydraulic loop. A model that includes external parameters (inertia, compressibility, pump response) is presented. A non-dimensional stability analysis of different cases is presented.

7.2 The Model

In this section a model to study the stability of two-phase flow systems is presented. This model includes: a constant pressure tank, P_{out}; a variable pressure tank in order to take into account the pump response and the pump evolution, $P_{in}(G_1, t)$; a heated section; two different surge tanks to simulate the effects of compressible volumes (non-condensable gas), V_{Si} and V_{So}; four incompressible pipe lines (inertia effects), L_i ; and finally four localised pressure drops in each section, K_i, as shown in Figure 7.1. Thus, the pressure difference between both tanks acts as the driving force and, according to the valves opening, the external characteristic ($\Delta P \ vs. \ G$) results in a quadratic decreasing curve. The implemented model is based on the following assumptions,

- One-dimensional model.
- Two-phase homogeneous model, [10].
- Thermodynamic equilibrium conditions, [6].
- Colebrook pressure drop correlation in the single phase region [12] and two-phase Müller-Steinhagen and Heck pressure drop correlation for two-phase flow region [7], see Appendix A.

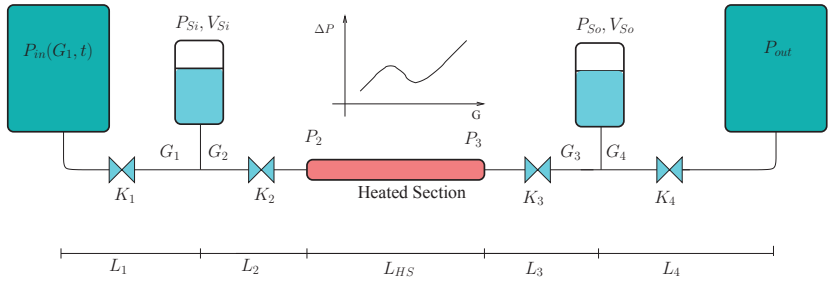

Figure 7.1: *Scheme of the implemented model.*

The mathematical description of the external system (pump, piping, surge tanks) corresponds to the conservation of momentum, since an adiabatic incompressible model is assumed for the pipes. In addition, an ideal isothermal gas model is assumed for the surge tanks. The equations of the external system can be expressed as

$$\dot{P}_{si} = \frac{P_{si}^2}{P_{si0}V_{si0}}\frac{A_{xs}}{\rho_l}(G_2 - G_1) \tag{7.1}$$

$$\dot{P}_{so} = \frac{P_{so}^2}{P_{so0}V_{so0}}\frac{A_{xs}}{\rho_l}(G_4 - G_3) \tag{7.2}$$

$$\dot{G}_1 = \left[P_{in}(G_1,t) - P_{si} - K_1\frac{G_1|G_1|}{2\rho_l}\right]\frac{1}{L_1} \tag{7.3}$$

$$\dot{G}_2 = \left[P_{si} - P_2 - (K_2+1)\frac{G_2|G_2|}{2\rho_l}\right]\frac{1}{L_2} \tag{7.4}$$

$$\dot{G}_3 = \left[P_3 - P_{so} - (K_3-1)\frac{G_3|G_3|}{2\rho_{out}}\right]\frac{1}{L_3} \tag{7.5}$$

$$\dot{G}_4 = \left[P_{so} - P_{out} - K_4\frac{G_4|G_4|}{2\rho_{out}}\right]\frac{1}{L_4} \tag{7.6}$$

The mathematical model used to describe the evolution of the heated section is the same as the one presented in previous chapters. The conservation equations can be expressed as

$$\frac{\partial\rho}{\partial t} + \frac{\partial G}{\partial z} = 0 \tag{7.7}$$

$$\frac{\partial G}{\partial t} + \frac{\partial}{\partial z}\left(\frac{G^2}{\rho}\right) + \frac{\partial P}{\partial z} + \frac{f}{D_H}\frac{G|G|}{2\rho} = 0 \tag{7.8}$$

$$\frac{\partial \rho h}{\partial t} + \frac{\partial G h}{\partial z} = Q\frac{P_H}{A_x} \tag{7.9}$$

As shown in Eqs. (7.1) to (7.6), the pressure drop in the valves is calculated using a homogeneous local pressure drop model, K_i, for each valve. Friction losses

are neglected in the energy equation and the friction factor in Eq. (7.8) is given by the known Colebrook correlation for the single phase regions (liquid or gas) and by Müller-Steinhagen and Heck correlation for the two-phase region [7]. All the fluid properties are updated in each point as a function of the local enthalpy and pressure.

Even if not all the introduced parameters are analysed in this chapter, their description is necessary to present a model that includes the main effects present in real industrial cases. None of the previous mentioned works analyse directly these external effects. In the next chapter ([8]) a complementary analysis to this chapter is made with focus on the *pressure drop oscillations*. The main parameters and criteria to study the stability of these systems were introduced in the last chapter, see Section 6.2.1.

7.3 Numerical description

7.3.1 The internal problem (heated section)

In accordance with the previous chapters the linearization of the internal system results in

$$\mathcal{L}_{int} = \begin{Bmatrix} \frac{\partial \bullet}{\partial z} & 0 & 0 \\ \frac{\partial \bullet}{\partial t} & \frac{\partial \bullet}{\partial z} & 0 \\ 0 & 0 & \rho^* \frac{\partial \bullet}{\partial t} + G^* \frac{\partial \bullet}{\partial z} \end{Bmatrix} \tag{7.10}$$

$$\mathbf{g}_{int} = \begin{Bmatrix} -\frac{\partial \rho^*}{\partial t} \\ -\frac{\partial}{\partial z}\left(\frac{G^{*2}}{\rho^*}\right) - \frac{f}{D_H}\frac{G|G|}{2\rho^*} \\ Q\frac{P_H}{A_x} \end{Bmatrix} \tag{7.11}$$

$$\mathbf{u}_{int} = \begin{Bmatrix} G \\ P \\ h \end{Bmatrix} \tag{7.12}$$

where G^* and ρ^* correspond to the old values of flow and density respectively. The initial condition boundary nodes are set to initial values for flow, pressure and enthalpy. In this chapter, the boundary conditions for enthalpy, flow are imposed at $z = 0$ and the boundary condition for the pressure is set at $z = L$.

7.3.2 The external problem (pump, piping, valves, surge tank)

The external system is solved only as a function of the time (one-dimensional). The operator description of this system, Eqs. (7.1) to (7.6) corresponds with

$$\mathcal{L}_{ext} = \begin{Bmatrix} \frac{\partial \bullet}{\partial t} & 0 & 0 & 0 & 0 & 0 \\ 0 & \frac{\partial \bullet}{\partial t} & 0 & 0 & 0 & 0 \\ 0 & 0 & \frac{\partial \bullet}{\partial t} & 0 & 0 & 0 \\ 0 & 0 & 0 & \frac{\partial \bullet}{\partial t} & 0 & 0 \\ 0 & 0 & 0 & 0 & \frac{\partial \bullet}{\partial t} & 0 \\ 0 & 0 & 0 & 0 & 0 & \frac{\partial \bullet}{\partial t} \end{Bmatrix} \tag{7.13}$$

$$\mathbf{g}_{ext} = \begin{Bmatrix} \frac{P_{si}^2}{P_{si0}V_{si0}} \frac{A_{xs}}{\rho_l}(G_2^* - G_1^*) \\ \frac{P_{so}^2}{P_{so0}V_{so0}} \frac{A_{xs}}{\rho_l}(G_4^* - G_3^*) \\ \left[P_{in} - P_{si}^* - K_1 \frac{G_1^*|G_1^*|}{2\rho_l}\right] \frac{1}{L_1} \\ \left[P_{si}^* - P_2^* - (K_2+1)\frac{G_2^*|G_2^*|}{2\rho_l}\right] \frac{1}{L_2} \\ \left[P_3^* - P_{so} - (K_3-1)\frac{G_3^*|G_3^*|}{2\rho_{out}^*}\right] \frac{1}{L_3} \\ \left[P_{so}^* - P_{out} - K_4 \frac{G_4^*|G_4^*|}{2\rho_{out}^*}\right] \frac{1}{L_4} \end{Bmatrix} \tag{7.14}$$

$$\mathbf{u}_{ext} = \begin{Bmatrix} P_{si} \\ P_{so} \\ G_1 \\ G_2 \\ G_3 \\ G_4 \end{Bmatrix} \tag{7.15}$$

where the * variables correspond to the values of the variables in the previous non-linear step.

7.3.3 Wavelet stability analysis

To evaluate the stability of the numerical solution the evolution of the inlet flow is analysed by using wavelet decomposition [1]. In particular, the "Mexican hat" wavelets family is used. This numerical technique is useful not only to analyse the frequency spectrum but also to obtain the evolution of the spectrum corresponding to the signal. For a given function $u(t)$, the "Mexican hat" wavelet transform is written as

$$\tilde{u}(\sigma, t) = \int u(t')\Psi(t - t', \sigma)dt' \tag{7.16}$$

where the function Ψ is the negative normalised second derivative of a Gaussian function,

$$\Psi(\sigma, t) = \frac{d^2 F_\sigma}{d^2 t} = \frac{2}{\sqrt{2\sigma}\pi^{\frac{1}{4}}} \left(1 - \frac{t^2}{\sigma^2}\right) e^{\frac{-t^2}{2\sigma^2}} \tag{7.17}$$

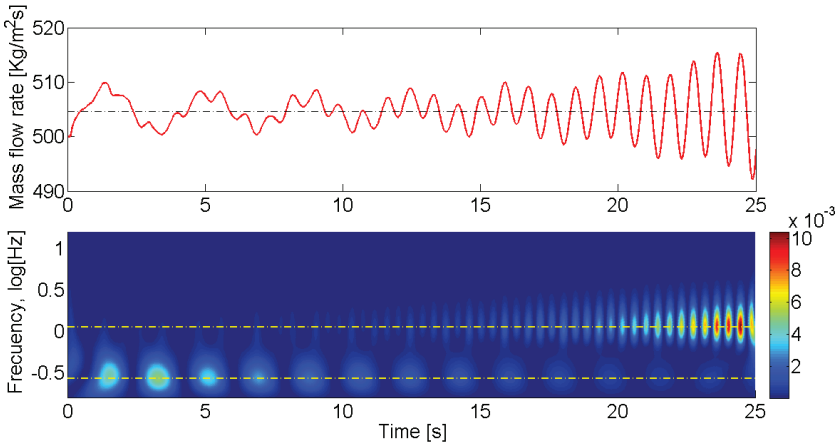

Figure 7.2: *Density wave oscillations and wavelet decomposition. Two different modes can be observed. This case corresponds to the example of Section 7.4.1.3. The pair (N_{pch},N_{sub}) for this case is (17,7.5).*

Finally the variable σ is transformed to frequency (Hz) and the signal spectrum is analysed. In Figure 7.2 the wavelet decomposition of a simulated case is presented. The color-bar corresponds to the percentage of energy for each coefficient of the wavelet decomposition. In this case the decomposition is characterised by two peaks at different frequencies. The lower frequency component behaves in convergent fashion, while the high frequency component evolves with a divergent behaviour. The peak position for each characteristic frequency is detected and an exponential curve is fitted to the maximum values. Then, according to the obtained exponential function, $f(t) = Ae^{-\alpha t}$, the stability criterion for each mode corresponds to Eq. (7.18). In this way, the use of wavelet analysis allows to analyse independently the evolution of different frequency modes.

$$\alpha > 0 \quad Stable \qquad \alpha < 0 \quad Unstable \tag{7.18}$$

As it is shown in Chapter 2, several mathematical and modelling techniques could be used to simplify this problem (linearization, Laplace transforms, etc.). Nevertheless, the main idea of using the direct simulation analysis is to use the same analysis as the one used in industrial systems, where those mathematical tools and modelling simplifications can not be applied.

7.4 Numerical Results

In the following simulations, the numerical order of approximation of time and space is $O_z = O_t = 4$. The number of elements in which the space is discretized is $N_e = 50$, the time step is $\Delta t = 10^{-2}$ sec, and the nonlinear relative error tolerance

for the Picard loop is $\varepsilon_{NL} = 10^{-8}$. In this chapter no hp-adaptive strategy is used, since the simulated times are in the order of a few oscillation cycles.

7.4.1 Inertia analysis

In the following examples the influence of the fluid inertia in the external pipes is discussed. The presence of compressible gases in the system is assumed to be negligible. All the simulations in this section are done in a system with the following characteristics:

- Fluid: R134a
- L_{HS} = 1m, D_H = 5mm
- P_{out} = 8 10^5 Pa, $P_{in} = P_{stationary}(G_{in} = 500$ [kg/m^{2}s])
- K_1 = 10, K_2 = 0, K_3 = 0, K_4 = 1
- $V_{si} = V_{so} = 0$

7.4.1.1 No external inertia

In this example a no external inertia case is analysed, $L_{1-2-3-4} = 0$. The corresponding stability map is presented in Figure 7.3. A total of 204 simulations have been used for the construction of this map. Most of these simulations are localised close to the stability limit to assure an accurate description of the system in that region.

The simplified stability criteria corresponding to Ishii [6] and Guido [4], describing the occurrence of *Ledinegg* and DWO are plotted in this figure. These limits follow the same trends as it was described in the previous chapter, Chapter 6. Therefore the usage of Guido's limit for both *Ledinegg* and DWO to real cases should be very carefully analysed, since these criteria do not seem to reflect the nature of the involved phenomena. In contrast, Ishii's limit seems to predict conservatively the occurrence of DWO. No high-order modes are observed in the analysed simulations for this case.

7.4.1.2 Inlet inertia

The same case as the previous section is analysed but in this example a one meter inlet pipe, $L_2 = 1m$ and $L_{1-3-4} = 0$ are used. A total of 226 numerical simulations have been used to construct the map in Figure 7.4. Similarly the stability limit criteria for DWO and *Ledinegg* instabilities are plotted. None of the stability limits seems to predict accurately the DWO stability limit, since the models used to obtain those limits do not reflect the influence of external parameters (pipe line lengths). Moreover, the system behaves in a more stable way when inertia is introduced at the inlet of the heated pipe. No high-order modes are observed in this case. A discussion and a comparison of this results is presented in the following sections.

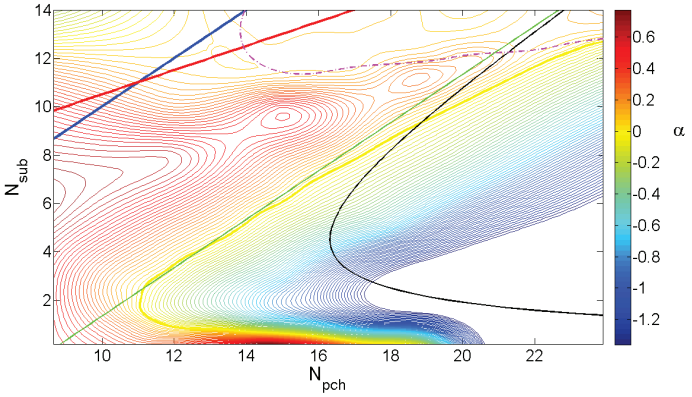

Figure 7.3: *Stability map for $L_{1-2-3-4} = 0$. This stability map corresponds to the normal DWO mode. Green and black lines are, respectively, Ishii's simplified criterion [5] and Guido's correlation [4]. Pink and red lines show the numerical stability limit and Guido's criterion for the occurrence of Ledinegg instability.*

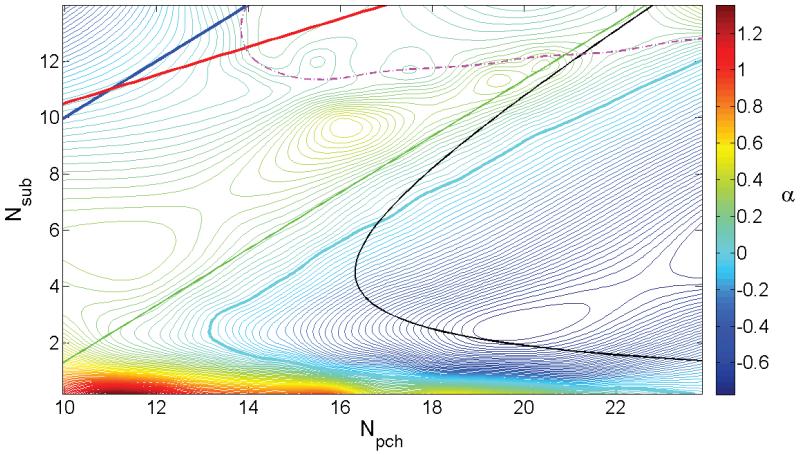

Figure 7.4: *Stability map for $L_2 = 1m$, $L_{1-3-4} = 0$. This stability map corresponds to the normal DWO mode. Green and black lines are, respectively, Ishii's and Guido's criteria. Pink and red lines show, respectively, the numerical stability limit and Guido's correlation for the occurrence of Ledinegg instability.*

7.4.1.3 Outlet inertia

In this example, an outlet one meter pipe is considered, (i.e. $L_{1-2-4} = 0$ and $L_3 = 1m$). A total number of 225 cases have been used to construct the stability map of Figure 7.5(a). Ishii's and Guido's stability limits for DWO and *Ledinegg* are also plotted. None of these criteria reflect the stability limits correctly, since none of them take into account external parameters such as the inertia of the fluid in non-heated pipes. In contrast with the other two examples, in this case high-order DWO appear for high sub-cooling numbers. The limits for the normal mode and the high-order modes are plotted in Figures 7.5(a) and 7.5(b). For $N_{sub} > 5$, the high-order modes become unstable even when the natural DWO mode is stable. Moreover, for $N_{sub} > 10$ the higher-order oscillations are not a pure frequency oscillation but, conversely, they correspond to the sum of different frequencies modes, as shown in the Figure 7.6. This last fact is completely in accordance with the experimental data presented in [13], where for higher sub-cooling the superposition of different higher-order modes is observed. The ratio between high-order and normal modes frequencies goes from 2.5 times ($N_{pch} = 14, N_{sub} = 5$) to approximately 10 times ($N_{pch} = 21, N_{sub} = 12$).

7.4.1.4 Discussion

In Figure 7.7 all the stability limits for the inertia examples are plotted. As it is possible to see, the effects of inlet external inertia stabilise the system. In contrast, the outlet inertia not only destabilises the system but also causes the occurrence of high-order DWO (type III). In conclusion, as an important design rule for two-phase systems, it is possible to say that the outlet pipes (two-phase outlet) should be shortened as much as possible in order to stabilise normal DWO and do not induce high-order modes. Moreover, the occurrence of high-order modes can affect more strongly the control systems since their frequency is higher than a normal DWO. The period of the normal oscillations does not seem to change significantly within these three different examples.

These stability limits are in accordance with the experimental data presented in [13]. These results seem to be the link between Sahas's and Yadigaroglu's experimental works. Regarding those cases, it is necessary to remark that the outlet pipe used in Yadigaroglu's experiment has had a strong influence over the system, inducing the described high-order modes. On the other hand in the case of the Saha's experiment, the use of a by-pass configuration and the long inlet section stabilise the system and as a result no high-order mode oscillations were observed.

7.4.2 Compressible volumes analysis

In this section the influence of the compressible volumes on the stability of the system is studied. The same methodology as described in the inertia cases is applied. All the simulations in this section are done in a system with the following characteristics:

- Fluid: R134a

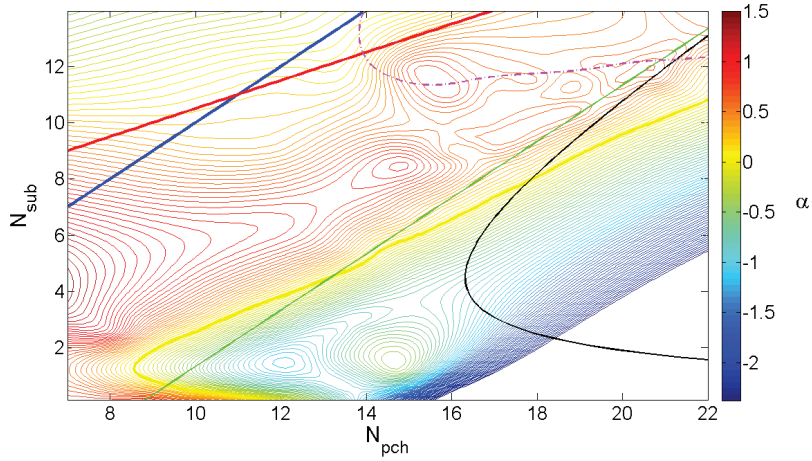

(a) Normal mode

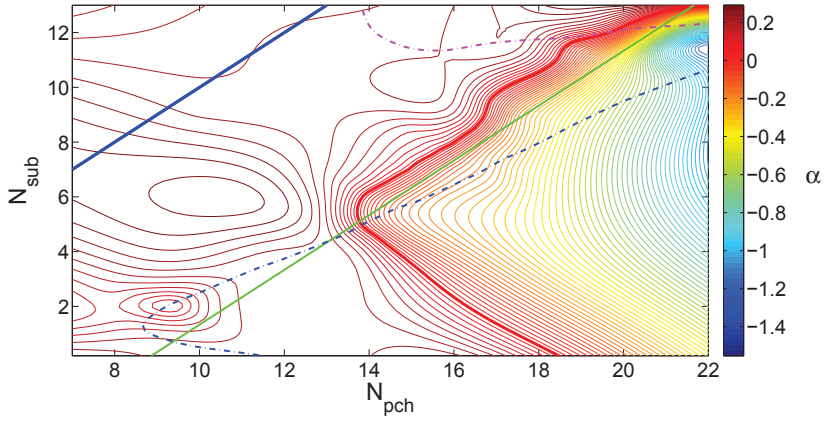

(b) High-order mode

Figure 7.5: *Stability maps for $L_{1-2-3} = 0,\ L_4 = 1m$. Normal (DWO - type II) (a) and high-order (DWO - type III) (b) stability maps are shown. Green and black lines represent, respectively, Ishii's and Guido's criteria. Pink and red lines show the numerical stability limit and Guido's correlation for the occurrence of Ledinegg instability.*

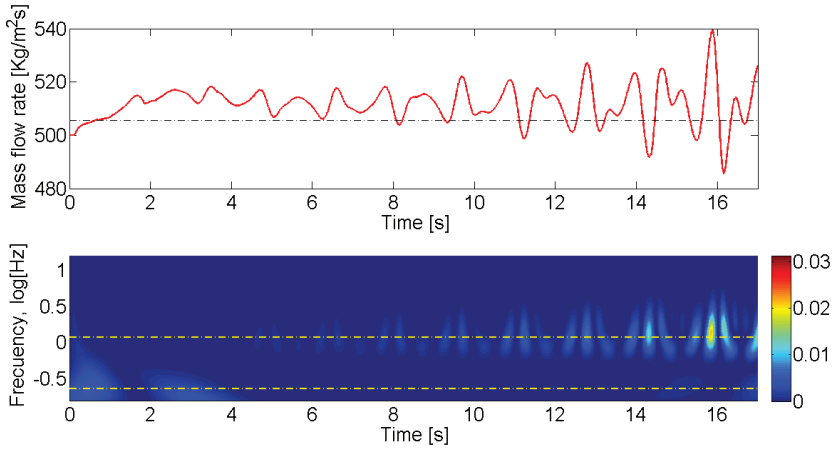

Figure 7.6: *Density wave oscillations and wavelet decomposition. (N_{pch},N_{sub}) for this case are (19,10.5). In this case the high-order modes (DWO - type III) are the sum of different frequency components.*

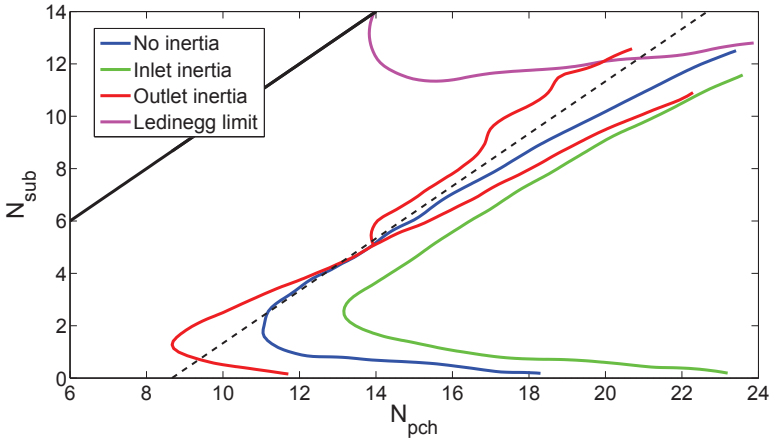

Figure 7.7: *Comparison of the stability limit for the three analysed examples. No external inertia (blue line), inlet inertia (green line) and outlet inertia (red line). In the case of outlet inertia higher-modes are observed in the system. The higher-mode stability limit is also plotted in red line.*

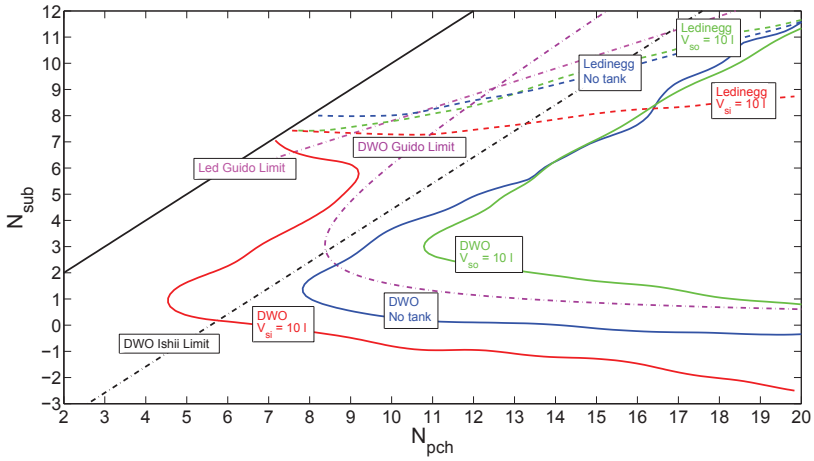

Figure 7.8: *Comparison of the stability limit for the case of inlet and outlet compressible volume. For DWO the different cases are: no compressibility case (blue lines), inlet compressibility (green lines) and outlet compressibility (red lines). Ishii's and Guido's stability limits are plotted in dashed lines.*

- L_{HS} = 1m, D_H = 5mm
- P_{out} = 8 10^5 Pa, $P_{in} = P_{stationary}(G_{in} = 500$ [kg/m^{2}s])
- K_1 = 10, K_2 = 0, K_3 = 0, K_4 = 4
- $L_1 = 1m, L_2 = L_3 = 0, L_4 = 1m$

Three different cases are presented: *no* compressibility, *inlet* compressibility and *outlet* compressibility. In the compressibility cases a 10 [l] volume upstream or downstream of the heated section, respectively, is modelled. The compressible volume is assumed to behave as an ideal gas, as described in Section 7.2. As shown above, one meter pipes are simulated at the inlet and outlet of the system. In Figure 7.8, the comparison between the stability limits of the three examples in this section is shown. Significant differences on the stability limits are observed. For all the cases the oscillations are mainly dominated by the main mode. Only in the no compressibility case high-order modes are observed for high sub-cooling numbers. The high-order modes are observed as a wave in the stability limit for sub-cooling number larger than 7. No high-order modes are observed in the cases where the compressible volume is taken into account. For the construction of the maps a total of 227 (no comp.), 260 (outlet comp.) and 280 (inlet comp.) simulations have been analysed. The soft undulations in the boundaries are due to the numerical approximation of the stability surface and they do not represent any physical effect.

7.4.2.1 Discussion

In Figure 7.8 the limit for both *Ledinegg* and DWO are presented for the three different cases. For the inlet compressibility case the stability limit of both *Ledinegg* and DWO are highly influenced. These two limits are more unstable compared to the case of no compressibility. The destabilisation of the *Ledinegg* limit is explained by the decoupling between K_1 section and the heated section due to the compressible tank. So in this case the external characteristic pressure drop vs. flow curve, intersecting the curve of the heated section, is not following the behaviour of the valve K_1. Moreover, in this case the *density wave* stability limit is changing its shape. It seems that the limit is influenced by the *Ledinegg* stability limit. So the influence of the compressible volume is not just moving the stability limit to the left (destabilising) but also adding a region close to the *Ledinegg* limit as unstable zone. It should be noted that the phenomena occurring in that region is not due to *pressure drop oscillations* but due to flow excursions (*Ledinegg*) instead.

In contrast, when a compressible downstream volume is simulated, then the limit for DWO is stabilised (moved to the right) for every sub-cooling number. It also stabilises the high-order modes, discussed on previous sections. The stabilisation of high-order modes seems to be the consequence of the decoupling between the heated section and the outlet pipe. In that sense it can not be directly concluded that a compressible volume stabilises high-order modes. This effect is a secondary consequence of fixing a compressible volume downstream the heater. In any case, the compressible volume can be used as a valid way of stabilising the system in a DWO sense. As analysed in [8], the influence of the compressible tanks are related with the distance respect to the heated section. So for both cases (inlet and outlet) the influence will be stronger as closer they are placed respect to the heated section.

In conclusion, the introduction of a compressible volume downstream the heated section can result in a more stable system. In addition, in most of the two-phase systems the tanks where vapor can produce the effect of compressible volume are located downstream the heated section. Thus, special attention has to be paid to the use of pressurisers and expansion volumes when they are fixed upstream of the heated section.

7.5 Summary

A general model to study the effects of several external parameters (external to the heated section) such as: fluid inertia in pipes, compressible gases and pump responses was presented. *Density wave* and *Ledinegg* phenomena were analysed with focus on the influence of these external parameters which have not been analysed in previous studies.

The inertia influence of the connecting pipes was analysed. It was found that the inlet inertia (longer inlet pipes) increases the stability of the system. On the contrary, for the increase of outlet inertia (longer outlet pipes) the stability of the system is not just decreased but also high-order oscillations are induced. The occurrence of high-order oscillation modes, reported experimentally, was described.

The frequency of these high-order oscillations was found to be between 2.5 and 10 times the frequency of the normal mode, according to the (N_{pch},N_{sub}) region. Different modes are induced for different set of parameters as observed experimentally. Wavelet decomposition was proved to be an efficient analysis technique for studying the evolution of different oscillatory modes.

The effects of compressible gases in the system were also studied. It was found that when a compressible volume is placed upstream of the heated section, then the system becomes highly unstable, for both *Ledinegg* and *density wave* phenomena. In contrast, when the compressible volume is fixed downstream of the heated section the system becomes more stable in the *density wave* sense.

Bibliography

[1] ADDISON P. S. *The illustrated wavelet transform handbook*. Institute of Physics Publishing, Bristol, UK, 2002. (Cited on page 143)

[2] DING Y., KAKAC S., AND X.J.CHEN . Dynamic instabilities of boiling two-phase flow in a single horizontal channel. *Experimental Thermal and Fluid Science*, 11:327–342, 1995. (Cited on page 139, 140)

[3] FUKUDA K. AND KOBORI T. Classification of two-phase flow instability by density wave oscillation model. *Journal of Nuclear and Technology*, 16:95–108, 1979. (Cited on page 140)

[4] GUIDO G., CONVERTI J., AND CLAUSSE A. Density wave oscillations in parallel channels – an analytical approach. *Nuclear engineering and Design*, 125:121–136, 1991. (Cited on page 145, 146, 258)

[5] ISHII M. AND N.ZUBER . Thermally induced flow instabilities in two-phase. *Proceedings of the forth international heat transfer metting*, 1970. (Cited on page 139, 146, 258)

[6] ISHII M. *Thermally induced flow instabilities in two-phase mixtures in thermal equilibrium*. PhD thesis, Georgia Institute of Technology, Michigan, 1971. (Cited on page 140, 145)

[7] MULLER-STEINHAGEN H. AND HECK K. A simple friction pressure drop correlation for two-phase flow pipes. *Chem. Eng. Prog.*, 20:297–308, 1986. (Cited on page 140, 142)

[8] RUSPINI L., DORAO C., AND FERNANDINO M. Modeling of dynamic instabilities in boiling systems. *Proceedings of 19th International Conference On Nuclear Engineering, ICONE19, Japan*, 2011. (Cited on page 142, 151)

[9] SAHA P., ISHII M., AND N.ZUBER . An experimental investigation of the thermally induced flow oscillations in two-phase systems. *Transactions of the ASME*, 1:616–622, 1976. (Cited on page 139, 140)

[10] WALLIS G. B. *One-dimensional two-phase flow*. McGraw-Hill, 1969. (Cited on page 140)

[11] WANG Q., CHEN X. J., KAKAC S., AND Y.DING . An experimental investigation of density-wave-type oscillations in a convective boiling upflow system. *Int. J. Heat and Fluid Flow*, 15, 1994. (Cited on page 139, 140)

[12] WHITE F. M. *Fluid Mechanics*. McGraw-Hill, 2003. (Cited on page 140)

[13] YADIGAROGLU G. AND BERGLES A. Fundamental and higher mode density-wave oscillations in two-phase flows. *Journal of heat transfer, Trans. ASME*, 94:189–195, 1972. (Cited on page 139, 147)

[14] YUNCU H. An experimental and theorethical study of density wave and pressure drop oscillations. *Heat transfer engineering*, 11:45–56, 1990. (Cited on page 139, 140)

CHAPTER VIII

Dynamic simulation of pressure drop oscillations

► In this chapter the pressure drop oscillation phenomenon is studied. The model used in the previous chapter is adopted in order to study the influence of several parameters. A comparison between a *dynamic* and the traditional *steady-state* models is made. Important differences in the prediction of the system evolution are obtained. It is proved that in several cases the results obtained with the *steady-state* models do not represent the nature of the involved phenomena. Moreover, the influence of several parameters such as compressible volumes and fluid inertia, downstream and upstream from the heated pipe, is investigated. It is observed that these parameters can affect the stability of the system and the frequency of the oscillations.

8.1 Introduction

In the last 60 years several aspects of the phenomenon called *pressure drop oscillations* have been studied. The main mechanisms involved in the occurrence of this phenomenon were explained in the Section 2.2.1.5. In the last years several experimental investigations described PDO in boiling systems, [17, 4, 8, 5]. In [4] the existence of a critical surge tank volume was experimentally proved. For this critical volume a transition between unstable-stable states takes place. Moreover, in [2] and [16] a deep experimental analysis on the interaction between dynamic instabilities in a horizontal tube was presented. In most of the experimental cases DWO are observed during the occurrence of PDO.

Several simplified theoretical methods have been applied to study PDO: Vander-Pol oscillator methods ([9]), D-partition methods ([15, 7]), planar models ([6]), bifurcation analysis ([10, 11]). These studies assume that PDO phenomenon is not related with other dynamic phenomena such as DWO. In consequence, they assume that the dynamic of the system is given by the evolution of the main variables in the external components (surge tank and piping). *Steady-state* models for the heated pipe are normally used. The main argument to study this phenomenon using simplified methods is that the time period of PDO is always much greater than the period for DWO. It is necessary to remark that these conditions are true only for

some kind of particular systems: big compressible upstream tank and short heated pipe. Moreover, it is found that the period of the oscillations is proportional to the amount of compressible gas in the surge tank, see [4]. It means that for low amount of non-condensable gases in the system (normal conditions in an industrial case) the frequency of these oscillations may result in the same order than *density wave* oscillations. On the other hand, even when in most of the experimental cases DWO have been observed overlapped with PDO, no work analyses the implementation of a *dynamic* model (normally used for DWO). More recently [14], the interaction between dynamic instabilities was briefly described. Nevertheless, no comparison with previous models or parameter analysis were presented in this last work. In addition none of the previous studies analysed the influence of compressible volumes downstream the heated section and its effect on PDO phenomenon.

The objective of this chapter is to analyse the validity of the previous mentioned models (steady-state heated pipe) used to simulate PDO. The *dynamic* model used in previous chapters is used to study this phenomenon. The effects of compressible volumes, both upward and downward from the heated section, and the effect of fluid inertia in the non-heated pipes are considered. Moreover, a parametric study regarding the system stability is also presented.

8.2 The Model

The model used in this chapter is the same as the one presented in the previous chapter. In this chapter a *steady-state* simplification is introduced in the model of the heated section in order to compare with the *dynamic* model. In the next section, these two models are described.

8.2.1 Heated section models

The model used in previous chapters will be called “dynamic” model. It corresponds with the resolution of the conservation equations, Eqs. (7.7) to (7.9). In this section the model used in previous PDO works, from now on called “steady-state”, is described.

8.2.1.1 Steady-state model

The *steady-state* model is based in the assumption that the temporal terms in the conservation equations, Eqs. (7.7) to (7.9), are negligible. In consequence, the flow can be assumed constant (G_{in}) and the momentum and energy equations become

$$\frac{\partial P}{\partial z} = -\frac{\partial}{\partial z}\left(\frac{G^2}{\rho}\right) - \frac{f}{D_H}\frac{G^2}{2\rho} \tag{8.1}$$

$$\frac{\partial h}{\partial z} = \frac{Q}{G}\frac{P_H}{A_x} \tag{8.2}$$

8.3 Numerical results

The numerical order of approximation for the time and the space are respectively $O_z = 5$ and $O_t = 4$. The number of elements in which the space is discretized is $N_e = 35$ and the time step is assumed to be $\Delta t = 10^{-2}$ sec. In addition the non-linear tolerance is $\varepsilon_{NL} = 10^{-6}$.

All the simulations in this section are done in a system with the following characteristics:

- Fluid: R134a
- L_{HS} = 1 [m], D_H = 5 [mm]
- Q = 1 [kW]
- P_{out} = 8 x 10^5 [Pa], $T_{in} = -23$ [^{o}C], $G_{in} = 500$ [kg/m^{2}s]
- L_1 = 1 [m], L_2 = 1 [m], L_3 = 1 [m], L_4 = 1 [m]

This case is representative of a typical industrial process where the total pressure drop is controlled by the external system (high K_1). The effects of K_1 on the system behaviour are fully described in [3]. Moreover, PDO are restricted to this kind of systems where the slope of the external characteristic is steeper than the slope of the internal characteristic ($K_1 >> K_2$). The values of K_2, K_3 and K_4 represent typical component pressure drop losses such as angles, curves, valves and they are in the order of the pressure drop of the heated pipe.

8.3.1 Dynamic vs. steady-state models

For the system described above both the *dynamic* and the *steady-state* models are solved. The results of these simulations are presented in Figure 8.1(a). It can be seen that despite the same initial conditions the evolution of the system results in completely different behaviours, both in frequency and in the amplitude of the oscillation. Moreover, while the steady model predicts a periodic oscillation, the *dynamic* model predicts a stable operation point. A detailed view of the beginning of these simulations, with same initial conditions, is presented in Figure 8.1(b). Similarly, several more cases were studied (V_S = 0.5,2,4,5,10 [l]). For all of them both models give different results. It implies that the results of the *steady-state* models can not be directly used in order to analyse the stability of these systems. It is observed that the dynamic behaviour of the heated channel affects both the amplitude and the frequency of the oscillations. In consequence, the nature of the phenomena involved are not well described by *steady-state* models.

8.3.2 Parametric study

All the simulations presented as a part of this parametric study are made using the *dynamic* model introduced in the previous sections.

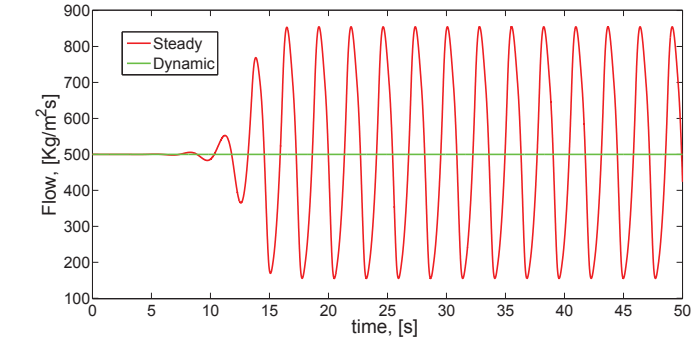

(a)

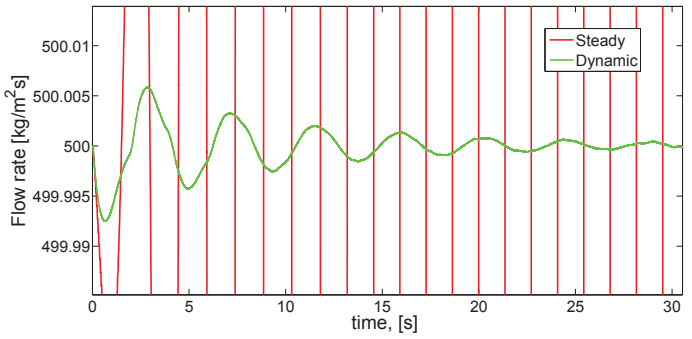

(b)

Figure 8.1: *Comparison of the dynamic and steady-state model results. A detail of the evolution at the beginning of the simulation from the same initial conditions is shown in (b).*

8.3.2.1 Inlet compressibility

In this section the effects of different volumes at the inlet surge tank are analysed. A comparison of the flow evolution is presented in Figure 8.2. According with this figure, for larger volumes the stability of the system is decreased and after a critical volume (≈ 1 [l]) the system evolves in an unstable diverging behaviour. In a detailed view of these simulations, Figure 8.3, it is possible to see that for the case of V_S = 0.5-1 [l], the system evolves in a stable manner. This change in behaviour according to the size of the surge tank was reported experimentally in [4].

As it is possible to see, in Figure 8.3 the frequency of the oscillations changes according to the volume of the surge tank ($T = 10s@V_{Si} = 5l$ - $T = 5s@V_{Si} = 1l$). It means that for small volumes the period of the oscillation will always become comparable to the particle transit time (approx. 2 [sec] in this case), related with the *density wave* oscillations periods. In consequence, the argument that *pressure drop oscillations* are always slower than *density wave* phenomenon, used to justify the use of *steady-state* models, results completely invalid for any system, since this phenomenon depends on the amount of compressible gas. Moreover, even for large

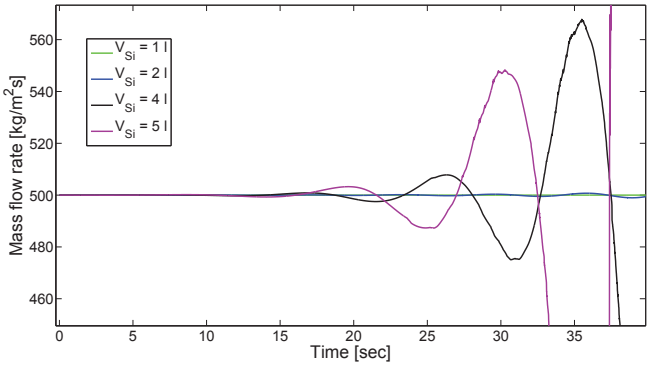

Figure 8.2: *Evolution of the system for different inlet surge tank volumes, V_{Si}.*

compressible volumes (slow oscillations) the *steady-state* model predicts always fast transitions when the system evolves from the all liquid to the two-phase flow state and vice-versa. Then the use of those models do not even fulfil its own assumptions, since the characteristic time of this transitions will depend on the parameters of the system.

In addition, it is necessary to remark that in this example (representative of a real system [13]) the unstable-stable critical volume is 5 times larger than the total volume of the heated pipe (V_S 1 $[l]$ and a heated pipe volume of 0.2 $[l]$). In consequence, the experimental cases normally described in the literature can not be used as a representation of a system with the presence of non-condensable gases. The study of *pressure drop oscillations* as it is normally presented is only representative of systems with a large compressible volume, even larger than the volume of the heated section, such as pressurisers and expansion tanks. In addition, the usage of normal control systems make those slow phenomena easy to control, changing for example the pressure in the surge tank, the valves opening, etc. The actual risk in the occurrence of these phenomena is exactly the higher frequency oscillation obtained with small compressible volumes, representative of non-condensable gases. In conclusion, it is necessary to use *dynamic* models in the modelling of the heated section in order to represent accurately the evolution of the involved phenomena.

8.3.2.2 Outlet compressibility

As commented before, in the classical description of PDO [1, 5], it is normally assumed that the surge tank at the inlet of the heated section represents any kind of compressible gas present in the system. In this section several simulations show the evolution of different cases in which the compressible volume is considered downstream from the heated section, V_{So} in Figure 7.1. In Figure 8.4 a comparison between the flow evolution for different outlet volume cases, for the same conditions as the example presented in the previous sections, is presented. A flow perturbation of 1 % respect to the steady-state solution is used as initial condition. As

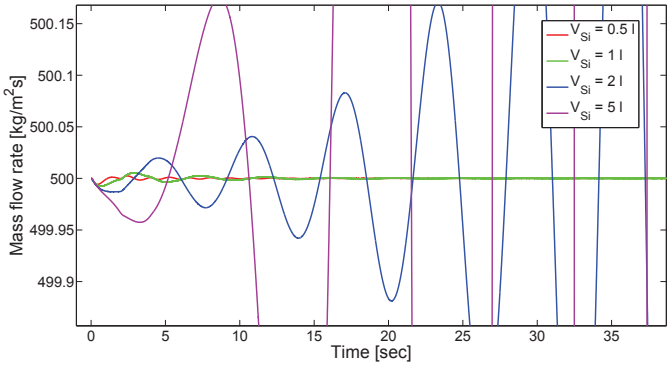

Figure 8.3: *Detailed view of the evolution of the system for different inlet surge tank volumes, V_{Si}.*

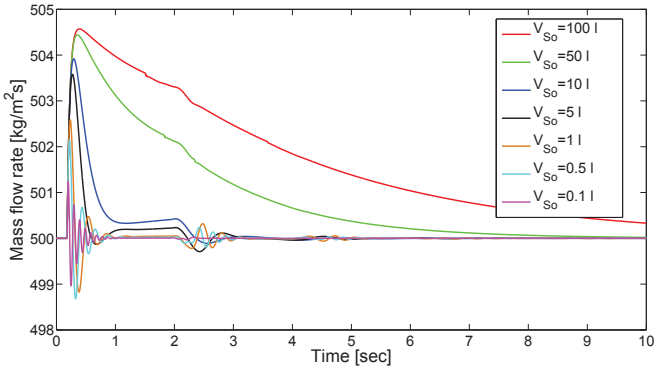

Figure 8.4: *Evolution of the system for different outlet surge tank volumes, V_{So}.*

a main result, for all the cases the system behaves in a stable manner. Moreover, for larger outlet volumes the system becomes more robust to system perturbations. These results are in agreement with [12] (Chapter 7) where it is proved that outlet compressible volumes stabilise the system for *density wave* phenomena.

8.3.2.3 Inertia stability analysis

The effects of fluid inertia in external pipes is analysed in this section. An inlet surge tank of $V_{Si} = 1l$ is used to perform the simulations. The inertia of the different sections is analysed by changing the length of each part independently. In Figure 8.5 the variation in the mass flux at the exit of the surge tank is presented. As it can be seen, for longer inlet sections (more fluid inertia) the system results slightly more unstable. It is necessary to remark that these changes are very small since an increase of 900 % in the inlet mass increases the amplitude of the oscillations

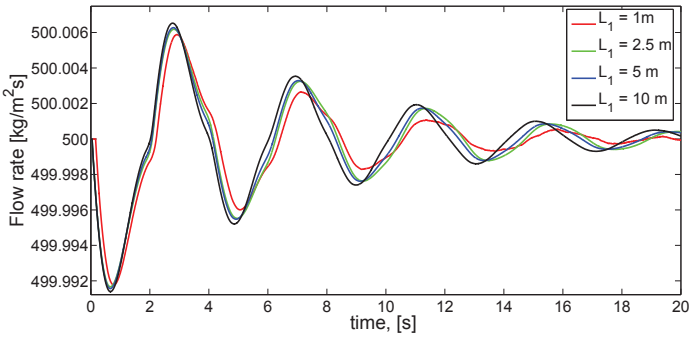

Figure 8.5: *Influence of the length L_1 on the system stability.*

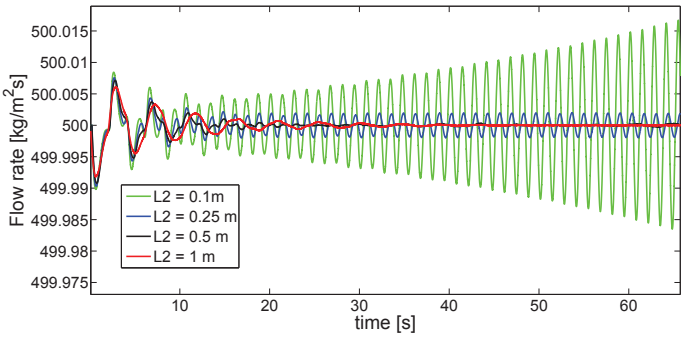

Figure 8.6: *Influence of the length L_2 on the system stability.*

in a 20 %. In the same way, for larger lengths the frequency is also increased. In conclusion, even if it is possible to see differences this effect will not represent a big problem for real systems since the variations are to small.

Regarding the inertia effects of the pipe connecting the surge tank and the heated pipe, the influence on the behaviour of the system is greater. A high influence on the stability of the system is observed by changing this parameter. For smaller L_2 the stability of the system is decreased, resulting for some values in a diverging behaviour. The critical value for this case seems to be close to $L_2 = 0.25$ [m] where a stable periodic oscillation is achieved. This behaviour is also reported experimentally in [4] where for smaller L_2 the stability of the system is decreased. The frequency of the oscillations seems also drastically influenced by the length of L_2. For smaller lengths the oscillations turn in an oscillation similar to a pure *density wave* oscillation, larger frequency, as can be observed in Figure 8.6. In contrast with the results of modifying L_1 and L_3, the destabilisation of the system is the result of the occurrence of DWO instead of PDO. These facts are in completely agreement with the results shown in [12] where the inertia effects on *density wave* oscillations are fully analysed.

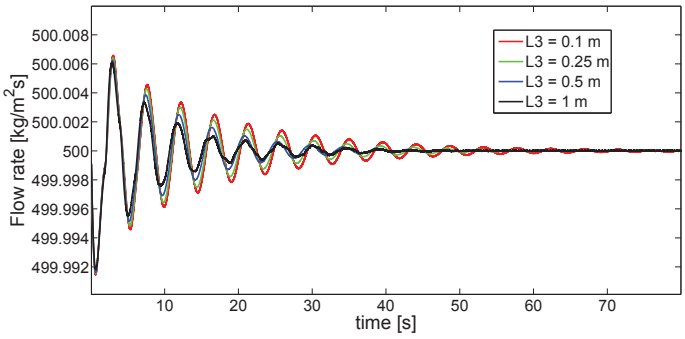

Figure 8.7: *Influence of the length L_3 on the system stability.*

Finally the stability influence of the length L_3 is also studied. As it is possible to see in Figure 8.7, for greater lengths the system becomes more stable. For a change of 90 % the amplitude of the oscillation is reduced in a 50 %. Then the effect of the inertia in the outlet pipe is not negligible. Is important to remark that even when the amplitude of the oscillations is small the validity of the numerical results is not affected, since the stability analysis is based on a local description. An important observation that should be made regarding the length L_3, is that for real systems the increase of L_3 is also an increase of the compressible volume and then the stability of the system is decreased. Therefore the stability of the system depends on the interaction between inertia and compressibility effects and none of them can be neglected.

8.4 Summary

In this chapter *pressure drop oscillations* were studied using a *dynamic* model. A comparison of the prediction with a *steady-state* model, commonly used in the literature, was presented. Remarkable differences were observed. While the *steady-state* predicts periodic oscillations for any size of compressible volume, the *dynamic* model predicts a transition between stable and unstable behaviour depending on the system parameters. It was also shown that in certain cases the results obtained with the *steady-state* model do not fulfil the assumptions needed to use this kind of models. In consequence, the usage of these results to describe real system should be carefully studied.

The effects of a compressible volume in the system were studied. When the compressible volume was located at the inlet of the heated section *pressure drop oscillations* were found. For small inlet compressible volumes the system evolves in a stable manner. In addition, the existence of a critical volume was proved through several simulations. Thus, for greater volumes than the critical volume the system becomes unstable. In contrast, when the compressible volumes are located at the outlet of the heated section then no PDO are found. It was also shown that the use of an outlet compressible volume makes the system more stable in the PDO sense.

Finally, the stability effects of the external fluid inertia were also analysed. It was found that for long inlet pipes (L_1) the system is slightly more unstable. Moreover, the variation of the length between the surge tank and the heated section had a strong influence on the stability of the system, as observed experimentally. For small length of the section connecting the surge tank and the heated pipe (L_2) the system was destabilised and the frequency of the oscillations jumped to higher frequencies due to a stronger coupling between the pipe and the surge tank dynamics. This coupling was due to the transition between *pressure drop* and *density wave* oscillations. It was also found that the outlet inertia (L_3) do not affect significantly the behaviour of the system, respect to PDO.

Bibliography

[1] BOURÉ J., BERGLES A., AND TONG L. Review of two-phase flow instabilities. *Nuclear Engineering and Design*, 25:165–192, 1973. (Cited on page 159)

[2] DING Y., KAKAC S., AND X.J.CHEN . Dynamic instabilities of boiling two-phase flow in a single horizontal channel. *Experimental Thermal and Fluid Science*, 11:327–342, 1995. (Cited on page 155)

[3] FU L., LEE S., VEZIROGLU T., AND KAKAC S. Mathematical modeling of two-phase flow instabilities in parallel channels. *Particulate phenomena and multiphase transport, washington Hemisphere*, 3, 1986. (Cited on page 157)

[4] GUO L., Z.P.FENG , AND X.J.CHEN . Pressure drop oscillation of steam-water two-phase flow in a helically coiled tube. *Int. J. of Heat and Mass Transfer*, 44:1555–1564, 2001. (Cited on page 155, 156, 158, 161)

[5] KAKAC S. AND BON B. A review of two-phase flow dynamic instabilities in tube boiling systems. *Int. Journal Heat Mass Tranfer*, 51:399–433, 2007. (Cited on page 155, 159)

[6] LIU H., KOCAK H., AND KAKAC S. Dynamical analysis of pressure-drop type oscillations with planar model. *Int.J. Multiphase Flow*, 20:1129–1142, 1995. (Cited on page 155)

[7] MAWASHA P. AND GROSS R. Periodic oscillations in a horizontal single boiling channel with thermal wall capacity. *Int. J. of Heat and Fluid Flow*, 22: 643–649, 2001. (Cited on page 155)

[8] O.KOMAKLI , KARSLI S., AND YILMAZ M. Experimental investigation of two-phase flow instabilities in a horizontal in tube boiling system. *Energy Conversion and Management*, 43:249–268, 2002. (Cited on page 155)

[9] OZAWA M., AKAGAWA K., SAKAGUCHI T., TSUKAHARA T., AND FUJII T. Oscillatory flow instabilities in air water two-phase flow systems. *Bulletin of JSME*, 22(174):1763–1773, 1979. (Cited on page 155)

[10] PADKI M., LIU H., AND KAKAC S. Two-phase flow pressure drop type and thermal oscillations. *Int. Journal of heat and fluid flow*, 12:240–248, 1991. (Cited on page 155)

[11] PADKI M., PALMER K., KAKAC S., AND VEZIROGLU T. Bifurcation analysis of pressure-drop oscillations and the ledinegg instability. *Int. Journal Heat Mass Transfer*, 35:525–532, 1992. (Cited on page 155)

[12] RUSPINI L. Study of inertia effects on dynamic two-phase oscillation phenomena. *14th International meeting on nuclear reactor thermal-hydraulics (NURETH-14), Toronto, Canada*, 2011. (Cited on page 160, 161)

[13] RUSPINI L., DORAO C., AND FERNANDINO M. Design of a two-phase flow forced convection loop for instability analysis. *Experimental Fluid Mechanics, Liberec, Czech Republic*, 2010. (Cited on page 159)

[14] SCHLICHTING W., LAHEY R., AND PODOWSKI M. An analysis of interacting instability modes, in phase change system. *Nuclear Engineering and Design*, 240:3178–3201, 2010. (Cited on page 156)

[15] SRINIVAS B. AND PUSHPAVANAM S. Determining parameters where pressure drop oscillations occur in a boiling channel using singularity theory and the d-partition method. *Chemical Engineering Science*, 55:3771–3783, 2000. (Cited on page 155)

[16] XIAO M., CHEN X. J., ZHANG M. Y., VEZIROGLU T. N., AND KAKAC S. A multivariable linear investigation of two-phase flow instabilities in parallel boiling channels under high pressure. *Int. J. Multiphase Flow*, 19:65–77, 1993. (Cited on page 155)

[17] YUNCU H. An experimental and theorethical study of density wave and pressure drop oscillations. *Heat transfer engineering*, 11:45–56, 1990. (Cited on page 155)

PART III

Experimental investigation

CHAPTER IX

Design and construction of an experimental facility to study two-phase flow phenomena

► In this chapter several aspects related to the design of two-phase components are investigated. A similarity criterion based on non-dimensional numbers is described. A brief stability analysis of boiling systems is presented. Both static and dynamic modelling of two-phase flow systems are presented. Moreover, the design of an experimental facility to study two-phase flow instabilities is presented. Several details of the construction, calibration and operation of this loop are described. Finally, some experimental results are shown.

9.1 Introduction

In Chapter 2 an extensive description of two-phase flow instabilities was presented. The main kinds of instabilities occurring in forced and natural convection loops were presented. As discussed, most of the investigations in the field are focused in boiling components for the nuclear industry. Nevertheless, the continues technological growth of the different industries is making two-phase components more and more used under many different conditions. Interesting cases of this kind of complex components can be found in liquefaction of natural gas (LNG). For example, components such a heat exchangers where both boiling and condensing phenomena take place are very used nowadays [27]. Furthermore, these open investigations related with LNG industry, are faintly focused in two-phase flow instabilities In consequence, the experimental and numerical study of two-phase flow instability phenomena for other fluids and conditions are still necessary.

In the Table 9.1 the used fluid and the main thermodynamic variables of several experimental investigations on two-phase flow instabilities are presented. As it is possible to see, most of the experimental investigations used water or freon 11/113 as a working fluid. However, in the last years, several experimental works utilise a new kind of hydro-fluorocarbon refrigerants [13, 2, 21]. In these last works, two-phase flow characteristics such as heat transfer and pressure drop were analysed.

Table 9.1: *Experimental conditions for some previous works describing two-phase flow instabilities.*

Reference	Type	Channels	Fluid	P_{in} [bar]	ΔT_{sub} [^{o}C]	D_H [mm]	L [m]	Q [W]
F.A. Jeglic and K.T Yang [9] (1965)	up	1	water	0.2 – 7	60	6	0,5	10 k
J.S. Maulbetsch and P. Griffith [15] (1965)	hor.	1	water	6	90	6	1,5	20 k
K. Akagawa and T. Sakaguchi [1] (1971)	hor.	1-3	freon-113	1 – 40	80	4	40	1500
S. Kakac et al. [11] (1974)	up	4	freon-11	4	100	6	≈ 2	1000
P. Saha et al. [25] (1976)	hor.	1	freon-113	34	110	10	2,8	100 k
M. Ozawa et al. [20] (1979)	hor.	1	freon-113	2	50	3.8	6	2000
T. Dogan et al. [4] (1983)	up	1	freon-11	6	70	3,8	1	700
R.P. Roy et al. [22] (1988)	up	1	freon-113	4,5	60	13	3,7	10 k
H. Yuncu [30] (1990)	hor.	1	freon-11	7	40	5	0,8	600
Q. Wang et al. [28] (1994)	hor.	1	water	30 –100	120	12	3,8	100 k
Y. Ding et al. [3] (1995)	hor.	1	freon-11	1-10	20	11	1	2500
L. Guo et al. [7] (2001)	hel.	1	water	5 – 35	30	15	6,5	160 k
O.Komakli et al. [19] (2002)	hor.	1	freon-11	7,5	28	11	3,8	22 k
U. Minzer et al. [16] (2004)	hor.	2	water	4	70	5	6	24 k
S. Kakac and Liping Cao [10] (2009)	up/hor.	1	freon-11	4	100	7,5	0,7	1000
C. Marcel et al. [14] (2010)	up	2	water	5	70	10	2	6000
G. Yun et al. [29] (2010)	up	2	water	120	70	10	1,5	120 k
Nan Liang et al. [12] (2011)	hor.	1	R-22	10	50	8	3	3000

Moreover, the thermodynamic properties of this kind of fluids are similar to the properties of hydrocarbons (propane, methane, etc.) highly used in several industries. In conclusion, it is still necessary more research in order to link the existing basic knowledge to the industrial equipment, fluids and process design.

The main objective of this chapter is to present a design methodology for two-phase flow components with main focus on thermo-hydraulic instabilities. In Section 9.2 the most used non-dimensional numbers in two-phase flow components are described. This non-dimensional criterion is used to select a proper fluid to represent the conditions in the liquid natural gas components. In Section 9.3 several simulations are used in order to characterise the parameter region for the occurrence of instabilities. The final characteristics, construction and operation details of the forced convection loop designed as a part of this work are presented in Sections 9.4 and 9.5. Finally, in Section 9.6 several experimental data are presented as a verification of the design methodology.

9.2 Similarity criteria

In order to assure the correspondence between the behaviour of different systems (i.e. from the laboratory to real systems and vice-versa), it is necessary to adopt a similarity criterion. The criterion presented in this chapter was introduced in [8] for boiling two-phase flow system. In this last work, the non-dimensional form of the characteristic equation for a general boiling system was obtained and seven non-dimensional groups were obtained. They are

- **Geometrical similarity**: The geometrical parameters can be expressed in a non-dimensional manner by using the axial characteristic length, such as

$$D^* = \frac{D}{L} \tag{9.1}$$

- **Subcooling number**: It takes into account the time lag effects in the liquid region

$$N_{sub} = \frac{h_f - h_{in}}{h_{fg}} \frac{\rho_{fg}}{\rho_g} \tag{9.2}$$

  this is one of of the fundamental parameters in the stability analysis, since it scales the subcooling of the fluid entering the heated section.

- **Phase change number**, or **Zuber number** [31]: It scales the change of phase due to the heat transfer to the system

$$N_{Zu} = N_{pch} = \frac{Q}{G_{in} A_{xs} h_{fg}} \frac{\rho_{fg}}{\rho_g} \tag{9.3}$$

  both N_{pch} and N_{sub} are significant in the stability analysis and also in the description of steady-state operational conditions.

- **Drift Number**: It takes into account the diffusion effects due to relative motion of the phases

$$N_{Drift} = \frac{V_{gj}}{v_{in}} \tag{9.4}$$

since V_{gj} depends on the flow regime, this group characterise the flow pattern.

- **Density number**: It scales the system pressure

$$N_{\rho} = \frac{\rho_g}{\rho_l} \tag{9.5}$$

since this number scales the pressure, it result quite important on the drift and two-phase frictional pressure drop terms.

- **Froud number**: It takes into account the effects of the gravity,

$$Fr = \frac{G_{in}^2}{\rho_l^2 g L} \tag{9.6}$$

- **Reynolds number**: It takes into account the hydrodynamic conditions

$$Re = \frac{G_{in} D}{\mu_l} \tag{9.7}$$

the Re and N_{Fr} numbers have the standard significance.

The main assumptions for obtaining this set of non-dimensional numbers are:

- The capillary body forces are negligible (mini-micro channels).
- The compressibility and dissipative effects are neglected in the energy conservation equation.
- The heat source is considered uniformly distributed.

In addition, the influence of external valves (inlet and outlet) has to be taken into account by the similitude criteria. This relation is quantified by the N_{τ} number, see [6], determined by

$$N_{\tau} = 2\frac{(K_i + K_o)}{(K_o + 1)} \tag{9.8}$$

where K_i and K_o are the pressure drop coefficients for the inlet and outlet valves respectively. Before continuing, it is necessary to remark that these non-dimensional numbers can generally be defined for any industrial system. In the next section the selection of a working fluid, based on this non-dimensional analysis, is presented.

9.2.1 Fluid selection and experimental conditions

Since two-phase flow instabilities phenomena are present in a very wide range of systems and conditions, a reference case will be used for the design of an experimental facility to study two-phase flow instabilities. In this chapter, the conditions in the LNG (Liquid Natural Gas) industry are taken as the reference case. In particular, in previous studies [18, 27], the use of plate-fin heat exchangers and hydrocarbons for LNG process is described. Due to the characteristics of the mentioned heat exchangers a horizontal condition is assumed. As a consequence, the Fr number is not considered in the following analysis. Moreover, to simplify the design analysis, a homogeneous condition is also assumed. Therefore, the N_{Drift} is not considered either. In the Table 9.2 the characteristics of the reference case are presented (red). In addition several candidate fluids are compared in terms of the non-dimensional numbers presented in the previous section. In order to assure similar characteristics to the reference fluids (propane, methane, butane) and taking into account the current environment protection regulations [17, 5], then the new generation of environmentally acceptable hydrocarbon products is taken into account. In the last years, they are gaining widespread acceptance for many industrial applications [13, 2, 21].

Fluid	Propane (Reference)	R134a	Co2	Pentane	water	R22
L/D	400	400	400	400	400	400
N_{sub}	8.7	8.7	8.7	8.7	8.7	8.7
N_{pch}	11.5	11.5	11.5	11.5	11.5	11.5
N_{ρ}	0.035	0.035	0.035	0.035	0.035	0.035
Re	7.6 10^4	7.6 10^4	7.6 10^4	7.6 10^4	7.6 10^4	7.6 10^4
D [mm]	10	5	5	5	5	5
L [m]	4	2	2	2	2	2
P [bar]	8	8.3	14.5	6.6	55	9.8
T_{in} [^oC]	-25	-5	< -72	70	160	-27
Q [W]	10000	4180	6900	4500	22500	4300
G [kg/m^{2}s]	900	2720	2500	1700	1500	2500

Table 9.2: *Comparison of similar two-phase conditions between different fluids.*

As it is possible to see in Table 9.2, the usage of CO2 for a similar condition than the reference case implies low temperatures (< -72 [^oC]) and pressures of at least 20 [bar]. Moreover, fluids such as propane, pentane or other pure hydrocarbons are flammable and that implies a more complex frame for the experiment. As discussed previously, the water has completely different characteristics than other fluids. Pressures in the order of 55 [bar] and temperatures of 160 [^{o}C] are needed to achieve the same conditions as the reference case.

In conclusion, the new family of hydro-fluorocarbons (R22, R134a) seems to meet the conditions imposed to the working fluid. The use of R134a implies an inlet temperature of -5 [^oC] while the R22 has to be below -27 [^{C}] as seen in Table 9.2. In conclusion, the refrigerant R134a seems to be an attractive solution for the design of this experimental two-phase flow loop. Moreover, its low boiling point (50 [^{o}C]

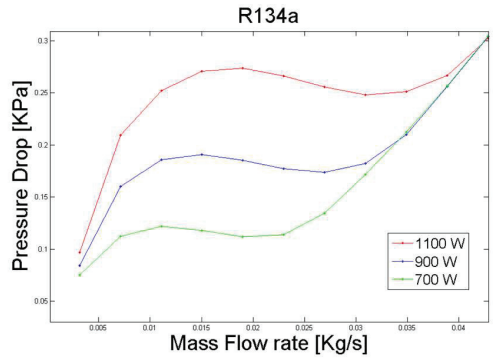

(a) Variation of heat power

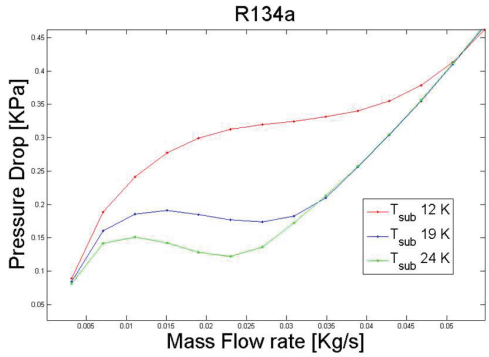

(b) Variation of sub-cooling temperature

Figure 9.1: *Typical N-shape curve for boiling R134a at 6 bar, varying the heat source (a) and the inlet temperature (b).*

@ 10 [bar]), the low latent heat of vaporisation (1.6 10^5 [J/kg] @ 10 [bar] – one order lower than water) and its non-flammable characteristics, also simplify the complexity of the design. In the next sections, the occurrence of instabilities for these particular conditions are presented.

9.3 Numerical simulations

The numerical solver developed and utilised in the last chapters is used in this chapter to simulate the phenomena occurring for the conditions obtained previously. The main goal of these simulations is to characterise the occurrence of instabilities for different parameter regions. Both steady-state and dynamic simulations provide useful information for the loop design.

9.3.1 Pressure drop characteristic curve

As presented in Chapter 2, the occurrence of *Ledinegg* and *pressure drop* instabilities depends on the slope of the characteristic pressure drop vs. flow, N-shape curve. In consequence, it is important to understand in which parameters region (power, pressure, temperature, length, diameter) the unstable behaviour is achieved (negative slope). A brief parameter analysis is presented here, in order to assure the occurrence of a negative slope in the designed loop. The characteristics of the simulated system are:

- fluid: R134a
- P_{in}: 8 [bar]
- T_{in}: -10 [^{o}C]
- Q: 900 [W]
- L: 2 [m], D: 9 [mm]

In Figure 9.1(a) the characteristic curve for different parameters are presented. For this set of curves all the parameters are kept constant but variations in the uniform power are analysed. As it is possible to see, even if the characteristic curve changes for different power levels, the relative shape (N-shape) do not change significantly its shape. It implies that for a wide range of powers the system present a negative slope characteristic curve. Similarly, the modification of the steady-state curve dues to variations in the inlet temperature is presented in the Figure 9.1(b). In this case, the shape of the curve is changing significantly with different sub-cooled inlet temperatures. Therefore, for this system, it is necessary to assure more than 30 [^oC] of sub-cooling at the inlet, in order to have a negative slope. In conclusion, in order to have a negative slope, it is necessary to assure a working inlet temperature minor than 0 [^oC] at 8 [bar].

9.3.2 Heat distribution effects

In real systems such as heat exchangers, reactors, re-boilers, etc, the heat source is not uniform due to several different factors. Thus, in order to understand the influence of the non-uniform heating in the thermo-hydraulic behaviour of the system, a steady-state analysis is performed in this section.

In Figure 9.2(a) different profiles of the heat source are presented, all of them with the same average value. In Figure 9.2(b) the corresponding characteristic curves for the different non-uniform sources are shown. According with this figure, an important influence of the heat distribution in the characteristic curve is observed. For those distributions applying more heat at the inlet, the N-shape amplitude is bigger. On the other hand, when the heat is applied at the outlet of the channel, then the slope of the characteristic curve is increased (stabilising effect). Consequently, a variable distribution heat source will be interesting to study these effects. Thus, different kinds of systems can be represented and studied in the same experimental facility.

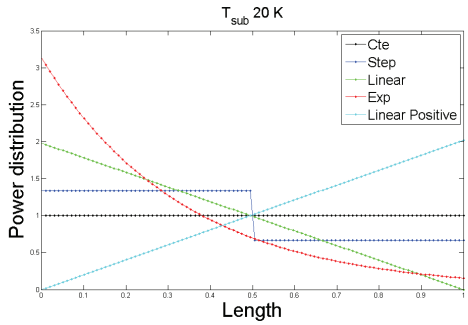

(a) Heat distribution

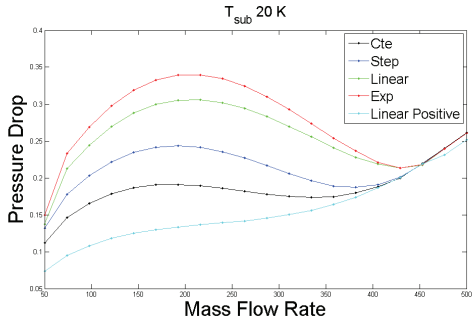

(b) Characteristic N-shape curve

Figure 9.2: *Comparison of the two-phase N-shape curve for different heat source distribution. (a) Heat source distribution, (b) Characteristic curves.*

9.3.3 Density wave oscillations

As seen in previous chapters, the occurrence of DWO is highly influenced by the sub-cooling and phase change numbers and the valves constants; N_{sub}, N_{pch}, K_{in} and K_{out}. According to the working parameter region the DWO can be asymptotically stable (converging), unstable (diverging) and marginally stable (periodic). Simulations of DWO for the conditions proposed in Table 9.2 are presented. The main parameters for these simulations are:

- fluid: R134a
- P_{out} = 8.0 [bar]
- Q: 500 [W]
- T_{in} 8 [^{o}C]
- L: 2 [m], D: 5 [mm]
- G_{in}: 230 – 250 – 280 [kg/m^{2}s]
- K$_{in}$ = 10

- K_{out} = 4

In Figure 9.3(a), three different simulations show the occurrence of *density wave* oscillations. The corresponding inlet initial mass flow rates are 230 – 250 – 280 $[kg/m^2s]$. The three different regimes (converging, periodic and diverging) can be seen in these examples. In addition, a stability map with the operation points of the three different simulations is shown in Figure 9.3. The approximated stability limit proposed by Zuber and Ishii [8] and the Guido's limit [6] are plotted.

It is necessary to remark that under the occurrence of this phenomenon the wall temperature can reach high temperatures producing burn-out. Consequently, an automatic safe system should be taken into account in the designed loop. This maximum temperature would be most of the times at the end of the pipe. On the other hand, regarding the acquisition times, it is seen that the oscillations period is about 10 [sec]. Moreover, the fastest oscillations will occur at the highest power and flow and lower subcooled inlet temperature. Under that conditions the oscillation time would be in the order of 1 [sec]. Nevertheless, as explained in Chapter 7, the occurrence of high-order modes would bound the acquisition time to at least 0.1 [sec] for the variables in the heated pipe.

9.4 Final Design

Based on the analysis carried out in the previous sections, the parameter region for the experimental loop design is:

- Fluid: R134a (easy to handle, low boiling point, low latent vaporisation heat)
- System pressure, P: 4–15 bar
- Mass flow rate, G: 5–2000 kg/m^{2}s
- Inlet temperature, T_{in}: -20 – 40 ^{o}C; Sub-cooling: 0–50 ^{o}C
- Max Power input, Q: 2 kW

In the Figure 9.4, a basic scheme of the main components in the loop is shown. In addition, some of the characteristics of this final design are explained in the following.

1. Two operating modes(Tanks/Pump): In order to study the influence of different external characteristics the loop has two operating modes. One using two tanks at different pressures (constant pressure condition) and another using a pump to circulate the fluid. The two-tanks operating mode is used for low flow rates (less than 0.06 l/min). In this operating mode, the flow rate is established by the difference in pressure between a high pressure tank (HP) and a low pressure tank (LP), and controlled by a regulating valve. The HP tank is pressurised with nitrogen. The LP tank is kept at constant saturation condition and thus the pressure and temperature are fixed by the conditions of the condenser. For higher flow rates, the tank-system does not provide enough

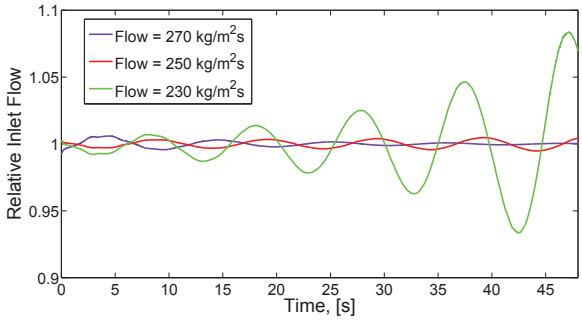

(a) Flow evolution

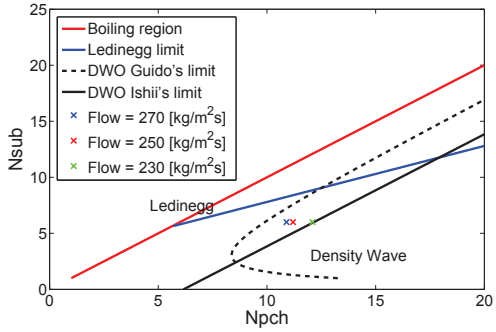

(b) Stability map

Figure 9.3: *Flow evolution and the corresponding Ishii-Zuber stability map (Ledinegg and DWO) for the designed two-phase loop. The operation points for the simulations of this section are plotted with crosses.*

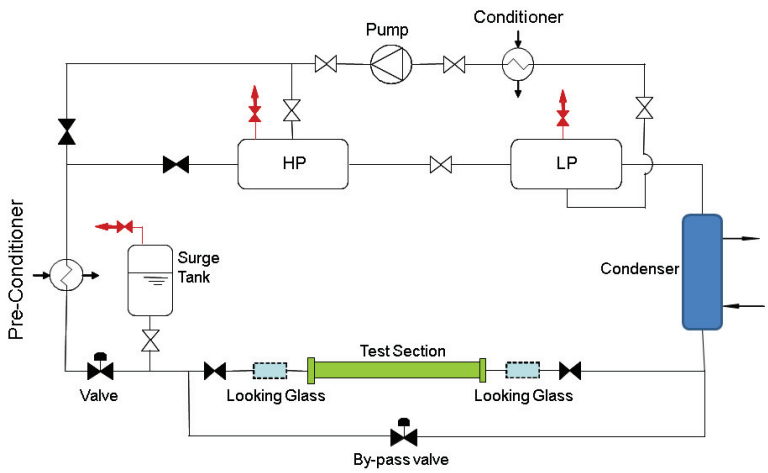

Figure 9.4: *Scheme of the final design of the two-phase loop.*

flow rate for a significant time and therefore the flow rate is controlled by a the pump.

2. Surge Tank: in order to study *pressure drop oscillations*, see Chapters 2 and 8, a compressible volume is mounted upstream from the heated section. In addition a second tank to characterise the effects discussed in previous chapters is placed at the outlet of the heated section. In operation these tanks are filled with nitrogen.

3. Pre–Conditioner: a heat exchanger is mounted before the test section in order to control the inlet conditions.

4. Distributed Source: As shown by Figure 9.5, the electrical "heat source" is split into five sections to achieve a non-uniform heat profile, as described in Section 9.3.2.

5. An adjustable valve provides the inlet pressure drop (K_i), while for the exit restriction an orifice valve is used. Design values of these two valves are $K_{in} \approx$ 5-500 and $K_{out} \approx$ = 2-50.

6. An adjustable valve is mounted in the by-pass branch in order to adjust the constant pressure drop boundary condition in the test section [8].

In Figure 9.4 a simplified sketch of the final design can be observed. In any of the two operating modes, the fluid is conditioned at the desired temperature with the pre-conditioner before entering the test section. A condenser is situated after the

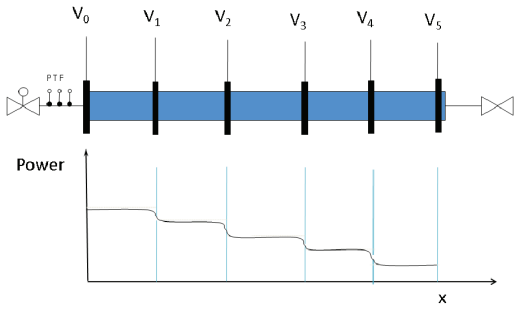

Figure 9.5: *Scheme of the distributed electrical DC heat source*

test section to condense the generated vapor before sending the fluid to the LP tank where it is stored. A conditioner (heat exchanger) is introduced before the pump in order to assure subcooled single phase flow into the pump. Two secondary circuits provide the refrigeration for the pre-conditioner, conditioner and condenser. In the next section a detailed description of each part is made.

9.5 The experimental facility

In the Figure 9.6 the detailed scheme of the constructed facility is plotted. In this figure all the main components an its localisation are sketched.

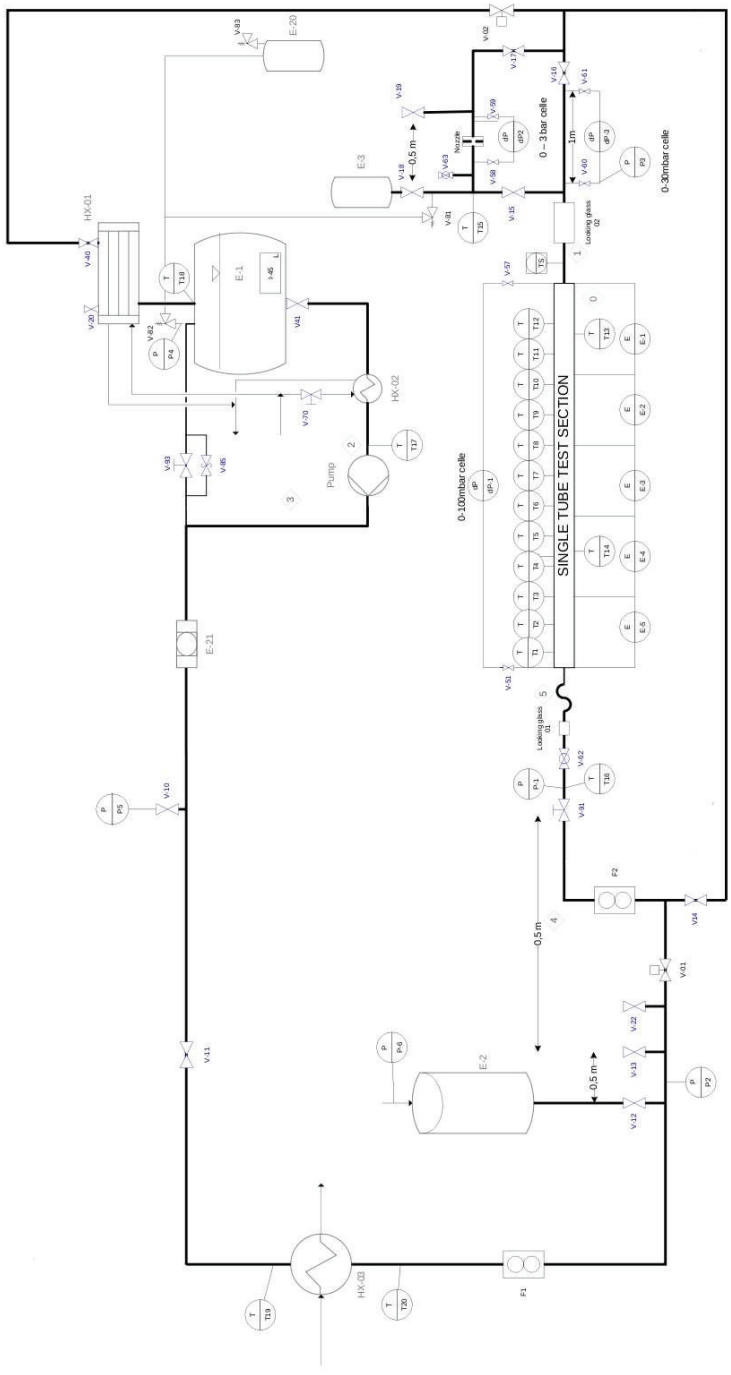

Figure 9.6: *Scheme of the experimental facility (main loop). T - thermocouples, P - Absolute pressure-meter, dP - Differential pressure-meter, F - Flow-meter, V - Valve, E - Tanks, HX - Heat exchanger, IX - Condenser. This sketch was made by Håvard Rekstad.*

In Figure 9.7(a) a view of the constructed loop is shown, where it is possible to see most of the main components: surge tank (left top), distributed power supply (right bottom), test section with instrumentation (center). The tanks, condenser and pump are located behind the distributed power supply. The electrical system is split in three different boxes: "main electrical box", "distributed power supply" (in the right side of Figure 9.7(a)) and the "instrumentation box". The main reason to split the electrical part is to isolate the instrumentation from the high voltage source (340 V). In the first step of the construction, the high pressure tank (HP) is omitted. Thus, the use of the pump and by-pass is the only the operation mode. Nevertheless, the design takes into account the incorporation of the HP tank in the future. Before continuing, it should be mentioned that a complete risk assessment report was presented by L.C. Ruspini and Erik Langørgen [24] (2011), in order to get the operation authorisation at the Thermal Laboratory, EPT, NTNU. Moreover, a technical report with the status and the final design was presented in L. Ruspini et al. [23] (2010). In the next section, the main components of this facility are described.

9.5.1 Test Section

The test section consists in a stainless steel tube of 5 mm of inner diameter and 8 mm outside diameter. In Figure 9.8 a sketch of the test section is presented. Some of the test section characteristics are listed in the next.

- 7 pressure taps for differential pressure drop measurements.
- 12 external thermocouples (wall temperature).
- 2 internal thermocouples to study heat transfer characteristics.
- 6 electrodes to control the heat distribution.

During the operation the test section is heated by Joule effect. A controller and rectifier circuit is used in order to convert the AC into a DC to heat each section. The total electrical input power is calculated from measurements of voltage and current in each of the heated sections, as it is explained in Section 9.5.7.1. In Figure 9.7(b) a detailed view of the test section is presented: copper electrodes with voltage measurements, pressure taps for differential pressure drop measurements (left) and thermocouples connections (right). The whole test section is mounted between two pieces of isolating material to reduce the heat exchange with the surroundings.

9.5.2 Looking glass and Image analysis

At the outlet of the heated section a looking glass is mounted to perform a photographic analysis. Moreover, the glass tube acts as a dielectric and thermal insulator between the electrically heated test section and the rest of the circuit. The glass tube consists in a borosilicate pipe (fabricated at RealFag, NTNU). The tube is 5 [mm] inner diameter, 8 [mm] external diameter and 20 [cm] long. It has undergone pressure testings up to 25 [bar] (maximum pressure to be used during operation, $\approx$ 15 [bar]). A high speed camera (Photron- FastCam SA3) is mounted in this glass tube to allow the study of flow patterns, similar to the experiment described in [26].

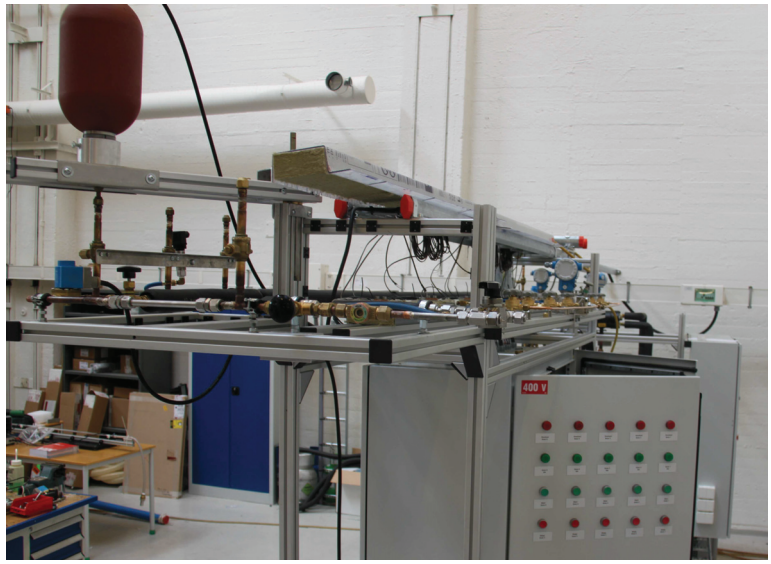

(a) General view of the facility

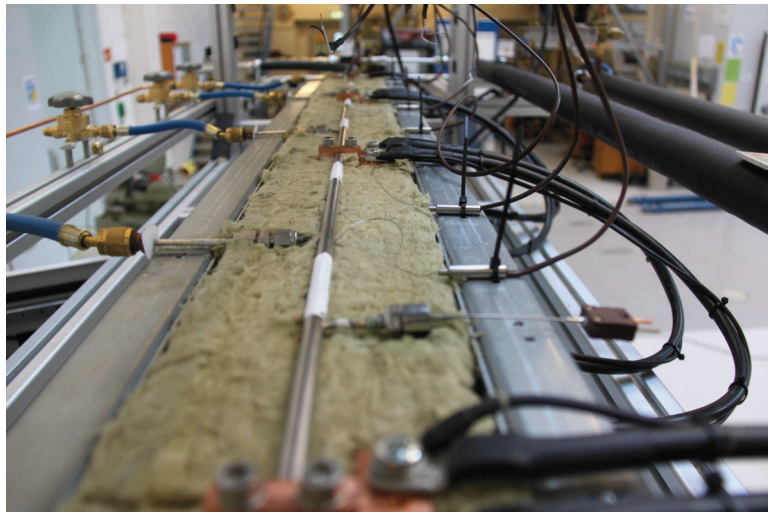

(b) View of the test section

Figure 9.7: *Views of the experimental facility. (a) Frontal view of the experimental facility. Surge tank (up-left), Heat source box (right), Test section (center). (b) Test section view. In the left side the pressure taps are shown (measurement of pressure drop inside the pipe). In the right side of the picture the internal and external thermocouples can be observed.*

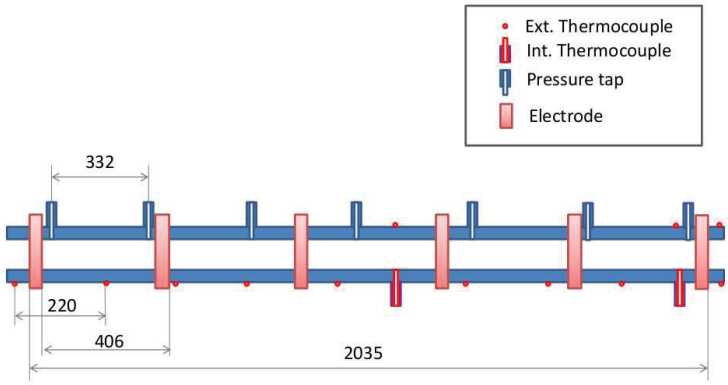

Figure 9.8: *Test section sketch.*

9.5.3 Outlet Arrangement

As shown in Figure 9.6, downstream from the test section is placed a parallel arrange to study pressure drop characteristics. These two different legs will be used to characterise distributed pressure drop (piping) and local pressure drop (orifice valve). A 1 [m] pipe, now on called "outside" section, is used to study distributed pressure drop. It is made of stainless steel with the same characteristics of the heated pipe (5 [mm]). On the other hand, in the Figure 9.9 a scheme of the orifice valve used in the other leg is shown. As it is possible to see the orifice can be changed to study the effects of different outlet local pressure drops. Orifices of 1.5, 2, 2.5, 3, 4, 5 and 7 [mm] were fabricated.

9.5.4 Heat exchangers and refrigeration chillers

Two secondary circuit are mounted in order to remove the heat from the heat exchangers and condenser. In Figure 9.10 a diagram of the two secondary circuits is shown. The chillers 1 and 2 are K9 and K6 models from the company "Applied Thermal Control" (ATC). The pre-conditioner is a plate-fin heat exchanger (B8THx14 SWEP) and the condenser is a shell and tube heat exchanger (CFC-12 – Alfa Laval). The secondary refrigerant is a solution of glycol and water. The two chillers are connected to the computer through the RS485 serial protocol. Thus, their reference temperature can be adjusted from the interface software, as will be described in Section 9.5.8.

9.5.5 Pump

A gear pump (GB – MICROPUMP) with a magnetic drive coupling is used. The velocity of the pump is controlled from the interface software. In this way, it is possible to control the flow in order to study the response of the system to particular

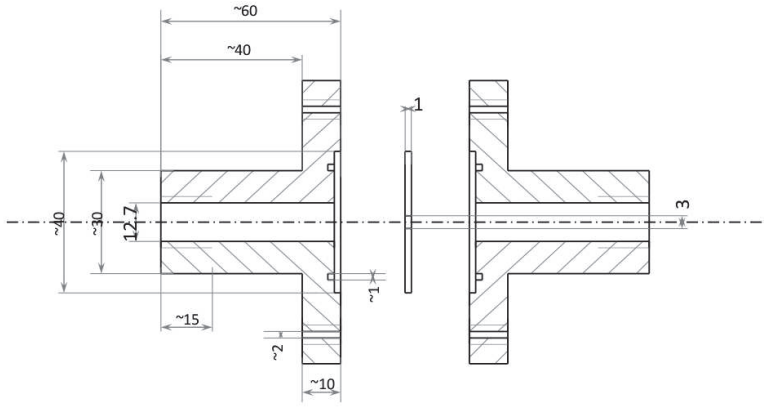

Figure 9.9: *Detailed scheme of the outlet orifice valve. Measures in [mm].*

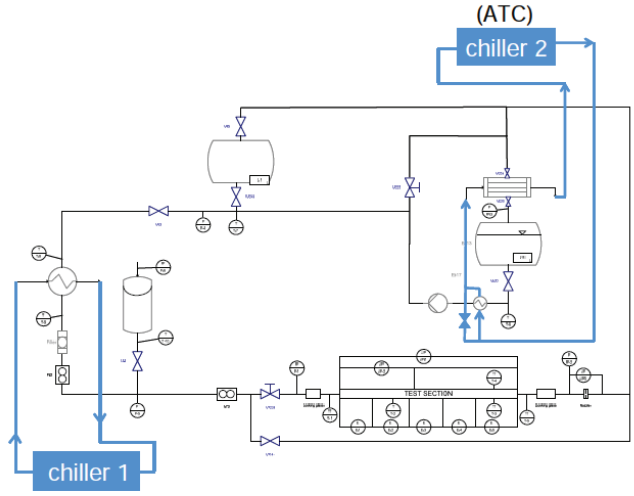

Figure 9.10: *Secondary circuits, heat exchangers and refrigeration chillers.*

signals. Moreover, a PID controller is implemented in order to assure the constant flow condition even when other parameters of the system change, see Section 9.5.8

9.5.6 Loop instrumentation

Absolute pressure transducers are used to measure the pressure in the tanks (LP and surge tank), after the surge tank, before and after the test section. In addition, differential pressure transducers are located in the test section, the inlet and the outlet valves. As shown in Figure 9.6, temperature measurements are placed: before and after the pre-conditioner, before the pump, before and after the test section. Two flow-meters, F1 and F2, are used to measure the refrigerant flow before and after the surge tank.

9.5.7 Accuracy of the measurements

In the next sections, a description of the calibration and the accuracy of the different measures taken in the experimental rig are described. In Table 9.3 the accuracy of the instruments and the statistical error for the different variables are presented. In the next section the description of the power calibration is presented.

9.5.7.1 Power calibration

As mentioned in previous sections, the applied heat is a difficult variable to measure. A controller-rectifier circuit is used in each of the heated sections in order to convert AC to DC. Due to the high current, the use of capacitors provoke overwarming and life span reduction of the transformers, used to convert the 340 [V] (AC) signal to 7 [V] (AC). Therefore, the high ripple of the signal made it difficult to estimate the actual heat applied to the different sections. In order to deal with this problem a full calibration of the heating system is needed. First, a digital oscilloscope (LeCroy) was used to obtain the actual shape of the applied voltage and current signals in each of the heated sections. Then, the voltage and current signals obtained with the oscilloscope were integrated numerically to get the DC component of the signal. An integration time corresponding to 20 periods was used to obtain the average values. On the other hand, the current measure chain used resistance in order to transform the current signal into voltage. In Figures 9.11(a) and 9.11(b) the calibrations of current and voltage signals are shown. The variables *Current PC* and *Voltage PC* are the values measured in the acquisition card. The total power is obtained by multiplying these two measurements, V_{cal} (calibrated voltage) and I_{cal} (calibrated current). Nevertheless, as the shape of the signals is not constant, then this power has to be corrected by a $\Phi_{AC/DC}$ factor. This last term takes into account the effects of ripple, specially important at low powers.

Name	Instrument type	Brand	Localisation	Range	Meass. Accuracy	Max. Stat. error	Max. Error
DP 1	Dp-cell	Endress+Hauser	Test section	0-1 [bar]	0.075 %	1 [mbar]	1 [mbar]
DP 2	Dp-cell	Endress+Hauser	Orifice valve	0-1 [bar]	0.075 %	5 [mbar]	5 [mbar]
DP 2	Dp-cell	Endress+Hauser	Outlet section	0-1 [bar]	0.075 %	2 [mbar]	2 [mbar]
DP 3	Dp-cell	Endress+Hauser	Inlet valve	0-1 [bar]	0.075 %	2 [mbar]	2 [mbar]
T 1-20	Thermocouple K	Standard	Whole loop	-50 – 100 [^{o}C]	0.1 [^{o}C]	0.1 [^{o}C]	0.2 [^{o}C]
P 1-5	Absolute Pressure	GE-UNIK 5000	Whole loop	1-16 [bar]	0.1 [bar]	< 10 [mbar]	0.1 [bar]
F 1-2	Flow-meter (Coriolis)	Bronkhorst Cori-Tech	Test section	0-3 [l/min]	0.01 [l/min]	< 0.01 [l/min]	0.05 [l/min]
Q 1-5	Power supply	Home made	Heated sections	0-2500 [W] (5 zones)	20 W, Eq. (B.9)	20 [W]	< 40 W

Table 9.3: *Accuracy of the instruments and measurement chains.*

In Figure 9.11(c) the values of the $\Phi_{AC/DC}$ factor vs. the calculated power are shown. The $\Phi_{AC/DC}$ factor is calculated as

$$\Phi_{AC/DC} = \frac{\int_0^{20T} i(t)v(t)dt}{V_{cal}I_{cal}} \tag{9.9}$$

and the total applied power will be calculated using the following expression

$$Q_{cal} = \Phi_{AC/DC}\, V_{cal}\, I_{cal} \tag{9.10}$$

this last value is the power shown at the interface software. The value of the $\Phi_{AC/DC}$ is calculated for each heated section independently. As can be seen this calibration allow to measured the actual applied power even when the pipe resistance change locally due to the subcooled or overheated conditions.

However, the effects of thermal losses to the environment should be taken into account to calculate the actual heat transferred to the fluid. The actual total heat is calculated as

$$Q_{real} = \Psi_{Thermal}\, Q_{cal} \tag{9.11}$$

where the $\Psi_{Thermal}$ is the thermal losses factor. For each condition of power, environment temperature and inlet temperature, this factor is calculated by using the inlet and the two internal thermocouples in the test section. Using the energy conservation, the actual heat transferred to the fluid is proportional to the the temperature increase. Thus, the thermal factor is calculated as,

$$\Psi_{Thermal} = \frac{Cp_l\, \Delta T_{12}\, G\, A_{xs}}{Q_{cal}} \frac{L_{Tot}}{L_{12}} \tag{9.12}$$

where ΔT_{12} is the temperature difference between two arbitrary points with a distance L_{12}; Cp_l the heat capacity of the liquid; and A_{xs} the cross sectional area. In the Figure 9.17 an example of the factor $\Psi_{Thermal}$ for a particular case is plotted. It is necessary to remark that, in the experimental cases, the heat losses are never higher than the 8 %. Finally, in Appendix B the error propagation for the measurement of the power is obtained.

9.5.8 Software Interface

The software interface to control the main parameters of the experimental rig was designed and implemented as a part of this work. The interface was made using NI Labview (2011). In the Figure 9.12 a view of the user screen is shown. In the following, some of the main features of the program are described:

- File acquisition
- On-line visualisation
- Power control:
  - Temporal PID Control of the power in the heated sections, (Constant - *Sin* function).

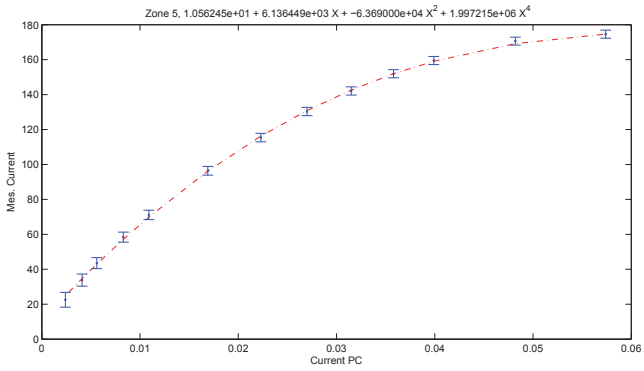

(a) “Current” signal calibration

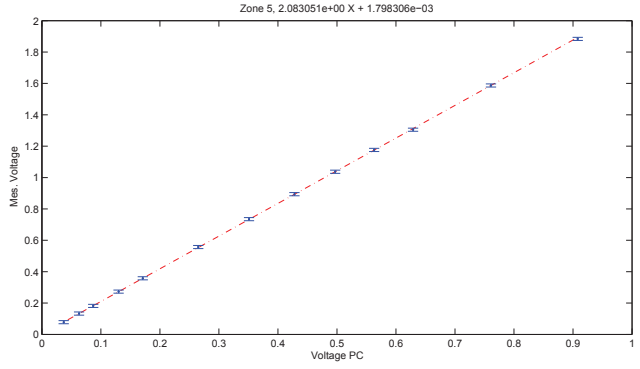

(b) “Voltage” signal calibration

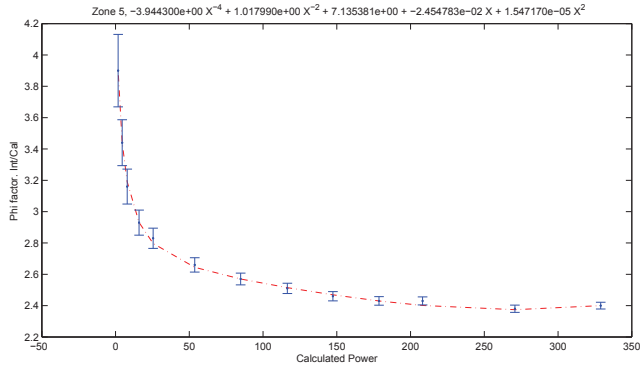

(c) $\Phi_{AC/DC}$ factor calibration

Figure 9.11: *Power calibration. The current and voltage signals are calibrated by measuring the integral of the actual current and voltage for each heated section. The total power is corrected by the $\Phi_{AC/DC}$ factor to take into account the signal shape.*

  - Space control of the heat distribution (Linear – Cos function).

- Pump control: Temporal PID Control of the flow, (Constant - Linear - Piecewise - *Sin* function).

- Chillers control:

  - RS485 Communication: with the chillers of the secondary circuits.
  - Chiller 1 (K9): PID Control of the inlet temperature, T_{in} (T20).
  - Chiller 2 (K6): PID Control of the tank pressure, P_{tank} (P4), through the chiller temperature.

- Alarm Control: As a safe system the heat source is shut-down when:

  - Maximum Temperature (190 [^{o}C]).
  - Maximum Current (200 [A]).
  - Maximum Pressure (15 [bar]).

9.6 Experimental results

In this section some general experimental cases are shown. The experimental results are presented as a validation of the methodology used in the designing of the experimental facility. The main parameters used for these experiments are:

- P_{out} = 8.3 [bar]
- Q_{real} = 0-1500 [W] (Uniform distribution)
- L_{heated} = 2 [m], $L_{total} \approx$ 6 [m], D: 5 [mm]
- $G_{in} \approx$ 0-500 [kg/m^{2}s]
- K$_{in} \approx$ 30
- K$_{out} \approx$ 20

9.6.1 Static characteristic curves

The characteristic ΔP vs. G curves for the pipe and the outlet orifice valve are presented in the Figure 9.13. In this case a orifice valve of 3 [mm] was used. As the phenomena involved into the pipe take place in the whole length of the pipe then the measured pressure drop results more accurate and less sensible to flow pattern changes. In contrast, for the case of the outlet valve the local effects that takes place into the orifice are instantly reflected in the pressure drop measurement, as shown by the error bars in the Figure 9.13(b). In this case the inlet temperature was bounded between (-13 – -9) [^{o}C] and the applied power was approximately 1200 [W].

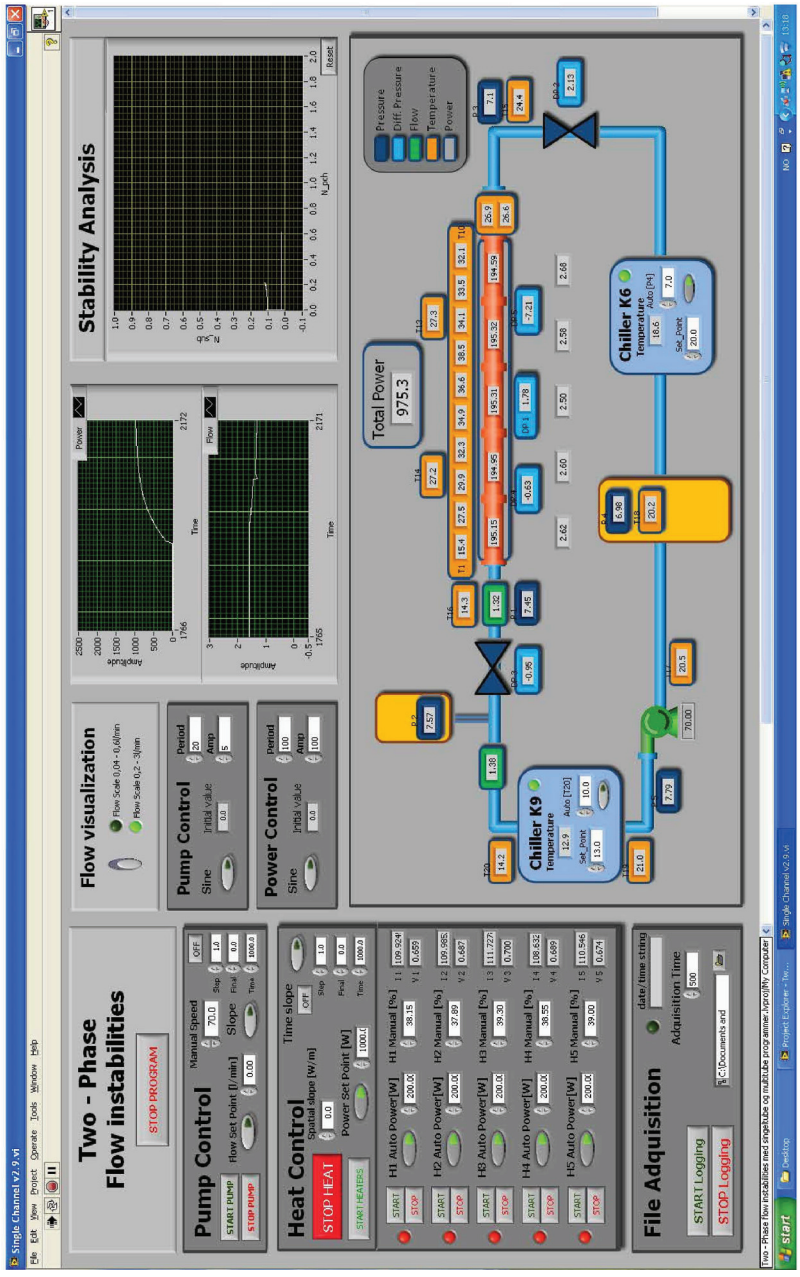

Figure 9.12: *Software interface to control the experimental loop.*

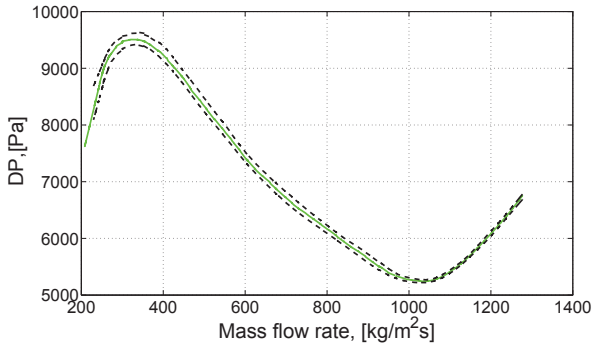

(a) ΔP vs. G curve, heater.

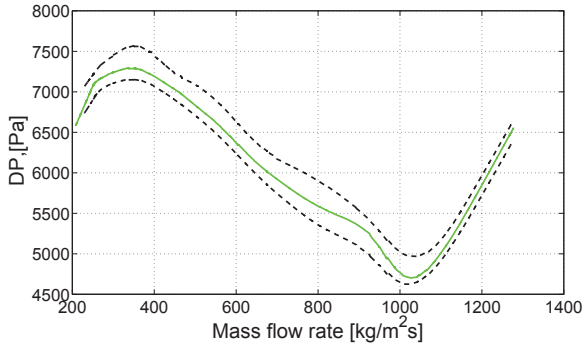

(b) ΔP vs. G curve, outlet valve.

Figure 9.13: *N-shape curve for the pipe and outlet valve. Green line represent the averaged value and dashed black lines show the error of the measurements.*

9.6.2 Density wave oscillations

In Figure 9.14 the beginning of a periodic oscillation is presented. This behaviour is the result of increasing the heat from a stable state to the corresponding of an unstable state condition, as described in the simulations of Section 9.3.3. The evolution of the applied heat is presented in Figure 9.14(b). As the figure shows the relative increase on the applied heat is smaller than 2%, when the transition from converging to periodic occurs. The characteristic time for these oscillations is approximately 3 seconds. Should be noticed that the difference with the simulations presented in Section 9.3.3, where the period of the oscillations are about 10 sec, are due to the differences in the sub-cooling number. In this case the sub-cooling number is smaller and the flow is higher making the period smaller. In Figure 9.15 it is possible to see the periodic state achieved, after a stabilisation time, by the same conditions as in the previous case. In this case the periodic behaviour does not correspond only with one pure frequency but the oscillation is slightly modulated by a component of lower frequency (non-linear effect). The change from a periodic to a stable state is shown in Figure 9.16. In this case the applied heat is decreased from 550 [W] to approximately 500 [W]. In this case as the flow decreases from the previous two cases, the period of the oscillation corresponds to about 5.5 seconds. The acquisition time for this experiments was 0.5 [sec].

9.6.3 Image analysis

In the Figure 9.17 the measured thermal factor for this case is shown. As it is possible to see, only at the low power points it is possible to use the temperature difference to measure this factor. Therefore, for the high power cases the thermal factor is extrapolated using a linear function as shown in the figure.

The characteristics of the flow patterns at the heat section outlet are studied using a fast camera, Section 9.5.2. In 9.18, the flow pattern for different conditions are studied. The basis system conditions are:

- $P_{tank} \approx$ 6.5 [bar]
- G_{in} = 0.6 [l/min] = 660 [kg/m^2 s]
- T_{in} = 0 [^{o}C]
- $Q_{real} \approx$ 0-2300 [W] (Uniform distribution)

in each case a different power was applied and a waiting period of 3 [min] was used in order to achieve stationary conditions. The corresponding thermodynamic equilibrium quality values are shown in the label of each image. In these images it is possible to see that subcooling boiling is significant (negative thermodynamic quality), Figures 9.18(a) and 9.18(b). On the other hand, for high power conditions the channel shows a dry-out condition, Figure 9.18(j). In this last case, the liquid do not wet the wall but it forms drops in the bulk of the gas. In these images the slug, intermittent and annular flow patterns are also shown.

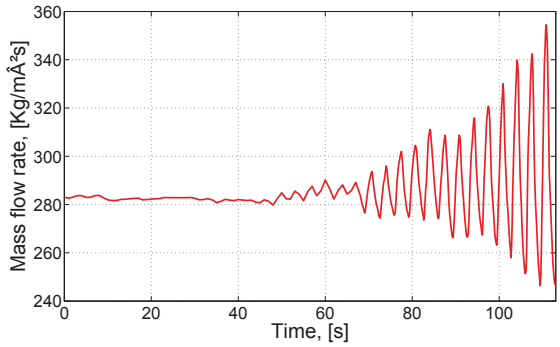

(a) Flow evolution

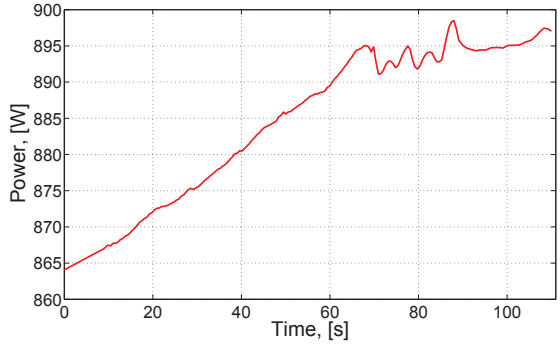

(b) Power evolution

Figure 9.14: *Starting of the periodic oscillation.* N_{sub} *= 3.7,* P_{in} *= 8.3 [bar],* T_{in} *= 17 [°C].*

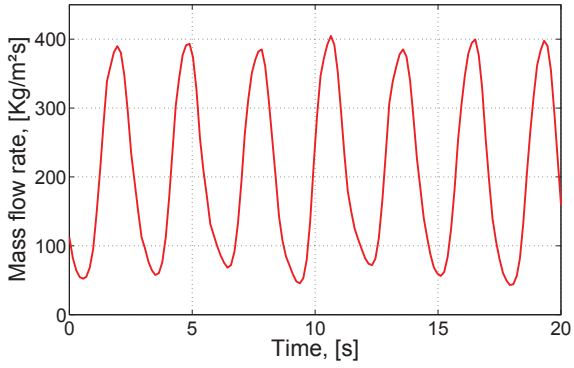

Figure 9.15: *Periodic evolution of the flow.* N_{sub} *= 3.8,* P_{in} *= 8.4 [bar],* T_{in} *= 17 [°C],* Q_{real} *= 870 [W].*

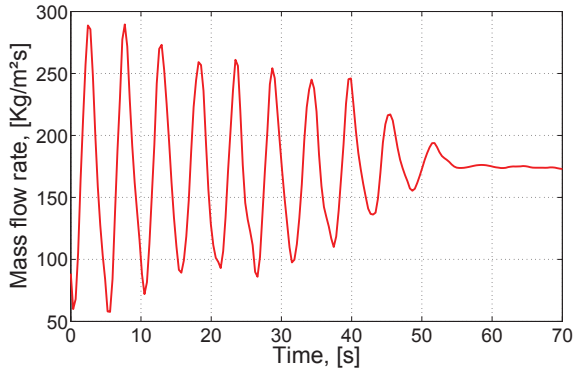

Figure 9.16: *End of the periodic oscillation.* N_{sub} *= 3.8,* P_{in} *= 8.3 [bar],* T_{in} *= 16 [*^{o}*C],* Q_{real} *= 550 [W].*

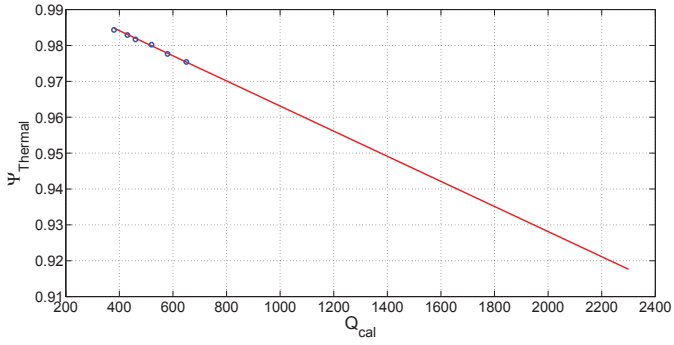

Figure 9.17: $\Psi_{Thermal}$ *factor for the image analysis case conditions.* P_{in} *= 6.5 [bar],* T_{in} *= 0 [*^{o}*C],* G *= 660 [*kg/m^2s*].*

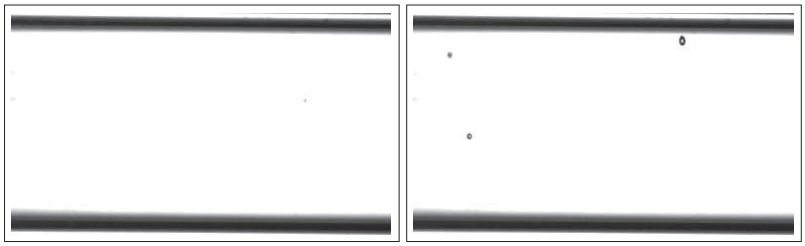

(a) Q_{real} = 374 [W] – x_{out} = -0.026 (b) Q_{real} = 423 [W] – x_{out} = -0.005

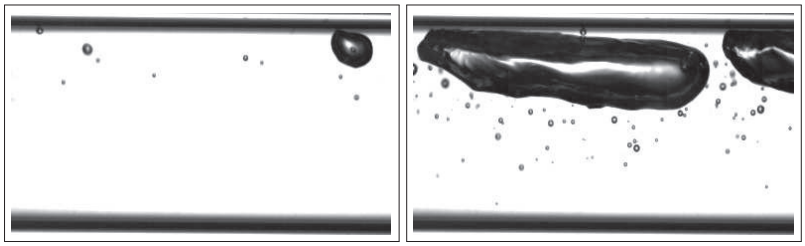

(c) Q_{real} = 451 [W]– x_{out} = 0.007 (d) Q_{real} = 509 [W] – x_{out} = 0.032

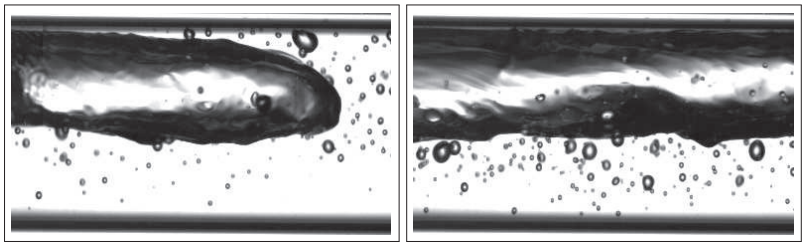

(e) Q_{real} = 567 [W] – x_{out} = 0.057 (f) Q_{real} = 634 [W] – x_{out} = 0.086

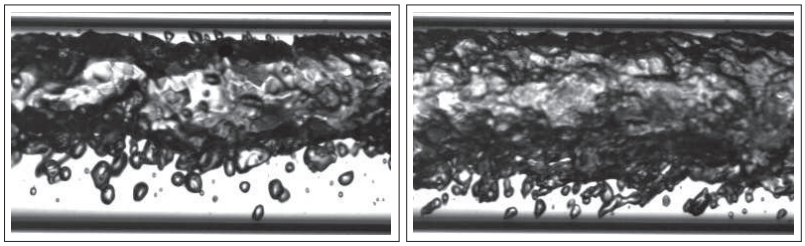

(g) Q_{real} = 776 [W] – x_{out} = 0.14 (h) Q_{real} = 964 [W] – x_{out} = 0.22

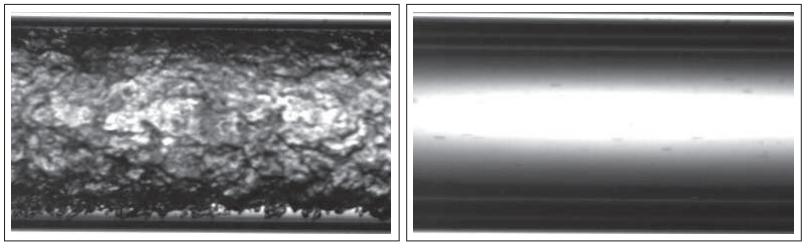

(i) Q_{real} = 1418 [W] – x_{out} = 0.43 (j) Q_{real} = 2110 [W] – x_{out} = 0.74

Figure 9.18: *Flow patterns for different applied powers. Different flow patterns are shown. (a) liquid-bubbles, (b) small bubbles, (c) small slugs, (d) slugs, (e) slugs, (f) big slugs, (g) intermittent, (h) intermittent-annular, (i) annular, (j) mist.*

9.7 Summary

A horizontal forced convection loop to study two-phase flow instabilities was designed. The theoretical basis for the design of two-phase components are described. The most used similarity criteria were described and used to design a facility using a heat exchanger in the LNG industry as a reference case. Several numerical simulations are used in order to study the steady and dynamic characteristics of the system. In addition, the influence of the heat distribution was studied, demonstrating its high-influence on two-phase instabilities. Several construction details and specifications of the designed loop were described. In the last part of the chapter, some experimental results of the final design loop were presented. The static characteristic curve for a heated pipe and an orifice valve were analysed. In addition, the occurrence of experimental *density wave* oscillations were also described. Finally, an image analysis (fast camera) is performed to show several different flow patterns for a particular case.

Bibliography

[1] AKAGAWA K. AND SAKAGUCHI T. Study on distribution of flow rates and flow stabilities in parallel long evaporatos. *Bulletin of JSME*, 14:837–848, 1971. (Cited on page 168)

[2] CASTRO H., GASCHE J., AND PRATA A. Pressure drop correlation for oil-refrigerant r134a mixture flaching flow in a small diameter tube. *Int. J. of refrigeration*, 32:421–429, 2009. (Cited on page 167, 171)

[3] DING Y., KAKAC S., AND X.J.CHEN . Dynamic instabilities of boiling two-phase flow in a single horizontal channel. *Experimental Thermal and Fluid Science*, 11:327–342, 1995. (Cited on page 168)

[4] DOGAN T., KAKAC S., AND VEZIROGLU T. Analysis of forced-convection boiling flow instabilities in single-channel upflow system. *Int. J. heat and fluid flow*, pages 145–156, 1983. (Cited on page 168)

[5] EUROPEAN PARLIAMENT , 2005. Resolution on *Winning the Battle Against Global Climate Change*. http://www.europarl.europa.eu. (Cited on page 171)

[6] GUIDO G., CONVERTI J., AND CLAUSSE A. Density wave oscillations in parallel channels – an analytical approach. *Nuclear engineering and Design*, 125:121–136, 1991. (Cited on page 170, 175)

[7] GUO L., Z.P.FENG , AND X.J.CHEN . Pressure drop oscillation of steam-water two-phase flow in a helically coiled tube. *Int. J. of Heat and Mass Transfer*, 44:1555–1564, 2001. (Cited on page 168)

[8] ISHII M. *Thermally induced flow instabilities in two-phase mixtures in thermal equilibrium*. PhD thesis, Georgia Institute of Technology, Michigan, 1971. (Cited on page 169, 175, 177)

[9] Jeglic F. and Yang K. The incipience of flow oscillations in force-flow subcooled boiling. Technical Report N66-15248, Heat transfer and Fluid Mechanics Institute University of California, 1965. (Cited on page 168)

[10] Kakac S. and Cao L. Analysis of convective two-phase flow instabilities in vertical and horizontal in-tube boiling systems. *Int. Journal Heat Mass Transfer*, 52:3984–3993, 2009. (Cited on page 168)

[11] Kakac S., Veziroglu T., Akyuzlu K., and Berkol O. Sustained and transient boiling flow instabilities in a cross-connected four-parallel-channel upflow system. *Proc. of the 5th int. conf. Heat Tranfer, Tokyo*, pages 235–239, 1974. (Cited on page 168)

[12] Liang N., Shuangquan S., Tian C., and Yan Y. Two-phase flow instabilities in horizontal straight tube evaporator. *Applied Thermal Engineering*, 31:181–187, 2011. (Cited on page 168)

[13] Longo G. Refrigerant r134a condensation heat transfer and pressure drop inside a small brazed plate heat exchanger. *Int. J. of refrigeration*, 31:780–789, 2008. (Cited on page 167, 171)

[14] Marcel C., Rohde M., and Van der Hagen T. Experimental investigations on flashing-induced instabilities in one and two-parallel channels: A comparative study. *Experimental Thermal and Fluid Science*, 34:879–892, 2010. (Cited on page 168)

[15] Maulbetsch J. and Griffith P. A study of system-induced instabilities in forced-convection flows with subcooled boiling. *MIT engineering projects Lab Report 5382-35*, 1965. (Cited on page 168)

[16] Minzer U., Barnea D., and Taitel Y. Evaporation in parallel pipes - splitting characteristics. *Int. J. Multiphase Flow*, 30:763–777, 2004. (Cited on page 168)

[17] Montreal Protocol , 2007. http://ozone.unep.org/Publications/MP_Handbook/Section_1.1 The Montreal Protocol. (Cited on page 171)

[18] Neeras B., Fredheim A., and Aunan B. Experimental data and model for heat transfer, in liquid falling film flow on shell-side, for spiral-wound lng heat exchanger. *International Journal of Heat and Mass Transfer*, 47:3565–3572, 2007. (Cited on page 171)

[19] O.Komakli , Karsli S., and Yilmaz M. Experimental investigation of two-phase flow instabilities in a horizontal in tube boiling system. *Energy Conversion and Management*, 43:249–268, 2002. (Cited on page 168)

[20] Ozawa M., Nakanishi S., Ishigai S., Mizuta Y., and Tarui H. Flow instabilities in boiling channels: Part 1, pressure drop oscillations. *Bulletin JSME*, 22(170), 1979. (Cited on page 168)

[21] POIATE E. AND GASCHE J. Foam flow of oil-refrigerant r12 mixture in a small diameter tube. *J. of the Braz. Soc. of Mech. Sci. & Eng*, 4:391, 2006. (Cited on page 167, 171)

[22] ROY R., JAIN P., AND S.P. K. Dynamic instability experiments in boiling flow system. *Int. J. Heat Mass Transfer*, 31:1947–1952, 1988. (Cited on page 168)

[23] RUSPINI L., MANAVELA E., REKSTAD H., TELLEBON R., DØLLNER M. Ø., DORAO C., AND FERNANDINO M. Two-phase flow instabilities and mal-distribution in lng heat exchangers: Experimental facility – project status. Technical report, EPT, NTNU, 2010. (Cited on page 180)

[24] RUSPINI L. AND LANGØRGEN E. Risk assessment report: Two-phase flow instabilities proyect. Technical report, NTNU, SINTEF, 2011. (Cited on page 180)

[25] SAHA P., ISHII M., AND N.ZUBER . An experimental investigation of the thermally induced flow oscillations in two-phase systems. *Transactions of the ASME*, 1:616–622, 1976. (Cited on page 168)

[26] SITU R., MI Y., ISHII M., AND MORI M. Photographic study of bubble behaviors in forced convection subcooled boiling. *Int- J. Heat and Mass transfer*, 47:3659–3667, 2004. (Cited on page 180)

[27] THONON B. A review of hydrocarbon two-phase heat transfer in compact heat exchangers and enhanced geometries. *Int. J. of refrigeration*, pages 633–642, 2008. (Cited on page 167, 171)

[28] WANG Q., CHEN X. J., KAKAC S., AND Y.DING . An experimental investigation of density-wave-type oscillations in a convective boiling upflow system. *Int. J. Heat and Fluid Flow*, 15, 1994. (Cited on page 168)

[29] YUN G., JUN H., GENGLEI X., AND HEYI Z. Experiment investigation on two-phase flow instability in a parallel twin-channel system. *Annals of Nuclear Energy*, 37:1281–1289, 2010. (Cited on page 168)

[30] YUNCU H. An experimental and theorethical study of density wave and pressure drop oscillations. *Heat transfer engineering*, 11:45–56, 1990. (Cited on page 168)

[31] ZUBER N. Hydrodynamic aspects of a boiling heat transfer. Technical Report AECU 4439, AEC, US, 1959. (Cited on page 169)

CHAPTER X

Pressure drop characterisation

► In this chapter different steady-state pressure drop models for single- and two-phase flow are experimentally analysed. In the first part, the distributed pressure drop in the "heated" and "outlet" sections, presented in the previous chapter, is studied. A modification to Blasius-Colebrook correlation is made in order to describe accurately the single-phase pressure drop. The distributed two-phase pressure drops, for "diabatic" and "adiabatic" cases, are also studied. A comparison of the most used correlations and experimental data is made. Finally, a new model for the "diabatic" friction pressure drop is introduced and its results are compared with previous models. In the last part, the same methodology is applied to the local pressure drops. Several well-known correlations, for orifice valves, are compared with experimental data for single- and two-phase flows.

As described in previous chapters, the stability of any two-phase flow system is highly dependent on the pressure drop losses along the circuit. In addition, it is well known that predicted two-phase pressure drop using leading methods differs by up to 100 % from experimental data. The main objective of the next sections, is to analyse the accuracy of the different correlations to describe the pressure drop losses in the thermo-hydraulic circuit presented in the previous chapter.

In the next sections, experimental and numerical results are analysed according to the next classification:

- Distributed pressure drop
  - Single-phase
  - Two-phase: Adiabatic case
  - Two-phase: Diabatic case
- Local pressure drop (orifice valve)
  - Single-phase
  - Two-phase: Adiabatic case

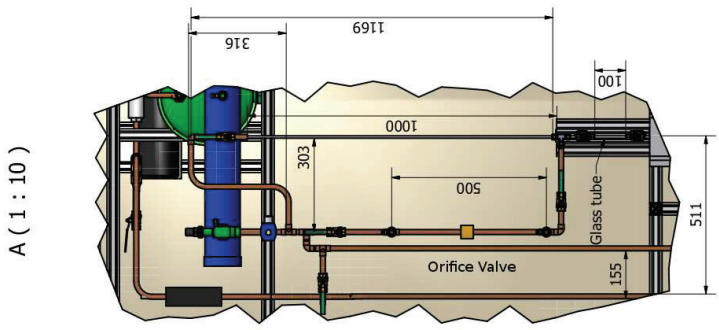

Figure 10.1: *Scheme of the "outlet" test section and the orifice valve, downstream the heated section (glass tube). This outlet parallel array is used to study distributed and local pressure drops. This sketch was made by Håvard Rekstad. The measures are in [mm].*

10.1 Distributed pressure losses

In this section, the distributed pressure drop losses for single- and two-phase flows are studied.

10.1.1 The experimental data

The general conditions for all the experimental data presented in this section are

- fluid: R134a
- P_{out}: 6.5 [bar]
- Q: 0-2000 [W]
- G_{in}: 0-3000 [kg/m^{2}s]
- L_{HS}: 1.6-2.05 [m], L_{out}: 1.00 [m]
- D_{in}: 5 [mm]

In the Figure 10.1 is shown the outlet arrange used to study the distributed and the local pressure drops at the outlet of the heated test section. As described in Section 9.5.3, a 1 meter pipe is placed downstream from the heated section to study adiabatic pressure losses. The characteristics of this pipe are the same of the pipe used as heated section. In the next sections single and two-phase pressure drop losses will be investigated.

10.1.2 Single-phase characterisation

Since all the pipes in this work are horizontal, it is possible to neglect the potential pressure drop. In a similar manner, the momentum pressure drop is neglected since the density does not suffer any significant change. Then, in accordance with the analysis made in Appendix A, the experimental friction factor is expressed as

$$f = \frac{D}{L}\frac{2\rho}{G^2}\Delta P_{fric} \tag{10.1}$$

where ΔP_{fric}, G,L and D are measured and ρ is calculated as a function of (T_{in},P_{in}).

In the next, the pressure drop in the *heated* and the *outlet* test sections are analysed independently since the *heated* section has pressure taps and inner thermocouples that can affect the friction terms. In order to analyse these friction pressure drop losses, four different data sets have been obtained experimentally. In Table 10.1 the main parameters for the experimental cases are shown.

Data Set	T_{in} [C^o]	P_{in} [m]	Q [W]
1	14	6.5	0
2	14	6.5	0
3	14	6.5	0
4	17	6.5	$\approx$ 1800

Table 10.1: *Average inlet parameters for the single phase pressure drop losses.*

10.1.2.1 Outlet test section friction factor

In the Figure 10.2, the experimental values for the friction factor and two of the most used correlations, smooth pipes (Blasius-Colebrook) and rough pipes (Colebrook), are shown. Four different experimental data sets are plotted. In the first three, the fluid is in liquid state (low Reynolds numbers), while in the last one the fluid is in super-heated vapor state (high Reynolds numbers).

As can be seen, none of the correlations reflects accurately the experimental values for low and medium Reynolds numbers. A roughness of $\epsilon/D = 0.01$ is used, for the rough pipe correlation (Colebrook). This value corresponds with normal roughness levels on stainless steel pipe, $\epsilon = \ 0.05[mm]$, as seen [12, chapter 6]. This last correlation seems to predict accurately the pressure drop at high Reynolds numbers. Nevertheless, at low Reynolds numbers the use of this correlation underestimate the pressure drop loss. In order to model the distributed friction pressure drop properly, a variation of Blasius-Colebrook correlations is proposed as follow

$$\begin{aligned} f &= 64/Re & Re < 10^3 \\ f &= 3.2/Re^{0.45} + 0.019 & 10^3 < Re < 10^{4.9} \\ f &= 1/(-1.8log_{10}((6.9/Re) + (\epsilon/3.7)^{1.11}))^2 & 10^{4.9} < Re \end{aligned} \tag{10.2}$$

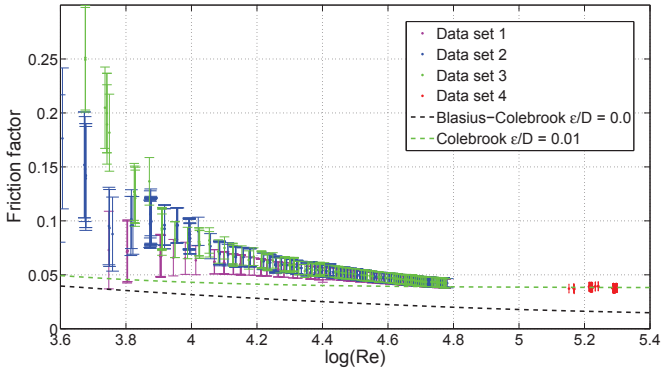

Figure 10.2: *Single-phase friction factor calculation for the "outlet" pipe. Comparison of the experimental values and the most used correlations.*

where the same roughness ($\epsilon/D = 0.01$) is used. The comparison with the experimental data, displayed in Figure 10.3, shows that for the working range of the system ($Re > 1e^{3.8} \Rightarrow G > 300kg/m^2s$) this last correlation reflects the experimental trends very accurately. The parameters of this correlation (constants and exponents) are obtained by minimising the difference between the experimental data and a function with the same functional shape as Blasius-Colebrook correlation. In accordance with the results shown in Figure 10.4, the total uncertainty of using this last correlation is minor to 5 % .

10.1.3 Heated section distributed friction factor

As mentioned earlier, the use of any well-know correlation that does not take into account the influence of roughness for middle Reynold number would underestimate the actual value of frictional pressure drop. Therefore, following the analysis of previous section, a modified "Blasius-Colebrook" correlation is obtained for the heated section pipe.

$$\begin{aligned} f &= 64/Re & Re < 10^3 \\ f &= 3.8/Re^{0.45} + 0.019 & 10^3 < Re < 10^{4.9} \\ f &= 1/(-1.8log_{10}((6.9/Re) + (\epsilon/3.7)^{1.11}))^2 & 10^{4.9} < Re \end{aligned} \tag{10.3}$$

notice that it is only changed the constant parameter in the term of the $Re^{-0.45}$. In this case, a roughness of $\epsilon/D = 0.015$ is used. This constant values are obtained by minimising the difference with the experimental data. In Figure 10.5, a comparison with the experimental friction factor values is shown. In the three sets of experimental data the fluid is in liquid state. Finally, the total pressure drop obtained using Eq. (10.3) is compared with the experimental values in the Figure 10.6. The total uncertainty for the working region of the facility results minor to 5 %.

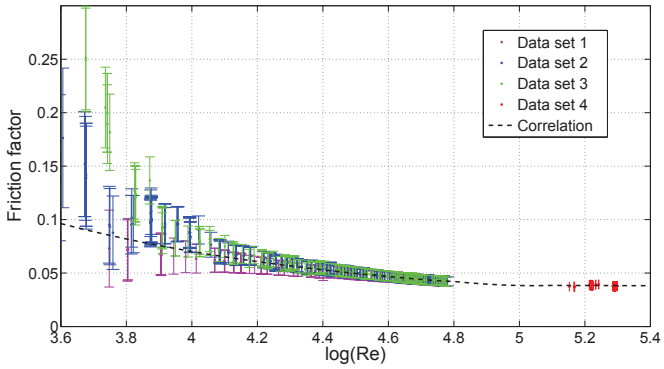

Figure 10.3: *Single-phase friction factor calculation for the "outlet" pipe. Comparison of experimental values and the correlation from Eq.* (10.2)*.*

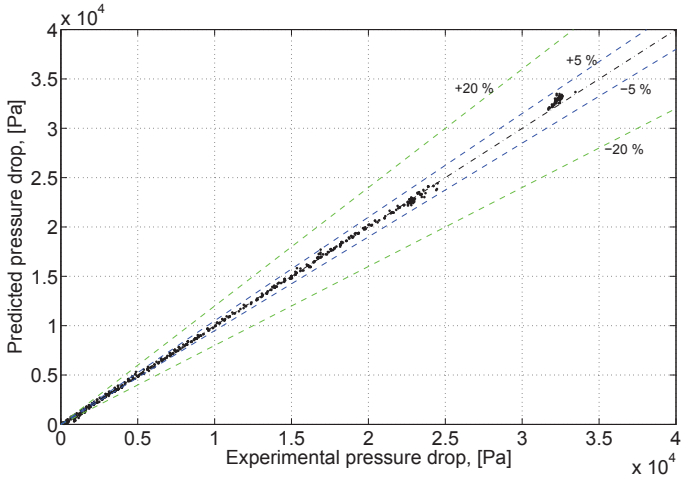

Figure 10.4: *Single-phase pressure drop for the "outlet" pipe. Comparison of experimental values and the correlation from Eq.* (10.2)*.*

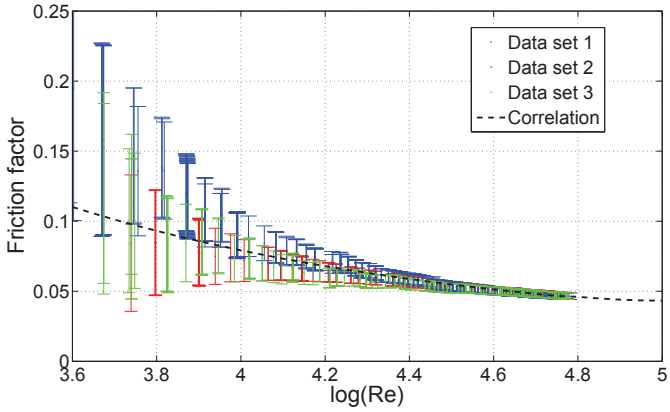

Figure 10.5: *Single-phase friction factor calculation for the "heated" test section. Comparison of experimental values and the correlation from Eq.* (10.3)*.*

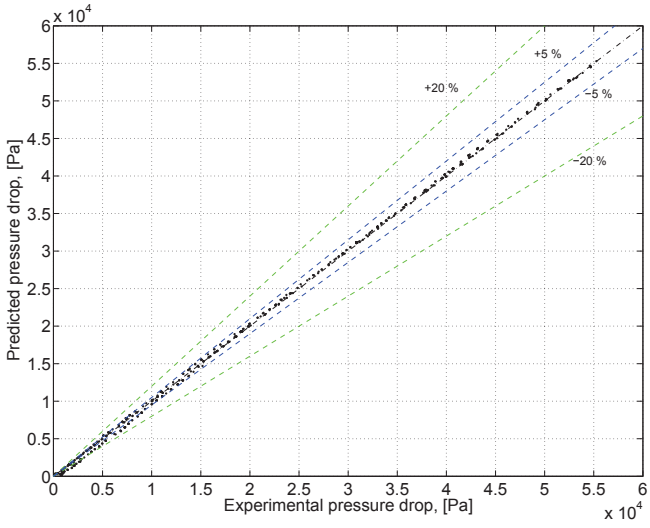

Figure 10.6: *Single-phase pressure drop for the "heated" test section. Comparison of experimental values and the correlation from Eq.* (10.3)*.*

10.2 Two-phase characterisation

It is well known that the two-phase pressure drop is highly dependent on the inlet conditions (Q,T_{in}, G_{in}). In this section, several sets of data are used in order to study pressure drop losses. In the Table 10.2, the average of the main thermo-hydraulic variables for those experimental cases are given. A waiting period, necessary for the stabilisation of the system was used in order to achieve the steady-state condition. Nevertheless, slight variations are observed for increasing and decreasing flow. These variations are probably due to flow pattern transitions and to the heat transfer modification in the heat exchangers. Then, this information is indicated as $\Uparrow$ and $\Downarrow$, respectively.

Case	Q [W]	T_{in} [C^o]	L_{HS} [m]	G evolution
1	1810	-15	2.05	$\Uparrow$
2	1840	-10	2.05	$\Uparrow$
3	1840	-10	2.05	$\Downarrow$
4	1870	-2	2.05	$\Uparrow$
5	1870	-2	2.05	$\Downarrow$
6	1660	-10	2.05	$\Uparrow$
7	1660	-10	2.05	$\Downarrow$
8	1385	-10	2.05	$\Uparrow$
9	1385	-10	2.05	$\Downarrow$
10	1410	-2	2.05	$\Uparrow$
11	1430	5	2.05	$\Uparrow$
12	1200	-10	1.65	$\Downarrow$
12	1200	-10	1.65	$\Downarrow$
13	925	-10	2.05	$\Uparrow$
14	930	-2	2.05	$\Uparrow$
15	930	-2	2.05	$\Uparrow$
16	960	5	2.05	$\Uparrow$
17	960	5	2.05	$\Downarrow$
18	990	10	2.05	$\Downarrow$
19	560	-10	1.65	$\Uparrow$
20	560	-10	1.65	$\Downarrow$
21	300	5	2.05	$\Downarrow$

Table 10.2: *Average inlet parameters for the experimental cases.*

10.2.1 Adiabatic case: Outlet test section

In order to model the “adiabatic” pipe, a thermal equilibrium model was implemented. As explained, gas and liquid are assumed to be at the same temperature in the two-phase region. Moreover, the total pressure in the outlet section can be calculated as

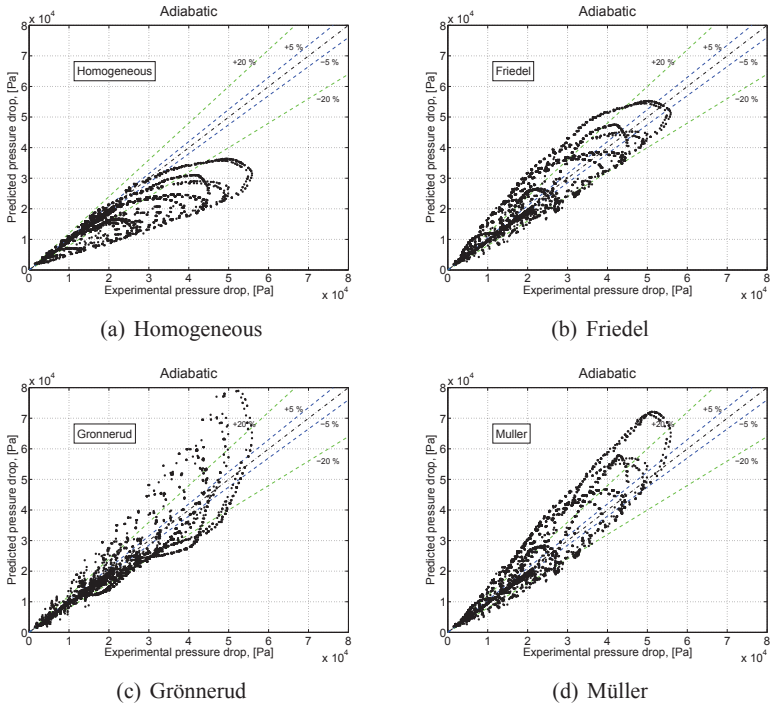

(a) Homogeneous (b) Friedel

(c) Grönnerud (d) Müller

Figure 10.7: *Two-phase pressure drop for the "outlet" test section (Adiabatic). Comparison of experimental values and most used correlations in the literature, Eqs. (A.2) to (A.18).*

$$\Delta P \quad = \quad \Delta P_{Fric} = \Delta P_{L0} \Phi_{TP}^2 \tag{10.4}$$

since this is a steady, adiabatic and horizontal problem. As presented before the single-phase pressure drop is given by

$$\Delta P_{L0} = \frac{f L}{D} \frac{G^2}{2\rho_l} \tag{10.5}$$

where G is the total mas flow rate and f correspond with the correlation obtained in Eqs. (10.2) and (10.3). The two-phase multiplier Φ_{TP}^2 is calculated following the description of Section A.1. The two-phase pressure drop correlations, given in Eqs. (A.2) to (A.18), are implemented. In the Figure 10.7, the numerical results are compared with the experimental values. The inlet conditions of the outlet pipe are the result of the model used in the next section for the heated pipe. As shown in these figures, the best performing model has an uncertainty larger than 40 %. In the following, a new adiabatic model is proposed.

10.2.1.1 A new model: adiabatic two-phase distributed pressure drop

As shown in Figure 10.7, for the present experimental conditions the most accurate results are obtained with the Grönnerud and Müller correlations. This last one, is specially characterised for its simplicity, since it depends only in the pressure drops for the all liquid and all vapor pressure drops and the quality. In the same manner, the empirical correlation proposed in this work, depends only on these parameters. At the same time some small variations in the pressure drop characteristic curve are observed for the transition to the annular flow pattern, see Figure 10.9. Thus, an empirical correlation is proposed to describe the frictional pressure drop, taking into account these small variations due to the flow pattern transition.

The main parameter of this correlation is the ratio between the pressure drop of all liquid and all vapor cases. It can be calculated as

$$\psi = \frac{\left(\frac{\partial P}{\partial z}\right)_{G0}}{\left(\frac{\partial P}{\partial z}\right)_{L0}} \tag{10.6}$$

Therefore the functional shape of the multiplier introduced in this work is

$$\Phi^2_{Rus} = (1-x) \; + \; \psi \, x \; + \; \frac{3.6}{\mathcal{S}} \, \psi \, x^2 \; (1-x)^{\frac{1}{2}} \tag{10.7}$$

where the value of $\mathcal{S}$ depends on the local flow pattern. The function of the two first terms on the right hand side is to make a smooth transition when $x \approx 0$ and $x \approx 1$. As explained, a clear change in the pressure drop characteristic curve is observed when the system evolves into the annular flow pattern. For that reason, a variation on the parameter $\mathcal{S}$ is introduced according the limit of this transition, expressed as a critical volumetric flux j_{crit}. In consequence, the parameter $\mathcal{S}$ is defined as

$$\begin{aligned} \mathcal{S} &= 1 & j < j_{crit} \\ \mathcal{S} &= \left(\frac{j}{j_{crit}}\right)^{\gamma} & j > j_{crit} \\ \gamma &= 1.5 \end{aligned} \tag{10.8}$$

where in this case the flow-pattern transition limit is given by

$$j_{crit} = 4.5 + 5\,x \; + \; 3\,x\,(1-x) \qquad [m/s] \tag{10.9}$$

Notice that for the slug, intermittent and bubbly flow patterns, the total volumetric flux j is always minor than j_{crit} and in consequence the parameter $\mathcal{S} = 1$. It is important to remark that this completely empirical flow pattern transition is based on the phenomenological variation of the pressure drop curve and not on visual observations. Moreover the range of application of this transition limit is only valid for inlet temperatures below $0\,C^o$. Although not of general applicability, this simple transition correlation give an accurate description of the pressure drop changes for this particular case. In Figure 10.8 a comparison of the experimental data and the

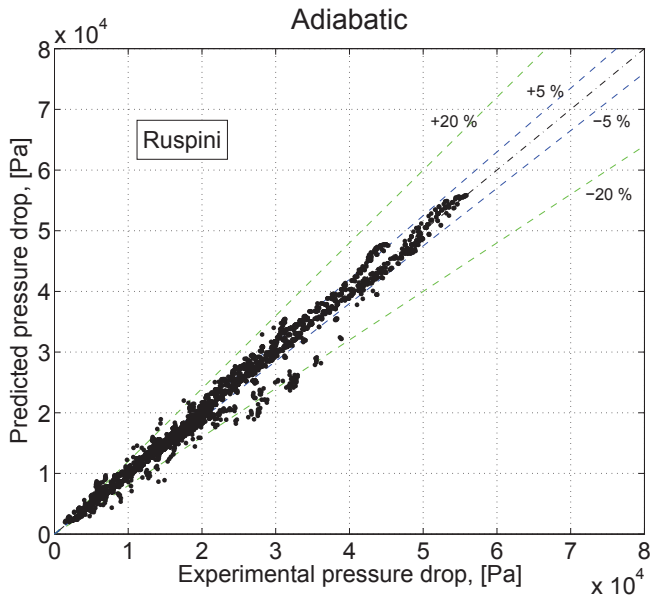

Figure 10.8: *Two-phase pressure drop for the "outlet" test section. Comparison of experimental values and the correlation introduced in Eq.* (10.7)*.*

predicted pressure drops, using the described model, is presented. As can be seen, the predicted values have and uncertainty less than 15 %. In Figures 10.9 and 10.10, two different experimental cases are used to put in evidence the predicted pressure drops for the different two-phase correlations studied in this work.

In Table 10.3 the uncertainties of the results for each correlation are compared. In accordance with the figures, it is easy to see that the correlation developed in this section predicts much more accurately the pressure drop for the outlet pipe.

	Adiabatic	
Model	In 20 % range	In 5 % range
Homogeneous	40.4	15.4
Martinelli	38.4	16.2
Friedel	57.6	19.2
Müller	55.4	19.6
Grönnerud	80.4	28.3
Ruspini, Eq. (10.7)	96.7	57.3

Table 10.3: *Adiabatic two-phase pressure drop. Comparison of the results and confidence intervals for the different correlations.*

In the end of this section, a discussion about the phenomenological description and the applicability to other cases of the different correlations, for both "adiabatic"

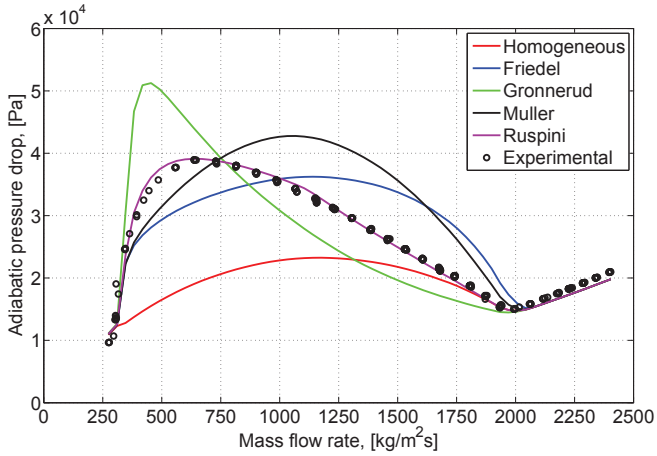

Figure 10.9: *Two-phase pressure drop for the "outlet" test section. Comparison of all correlations and the experimental pressure drops for case 10 in Table 10.2.*

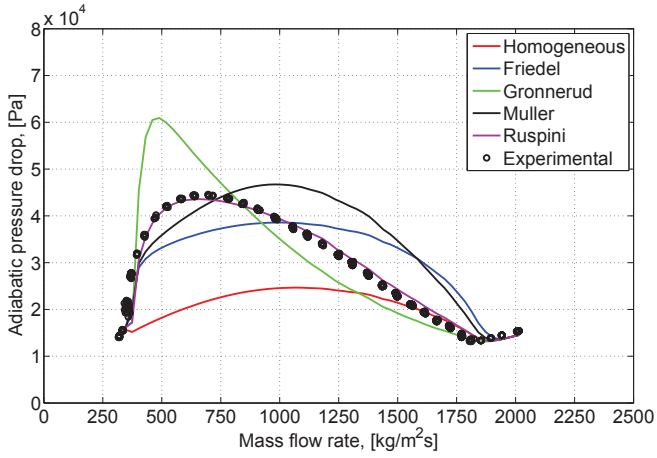

Figure 10.10: *Two-phase pressure drop for the "outlet" test section. Comparison of all correlations and the experimental pressure drops for case 6 in Table 10.2.*

and “diabatic” cases, is presented.

10.2.2 Diabatic case: Heated test section

The most important difference in the diabatic case, respect to the adiabatic case, is the addition of heat to the fluid. It makes that the involved phenomena occurring are significantly different. As the fluid is flowing through the pipe, then it is heated. According to that, bubbles start been generated close to the wall even when the average temperature is less than the saturation temperature (subcooling boiling). Then, more vapor is generated and the different flow patterns take place over the pipe. In this case the total frictional pressure drop is the sum of the local pressure drops caused by different flow patterns. Another important difference respect to the adiabatic case, is that the momentum pressure drop becomes non-negligible. In addition, the experimental measured pressure drop is the sum of both, momentum and frictional pressure drops and it is not possible to distinguish between them. This is one reason because the model of momentum pressure drop plays an important role in the prediction of the diabatic pressure drop. As explained in [5], momentum pressure drop is caused by changes in the density profile that, in the boiling case, produce a flow acceleration along the pipe.

The model used in this section, takes into account the sub-cooled boiling phenomenon following P. Saha and N. Zuber [8] (1974). In addition, a separated flow model is used to calculate the momentum pressure drop, see [5]. The expression for this component is

$$\Delta P_{Mom} = \frac{G^2 L}{2}\left(\frac{1}{\rho'_{in}} - \frac{1}{\rho'_{out}}\right) \tag{10.10}$$

where the momentum density is given by

$$\frac{1}{\rho'_i} = \left[\frac{1}{\rho_l}\frac{(1-x_i)^2}{(1-\alpha_i)} + \frac{1}{\rho_g}\frac{(x_i)^2}{(\alpha_i)}\right] \tag{10.11}$$

The friction components are calculated using the same correlations as for the adiabatic case. Finally, the total pressure drop is calculated as the sum of the frictional and momentum terms

$$\Delta P_{Tot} = \Delta P_{Mom} + \Delta P_{Fric} \tag{10.12}$$

the potential pressure drop is neglected since in this case the pipe is horizontal.

In Figure 10.11, the comparison of experimental and predicted values is shown. In accordance with these results the correlation of Eq. (10.7) is found to be the most accurate, followed by the Grönnerud correlation. These results are reflected in Table 10.4, where an uncertainty comparison of the results is made. According to this analysis, it is proved that also in the adiabatic case, the empirical correlation introduced in this work produce better results than the other correlations.

In Figures 10.12 and 10.13, two experimental cases and the predicted pressure drops are depicted. In these figures, the total pressure drop (momentum and friction) is presented. It is important to remark that the correlation introduced in the previous

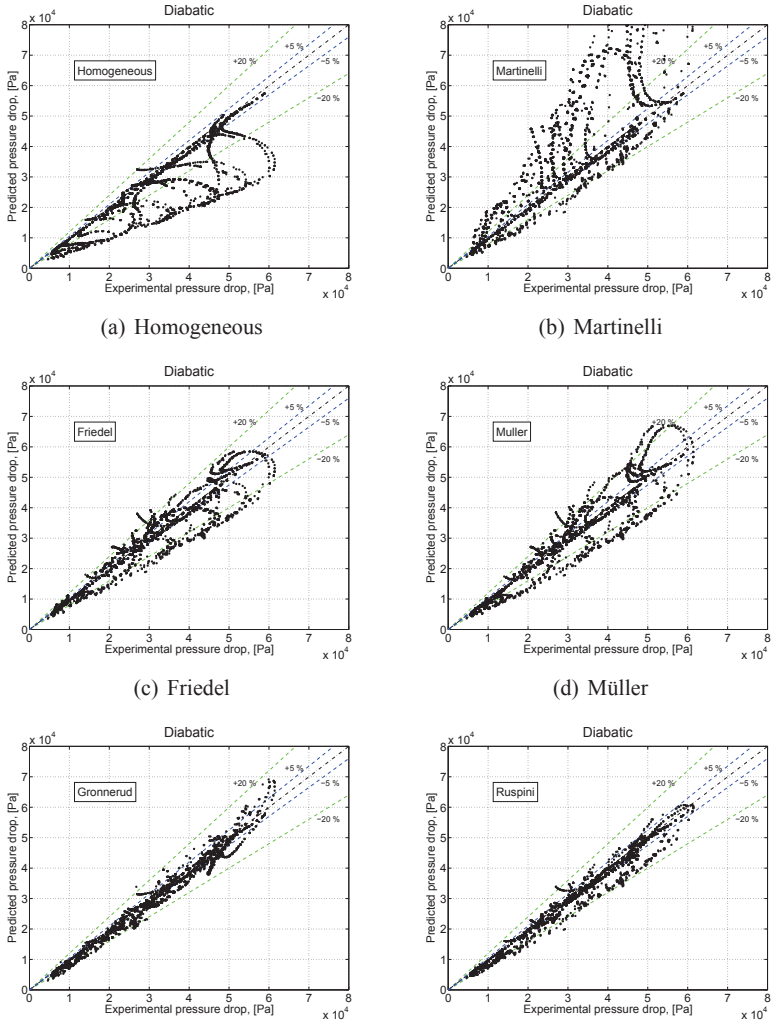

(a) Homogeneous

(b) Martinelli

(c) Friedel

(d) Müller

(e) Grönnerud

(f) Ruspini, Eq. (10.7)

Figure 10.11: *Total two-phase pressure drop for the "heated" test section (Diabatic). Comparison of experimental values and several correlations.*

	Diabatic	
Model	In 20 % range	In 5 % range
Homogeneous	78.8	46.0
Martinelli	60.2	35.9
Friedel	88.8	46.3
Müller	85.8	47.2
Grönnerud	95.8	51.2
Ruspini, Eq. (10.7)	96.1	61.4

Table 10.4: *Diabatic two-phase pressure drop. Comparison of the results uncertainties and confidence intervals for the different models.*

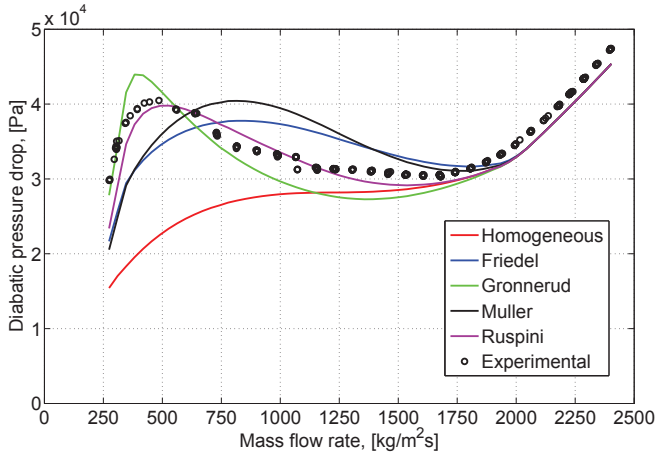

Figure 10.12: *Two-phase pressure drop for the "heated" test section. Comparison of all correlations and the experimental total pressure drop (Momentum + Friction) for case 10 in the Table 10.2.*

sections, not only describe more accurately the total pressure drop but also the slope of the characteristic pressure drop vs. mass flow rate curve ($\partial \Delta P \; vs. \; \partial G$). This last parameter is of paramount importance in the description of any kind of two-phase flow instabilities, as described in previous chapters. In addition, in Figure 10.14 the different pressure drop components (momentum and friction) are shown independently, for the case 17 in the Table 10.2. In accordance with these results, the momentum pressure drop can not be considered negligible, been approximately the 15 % of the total pressure drop. In the next section, a general discussion about the modelling of these pressure drop terms is presented.

10.2.3 Discussion

The analysis presented previously put in evidence the higher accuracy of the correlation introduced in this work compared to the most used correlations in the

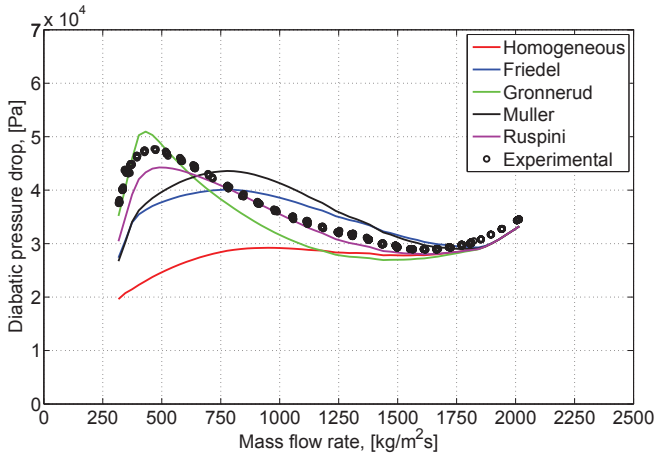

Figure 10.13: *Two-phase pressure drop for the "heated" test section. Comparison of all correlations and the experimental total pressure drop (Momentum + Friction) for case 6 in the Table 10.2.*

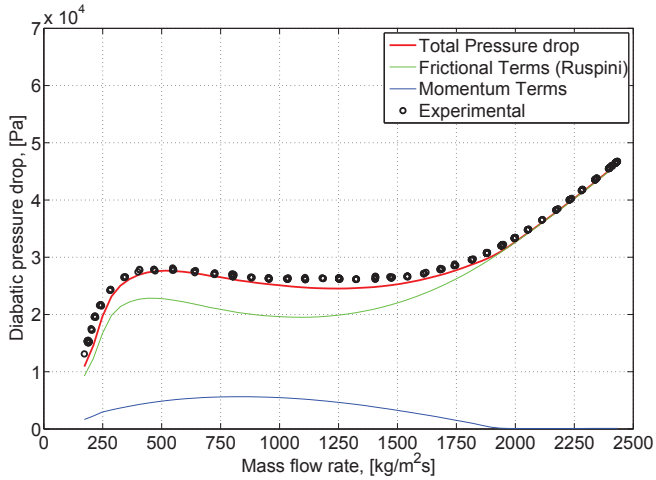

Figure 10.14: *Two-phase pressure drop for the "heated" test section (Diabatic). Momentum and frictional pressure drop components, using Eq.* (10.7)*. (Case 17 in the Table 10.2)*

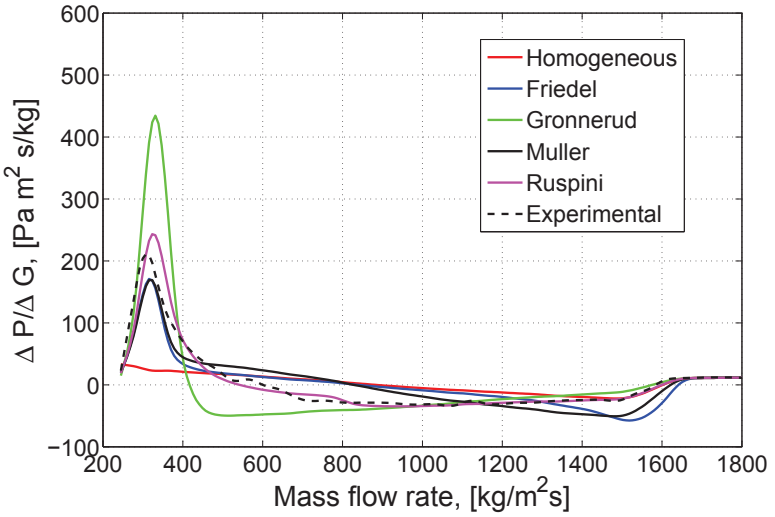

Figure 10.15: *Characteristic curve slope from the curve presented in Figure 10.10. It corresponds to the case number 6 in Table 10.2 (Adiabatic).*

literature. For approximately 900 experimental points, the percentage of data points correctly predicted within the 5 % is 57.3 % and 61.4 % for the adiabatic and the diabatic cases respectively. Nevertheless, should be remarked that its applicability range is limited due to the use of a empirical correlation, Eq. (10.9), for the flow pattern transition. As commented, the validity of this flow-pattern limit is reduced to these experimental cases and operation ranges. In addition, should be noticed that the experimental points out of the 5% group are, in general, those points corresponding with high qualities where the slope of the characteristic curve increases considerably. Therefore, a dryout model would be useful to better describe the pressure drop terms.

In addition as seen in previous chapters, the slope of the characteristic curve has a high influence on the stability of thermo-hydraulic instabilities. In Figures 10.15 and 10.16 the slope of the characteristic curves for an adiabatic and a diabatic cases are shown. These experimental cases correspond with the Figures 10.10 and 10.13 respectively. As indicated in these figures, the correlation introduced in this work predicts the slope more accurately than the other correlations. For that reason it results convenient to describe the pressure drop terms using this correlation.

Regarding the performance of the other correlations, Grönnerud correlation is the most accurate. For the diabatic case it predicts a percentage of 51.2 % data points within the 5 %. However, in the adiabatic case the percentage of well predicted points drops dramatically to 28.3 %. The same trend is followed by the rest of the correlations. Furthermore, in accordance with Figures 10.15 and 10.16, the slope of the characteristic curves is well described only for low qualities (higher mass flow rate). As can be seen, this correlation over-predicts the slope for low

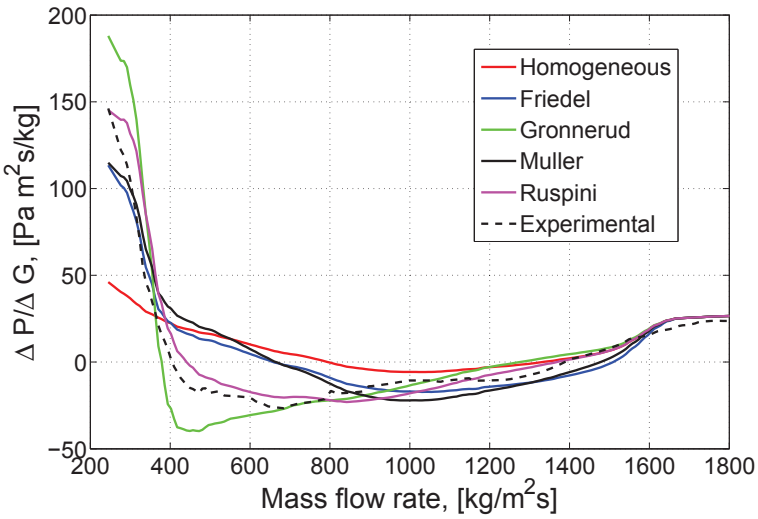

Figure 10.16: *Characteristic curve slope from the curve presented in Figure 10.13. It corresponds to the case number 6 in Table 10.2 (Diabatic).*

mass flow rates.

Before concluding this section, a last remark should be taken regarding the current pressure drop models based in a flow pattern description, J.M. Quiben and J.R. Thome [6, 7]. Although the limited application range of the used flow pattern maps (L. Wojtan et al. [14]), they use a continues void fraction model that does not take into account the different flow pattern structures. In the mentioned studies, a modified version of the Rouhani and Axelsson (1970) void fraction correlation presented in [9, 13] is used. This choice is supported by the results obtained in [13] for only slug flow, but applied to all the flow pattern regimes. As proved in [15], none of 68 different void fraction correlations (included Rouhani and Axelsson) is able to predict experimental values with more than 45 % of uncertainty in a wide number of experimental conditions, with different flow pattern structures. In addition, most of the experimental results supporting the use of those correlation have historically been developed for air-water and air-kerosene mixtures. Moreover, as proved in [1], when J.M. Quiben and J.R. Thome [6] flow pattern model is applied to a case with a different operation range, it predicts the pressure drop loss with the same degree of exactitude than Grönnerud, Müller or Friedel correlations.

The last issue to remark, regarding pressure drop models based in flow pattern maps, is the choice of the momentum pressure drop. In J.M. Quiben and J.R. Thome [6], as well as in this work, a separated flow model is used. In Figure 10.17 the predicted momentum pressure drop is shown, using three different models. A separated and a homogeneous model for the momentum pressure drop are used. The separated model is tested with an homogeneous void fraction and using the Rouhani and Axelsson void fraction model introduced in [9]. As can be seen, a difference of almost 2 exist when using the separated model, compared with the homogeneous

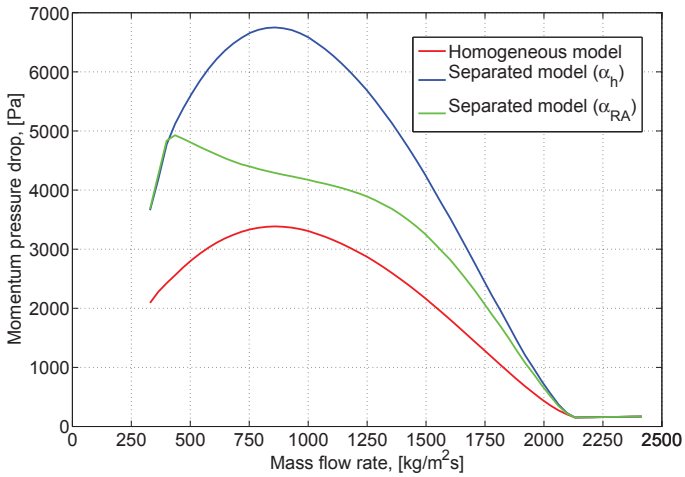

Figure 10.17: *Momentum pressure drop for the "heated" test section (Diabatic). (Case 6 in the Table 10.2)*

case. This figure also shows the large influence of the void fraction model in the momentum pressure drop. In summary, it is proved that flow pattern based methods can be significantly more precise than the most common methods. However, several incompatibilities between the void fraction (slip velocity), momentum pressure drop and flow pattern structures should be addressed in order to obtain a method that accurately reflects the physical phenomena taking place in two-phase flow mixtures.

10.3 Local pressure drop

In this section, the pressure loss in an orifice valve is studied following the same methodology presented before. First, the single-phase pressure drop is analysed. Then, several pressure drop correlations for two-phase flow are compared with experimental data. Finally, a brief discussion about the results is presented.

10.3.1 The experimental data

The general conditions for the experimental data used in this section are:

- fluid: R134a
- P_{out}: 6.5 [bar]
- Q: 0-2000 [W]
- G_{in}: 0-3000 [kg/m^{2}s]
- D_{piping} = 12.5 [mm]

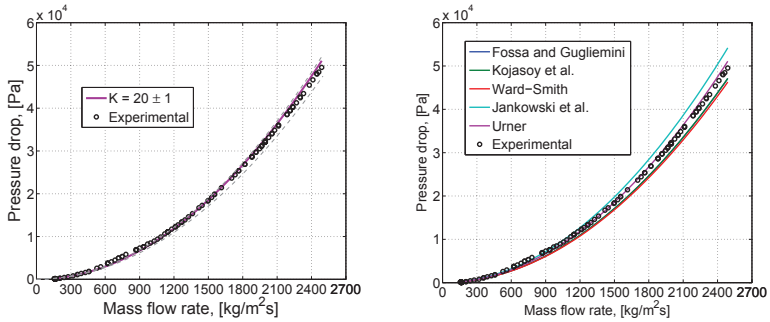

Figure 10.18: *Single-phase pressure drop at the orifice valve. (a) corresponds to the best fitting of the constant K. (b) presents a comparison of several methods to estimate this constant from geometrical characteristics.*

- $D_{orifice}$ = 3.0 [mm]
- l = 1.0 [mm] (Orifice Length)

The orifice valve used in this section, see Figure 9.9, is placed in a parallel configuration respect to the "outlet pipe", as shown in Figure 10.1. All the experimental points are taken in steady-state conditions. A stabilisation period of some minutes was waited before recording the data points.

10.3.2 Single phase characterisation

As explained in the Section A.2, the local single-phase pressure drop of an orifice valve is characterised by a constant K. This constant is the analogous to the Darcy friction factor, used in distributed pressure drop calculations. Thus, the total pressure drop in the orifice is represented by

$$\Delta P = K\frac{G^2}{2\rho_l} \tag{10.13}$$

In the Figure 10.18, the single-phase pressure drop for the valve described before is plotted. In this case, the fitted valve constant corresponds to $K = 20 \pm 1$. There exist, in the literature, several models to obtain the values of K based on the geometrical characteristics of the orifice, see M. Fossa and G. Guglielmini [2], G. Kojasoy et al. [4], A.J. Ward-Smith [11], T.A. Jankowski et al. [3], Gerd Urner [10]. Among them, Urner's model is producing the best prediction of K, as shown in Figure 10.18(b). In the following, the two-phase pressure drops in the orifice valve are analysed.

Case	Q [W]	T_{in} [C^o]
1	1810	-15
2	1840	-8
3	1870	-2
4	1365	-15
5	1385	-8
6	1410	-2
7	910	-15
8	925	-8
9	930	-2

Table 10.5: *Average inlet parameters for the experimental cases used to study the local pressure drop in an orifice valve.*

10.3.3 Two-phase characterisation

Remembering, the pressure drop for two-phase flow in an orifice valves is given by

$$\Delta P_{TP} = \Delta P_{L0} \Phi_{TP}^2 \tag{10.14}$$

where ΔP_{L0} is the single-phase pressure drop given by Eq. (10.13), using the liquid density and Φ_{TP}^2 is the two-phase multiplier. Several correlations describing this multiplier are described in Appendix A.2. The quality x at the valve is calculated using the output from the *heated* test section model introduced in the Section 10.2.2. In the following, a comparison of experimental and calculated results is presented. In Table 10.5 the average values of the main thermo-hydraulic variables for the experimental cases are shown.

The correlations given in Eqs. (A.20) to (A.21) are used to predict the two-phase multiplier. In Figure 10.19, the calculated and the experimental points are compared. In the same way as in the previous section, the percentage of well-predicted points is used to characterize the different correlations. In Table 10.6, the percentage of well predicted points within the 20 % and 5 % are shown. In accordance with these results, Chisholm correlation is the most accurate, predicting almost 39 % of points within the 5% of error. The second best performance is for Simpson correlation with 35 % of well predicted points within 5 %.

In Figures 10.20 and 10.21 the predicted and experimental pressure drops are plotted against the mass flow rate to compare the characteristic curves, for cases number 1 and 6 in the Table 10.5. As can be seen, in an opposite way from the distributed pressure drop models, the homogeneous approximation over-estimate in all the cases the pressure drop.

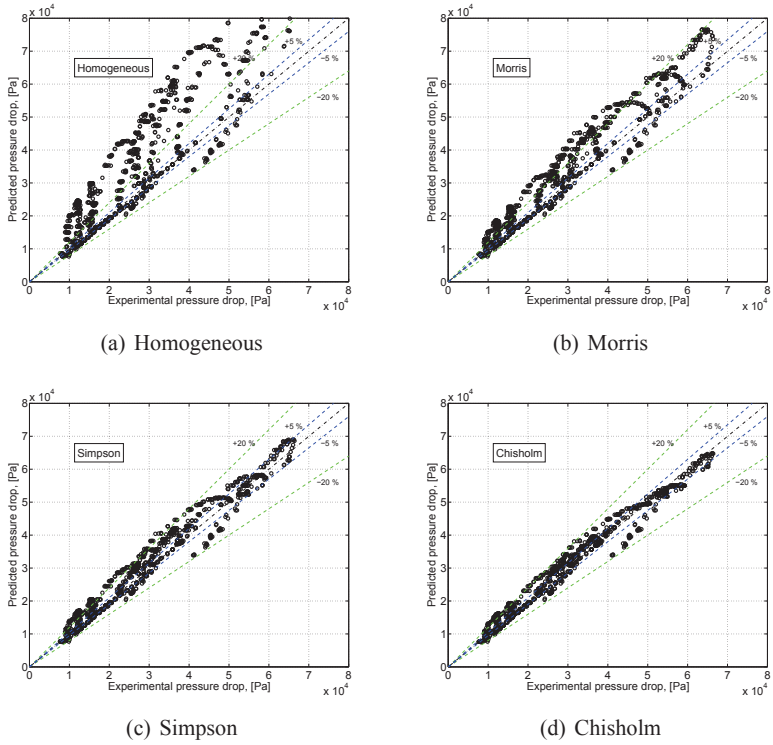

(a) Homogeneous (b) Morris

(c) Simpson (d) Chisholm

Figure 10.19: *Two-phase pressure drop in the orifice valve. Comparison of the experimental and predicted values for each of the correlations.*

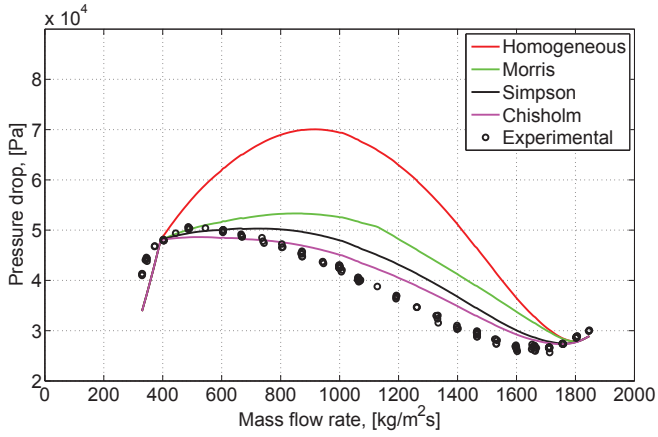

Figure 10.20: *Two-phase pressure drop for the orifice valve. Comparison of predicted and experimental pressure drops for case 1 in Table 10.5.*

	Orifice valve	
Model	In 20 % range	In 5 % range
Homogeneous	48.5	18.1
Morris	66.0	21.4
Simpson	86.5	34.4
Chisholm	92.0	38.7

Table 10.6: *Adiabatic two-phase pressure drop in an orifice valve. Comparison of the results uncertainties and confidence intervals for the different models.*

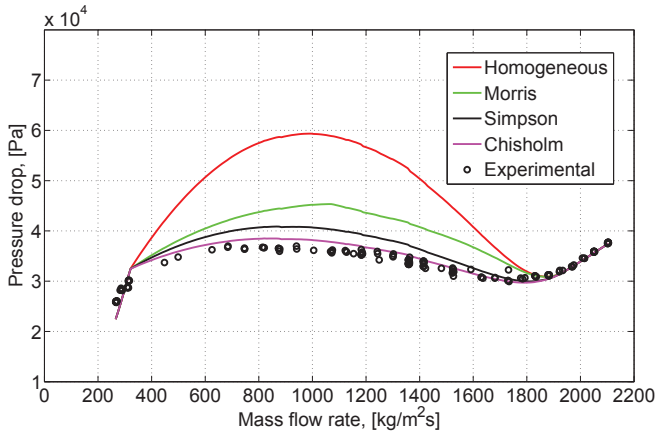

Figure 10.21: *Two-phase pressure drop for the orifice valve. Comparison of predicted and experimental pressure drops for case 6 in Table 10.5.*

10.4 Summary

In this chapter an experimental investigation on the distributed and local pressure drops was made. In addition, the experimental results were compared with the most used pressure drop correlations in the literature. In the first part, the distributed pressure drop losses were analysed. A modification of the well known Blasius-Colebrook correlation, for single-phase flows, was made in order to described accurately the pressure drop on different sections of the experimental loop. The two-phase flow pressure drops were analysed. Among the most used correlations, Grönnerud proved to be the most accurate. An empirical correlation for distributed two-phase pressure drop was proposed. Even if not of general application, it proved to describe the pressure drop in the system more accurately than any of the other correlation. Finally, the local pressure drops for single and two-phase flows were analysed. Chisholm correlation was the most accurate predicting the two-phase pressure drop in an orifice valve.

Bibliography

[1] CHENG L., RIBATSKI G., QUIBÉN J. M., AND THOME J. A flow pattern based phenomenological two-phase frictional pressure drop model for c02 evaporation in macro and micro-channels. *5th European Thermal-Sciences Conference, The Netherlands*, 2008. (Cited on page 215)

[2] FOSSA M. AND GUGLIELMINI G. Pressure drop and void fraction profiles during horizontal flow through thin and thick orifices. *Experimental Thermal and Fluid Science*, 26, 2002. (Cited on page 217)

[3] JANKOWSKI T., SCHMIERER E., AND PRENGER F. A series pressure drop representation for flow through orifice tubes. *Journal of Fluids Engineering*, 130, 2008. (Cited on page 217)

[4] KOJASOY G., LANDIS F., KWAME-MENSAH P., AND CHANG C. Two-phase pressure drop in multiple thick- and thin-orifice plates. *Experimental Thermal and Fluid Science*, 15, 1997. (Cited on page 217)

[5] LAHEY R. AND MOODY F. *The thermal hydraulics of a boiling water nuclear reactor*. Amer Nuclear Society, 1977. (Cited on page 210)

[6] QUIBEN J. AND THOME J. Flow pattern based two-phase frictional pressure drop model for horizontal tubes. part i: Diabatic and adiabatic experimental study. *Int. J. Heat Fluid Flow*, 28:1049–1059, 2007. (Cited on page 215)

[7] QUIBEN J. AND THOME J. Flow pattern based two-phase frictional pressure drop model for horizontal tubes. part i: New phenomenological model. *Int. J. Heat Fluid Flow*, 28:1060–1072, 2007. (Cited on page 215)

[8] SAHA P. AND ZUBER N. Point of net vapor generation and vapor void fraction in subcooled boiling. *Procedings of the fifth International Heat Tranfer*, B4.7: 175–179, 1974. (Cited on page 210)

[9] STEINER D. Vdi-warmeatlas (vdi heat atlas) chapter hbb. *In: Verein Deutscher Ingenieure, editor. VDI-Gesellschaft Verfahrenstechnik und Chemieingenieurwesen (GCF), Translator: J.W. Fullarton, Dusseldorf*, 1993. (Cited on page 215)

[10] URNER G. Pressure loss of orifice plates according to iso 5167-1. *Flow Measurement and Instrumentation*, 8, 1997. (Cited on page 217)

[11] WARD-SMITH A. *Pressure Losses in Ducted Flows*. Butterworths, London, 1971. (Cited on page 217)

[12] WHITE F. M. *Fluid Mechanics*. McGraw-Hill, 2003. (Cited on page 201)

[13] WOJTAN L., URSENBACHER T., AND THOME J. R. Interfacial measurements in stratified types of flow. part ii: Measurements for r-22 and r-410a. *International Journal of Multiphase Flow*, 30:125–137, 2004. (Cited on page 215)

[14] WOJTAN L., URSENBACHER T., AND THOME J. Investigation of flow boiling in horizontal tubes: Part i-a new diabatic two-phase flow pattern map. *International Journal of Heat and Mass Transfer*, 48:2955–2969, 2005. (Cited on page 215)

[15] WOLDESEMAYAT M. A. AND GHAJAR A. J. Comparison of void fraction correlations for different flow patterns in horizontal and upward inclined pipes. *International Journal of Multiphase Flow*, 33:347–370, 2007. (Cited on page 215)

CHAPTER XI

Experimental investigation of two-phase flow instabilities

► In this last chapter two-phase flow instabilities are experimentally investigated. The phenomena called *density wave* and *pressure drop* oscillations are studied. A discussion of the nature of the involved phenomena in the occurrence of these phenomena is made. The influence of flow patterns transitions and non-linear effects are discussed. The interaction between different kinds of instabilities is studied. In addition, the stability of the system is investigated both experimental and numerically. A comparison of the results is made and also extended to the occurrence of high amplitude oscillations. Finally, the DWO stability limits are analysed experimentally to characterise the influence of a compressible volume in the inlet of the heated section.

11.1 Introduction

Several aspects of *density wave* and *pressure drop* oscillations were investigated in previous chapters. In Chapter 2 the main instability mechanisms triggering these phenomena were introduced. R.T. Lahey and D.A. Drew [4] (1980) made an extensive review of the experimental and analytical research regarding the occurrence of these phenomena. The need for more investigation on the interaction between different instability modes was presented as one of the main conclusions of that study. On the other hand, other investigations discuss the need of more research in the interaction of different instability modes [5]. In the last years several studies analysed PDO experimentally [8, 16, 1, 2] and numerically [9, 10, 14, 6, 13, 7, 3]. However, even when in most of the cases DWO are observed during the occurrence of PDO, very few studies on the interaction of these phenomena have been published. It is also necessary to remark that none of the numerical models used to simulate pressure drop oscillations in the past are able to describe DWO phenomenon. More recently, [12] describes numerically a case of interaction between these two instability modes. However, the main focus of the investigation was the description of DWO phenomenon.

The main objective of this chapter is to analyse the interaction between *density*

wave and *pressure drop oscillations*, both experimentally and numerically. In Section 11.2 this interaction is described experimentally. In Section 11.3 the modelling of the experimental setup described in the last sections is presented. Moreover, the experimental and numerical stability limits are compared. The description of large amplitude oscillations is also presented. Finally in Section 11.4, the effects of the compressible volume on the stability of *density wave oscillations* are studied.

11.2 PDO-DWO interaction

In this section the influence of *density wave* phenomena on *pressure drop* oscillations is investigated. The main parameters used for the experiments presented in this section are:

- $P_{out} \approx$ 8.3 [bar]
- $T_{in} \approx$ - 13 [^{o}C]
- $Q \approx$ 1380 [W] (Uniform distribution)
- $G_{in} \approx$ 0-1500 [kg/m^{2}s]
- L_{HS} = 2 [m], D_H: 5 [mm]
- K$_{out} \approx$ 20 (3 [mm] orifice)
- $V_S \approx$ 9 [l]

11.2.1 Density wave mode

In the Figure 11.1 the transition from a stable operation point to an unstable point is presented. In this case the power is uniformly distributed and kept constant at $\approx$ 1380 [W]. The pump velocity is decreased until the unstable oscillatory behaviour is observed. In the unstable state the system evolves into a periodic oscillation. This way of inducing the oscillation (constant power) is different from the cases presented in Chapter 9. In this case the external characteristic is changed (pump velocity) until the unstable state is achieved. These results will be useful to analyse the interaction of DWO and PDO where the power is kept constant.

The characteristic time of these DWO is of approximately 6 seconds. No high-order oscillations are founded, even when the flow was decreased sufficiently to achieve the over-saturated conditions (dryout). As shown in 11.1, the shape of the oscillation differs from a pure mode for large amplitude oscillations. However, it should be remarked that this change of shape is not due to high-order modes but it is the results of the non-linear terms. In addition, even when the amplitude of the oscillation is significant, back-flow is not observed. In the next section, the interaction of this phenomenon with the PDO in the same system is investigated.

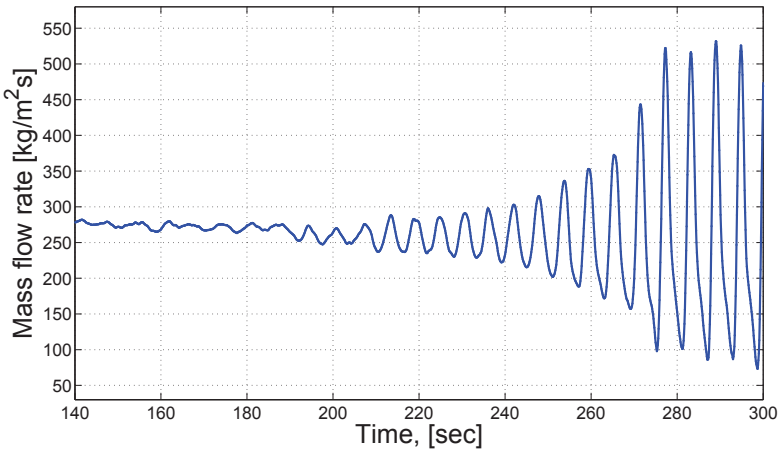

Figure 11.1: *Density wave oscillations obtained by reducing the flow for a uniform heat of 1380 W. Over-saturated conditions in the outlet are achieved.*

11.2.2 Pressure drop oscillation mode

In this section a surge tank of approximately 9 litres is used at the inlet of the test section as described in Chapter 9. In the Figures 11.2(a) and 11.2 the evolution of the flow before and after the surge tank is presented. The initial point corresponds with the all liquid condition ($G > 1200$ $[kg/m^2s]$). A quasi-steady evolution is induced by decreasing the pump flow with a small slope (compared to the PDO and DWO periods). As shown in these figures an unstable evolution is observed after $t = 1000$ $[s]$. However, the amplitude of this phenomenon is small (< 10 %) and it remains bounded. On the other hand, after $t = 3000$ $[s]$ a fast transient phenomenon takes the system completely out of the operation conditions and a high amplitude oscillation is observed (> 250 %). A detailed view of the fast transient phenomena that triggers the high amplitude oscillations is presented in the Figure 11.3. As it is possible to see the flow evolves to the negative region and back-flow takes place in short time periods. In contrast with the DWO presented in the previous sections, the oscillatory phenomenon present in this case is faster and stronger (larger amplitudes). In this case the external characteristic curve can be considered almost horizontal since the surge tank decouples the effects of the pump (external characteristic) and the boiling section (internal characteristic). In consequence, the DWO mode becomes more unstable than the case analysed in the previous section (without a compressible volume). In conclusion the system evolves in a DWO mode and it triggers the high amplitude PDO. This phenomenon was already observed since in most of the previous experimental cases both oscillation are reported to take place at the same time. Nevertheless, most of the models used to simulate PDO in the past do not take into account the mechanism that produce de DWO phenomenon. The coupling between these phenomena is normally neglected in the assumption of describing PDO as a pure and independent mode.

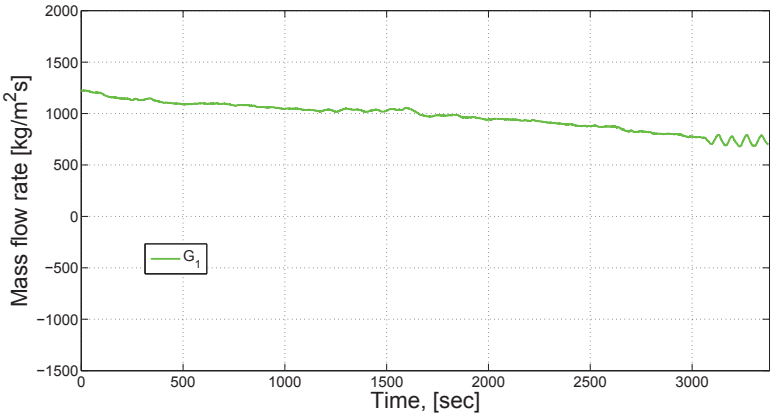

(a) Inlet flow (before the tank)

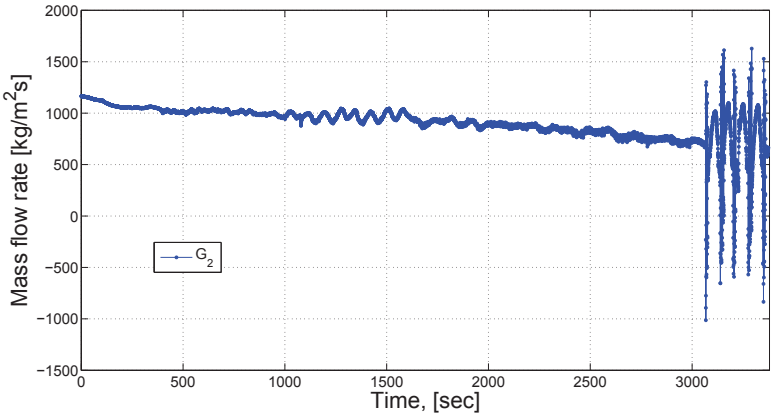

(b) Heated pipe flow (after the tank)

Figure 11.2: *Evolution of mass flow before and after the compressible tank. Pressure drop oscillations and density wave phenomena are observed.*

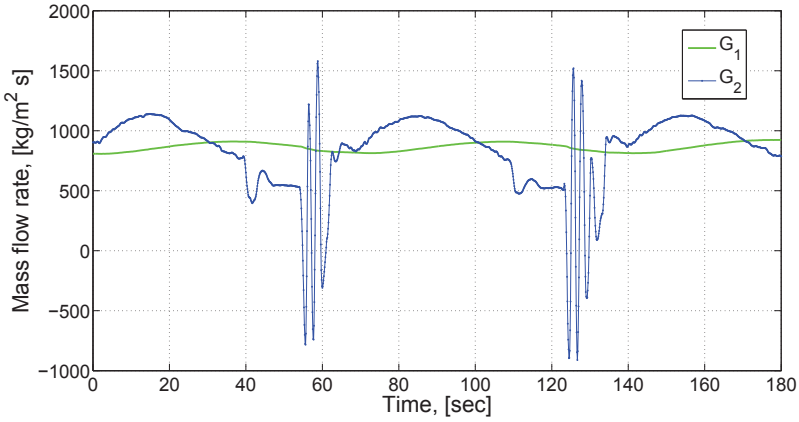

Figure 11.3: *Detailed view of the mass flows after and before the compressible tank. The pressure drop oscillations are triggered by density wave oscillations.*

The phase diagram corresponding to the oscillatory state is presented in the Figure 11.4. The internal and external characteristic curves are also shown. The internal N-shape curve is measured and the external characteristic curve is extrapolated from the oscillatory evolution (green line). In these diagrams, the area contained in the two evolution figures (internal in blue and external in green) is representative of the inertia terms which take place into the systems. As it is shown, the DWO phenomena takes place in the left part of the figure. The interaction between the different phenomena makes this kind of diagrams completely different from those normally reported in previous studies. In conclusion, none of the models used in the past to describe PDO is able to represent these physical phenomena. Furthermore is proved experimentally that even when DWO is faster than PDO, it gives the necessary energy to provoke a high amplitude oscillation. Thus, the PDO cannot be considered as a pure phenomena, not even when a large compressible volume is considered, since it interacts via energy exchange with the DWO phenomenon.

Finally, the evolution of the system for a quasi-steady increase of the flow is presented in the Figure 11.5. In contrast with the evolution presented in the Figure 11.2, in this case the high amplitude oscillations are observed in a wider region of parameters, since the DWO phenomenon continues triggering PDO. Even in regions where the system was stable in the case presented in Figure 11.2. The coupling between these two phenomena avoids the system to go into a stable operation point. The system becomes stable only after DWO disappears. In the following sections a comparison between experimental and numerical results are presented.

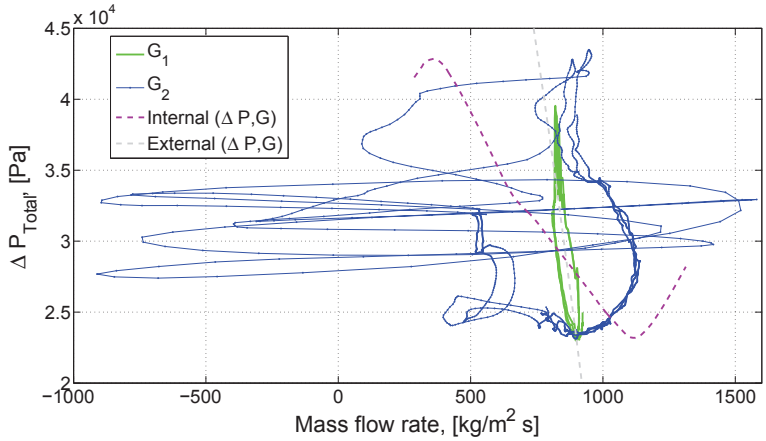

Figure 11.4: *Phase diagram of the stable oscillations. Dashed lines correspond with the internal (N-shape) and the external characteristic curves.*

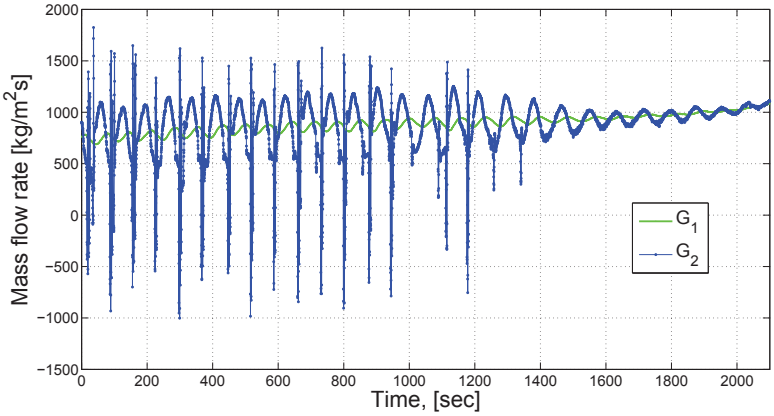

Figure 11.5: *Evolution of the heated pipe and inlet flows. High amplitude pressure drop oscillations triggered by density wave oscillations are present in the whole evolution of the system.*

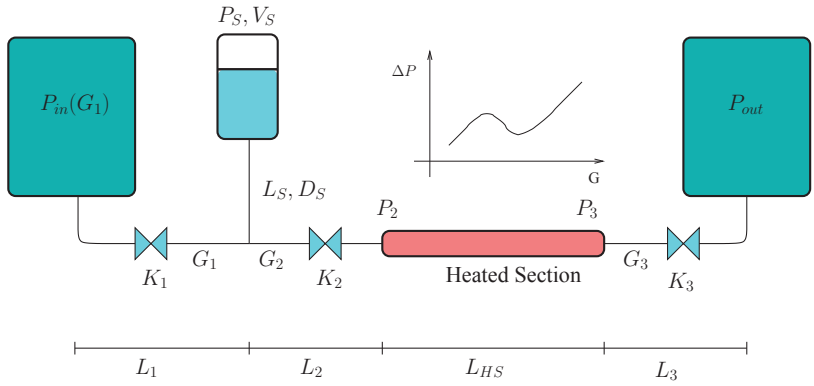

Figure 11.6: *Scheme of the model used to describe the loop presented in Chapter 9.*

11.3 Numerical validation

In Figure 11.6 it is shown the scheme of the model used in this chapter to describe the facility presented in Chapter 9. This model corresponds to the one introduced in Chapter 8. The main difference is that the pressure drop and inertia of the pipe connecting the surge tank with the loop (L_S, D_S) are taken into account. In addition, the different diameters of the piping and the heated section are also modelled. Several parameters such as the valves constants, pump response are estimated from the measurement of the absolute pressures in the loop, as described in the next sections. The mathematical formulation of this model was described in Section 8.2. In the next sections, the most important features of this model are described.

11.3.1 Heated section model

The conservation equations for the heated section model were introduced in Eqs. (7.7) to (7.9). The model used in this chapter is based on:

- Pressure drop correlation, Eq. (10.7): The pressure drop correlation for diabatic and adiabatic cases, developed in Chapter 10, is implemented in this model.
- Back-flow boundary condition: In order to take into account the back-flow phenomenon, the domain is extended at the inlet. In this new section an adiabatic condition is assumed.
- Subcooled boiling model: P. Saha and N. Zuber [11] (1974).

11.3.2 Pump response

As explained in Chapter 9, during the experiments the outlet tank pressure (after the condenser) is kept constant and it is used as the reference pressure by modifying the saturation conditions in the condenser (temperature). Thus, it is possible to

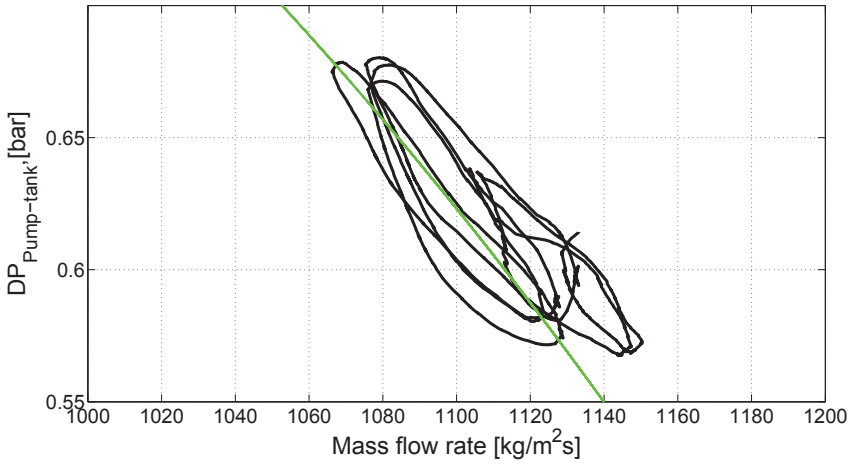

Figure 11.7: *Experimental pump response. The green line corresponds to the Eq.* (11.1) *and it is used for the numerical stability analysis.*

get the pump response by measuring the pressure at the pump outlet and at the tank. In Figure 11.7 this pressure difference vs. the mass flow rate, ($P_{Pump} - P_{Tank}$) vs. (G_1), it is plotted (black line). This characterisation is made during a pressure drop oscillation, where it can be assumed that the external characteristic is kept constant. Moreover, the hysteresis in the pump response curve is due to the fluid inertia, as seen before. Several pump response curves were analysed and the following expression was obtained

$$DP_{Pump-Tank} = 1.1 + A_0 \frac{G_1^4}{G_0^4} [bar] \tag{11.1}$$

where A_0 and G_0 are two constants used to describe the average values of the pressure drop and the mass flow during the oscillation. In the numerical analysis presented in the following section, G_0 corresponds with the initial flow and A_0 is the constant such that the internal and the external characteristic curves intersect at the flow G_0. Finally, should be remarked that this equation is obtained when both bypass valves are completely closed, see Section 9.5.

11.3.3 Stability analysis

In this section the experimental and numerical stability maps are compared. The setup used in this section has the following characteristics:

- $P_{out} \approx$ 6.5 [bar]
- $T_{in} \approx 0 - -15$ [^{o}C]
- $Q \approx$ 0-1380 [W] (Uniform distribution)

- $G_{in} \approx$ 0-1500 [kg/m^{2}s]
- L_{HS} = 1.65 [m], $L_1 \approx$ 6 [m], $L_2 \approx$ 1.5 [m], $L_3 \approx$ 1.5 [m]
- D_H = 5 [mm], D_{piping} = 12.4 [mm]
- L_S = 0.5 [m], D_S = 5 [mm]
- $K_1 \approx 5$, $K_2 \approx 15$
- $V_S \approx 9$ [l]

In contrast with the experimental cases presented in the last section, in this case the outlet test section is used instead of the orifice valve, as described in Chapter 10. The numerical stability was performed using the following numerical parameters: $\Delta t = 2\ 10^{-1}\ [sec]$, $O_z = 4$ and $O_t = 4$, $N_e = 80$ and the maximum non-linear error, as described in Eq. (3.26), is $\varepsilon_{NL} = 10^{-8}$.

In Figures 11.8(a) and 11.8(b) the numerical stability maps for the PDO and DWO modes are plotted. This stability map was constructed using 128 simulation cases. These stability limits are obtained in the same way as the limits presented in Chapter 6. In Figure 11.9 a comparison between the numerical and the experimental stability limits is presented. As can be seen, the used model predicts the PDO stability limit with a good degree of accuracy. In addition, the stability limit for the occurrence of the DWO$_I$ mode is predicted in a conservative manner. This last fact is in agreement with the results obtained in [15] using the homogeneous model in a low pressure system. Regarding the performance of this model compared with the simpler lumped models used in the literature, described on Chapter 8, it is necessary to remark the fact that none of the previous models are able to describe or predict *density wave* oscillations. Moreover, the application of those models [13, 7, 6, 9, 10, 16, 1, 8, 2] can not be extended to industrial systems, since they are only focused in the physical mechanisms involved with the PDO mode.

Regarding the current used model it should be noticed that, apart from the errors in the parameter values, there are several important differences between the numerical and experimental cases. For example, the model used for the compressible volume supposes nitrogen as a perfect gas at constant temperature. Thus, in order to improve the description of the stability limits a better model of the tank (nitrogen and R134a, not constant temperature) should be used. Regarding the heated section model, the effects of slip and wall heat transfer could also improve the accuracy of the results, especially to describe the DWO mode. Finally, there are dynamic phenomena such as the triggering of DWO by sudden flow pattern transitions, that this model is not able to describe and as proved in the last section can provoke the occurrence of high amplitude PDO.

11.3.4 Large amplitude oscillations

In this section a comparison between a simulation and the experimental evolution of a large amplitude oscillation is presented. In the numerical simulation the hp-adaptation strategy was used in order to improve the computational time. The

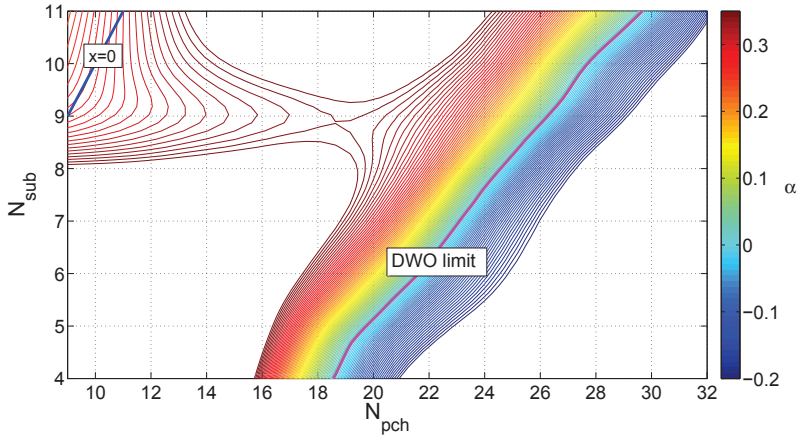

(a) Density wave mode (DWO_{II})

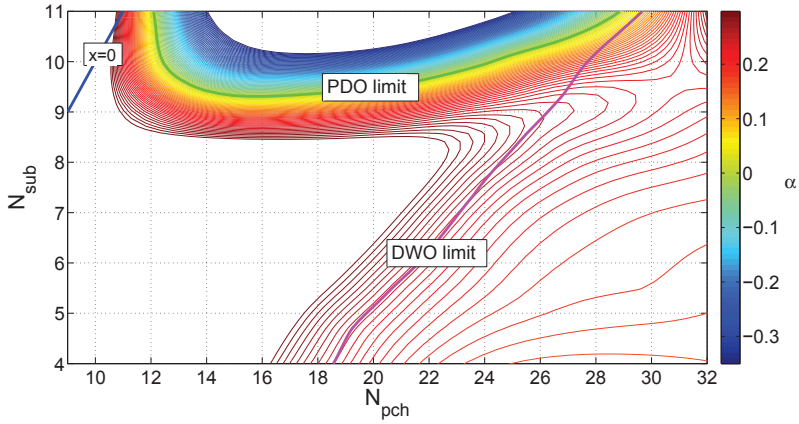

(b) Pressure drop oscillation mode (PDO)

Figure 11.8: *Stability maps for the density wave and pressure drop oscillations modes.*

adaptive strategy corresponds to varying the time step between $\Delta t = 5\ 10^{-2}\ [sec]$ and $\Delta t = 5\ 10^{-1}\ [sec]$ with a multiplicative factor of 2. A constant high order for both time and space, $O_z = 4$ and $O_t = 4$ is used. The number of elements in which the space is discretized is $N_e = 120$ and the maximum non-linear error is $\varepsilon_{NL} = 10^{-8}$.

In Figure 11.10 the experimental case is shown. The measured absolute pressure in different points of the loop are shown in Figure 11.10(a), following the nomenclature of Figure 11.6. As can be seen the time response of the pressure-meters is not enough to describe properly the DWO mode. In addition, it is possible to see that the outlet tank pressure (reference) is not constant during the oscillation. Thus the assumption of a constant pressure is not fulfilled for large amplitude oscilla-

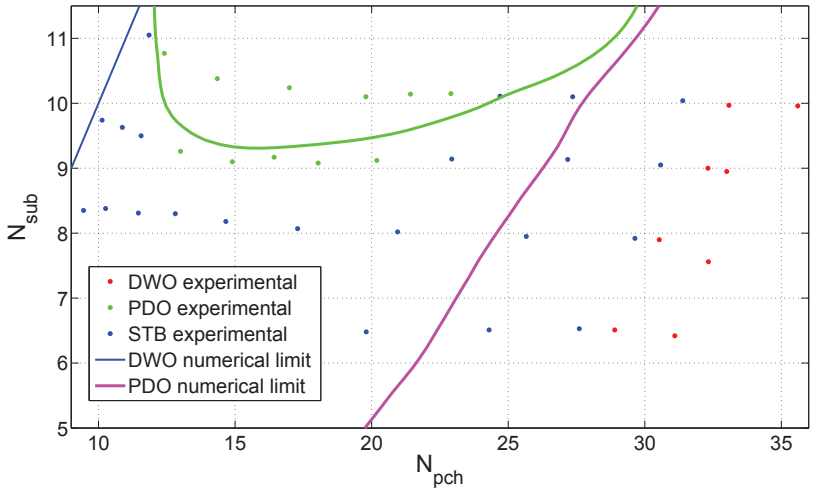

Figure 11.9: *Comparison between the numerical and the experimental stability limits for PDO and DWO modes.*

tions. In Figure 11.10(b) the measured mass flow before and after the surge tank are presented. In Figure 11.11 the simulated values for the absolute pressures and the mass flow rates are shown. The main difference between the experimental and the numerical case is that in the simulations the mass flow is slightly smaller than the experimental case. In addition, as described in the previous section, the numerical simulation is more unstable for the DWO mode. As shown in the figure, the DWO mode is observed during a longer time than for the experimental case. Furthermore, the influence of the DWO mode in the G_1 seems to be exaggerated in the numerical case. This effect can be seen in Figure 11.11(b). As commented in the last section, there are still several modelling issues that can be improved for a better description of the physical phenomena in the system. However, most of the complex phenomena which take place in the experimental example are also reflected in the numerical results. For example the back-flow, the interaction between PDO and DWO modes and the phase-shift of the inlet and outlet variables. Most of these effects are not represented by the models used in the past to describe PDO mode.

11.4 Experimental stability analysis of the DWO mode

In this last section, the effects of the compressible volume on the stability of the DWO mode is analysed. In addition, the hysteresis of the DWO phenomenon is studied experimentally. The characteristics of the experimental setup are:

- $P_{out} \approx 7$ [bar]
- $T_{in} \approx 20 - -15$ [^{o}C]

- $Q \approx 1380$ [W] (Uniform distribution)
- $G_{in} \approx$ 0-1500 [kg/m^{2}s]
- L_{HS} = 1.65 [m], $L_1 \approx 6$ [m], $L_2 \approx 1.5$ [m], $L_3 \approx 1.5$ [m]
- D_H = 5 [mm], D_{piping} = 12.4 [mm]
- L_S = 0.5 [m], D_S = 5 [mm]
- K$_1 \approx 5$, K$_2 \approx 15$

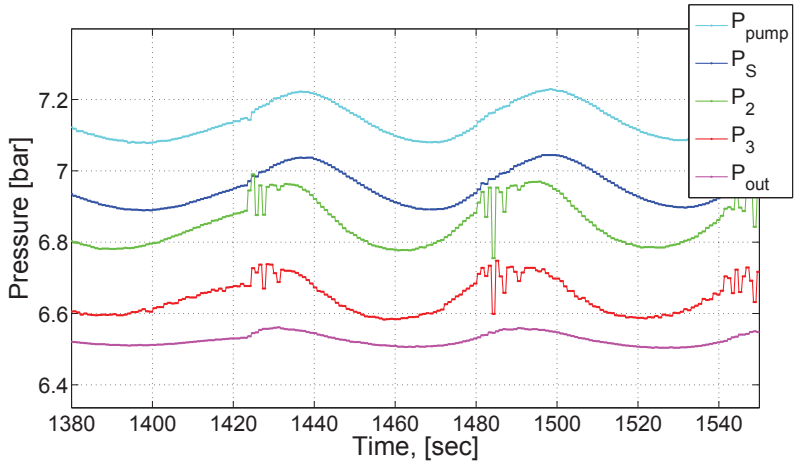

(a)

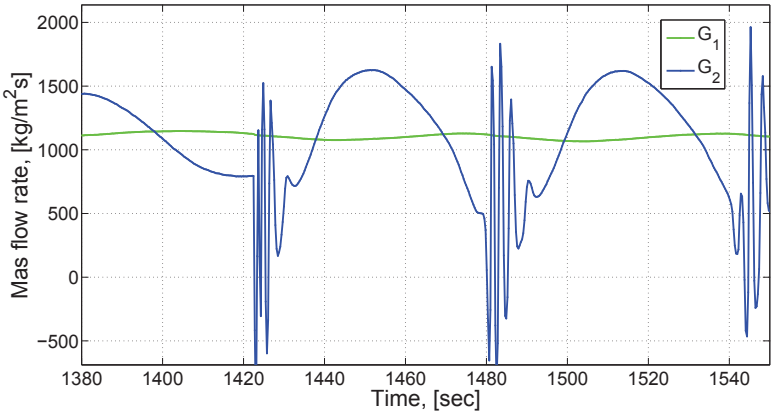

(b)

Figure 11.10: *Experimental absolute pressures (a) and mass flow rates (b) during a large amplitude oscillation.*

- $V_S \approx 8$ [l]

the one meter outlet section is used as a external pressure drop. Moreover, the pump by-pass valve was opened in order to destabilise the DWO mode when no compressible volume is used.

11.4.1 Compressibility volume effects

In this section the occurrence of DWO in the system previously described is studied. The main idea is to analyse the effects of the compressible volume on the

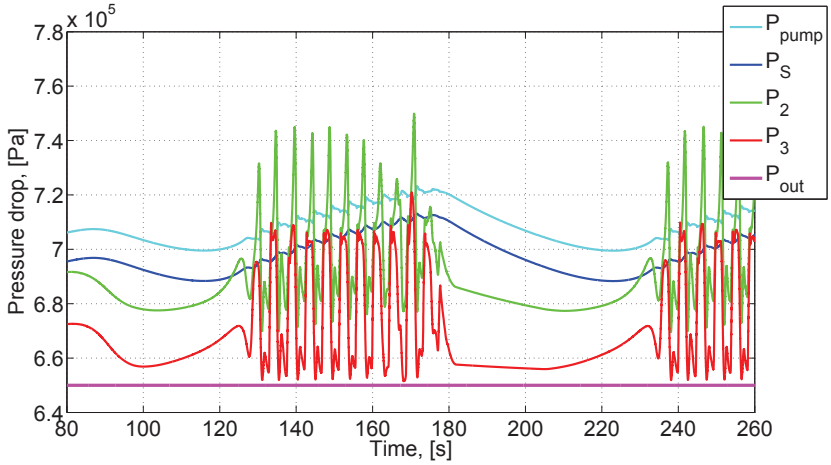

(a)

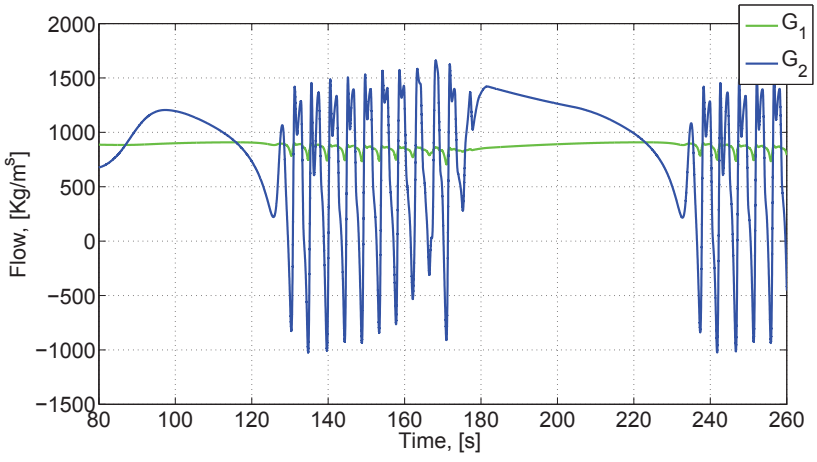

(b)

Figure 11.11: *Numerical absolute pressures (a) and mass flow rates (b) during a large amplitude oscillation.*

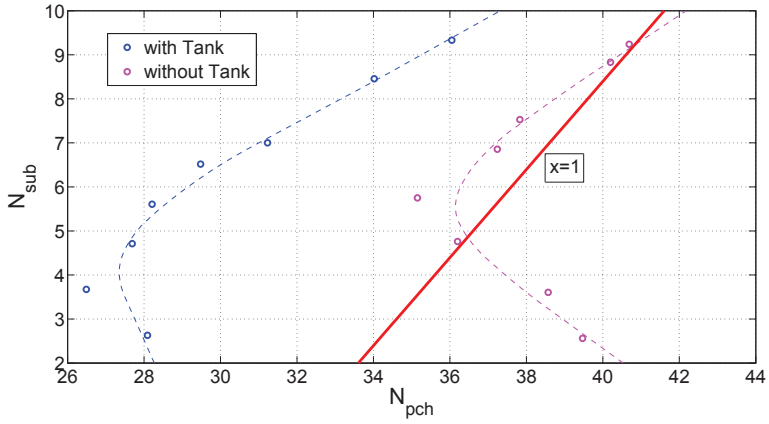

Figure 11.12: *Experimental stability limit for the DWO with and without the compressible volume at the inlet.*

stability limits. In Chapter 7 these effects were analysed numerically. In Figure 11.12 the effect of the compressible volume on the stability limits is shown. The stability limits for two cases, with and without the compressible volume, are plotted. As can be seen, the compressible volume have a high destabilising effect on the DWO mode. This same conclusion was obtained in the numerical analysis of Chapter 7. In this experimental cases no high-order modes (DWO_{III}) are observed.

11.5 Summary

In this chapter *density wave* and *pressure drop* oscillations were investigated both experimental and numerically. The interaction between these two phenomena were experimentally studied. It was proved that the occurrence of PDO it is directly related to the DWO phenomenon. In all the cases the DWO mode triggers a high amplitude PDO. In addition, the stability of PDO and DWO was also analysed using the model described in previous chapters. Numerical and experimental stability limits were compared. In the PDO mode the agreement between these the two limits was good. Moreover, for the DWO mode the predicted stability limit was conservative. In addition, the results of a high amplitude PDO with imposed DWO were used to validate the numerical model. Most of the fundamental mechanisms taking place in the experimental results were well described in the simulated case. In the last part of the chapter, the effects of the compressible volume in the stability limits of DWO were studied. It was demonstrated that the inlet compressibility notably reduces the stability of the system. This last result is in accordance with the numerical analysis presented in Chapter 7.

Bibliography

[1] GUO L., Z.P.FENG , AND X.J.CHEN . Pressure drop oscillation of steam-water two-phase flow in a helically coiled tube. *Int. J. of Heat and Mass Transfer*, 44:1555–1564, 2001. (Cited on page 223, 231)

[2] KAKAC S. AND BON B. A review of two-phase flow dynamic instabilities in tube boiling systems. *Int. Journal Heat Mass Tranfer*, 51:399–433, 2007. (Cited on page 223, 231)

[3] KAKAC S. AND CAO L. Analysis of convective two-phase flow instabilities in vertical and horizontal in-tube boiling systems. *Int. Journal Heat Mass Transfer*, 52:3984–3993, 2009. (Cited on page 223)

[4] LAHEY R. AND DREW D. An assesstment of the literature related to LWR instability modes. Technical Report NUREG/CR-1414, Rensselaer Polytechnic Institute, U.S. Nuclear Regulatory Commission, 1980. (Cited on page 223)

[5] LAHEY R. AND PODOWSKI M. On the analysis of varius instabilities in two-phase flows. *Multiphase Science and Technology*, pages 183–370, 1989. (Cited on page 223)

[6] LIU H., KOCAK H., AND KAKAC S. Dynamical analysis of pressure-drop type oscillations with planar model. *Int.J. Multiphase Flow*, 20:1129–1142, 1995. (Cited on page 223, 231)

[7] MAWASHA P. AND GROSS R. Periodic oscillations in a horizontal single boiling channel with thermal wall capacity. *Int. J. of Heat and Fluid Flow*, 22: 643–649, 2001. (Cited on page 223, 231)

[8] O.KOMAKLI , KARSLI S., AND YILMAZ M. Experimental investigation of two-phase flow instabilities in a horizontal in tube boiling system. *Energy Conversion and Management*, 43:249–268, 2002. (Cited on page 223, 231)

[9] PADKI M., LIU H., AND KAKAC S. Two-phase flow pressure drop type and thermal oscillations. *Int. Journal of heat and fluid flow*, 12:240–248, 1991. (Cited on page 223, 231)

[10] PADKI M., PALMER K., KAKAC S., AND VEZIROGLU T. Bifurcation analysis of pressure-drop oscillations and the ledinegg instability. *Int. Journal Heat Mass Transfer*, 35:525–532, 1992. (Cited on page 223, 231)

[11] SAHA P. AND ZUBER N. Point of net vapor generation and vapor void fraction in subcooled boiling. *Procedings of the fifth International Heat Tranfer*, B4.7: 175–179, 1974. (Cited on page 229)

[12] SCHLICHTING W., LAHEY R., AND PODOWSKI M. An analysis of interacting instability modes, in phase change system. *Nuclear Engineering and Design*, 240:3178–3201, 2010. (Cited on page 223)

[13] SRINIVAS B. AND PUSHPAVANAM S. Determining parameters where pressure drop oscillations occur in a boiling channel using singularity theory and the d-partition method. *Chemical Engineering Science*, 55:3771–3783, 2000. (Cited on page 223, 231)

[14] XIAO M., CHEN X. J., ZHANG M. Y., VEZIROGLU T. N., AND KAKAC S. A multivariable linear investigation of two-phase flow instabilities in parallel boiling channels under high pressure. *Int. J. Multiphase Flow*, 19:65–77, 1993. (Cited on page 223)

[15] YUN G., JUN H., GENGLEI X., AND HEYI Z. Experiment investigation on two-phase flow instability in a parallel twin-channel system. *Annals of Nuclear Energy*, 37:1281–1289, 2010. (Cited on page 231)

[16] YUNCU H. An experimental and theorethical study of density wave and pressure drop oscillations. *Heat transfer engineering*, 11:45–56, 1990. (Cited on page 223, 231)

PART IV

Final Remarks & Conclusions

CHAPTER XII

Conclusions

► The main conclusions and recommendations for future work are described here based in the analysis and discussions presented in the previous chapters.

12.1 About this work

The main goal of this work was to analyse the occurrence of instabilities in two-phase flow components. The partial results obtained along the thesis can be found at the end of each chapter. In the next sections only the main conclusions, observations and remarks are presented. As this work was split in four different parts, the same division will be used to present the conclusions.

12.2 Literature review

In this first part of the thesis (Chapter 2), an extensive review on two-phase flow instabilities was presented. A detailed description of the main mechanism involved in the occurrence two-phase flow instabilities has been given. Moreover, several experimental and analytical works were used to expose the current state of the research in the open literature. A discussion on the problems, challenges, and needs was presented.

12.3 Part I : Numerical investigation

The use of the *least squares method* was presented as an attractive alternative to solve general thermo-hydraulic problems. A *hp*-adaptive time-space spectral method was discussed for simulating a natural circulation loop given by the so called Welander's problem. This method has shown to be quite robust for solving this kind of problems using different order of approximation and discretization. It was also shown that low order discretization approaches can affect the nature of the problem by damping the dynamics of an unstable case. In addition, it was proved that the use of an adaptive strategy reduces significantly the computational costs. Furthermore, the main structure of a general *hp*-adaptive method used to solve transient two-phase

problems was presented. The stability of the solver was tested using a shock-tube problem example in which the propagation of discontinuities is simulated.

12.4 Part II: Modelling of two-phase flow instabilities

The transient evolution of flow excursion instability (Ledinegg) was analysed. The dynamic changes of the characteristic pressure drop vs. flow rate curve due to delays in the propagation of the enthalpy information were studied. Furthermore, the occurrence of *Ledinegg* and *density wave* instabilities were discussed for the cases of boiling and condensing systems. The stability limits for the occurrence of these two phenomena (Ledinegg and DWO) were obtained and compared with previous simplified criteria. In the case of condensing systems, it was found that due to the characteristic positive slope of the density profile, it is not possible to find frictional density wave phenomenon (DWO_{II}).

Respect to the stability of *density wave* instability, several external parameters (external to the heated section) such as fluid inertia in pipes, compressible gases and pump response were introduced in a simple model. It was found that the inlet inertia (longer inlet pipes) increases the stability of the system. On the contrary, the increase of the outlet inertia (longer outlet pipes) the stability of the system was not just decreased but also high-order oscillations (DWO_{III}) were induced. The occurrence of high-order oscillation modes was analysed. The effect of compressible gases in the system was also studied. It was proved that a compressible volume upstream from the heated section produces a high destabilising effect for both *Ledinegg* and *density wave* instabilities. In contrast, when the compressible volume was placed downstream of the heated section, then the system becomes more stable.

Pressure drop oscillations and its relation with density wave oscillations was investigated numerically. A comparison of the results using a dynamic and a steady-state models was presented and some remarkable differences were founded. While the steady state predicted periodic oscillations for any size of compressible volume, the dynamic model predicts a transition between stable and unstable depending on the amount of compressible volume, as seen experimentally. The effects of a compressible volume in different parts of the system were studied. For the case of upstream compressible volume, the occurrence of pressure drop oscillations was reported. In contrast, when the compressible volumes were located downstream from the heated section, no PDO were found.

12.5 Part III: The experimental investigation

The complete design of a horizontal forced convection loop to study two-phase flow instabilities was presented and a review of the necessary theoretical basis for the safe design of two-phase components was made. Some experimental results of the final design loop are used in order to compare with the theoretical analysis made in the design.

In the last part of this work, an experimental investigation on the distributed and local pressure drops is made. The experimental results were compared with pressure

drop correlations used in the literature. Moreover, a correlation for the distributed pressure drop in the loop was proposed and compared with the experimental data, proving to be more accurate than other correlations in this case.

Finally, *density wave* and *pressure drop* oscillations were investigated experimentally. The main focus of this experimental study was to described the interaction between these two oscillations modes. Several aspects of this interaction were addressed. Moreover, a comparison of the experimental and the numerical stability limits was made. For the *density wave* phenomenon, the numerical stability limit were found to be conservative respect of the experimental values. On the other hand, the *pressure drop oscillation* stability limit was predicted very accurately. A discussion about improvement of the two-phase flow modelling necessary to describe better these phenomena is presented.

12.6 Future works

From the results and conclusions obtained in this work, it is evident that further research is still needed in order to extend the researching directions posed in this work.

Regarding the numerical aspects, this work only showed that it is possible to use high-order methods and adaptive techniques in the simulation of thermo-hydraulic systems. Moreover, further effort should be directed in the application of these tools to other formulations. In addition, the extension of these concepts in the analysis of other thermo-hydraulic problems can be also used to generalise the application of the described high-order methods.

Respect to the modelling of transient two-phase flow systems, several aspects need to be improved. Further work is needed on the modelling of the interaction between the different instabilities. According to that, the treatment of these phenomena in a separated manner should be avoided, since there is a lot of experimental evidences proving that different modes interact with each other in real systems.

In addition, as presented in the literature review of Chapter 2, there is a large amount of investigations analysing the same effects (e.g. system pressure, inlet/outlet throttling, etc.) while there is still a huge number of parameters from real systems that are not considered in the numerical investigations (e.g. fluid inertia, compressible gases, external components response, etc.). Thus more effort should be made in the analysis of these parameters.

Regarding the experimental investigation, more research is still needed in the understanding of the mechanisms causing DWO_{III}. The involved physical mechanisms can be analysed by using test sections where the momentum pressure drop term is dominating.

In addition, more experimental research is needed regarding the interaction of PDO-DWO and in general analysing the interaction of different instabilities. Finally, the investigation of several parameters as the fluid inertia and the compressible volumes in two-phase flow instabilities is still necessary.

Finally, the use of different models in the resolution of this kind of problems is well investigated. However, most of the models depend on empirical correlations (e.g. pressure drop, heat transfer) that are developed in steady-state conditions. Further research should be made in the studying of the transient effects influence on the existing closure laws.

Appendixes

APPENDIX A

Pressure drop correlations for two-phase flows

The field of two-phase flow is empirically based, since it must rely heavily on correlations synthesised from experimental data. The prediction of pressure drop is a particularly good example of the empirical basis of these calculations. In flowing two-phase systems, it has been observed experimentally that for a given mass flux, the pressure drop can be much greater than for a corresponding single-phase system. The classical approach, which has been taken to correlate two-phase frictional losses, is to multiply the equivalent saturated single-phase pressure loss by an empirical multiplier, Φ^2_{TP}, which is a function of at least quality and system pressure. That is,

$$\Delta P_{fric} = \Phi^2_{TP} \Delta P_{L0} \tag{A.1}$$

A.1 Distributed pressure drop correlations

A.1.1 Homogeneous

As explained in [8], the homogeneous friction factor can be expressed as

$$\Phi^2_{Hom} = \left[1 + x\left(\frac{\rho_l}{\rho_g} - 1\right)\right]\left[1 + x\left(\frac{\mu_l}{\mu_g} - 1\right)\right]^{-0.25} \tag{A.2}$$

A.1.2 Lockhart and Martinelli

Introduced [4], the Lockhard and Martinelli correlation is calculated as

$$\Delta P_{fric} = \begin{cases} \Phi^2_{Ltt} \Delta P_L & Re_L > 4000 \\ \Phi^2_{Gtt} \Delta P_G & Re_L < 4000 \end{cases} \tag{A.3}$$

$$\Phi^2_{Ltt} = 1 + \frac{C}{X_{tt}} + \frac{1}{X^2_{tt}} \tag{A.4}$$

$$\Phi^2_{Gtt} = 1 + CX_{tt} + X^2_{tt} \tag{A.5}$$

where X_{tt} is the Martinelli parameter, in the turbulent regimes is defined as

$$X_{tt} = \left(\frac{1-x}{x}\right)^{0.9} \left(\frac{\rho_g}{\rho_l}\right)^{0.5} \left(\frac{\mu_l}{\mu_g}\right)^{0.1} \tag{A.6}$$

The value of C is given by

Liquid	Gas	C
Turbulent	Turbulent	20
Laminar	Turbulent	12
Turbulent	Laminar	10
Laminar	Laminar	5

A.1.3 Friedel

The two-phase multiplier given for the Friedel correlation [2]

$$\Phi_{Fr}^2 = E + \frac{3.24FH}{Fr_H^{0.045} We_L^{0.035}} \tag{A.7}$$

and the rest of the variables given by

$$Fr_H = \frac{G^2}{gD_H\rho_H^2} \tag{A.8}$$

$$E = (1-x)^2 + x^2\frac{\rho_l f_g}{\rho_g f_l} \tag{A.9}$$

$$F = x^{0.78}(1-x)^{0.224} \tag{A.10}$$

$$H = \left(\frac{\rho_l}{\rho_g}\right)^{0.91} \left(\frac{\mu_g}{\mu_l}\right)^{0.19} \left(1-\frac{\mu_g}{\mu_l}\right)^{0.7} \tag{A.11}$$

$$We_L = \frac{G^2 D_H}{\sigma\rho_H} \tag{A.12}$$

$$\rho_H = \left(\frac{x}{\rho_g} + \frac{1-x}{\rho_l}\right)^{-1} \tag{A.13}$$

This correlation is typically used when the ratio (μ_l/μ_g) is less than 1000.

A.1.4 Grönnerud

Grönnerud correlation, presented in [3], is given by the following expression

$$\Phi_{Gro}^2 = 1 + (\frac{dp}{dz})_{Fr}\left[\frac{(\frac{\rho_l}{\rho_g})}{(\frac{\mu_l}{\mu_g})^{0.25}} - 1\right] \tag{A.14}$$

with

$$(\frac{dp}{dz})_{Fr} = f_{Fr}\left[x + 4(x^{1.8} - x^{10} f_{Fr}^{0.5})\right] \tag{A.15}$$

$$f_{Fr} = Fr_L^{0.3} + 0.0055(ln\frac{1}{Fr_L})^2 \tag{A.16}$$

$$Fr_L = \frac{G^2}{gD_H\rho_l^2} \tag{A.17}$$

A.1.5 Müller-Steinhagen and Heck

Presented in [6] and characterised by its simplicity the Müller-Steinhagen and Heck correlation is given by

$$\Phi_{Mu}^2 = (1 + 2\,(1-\psi)\;x)\,(1-x)^{1/3} \;+\; \psi x^3 \tag{A.18}$$

with

$$\psi = \frac{\left(\frac{\partial P}{\partial z}\right)_{G0}}{\left(\frac{\partial P}{\partial z}\right)_{L0}} \tag{A.19}$$

A.2 Local pressure drop correlations

Following the same method as used to calculate distributed pressure drop, a multiplicator factor is used in order to calculate a local pressure drop loss, given by Eq. (A.1).

A.2.1 Homogeneous

As presented in [8], it is expressed as

$$\Phi_{homogeneous}^2 = 1 + x\left(\frac{\rho_l}{\rho_g} - 1\right) \tag{A.20}$$

A.2.2 Simpson

The Simpson model [7] is used for large pipes (up to 127 [mm]) assuming separated flow.

$$\Phi_{simpson}^2 = \left[1 + x\,(S-1)\right]\left[1 + x\left(S^5 - 1\right)\right] \tag{A.21}$$

with

$$S = \left(\frac{\rho_L}{\rho_V}\right)^y \tag{A.22}$$

where the exponent y ranges from 0 in case of homogeneous flow to 0.5 for maximum slip. H.C. Simpson et al. [7] proposed a value of 1/6 based in their own experimental data.

A.2.3 Morris

First introduced in [5], The Morris multiplier can be written as

$$\Phi^2_{morris} = \left[x\frac{\rho_L}{\rho_V} + S\left(1-x\right)\right]\left[x + \left(\frac{1-x}{S}\right)\left(\frac{\left(S-1\right)^2}{\left(\rho_L/\rho_V\right)^{1/2}-1}\right)\right] \tag{A.23}$$

The value of the slip ratio is given by

$$S = \left[1 + x\left(\frac{\rho_L}{\rho_V} - 1\right)\right]^{\frac{1}{2}} if\ \chi_{tt} > 1 \tag{A.24}$$

$$S = \left(\frac{\rho_L}{\rho_V}\right)^{\frac{1}{4}} if\ \chi_{tt} < 1 \tag{A.25}$$

where the Lockart and Martinelli parameter is evaluated as

$$\chi_{tt} = \left(\frac{1-x}{x}\right)^{(2-n)/2}\left(\frac{\rho_V}{\rho_L}\right)^{0.5}\left(\frac{\mu_L}{\mu_G}\right)^{n/2} \tag{A.26}$$

A.2.4 Chisholm

Chisholm correlation [1], is calculated as

$$\Phi^2_{chrisholm} = 1 + \left(\frac{\rho_L}{\rho_V} - 1\right)\left[Bx\left(1-x\right) + x^2\right] \tag{A.27}$$

In the case of orifice valves, the parameter B is assumed

$$B = 0.5 \qquad s/d < 0.5 \tag{A.28}$$

$$B = 1.5 \qquad s/d > 0.5 \tag{A.29}$$

where s is the length and d the internal diameter of the orifice.

Bibliography

[1] CHISHOLM D. *Two-phase flow in pipelines and heat exchanges*. George Godwin, London and New York, 1983. (Cited on page 250)

[2] FRIEDEL L. Improved friction pressure drop correlation for horizontal and vertical two-phase pipe flow. *Eur. Two-phase Flow Group Meeting Pap., E2 18 (1979)*, pages 485–492, 1979. (Cited on page 248)

[3] GRÖNERUD R. Investigation of liquid hold-up, flow resistance and heat transfer in circulation type of evaporator, part iv: two-phase flow resistance in boiling refrigerants. *Annexe 1972-1, Bulletin, de l'Institut du Froid, 1979*, 1979. (Cited on page 248)

[4] LOCKHART R. W. AND . MARTINELLI R. C. Proposed correlation of data for isothermal two-phase two-component flow in pipes. *Chern. Eng. Progr.*, 45, 1949. (Cited on page 247)

[5] MORRIS S. Compressible gas-liquid flow through pipeline restrictions. *Chemical Engineering Process*, 30, 1991. (Cited on page 250)

[6] MULLER-STEINHAGEN H. AND HECK K. A simple friction pressure drop correlation for two-phase flow pipes. *Chem. Eng. Prog.*, 20:297–308, 1986. (Cited on page 249)

[7] SIMPSON H., ROONEY D., AND GRATTAN E. Two-phase flow gate valves and orifice plates. *International Conference Physical Modelling of Multi-Phase Flow*, 1983. (Cited on page 249, 250)

[8] WALLIS G. B. *One-dimensional two-phase flow*. McGraw-Hill, 1969. (Cited on page 247, 249)

Power measurement error estimation

From Eqs. (9.10) and (9.11)

$$\begin{aligned}\Delta Q_{real} &= \left|\frac{\partial Q_{real}}{\partial \Psi_{Thermal}}\right| \Delta \Psi_{Thermal} + \left|\frac{\partial Q_{real}}{\partial \Phi_{AC/DC}}\right| \Delta \Phi_{AC/DC} \cdots \\ &+ \left|\frac{\partial Q_{real}}{\partial V_{cal}}\right| \Delta V_{cal} + \left|\frac{\partial Q_{real}}{\partial I_{cal}}\right| \Delta I_{cal} \end{aligned} \tag{B.1}$$

using the expression of the relative error (ε) it is obtained,

$$\frac{\Delta Q_{real}}{Q_{real}} = \varepsilon Q_{real} = \varepsilon \Psi_{Thermal} + \varepsilon \Phi_{AC/DC} + \varepsilon V_{cal} + \varepsilon I_{cal} \tag{B.2}$$

From Eq. (9.12) and neglecting the length error, the relative error of $\Psi_{Thermal}$ can be obtained as

$$\varepsilon \Psi_{Thermal} = \varepsilon DT_{12} + \varepsilon G = \frac{\Delta DT_{12}}{DT_{12}} + \frac{\Delta G}{G} \tag{B.3}$$

Moreover, using the maximum errors from Table 9.3 for the temperature and flow, taking DT_{12} as the difference between the inlet temperature and the first thermocouple value (T_{13} in Figure 9.6) and assuming that the $\Psi_{Thermal}$ will be measured with a electrical power bigger than 200 W (ΔT = 10 ^{o}C), then

$$\frac{\Delta DT_{12}}{DT_{12}} = \frac{2\ \Delta T}{T_{13} - T_{in}} < \frac{2\ 0.1}{10} \frac{[^oC]}{[^oC]} = 2\% \tag{B.4}$$

$$\frac{\Delta G}{G} < \frac{0.01}{0.5} \frac{[l/min]}{[l/min]} = 2\% \tag{B.5}$$

On the other hand, from Figures 9.11(a) to 9.11(c) the errors of $\Phi_{AC/DC}$, V_{cal} and I_{cal} are estimated as

$$\frac{\Delta \Phi_{AC/DC}}{\Phi_{AC/DC}} < 4\% \tag{B.6}$$

$$\frac{\Delta V_{cal}}{V_{cal}} < 0.5\% \tag{B.7}$$

$$\frac{\Delta I_{cal}}{I_{cal}} < 1\% \tag{B.8}$$

where is assumed an electrical power higher than 200 W (40 W each section).

Finally, replacing these values in Eq. (B.2) the accuracy of the real heat is estimated as

$$\Delta Q_{real} \approx 20[W] \quad \varepsilon Q_{real} < 10\% \tag{B.9}$$

It is important to remark that the accuracy of the power measure chain was taken assuming a power higher than 200 [W], for smaller powers then the measurement could be less accurate.

List of Figures

List of Tables